AWARD NUMBER: W81XWH-11-2-0021

TITLE: Threshold-Switchable Particles (TSPs) To Control Internal Hemorrhage

PRINCIPAL INVESTIGATOR: James H. Morrissey, Ph.D.

CONTRACTING ORGANIZATION: University of Illinois
Urbana, IL 61801-3620

REPORT DATE: September 2016

TYPE OF REPORT: Final

PREPARED FOR: U.S. Army Medical Research and Materiel Command
Fort Detrick, Maryland 21702-5012

REPORT DOCUMENTATION PAGE

Form Approved
OMB No. 0704-0188

1. REPORT DATE	2. REPORT TYPE	3. DATES COVERED
SEPT-2016	Final	23 NOV 2010 – 22 JUN 2016

4. TITLE AND SUBTITLE
Threshold-Switchable Particles (TSPs) To Control Internal Hemorrhage

5a. CONTRACT NUMBER

5b. GRANT NUMBER W81XWH-11-2-00 21

5c. PROGRAM ELEMENT NUMBER

6. AUTHOR(S)
James H. Morrissey, Rustem Ismagilov, Ying Liu, Galen Stucky, and Christian Kastrup

E-Mail: jhmorris@illinois.edu

5d. PROJECT NUMBER

5e. TASK NUMBER

5f. WORK UNIT NUMBER

7. PERFORMING ORGANIZATION NAME(S) AND ADDRESS(ES)

UNIVERSITY OF ILLINOIS
GRANTS AND CONTRACTSOFFICE
506 S WRIGHT ST, 364 HENRY ADMIN BLDG
URBANA IL 61801-3620

8. PERFORMING ORGANIZATION REPORT NUMBER

9. SPONSORING / MONITORING AGENCY NAME(S) AND ADDRESS(ES)

U.S. Army Medical Research and Materiel Command
Fort Detrick, Maryland 21702-5012

10. SPONSOR/MONITOR'S ACRONYM(S)

11. SPONSOR/MONITOR'S REPORT NUMBER(S)

12. DISTRIBUTION / AVAILABILITY STATEMENT

Approved for Public Release; Distribution Unlimited

13. SUPPLEMENTARY NOTES

14. ABSTRACT
The final goal of this project was to develop smart particles to stop internal hemorrhage at local sites. Four collaborating laboratories worked together under this contract to define threshold levels of activators of blood clotting such that the candidate clotting activators will circulate in the blood at a concentration below the threshold necessary to trigger clotting, but accumulation of the activators at sites of internal injury/bleeding will cause the local concentration of clotting activators to exceed the clotting threshold and restore hemostasis. During the past year we have applied our improved methods for covalently attaching inorganic polyphosphate (a potent initiator and accelerator of blood clotting) to nanoscale solid supports including silica- and gold-based nanoparticles that have been fabricated using a variety of derivatization and passivation methods. We have conducted extensive testing of candidate procoagulant nanoparticles to quantify their ability to trigger and/or accelerate blood clotting and have made significant progress toward the goal of adjustable procoagulant activities of the particles to render them sub- or supra-threshold with regard to initiation of the clotting cascade.

15. SUBJECT TERMS
Internal hemorrhage; Bleeding; Blood clotting; Nanoparticles; Trauma

16. SECURITY CLASSIFICATION OF:			17. LIMITATION OF ABSTRACT	18. NUMBER OF PAGES	19a. NAME OF RESPONSIBLE PERSON
a. REPORT	b. ABSTRACT	c. THIS PAGE			USAMRMC
Unclassified	Unclassified	Unclassified	Unclassified	88	19b. TELEPHONE NUMBER *(include area code)*

Table of Contents

FINAL REPORT FOR WQ81XWH-11-2-0021: "Threshold-Switchable Particles (TSP) to Control Internal Hemorrhage"

1. INTRODUCTION

The overall goal of this research project was to develop smart particles to stop internal (incompressible) hemorrhage at local sites. Our research comprised five collaborating laboratories working to develop new types of pro-hemostatic nanoparticles and to define threshold levels of these particles such that the candidate nanoparticles will circulate in the blood at a concentration below the threshold necessary to trigger clotting. On the other hand, when the particles accumulate at sites of internal injury/bleeding, their local concentration should exceed the clotting threshold and restore hemostasis. Our approaches included the development and application of chemistries for attaching inorganic polyphosphate (polyP—a potent trigger and accelerator of blood clotting) to nanoscale solid supports, development of candidate nanoparticles with varying abilities to trigger and/or accelerate blood clotting, and defining the threshold levels and flow conditions under which these particles will or will not trigger blood clotting.

2. KEYWORDS

- Internal hemorrhage
- Incompressible hemorrhage
- Bleeding
- Blood clotting
- Nanoparticles
- Trauma

3. OVERALL PROJECT SUMMARY

Comments on Administrative and Logistical Matters

Overview of subcontracts — Five laboratories participated in this project, headed by Drs. James Morrissey (University of Illinois at Urbana-Champaign), Ying Liu (University of Illinois at Chicago), Rustem Ismagilov (Caltech), Galen Stucky (University of California at Santa Barbara), and Christian Kastrup (University of British Columbia in Vancouver, BC, Canada. Dr. Morrissey served as the lead on this multi-site project.

No-cost extension — Relocating the Ismagilov lab to Caltech delayed progress on certain subtasks, and granting our request for a new subaward to Dr. Kastrup resulted in further unavoidable delays in this project. We therefore requested and received an additional, one-year, no-cost extension, resulting in a new expiration date of 22 June 2016.

Human Anatomical Substances use approval (Milestone #2) — Some of the studies in Dr. Ismagilov's lab were designed to employ blood samples from human volunteer blood donors. Dr. Ismagilov obtained IRB approval from Caltech for these studies (RI-334, approved on December 5, 2011) and Dr. Ismagilov was notified on March 20, 2012 that the protocol was approved by the Office of Research Protections. On 28 October 2014, the Ismagilov lab submitted a request to close the protocol to the US Army Medical Research and Materiel Command (USAMRMC), Office of Research Protections (ORP), Human Research Protection Office (HRPO). The final report and supporting documents were reviewed by HRPO and found to be acceptable. The protocol was therefore closed in October 2014 and no additional studies with human subjects were undertaken for the remainder of this project.

Approval for animal studies (Task #5) — Initially, we had hoped to be able to test candidate TSPs in a pig arterio-venous shunt model, and later we proposed using a mouse tail bleeding model as a substitute approach for testing these particles in an experimental animal. Although we did receive local IACUC approval for the mouse studies at the University of Illinois at Urbana-Champaign, loss of key trained personnel in the Morrissey lab during the final year of the project precluded our moving forward with the bleeding model. We therefore did not apply for approval from the USAMRMC Animal Care Use and Review Office (ACURO) for these studies. We therefore did not initiate any studies in experimental animals under this project, and Task #5 remained unaddressed.

Scientific Progress

BACKGROUND

Inorganic polyphosphates (polyP) are linear polymers of phosphate monomers. Ubiquitous across a diverse range of organisms, the physiological function of polyP in humans and other complex eukaryotes has only recently been investigated in detail [1]. PolyP is secreted from activated blood platelets and research from the Morrissey lab and others has shown that polyP acts at various stages of the coagulation cascade, depending on its polymer length [2]. Long-chain polyP (>300 phosphates long) is a potent activator for the contact pathway of blood clotting, while shorter polyP polymers of 60-100 phosphate units (the size secreted by platelets) accelerate the activation of coagulation factor V and slow fibrin clot lysis [2, 3]. With its role now clearly established as a critical hemostatic agent within the body, polyP could potentially serve as a useful and safe procoagulant compound to address multiple bleeding disorders including internal hemorrhage.

When intravenously administered, nanoparticle therapies have been devised to target activated platelets with some success, but the goal of functionally delivering a procoagulant therapy to treat internal hemorrhage in practice has yet to be fully realized [4]. In this project, we worked to develop novel approaches for the targeted delivery of nanoparticles functionalized with controlled amounts of polyP as the clot-promoting payload. The concept is that these tunable particles will be able to selectively target sites of injury in response to appropriate stimuli without the induction of clotting anywhere else in the body, a property that aqueous polyP unfortunately does not possess. Therefore, the overall goal of this study was to understand the process of particle-induced blood clotting, ultimately leading to optimally engineered particles for treating internal bleeding. We made substantial progress on this project, as outlined in the sections below.

Task 1 — Conduct spatially-defined numerical simulations to identify threshold conditions. The simulations will utilize Comsol Multiphysics modeling software to screen concentrations of activators and particles, reaction rates, temporal dynamics, shear and external fields.

The Ismagilov led the studies under Task 1 by conducting simulations to test the points of the coagulation cascade that are most susceptible to initiation. These simulations used a previously reported model that describes enzyme kinetics and stoichiometric inhibition in blood coagulation with 42 differential rate equations for 45 interacting species. For these preliminary tests, only kinetics were of interest and diffusion and fluid flow were not included. For activation of individual factors, preliminary results indicated that coagulation is initiated only if particular enzymes are activated: factors XIIa, XIa, Xa, IXa, or IIa (thrombin). Activation of other individual enzymes such as plasma kallikrein, factor VIIIa or factor Va did not lead to initiation of coagulation. The Ismagilov lab also investigated the threshold concentration of each factor required to initiate clotting in the simulation. Intrinsic pathway factors IXa and XIa required only 10 pM concentrations, whereas downstream pathway factors thrombin and XI required 100 pM. The Ismagilov group also tested whether activating multiple factors is more efficient than activating single factors, and found that the clotting is accelerated up to four-fold by activating pairs of factors. Consistent with previous results, the fastest combinations included thrombin and either factor XIa or IXa. No further acceleration was obtained by activating three factors at once, which tells us that prototype nanoparticles need produce, aggregate, or accumulate only one or two activated factors in order to have a strong effect.

The Ismagilov Lab compared the effect of polyP on coagulation when polyP is localized on a surface instead of solubilized in plasma. To this end, we used a two-dimensional numerical simulation that considered reaction, diffusion, and convection of the chemical species involved in blood clotting *in vivo*. In addition to running 40 reactions to describe the human coagulation cascade [1], four additional reactions were performed to compare the effect of polyP:

Reaction 41) V + Xa + polyP ↔ Va + Xa + polyP
Reaction 42) XI + IIa + polyP ↔ XIa + IIa + polyP
Reaction 43) XI + XIa + polyP ↔ XIa + XIa + polyP
Reaction 44) TFPI + polyP ↔ TFPI - polyP

The components and rate constants for the 40 coagulation reactions were taken from an established kinetic model for the human coagulation network [5]; the enhanced V and XI activation rates and TFPI abrogation rate due to the presence of polyP in Reactions 41-44 were estimated from kinetic assays [2, 6]. In the simulation, 2.76 fmol polyP was either spatially localized onto a 50 μm patch of a cylindrical channel (pink line in **Figure 1B**) or dispersed throughout its volume; plasma flowed

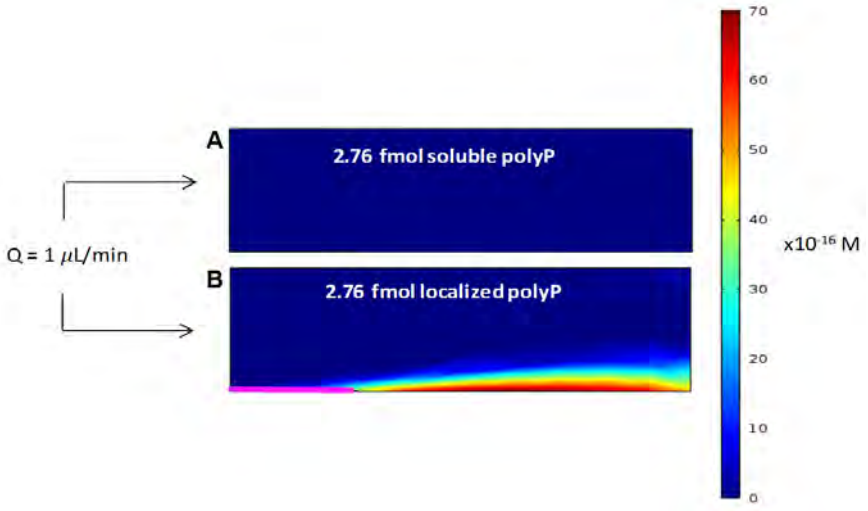

Figure 1. Thrombin concentration in the cylindrical channels when the same amount of polyP (2.76 fmol) was (A) solubilized in plasma or (B) localized on the surface in a 50 μm patch (pink line). The color scale ranges from 0 fM (blue) to 7 fM (red). Plasma flowed through each channel at a flow rate of 1 μL/min with the wall shear rate 12 s^{-1}. The rectangles are 2D representations of a 3D cylindrical geometry with the top side as the radial axis of symmetry.

through each channel at 1 µL/min. When polyP was dispersed, the maximum thrombin concentration in the channel was only 0.015 fM, whereas when polyP was localized, 7 fM was generated (**Figure 1**). A thrombin burst is what initiates fibrin formation, so the higher thrombin concentration in the localized scenario suggests that localized polyP increases the coagulability of flowing blood in comparison to solubilized polyP.

Shear rate may be a threshold condition by which particles can aggregate and trigger blood clotting. To test this hypothesis, Dr. Kastrup's and Dr. Ismagilov's labs have designed several microfluidic devices with varying channel widths to test the effects that different shear rates have on clotting. To aid in experimental design and interpretation of results, the Ismagilov laboratory simulated the shear rate of fluid flow inside a microfluidic channel with a 500 µm width 100 µm height using COMSOL Multiphysics modeling software. As **Figure 2** shows, as expected, the shear rate in the entrance region of the channel is different from that of the midplane (particularly in the corners). Thus, simulations will be used to design experiments and to interpret experimental findings of how shear affects coagulation.

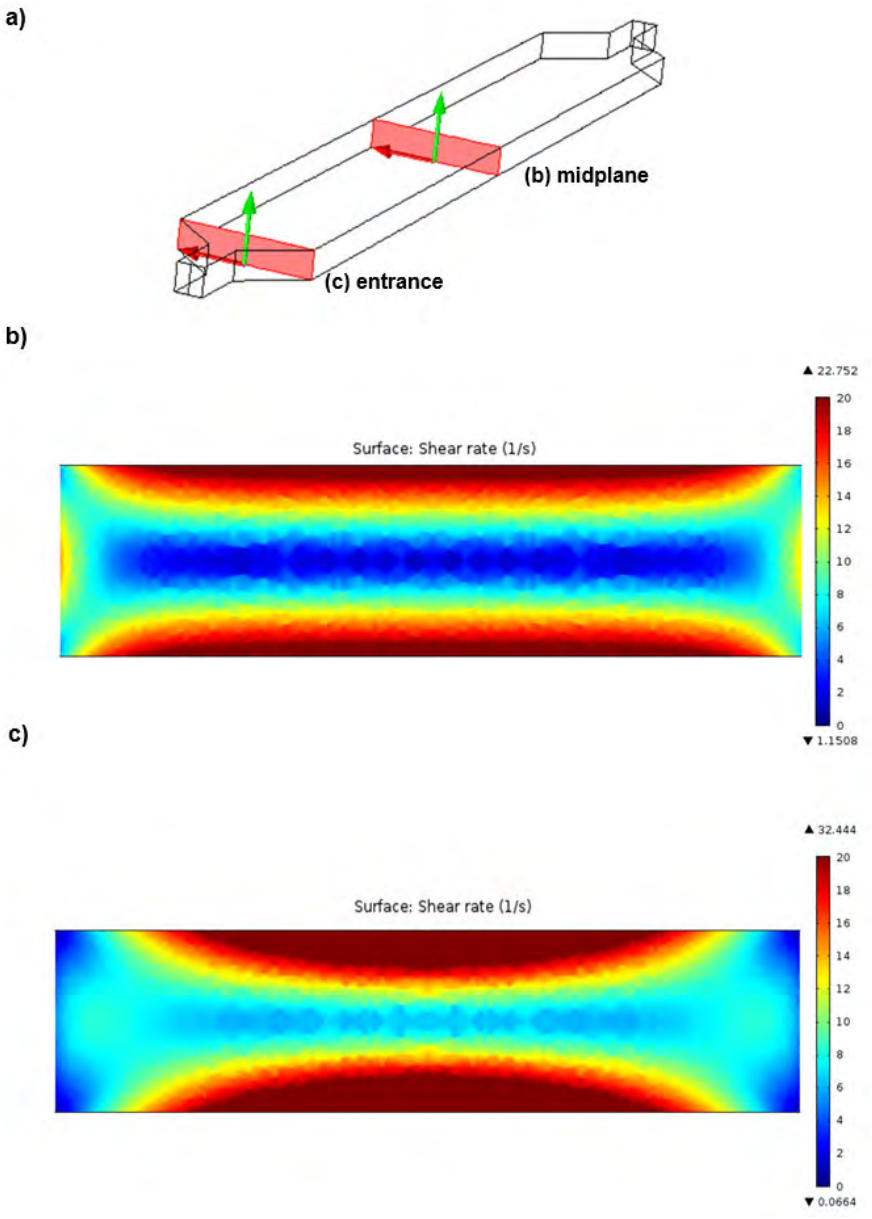

Figure 2. (A) Schematic of the microfluidic channel. (B) Shear rate simulation for the mid-plane of the channel, where different colors represent different shear rates. (C) Shear rate simulation for the entrance of the channel, where different colors represent different shear rates.

To examine how localizing polyP onto surfaces affects thrombin generation, we used a two-dimensional numerical simulation that considered diffusion, convection, and the rates of 41 reactions of the coagulation cascade. An established kinetic model for the coagulation cascade [7] was used with the addition of $polyP_{>1000}$ in three reactions that were previously characterized in kinetic assays [2, 8-11]. PolyP (7.54×10^{-9} moles, 30 µM) was either spatially localized onto the surface of a cylindrical channel or dispersed throughout its volume. When polyP was localized onto the surface of the channel with a shear rate of 1 s^{-1}, the local thrombin concentration was 782-fold higher than when polyP was dispersed throughout the volume (1.83×10^{-8} M versus 2.34×10^{-11} M) (**Figure 3A-B**). The difference in the concentration of thrombin generated can be attributed to the higher local concentration of polyp, which led to increased positive feedback from the coagulation cascade. However, simulations showed that the effectiveness of localizing polyP decreases as shear rate increases (**Figure 3C**).

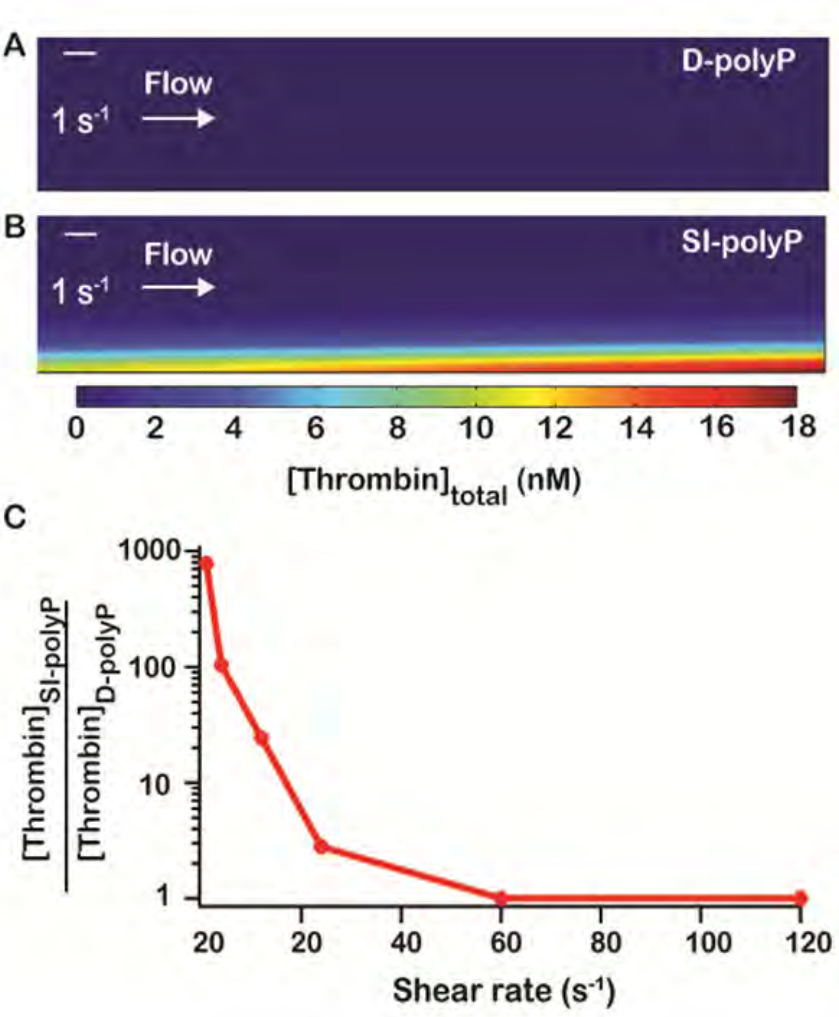

Figure 3. Localization of polyP accelerates thrombin production in the presence of flow. Two-dimensional numerical simulations of the human blood coagulation cascade, comparing the generation of thrombin by polyP dispersed throughout a cylindrical channel versus polyP immobilized on the channel surface. The overall number of polyP molecules was the same in all simulations (7.54×10^{-9} moles). (A) Plots show $[thrombin]_{total}$, the sum of [thrombin] and [meizothrombin], for a two-dimensional longitudinal cut of the cylinder from simulations where polyP was either dispersed throughout the volume or was immobilized onto the surface of the channel. $[Thrombin]_{total}$ was sampled at 500 s in both cases. (B) The fold difference in maximum [thrombin] generated when polyP is surface-immobilized versus dispersed at varying shear rates.

Simulation Methods

Thrombin generation was modeled using the *Transport of Diluted Species* module of Comsol Multiphysics 4.4 by adding diffusion and convection to a previously reported kinetic model by Chaterjee, et al. [7]. The following modifications were made to the Chaterjee model: i) Reactions 28, 29 and 35 were omitted because our experiments did not include a thrombin detection agent, a surface that activates factor XII, or CTI; ii) Reactions 50-57 describe the fibrinolysis reactions and were omitted to conserve computational resources; and iii) three rate equations were added to describe the activation the clotting cascade by polyP [2, 8-11], as follows:

Reaction 58: TFPI + polyP ↔ TFPI-polyP; k58_on = 1.0×10^{6} $M^{-1}s^{-1}$, k58_off = 1.0×10^{-2} s^{-1}
Reaction 59: V + Xa + polyP → Va + Xa + polyP; k59 = 2.0×10^{13} $M^{-2}s^{-1}$
Reaction 60: XI + IIa + polyP → XIa + IIa + polyP; k60 = 2.2×10^{10} $M^{-2}s^{-1}$

In the Chaterjee et al. model, rate constants were modified to include the effect of platelet activation using parameters ϵ and η. As our microfluidic experiments used platelet-poor plasma, these modifications to the rate constants were ignored and original literature values were used (columns 2-4 of Table 1 in reference [7]). The rate constants for the three extra polyP reactions were estimated from kinetic assays in references [2, 8-11].

The diffusion coefficient for all soluble species was 5×10^{-11} m^2/s and the velocity profile varied with the shear rate, $v_z(r) = \frac{\gamma_w R}{2}\left(1 - \frac{r}{R}\right)^2$, where v_z is the velocity in the axial direction at each radial coordinate r, R is the cylinder radius, and γ_w is the shear rate at the cylinder wall. The chemical species were flowed into a cylindrical geometry of radius 2 mm and length 20 mm at varying shear rates (1, 4, 12, 24, 60, 120 s^{-1}), and polyP reacted with the clotting factors as a species either immobilized on the surface of the cylinder or dispersed throughout its volume. For each shear rate, [thrombin] was sampled after the incoming flow had displaced the channel volume 12.5 times.

Task 2 — Conduct in vitro experiments to test recommended threshold conditions with human plasma and whole blood.

The Liu Group, collaborating with the Morrissey Group, focused on using two candidate TSP formats, namely the Artificial Dense Granule (ADG) DDS and the polyP-gold nanoparticle (polyP-GNP) drug delivery systems (DDS). These studies used *in vitro* clotting experiments with citrated human plasma, as well as other tests assaying the contact pathway of clotting. ADG and polyP-GNP syntheses are outlined in depth below in **Task 3**. The contact activity of bare polyP nanoparticles (NPs) were first assessed in citrated human plasma and with an isolated clotting factor assay for factor XII (FXII) zymogen activation in order to contrast it with the procoagulant ability of molecularly dissolved polyP. When bare polyP NPs are added to human plasma, the particles are able to activate the contact pathway of clotting more robustly as compared to their molecularly dissolved counterparts by theoretically serving as a superior templating surface for FXII (cf. **Figures 5** and **6** in **Publication 3**). Precipitated short-chain polyP is able to autoactivate FXII even though evidence suggests that this polymer length is too short to serve as a significant contact surface in solution (cf. **Figure 4** in **Publication 6**) [12]. Therefore, encapsulating polyP granules in phospholipid vesicles was envisioned as a way to efficiently deliver procoagulant actors to the injury site to promote hemostasis. For targeting, the ADG DDS relies on the overexpression of inflammatory enzymes that degrade phospholipid vesicles called phospholipases, which can be secreted into the circulation. Certain isoforms such as secreted phospholipase A_2 ($sPLA_2$), typically found at ng/ml concentrations in the blood stream, could potentially reach concentrations approaching µg/ml directly adjacent to cancerous neoplasms and hemorrhage sites [13]. It is thus envisioned that ADGs will remain intact until flowing past a traumatic injury location where these enzymes are above the threshold concentration necessary to degrade the protective vesicular envelope and unload the procoagulant polyP granule inside [14] (cf. **Figure 4** in **Publication 6**). Dynamic light scattering studies (DLS) reveal that $sPLA_2$ and an intracellular isoform PLC, which is involved in platelet granule secretion [15, 16], are able to hydrolyze phospholipid vesicles at µg/ml concentrations (cf. **Figure 3** in **Publication 6**). A proof-of-concept study was conducted with the nonionic detergent Tween 20 to prove that the polyP NP inside the ADG is capable of FXII autoactivation. ADGs not treated with detergent exhibit no ability to initiate conversion of FXII to FXIIa, whereas ADGs treated with the detergent were able to autoactivate FXII in a manner approximately equivalent to the bare polyP NP. Next, a similar experiment was undertaken with the phospholipase, PLC. Again ADGs not exposed to enzyme manifested very little FXII conversion activity, whereas ADGs treated with 30 µg/ml PLC autoactivated FXII like their bare polyP NP and ADG + detergent counterparts (cf.

Figure 4 in **Publication 6**). The clotting activity of the ADG DDS was further investigated in human plasma. Results from a turbidometric contact pathway assay indicate that 10 μM ADGs incubated with PLC reduced the time to clot compared to control with no clotting activators present by approximately 20% (cf. **Figure 5** in **Publication 6**). Taken together, the data indicate that the ADG DDS is able to initiate the contact pathway of clotting once sufficient phospholipase concentrations rise above threshold.

The polyP-GNPs' ability to initiate the contact pathway of coagulation was evaluated by two distinct methods: colorimetric assay and coagulometry. This allows for the investigation of clot formation optically and viscomechanically. Both techniques show that polyP-GNPs synthesized with 10 nm- and 50 nm-diameter GNPs are significantly more procoagulant compared to dispersed polyP of the same chain length. In addition, the polyP-GNPs approximate the clotting activity of very long chain polyP ($polyP_{800}$). In other words, the confinement of shorter polyP chains on nanoscale surfaces enhances their ability to activate FXII and the recruit other proteins including prekallikrein and high molecular weight kininogen (HMWK) (cf. **Figures 3** and **4** in **Publication 5**).

Ongoing work in the Liu Group is focusing on exploiting polyP's role as a generic, non-proteinaceous molecular chaperone, with the polymer possessing high binding affinity for a diverse class of proteins [17]. In particular, current efforts are directed towards the delivery of factor VIII (FVIII) as a novel, targeted therapy for hemophilia A, a congenital disorder characterized by low circulating concentrations of FVIII and prolonged partial thromboplastin times (a clotting test based on contact pathway activity). Therefore, *in vitro* experiments regarding this Task have entailed assaying for contact activity with FVIII-deficient plasma. Preliminary results appear promising. **Figure 4** shows a FXII autoactivation assay with ADG/FVIII demonstrating, as a proof-of-concept, that the polyP particles can still activate FXII zymogen. **Figure 5** shows that only 10 μM ADG/FVIII incubated with 10 μg/ml PLC is able to suitably initiate clotting in an hour timescale in FVIII-deficient plasma, while ADG/FVIII without PLC digestion does not appreciably coagulate. PolyP and FVIII must act synergistically to initiate clotting in FVIII-deficient plasma: PolyP NPs alone do not initiate clotting. Interestingly, addition of an equivalent amount of FVIII alone also does not rescue normal clotting time. This is reasonable because the FVIII concentration was not physiological and has not been optimized for rescuing the normal bleeding time. Excess free floating FVIII was not removed in this assay and the ADG/FVIII samples are referred to as "before centrifugation" (BC). The design and synthesis of "ADG/FVIII," with polyP as the delivery vehicle, is outlined below in **Task 3**.

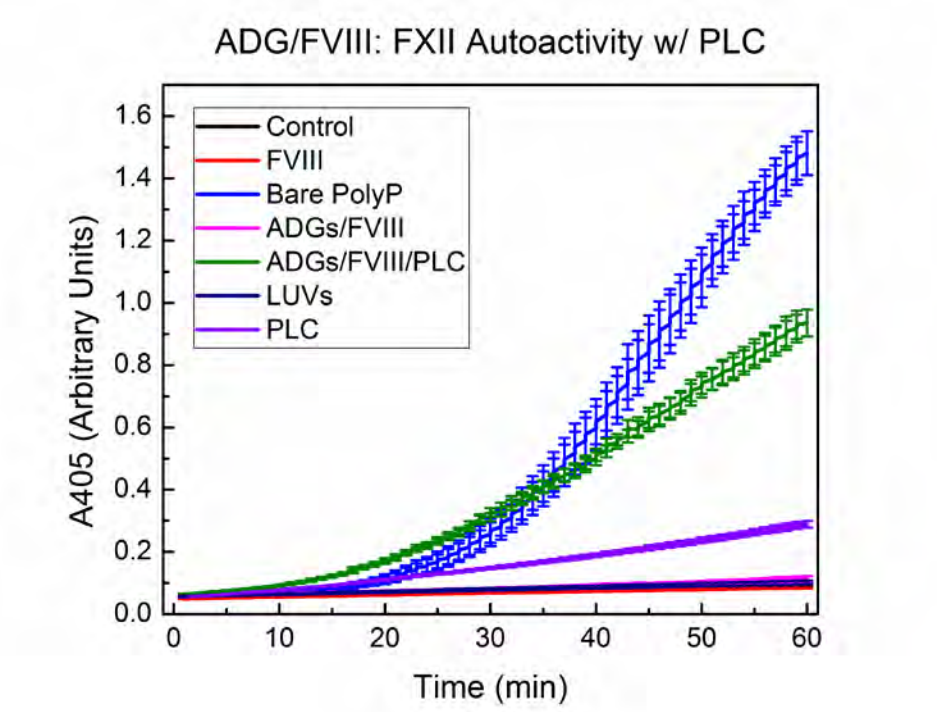

Figure 4. FXII Autoactivation Assay with ADG/FVIII after PLC Triggering.

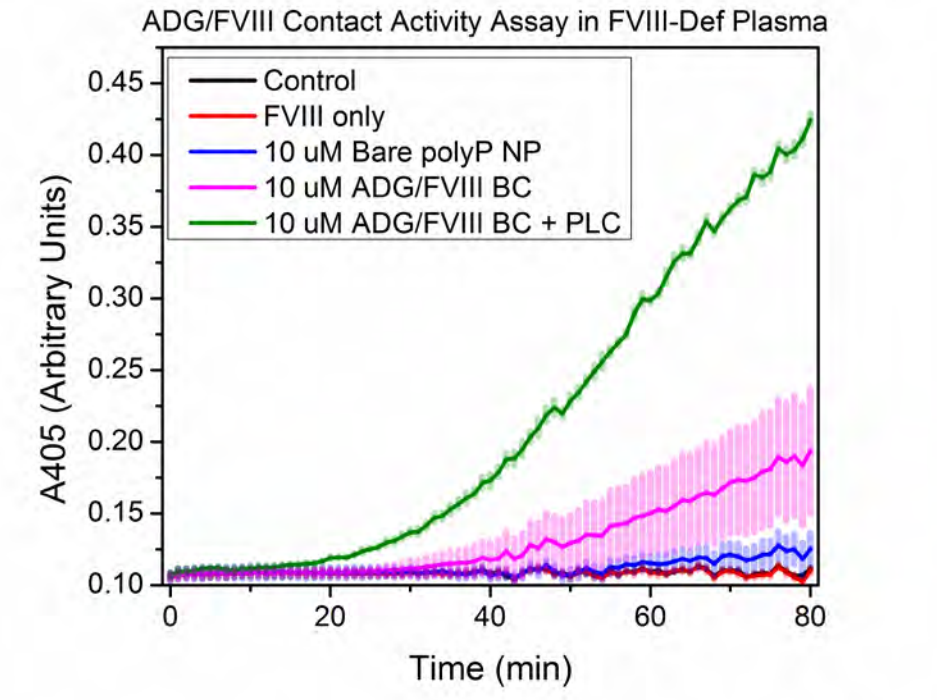

Figure 5. Contact activity of ADG/FVIII in FVIII-Deficient Plasma before centrifugation.

Task 3 — Design and test particles that will function as candidate TSPs.

The Morrissey Group provided large quantities of carefully size-fractionated polyP preparations to the other sites as a key ingredient in preparing and testing candidate TSPs, with polyP being the clot-promoting payload in many of the particles. We developed improve, scalable methods for size-fractionating polyP and for rapidly estimating the polymer lengths using PAGE (manuscripts in preparation), and we made these technologies available to all sites within the project. Prior to 2010, there was really no chemistry available in the literature for covalently end-labeling polyP molecules, but our group reported a facile method for creating stable, covalent phosphoramidate linkages between the terminal phosphates of polyP and almost any primary amine using water-soluble carbodiimide-mediated coupling [18]. During the current project period, the Morrissey lab optimized these coupling reactions and extended them to identify robust conditions for covalently coupling alcohols to the terminal phosphates of polyP to create phosphoester bonds (**Publication 2**), thereby increasing the types of coupling chemistries available for formulating polyP-containing candidate TSPs. These technologies were also widely shared among the sites. **Publication 2** also reported the synthesis of a series of chromogenic and fluorogenic polyP-based substrates that now allow high-throughput methods for detecting and quantifying enzymes that degrade polyP (both exo- and endopolyphosphatases). More recently, we have further extended these coupling chemistries to include covalently attaching small synthetic oligopeptides to the terminal phosphates of polyP, which allows us to further expand both the number and the types of functional chemical groups that can be stably attached to polyP. This includes attaching multiple free amines, sulhydryls, and carboxylates to the termini of polyP, as well as attaching dyes, fluorophores, biotin, and peptide epitope tags to polyP (manuscript in preparation).

The Liu Group concentrated its efforts during the grant period to achieve the Task's objectives by leveraging its expertise in size-controlled synthesis of polymeric nanoparticles (NPs) and the design of inexpensive, facile, bio-inspired and biocompatible routes for creating efficacious drug delivery systems (DDS), together with the expertise of the Morrissey Group in polyP chemistry and the blood clotting system. As such, we followed nature's example in the case of polyP in order to synthesize a "smart" threshold-switchable particle with procoagulant functionality suitable for mitigating detrimental outcomes associated with internal hemorrhage. PolyP is often localized on the nanoscale in electron-dense, subcellular bodies called acidocalcisomes in unicellular organisms, such as species in the genera Protozoa and Archaea. Its name arises from the fact that the pH in the organellar lumen is slightly acidic and from its propensity to store divalent metal cations including calcium, magnesium, and zinc at high concentrations [19]. Analogous polyP granules also exist in human platelets, first characterized by Ruiz et al. [20], who discovered that human platelet dense granules contain abundant stores of polyP. These polyP storage pools are approximately 200-250 nm in diameter, surrounded by a phospholipid bilayer, which contains several ATP-driven transmembrane proton pumps to maintain a mildly acidic environment. Upon platelet activation, these granules are secreted in concert with other platelet bodies as a first act to achieve hemostasis [21]. Using nature as a guide, the Liu Group devised a DDS entailing the encapsulation of polyP NPs in sterically stabilized liposomes decorated with poly(ethylene glycol) (PEG) to promote clotting at internal hemorrhage sites (cf. **Figure 1** in **Publication 6**).

First, polyP nanoprecipitation was systematically investigated in the presence of biologically significant concentrations of divalent metal cations such as Ca^{2+} and Mg^{2+}. Dynamic light scattering (DLS) is a pragmatic means to interrogate the solubility behavior of polyP in an aqueous environment, as the molecularly dissolved polymer will scatter little light radiation, whereas polymeric precipitates will produce significant scattering. Therefore, exploring the scattering phenomena of the polymer across a wide concentration range will reveal two distinct thermodynamic regimes. The first is characterized by low scattering; this occurs when polyP is still free floating. Between the first and second regimes, there is an abrupt transition in the relationship between the scattering count rate and monoP concentration. In the latter regime, the count rate rises as the number of particles that are able to scat-

ter light increases concomitantly with the addition of more polyP polymer. The inflection point is defined to be polyP's solubility, in a manner analogous to the treatment of a surfactant critical micelle concentration (CMC).

The scattering behavior of three polyP polymer lengths (70, 250, and 1000+ phosphate units) was determined using carefully size-fractionated polymer preparations prepared by the Morrissey Group. Longer polyP, usually localized in acidocalcisomes in bacteria, is able to nanoprecipitate much more easily than shorter chains, like those commonly encountered in human platelet dense granules. The variation in polyP solubility may explain the divergent procoagulant/hemostatic behavior of polyP, especially in terms of initiation of the contact pathway of clotting. Typically, negatively charged nanoscale surfaces are required to act as a template to localize Factor XII (FXII) and its binding partners. The solubility of polyP was subsequently assessed by varying the metal cation concentration. PolyP readily precipitates in 5 mM $CaCl_2$, typical of many *in vitro* clotting tests, as well as in the ionic calcium concentration measured in human blood plasma (1.2 mM), although not as robustly. Including other divalent metal cations such as 0.4 mM Mg^{2+} or 10 μM Zn^{2+} promotes increased nanoprecipitation (cf. **Figure 1** in **Publication 3**).

The colloidal stability of polyP NPs under aqueous conditions containing 1.2 and 5 mM $CaCl_2$, respectively, as well as in 35 mg/ml bovine serum albumin (BSA) suspension (in order to gain insights into colloidal behavior at conditions resembling human plasma) was also investigated using DLS (cf. **Figure 2** in **Publication 3**). In aqueous calcium, the polyP NPs manifest Ostwalt ripening behavior as the particle diameter grows following a power law over a time scale of hours. In BSA suspension, the particles immediately shrink 50% from their initial size, and then the effective diameter is unchanged over three hours. The decrease in the NP diameter does not involve multiple scattering effects caused by saturation of the DLS detector. Rather, it is hypothesized that the polyP NPs interact with BSA in a manner mediated by the presence of the calcium cation.

The NP effective diameter is controlled solely by the metal cation concentration regardless of the monoP concentration (supersaturation ratio). Increasing the Ca^{2+} concentration forces polyP to nanoprecipitate more robustly. On the other hand, decreasing the Ca^{2+} concentration forces more polyP into solution. In this way, polyP nanoprecipitation is a thermodynamic equilibrium process governed by the metal cation concentration (cf. **Figure 3** in **Publication 3**). Whereas the particle formation is dependent on the metal ion concentration, the particle behavior displays dilution-dependent hysteresis across a range of monoP concentrations (or supersaturation values). $PolyP_{250}$ was nanoprecipitated at several times its solubility concentration in 5 mM $CaCl_2$, and then diluted serially in more 5 mM $CaCl_2$. The scattering count rate remained elevated as compared to the forward direction of the solubility curve, even maintaining its particle format past the solubility concentration (cf. **Figure 3** in **Publication 3**). This hysteric behavior suggests that the polyP NPs do not dissolve immediately upon dilution, a phenomena having potentially significant ramifications in hemostasis, e.g. in dense granule secretion, implying that polyP NPs may maintain its particle format downstream in circulation.

After completion of a comprehensive study of polyP NP formation, A DDS with targeted, procoagulant functionality was sought that would be modeled after the human body's granular polyP bodies. The polyP DDS is heretofore referred to as Artificial Dense Granules (ADGs), as they are inspired by the same nanostructures in human blood platelets (cf. **Figure 1** in **Publication 6**). Platelet-sized polyP was nanoprecipitated in 5 mM $CaCl_2$, forming ~160 nm granular particles. The polyP NPs were then mixed with an excess of 200 nm sterically stabilized liposomes decorated with 5 mol% PEG. Sonication of the resulting dispersion yielded high encapsulation of polyP NPs in the vesicles as demonstrated by colloidal stability and calcium modulation experiments using DLS. After 10 minutes of sonication, the ADG hydrodynamic diameter is ~165 nm and does not change after 1 h, whereas the bare polyP NPs undergo Ostwalt ripening as discussed above. The encapsulation efficiency was determined by changing the Ca^{2+} concentration from 5 mM to 7.5 mM 30 minutes after ADG synthesis to examine any perturbation in the ADG effective diameter. As particle precipitation is a thermody-

namic equilibrium process controlled by the Ca^{2+} concentration, any shift in concentration will elicit a change in NP size. The ADG hydrodynamic diameter is only altered upon addition of extra calcium and a nonionic detergent (Tween 20), which dissolves the phospholipid envelope and allows the polyP NPs to further precipitate in the more concentrated calcium environment. Without inclusion of detergent, ADGs maintain their integrity in the higher calcium environment, evinced by the lack of any size perturbation (cf. **Figure 3** in **Publication 6**).

The morphology, structure, and composition of the ADG DDS and bare polyP NPs were studied by various imaging and spectroscopic techniques, including transmission electron microscopy (TEM), high resolution scanning transmission electron microscopy (HR-STEM), electron energy loss spectroscopy (EELS), and X-Ray photoelectron spectroscopy (XPS). When polyPs of any polymer length are nanoprecipitated in 5 mM $CaCl_2$ and prepared for imaging with TEM, the particles are homogenously electron dense and granular in morphology with diameters of approximately 150-250 nm. Upon prolonged exposure with the electron beam, the particles appear like sponges or soccer balls, with dispersed, bright white spots of lesser electron density [21]. XPS data reveals that the NPs are composed solely of P, Ca, and O, with a P:Ca ratio of 67:32 (cf. **Figure 4** in **Publication 3**).

Imaging and spectroscopic analysis of the ADG DDS demands more sophisticated techniques in order to elucidate the core-shell nanoarchitecture. As such, the ADGs and bare polyP NPs, respectively, were sandwiched between two graphene monolayers in a biocompatible manner using benign aqueous conditions. The graphene mitigates the harmful effects of the electron beam, hindering mass loss and enhancing resolution to the Ångstrom level [22]. ADGs examined by this approach with HR-STEM appear to have a dense core approximately 120 nm in diameter surrounded by a ~25 nm corrugated shell of lighter electron density. Spectroscopic measurements confirm the presence of a phospholipid-encapsulated granular polyP NP, as indicated by the homogenous distribution of P, Ca, and O in the core, and only P, C, and O in the shell. Further investigation of the L-edge demonstrates without equivocation that the phosphate in the core is polymerized (i.e. inorganic polyP) and the phosphate in the shell is not (i.e. phospholipid). An analysis of the bare polyP NPs by HR-STEM corroborates the observation that electron damage is the cause of the white spots. In the electronically insulated environment of the graphene sandwich, the bare polyP granules appear uniformly electron dense and with approximately the same diameter as determined by DLS and TEM. Moreover, EELS provides additional evidence (in conjunction with the XPS data) that the bare particles contain homogenous distributions of P, Ca, and O (cf. **Figure 2** in **Publication 6**).

In addition to investigating polyP nanoprecipitation as a means toward a procoagulant DDS with threshold-switchable properties, synthetic routes toward decorating polyP on a distinct nanoparticle scaffold were also devised. The Liu Group investigated the nanoscale confinement of polyP on colloidal surfaces using inorganic and polymeric substrates, including gold sols and dendrimers via chemical modification and/or functionalization. To this end, nanolocalization of polyP was hypothesized as a route to assemble activators of the coagulation cascade above their threshold concentration to elicit a robust procoagulant stimulus greater than the sum of the equivalent amount of molecularly dissolved actors dispersed in solution. Platelet-sized polyP (~70 orthophosphate) was covalently linked to the disulfide molecule cystamine via N-(3-(dimethylamino)propyl)-N′-ethylcarbodiimide hydrochloride (EDAC)-mediated modification of the terminal phosphate under benign aqueous conditions (cf. **Figure 1** in **Publication 5**). The EDAC coupling chemistry was devised by the Morrissey Group in 2010 [18]. After synthesis of the polyP-cystamine ligand at high yield (70-80%) (cf. **Table 1** in **Publication 5**), it was allowed to react with citrated colloidal gold nanoparticles of various sizes (10 nm, 15 nm and 50 nm). Ligand replacement and reduction of the disulfide group, in conjunction with an increase in the ionic strength, allowed the polyP-cystamine ligand to decorate the GNP surface. Excess, free polyP-cystamine ligand was removed by centrifugation (cf. **Table 6** in **Publication 5**). The degree of polyP decoration on the nanoparticle surface was also controlled by introducing PEG-thiol. In other words, the polyP aggregation number (the number of polyP molecules per particle) was modulated by the inclusion of a known amount of PEG-thiol. Ursula Jakob and colleagues at the Uni-

versity of Michigan argue that polyP is an ancient macromolecule protecting a myriad of proteins from denaturation [17]. The Liu Group intends to use this functionality to design a bioinspired drug delivery vehicle and construct an enhanced procoagulant TSP. It is envisioned that polyP's action as a molecular chaperone can be leveraged to encapsulate clotting factors inside granular polyP NPs to treat specific bleeding disorders. The Liu Group has centered its primary efforts initially on FVIII for development of a TSP for Hemophilia A. FVIII and polyP are first mixed together and subsequently co-precipitated in 5 mM $CaCl_2$, creating coacervated polyP NPs containing the clotting factor. The polyP/FVIII NPs are mixed with a stoichiometric excess of sterically stabilized, PEGylated liposomes, and sonicated to achieve encapsulated particles. The ADG/FVIII are then centrifuged to remove excess unencapsulated polyP, FVIII, and empty liposomes. Experiments are ongoing to determine the encapsulation efficiency and protein loading. **Figure 6** shows the colloidal stability of ADG/FVIII after encapsulation.

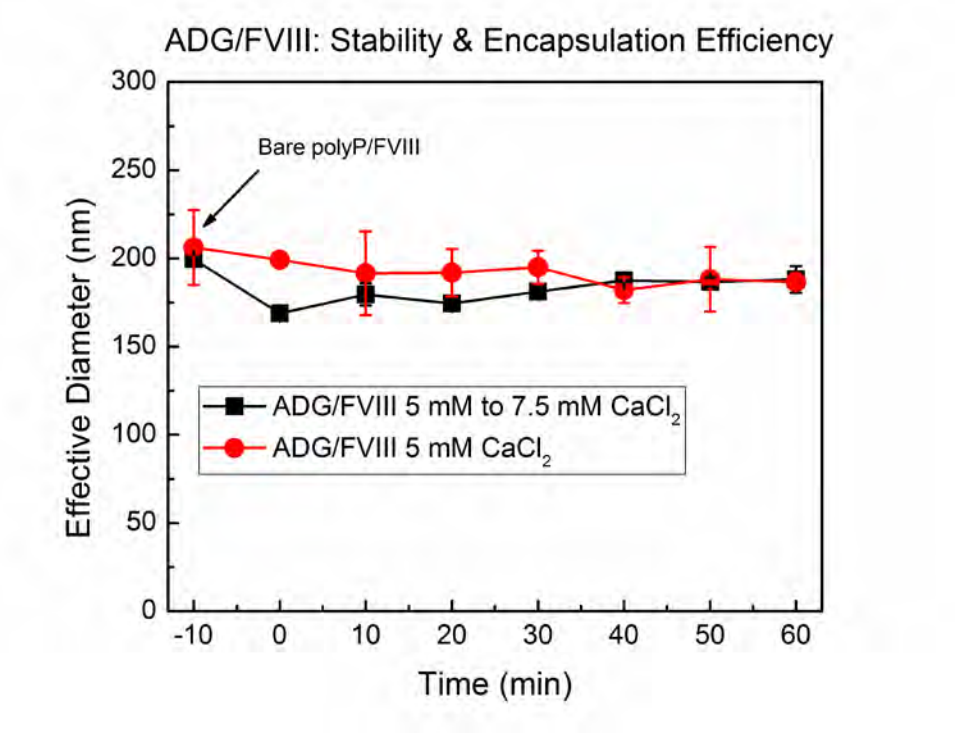

Figure 6. ADG/FVIII Colloidal Stability in aqueous 5 mM and 7.5 mM $CaCl_2$.

SUBTASK 3.a

Research in the Stucky group focused on polyP-functionalized silica nanoparticles (SNP) (polyP-SNP) as a promising TSP candidate for delivering a large enough dose to activate coagulation in internal injuries. As previously discovered, the ideal SNP-polyP candidate uses roughly 70-monomer polyP provided by the Morrissey group to synthesize polyP-SNP. The ideal concentration for minimizing clot time was approximately 0.25 mg/ml, though the clot time remains under 2 min for concentrations as low as 0.05 mg/ml POLYP-SNP. Below 0.05 mg/ml, the concentration was too low to significantly activate coagulation (**Figure 3** in **Publication 4**). In vitro blood clotting experiments were conducted on a thromboelastograph (TEG).

SNPs served as the scaffold for the majority of TSP studies. Using the reverse micelle method and the modified Stöber method [23], we were able to control the size of SNPs produced based on reagent ratios and synthesis conditions. This controlled synthesis ensured that SNPs post functionalization with polyP were within the desired size regime. In addition, we refined our synthesis protocol to prevent particle aggregation. For instance, smaller SNPs and storing the particles in solution (**Figure 7**) minimized aggregation. Nanoparticle size was determined by dynamic light scattering (DLS).

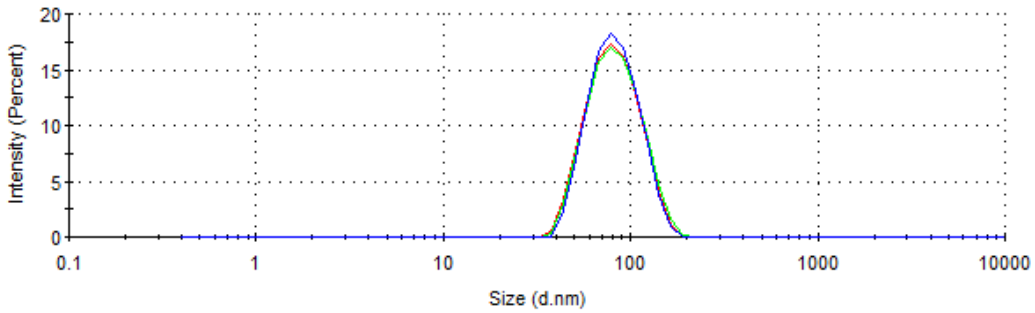

Figure 7. Size of monodisperse SNPs determined to be 83.73 ± 26.03 nm by DLS with a polydispersity index (PdI) of 0.081. SNPs were synthesized by the modified Stöber process in ethanol.

In our tests with silica nanoparticles (SNPs) and polyP-functionalized silica nanoparticles (polyP-SNP), we measured the effect of the silica particles' size and concentration on coagulation. Particles above 10nm were synthesized in the laboratory following the modified Stöber method and recovered using centrifugation. The different nanoparticle sizes were obtained by varying the amounts of tetraethoxysilane (TEOS) and ammonia (NH_4OH) (**Figure 8**). Further tests were conducted using Ludox silica nanoparticles (Sigma Aldrich) below 10 nm. We isolated silica nanoparticles below 50 nm by ultrafiltration and ultracentrifugation to develop a stock for coagulation and functionalization experiments. Yield posed a problem for syntheses using less than 4 % NH_4OH. Syntheses below 4 % NH_4OH produced a yield below 40 % (**Figure 9**). The lack of ammonia likely prevents catalysis of the TEOS hydrolysis reaction. Zeta potential tests showed that SNPs have a negative charge in simulated body fluid, which helps activate the intrinsic pathway by activating FXII [24]. However, zeta potential exhibits no systematic change in coagulation with respect to size or pH.

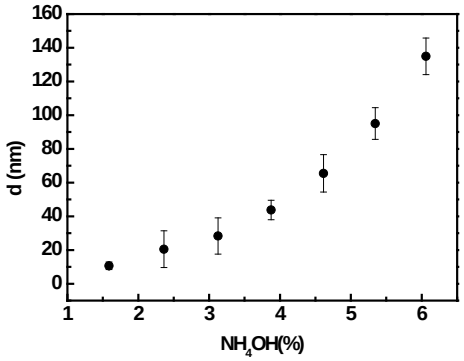

Figure 8. Particle size of SNP based on % NH_4OH added.

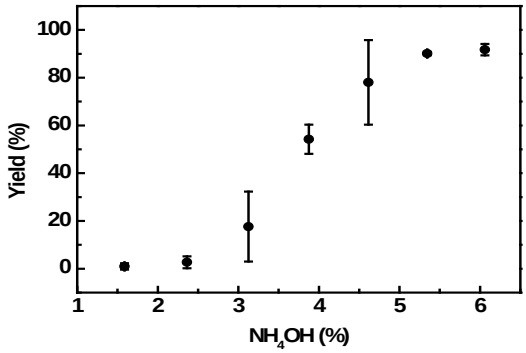

Figure 9. Silica yield based on % NH_4OH added.

Apart from the clotting time (R) other parameters were evaluated, such as rate of clot formation, and clot size, since the agents attached to the particle might not affect the initial clot formation time, but could accelerate the clotting when this is initiated or result in the formation of a bigger clot. Tests confirmed that the particles maintain stability and size, at all concentrations of interest, indicating particle sizes vary solely due to synthesis conditions.

In addition to solid non-porous nanoparticles, large-pore mesoporous nanospheres (MSN) [25] were tested for delivering procoagulant proteins such as thrombin, prothrombin or tissue factor to wounds. The large pore size and increased accessible surface likely increases coagulation by allowing proteins to adsorb to the surface and activate [26]. While cytotoxicity studies on mesocellular foam silica particles (MCF) show that MCF is safer for use in the body compared to the current acceptable

materials such as kaolin (**Publication 1**), MSNs were found to be too large to function as a viable TSP.

In addition to silica, the Stucky group looked at other oxide nanoparticle materials as polyP delivery platforms. Titanium dioxide and calcium hydroxyapatite were found to have greater aggregation and were not as easily functionalized as silica. After silica, the next best scaffold was iron-oxide (Fe_3O_4) In contrast to silica, iron oxide particles are not as strongly procoagulant, which means the particles will not significantly activate the intrinsic pathway. Furthermore, iron oxide can be detected using magnetic resonance imaging (MRI) technology to track particle biodistribution within in the cardiovascular system. The main obstacle in using iron oxide nanoparticles was converting the particles from the organic solvent in which they were synthesized to a more biocompatible solvent, while retaining the small particle size. One method of preparing biocompatible iron oxide was to add poly(acrylic) acid (PAA) to the particles' surface. However, addition of PAA resulted in nanoparticle aggregation (**Figure 10**). Despite testing several functionalization strategies, SNPs were determined to be the best scaffold for a variety of candidate TSPs.

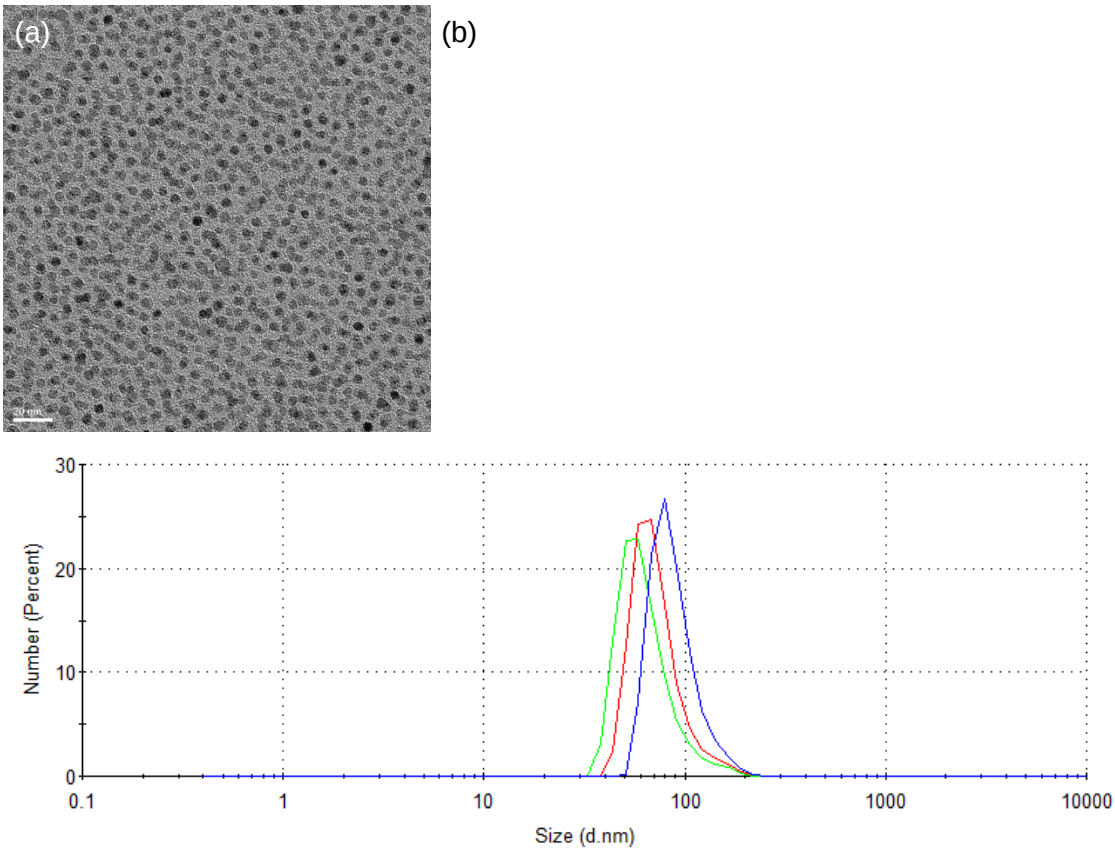

Figure 10. (a) TEM image and (b) Iron oxide particles (73.44 ± 24.93 nm, PdI 0.307) suspended in deionized water.

SUBTASK 3.b Develop and refine procedures for chemically (covalently) attaching molecules that can trigger or enhance blood clotting (polyphosphate, tissue factor, etc.) to solid supports.

Originally, candidate TSPs were theorized to deliver recombinant proteins such as thrombin. However, the best candidate TSP produced by the Stucky group was polyP-SNP. The synthesis, characterization, and *in vitro* research on polyP-SNP are described in **Publication 4**.

A second pathway used APTES to form a bridge between the nanoparticle and the procoagulant material. The primary amine terminus of APTES readily binds with proteins or EDAC -modified polyP (**Figure 11**). The Morrissey group has shown how polyP binds to amine surface strip wells using EDAC, polyP, APTES-modified silica, and 2-(N-morpholino)ethanesulfonic acid (MES) [18]. Zeta potential and Fourier transform infrared (FTIR) spectroscopy showed that the nanoparticles had been functionalized with APTES. Zeta potential measurements were used to ensure that the polyP bound to the particles.

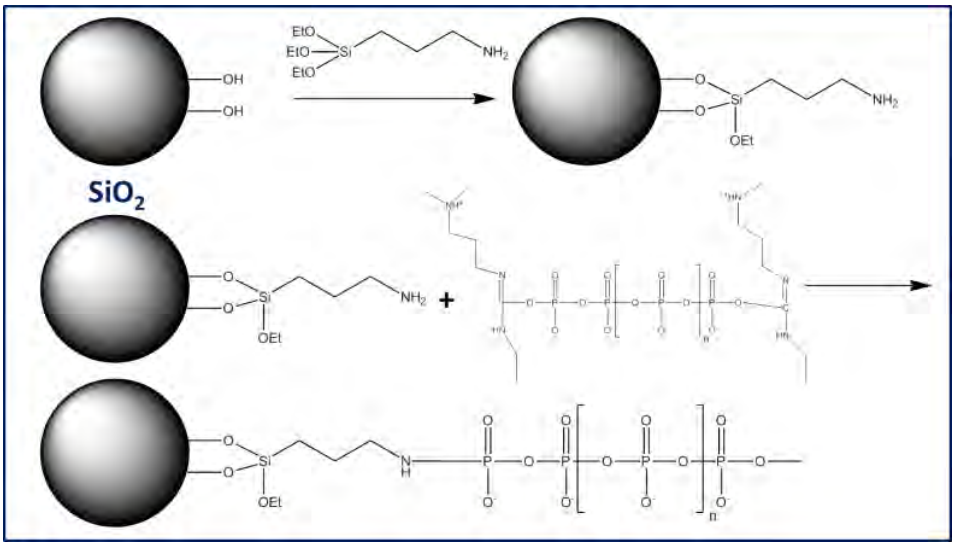

Figure 11. Schematic of SNP core and P70 corona via an APTES bridge and EDAC cross-linker.

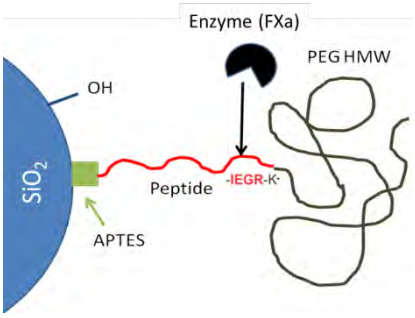

Figure 12. FXa (found in the wound site) recognizes peptide sequence (IEGR) and cleaves PEG off the TSP to selectively activate coagulation.

Conjugation Discussion. In comparison to external hemorrhage, the lack of tissue damage greatly impairs treatment. The particles are designed to be injected into the bloodstream and to only target bleeding sites. Thus, the particles require a second functionalization designed to protect the nanoparticles from initiating clotting in healthy vessels and inducing a heart attack or stroke. Nanoparticles designed for drug delivery often coat their particles with polyethylene glycol (PEG) to prevent unwanted activation. PEGylated nanoparticles increase the half-life of silica in the blood stream, limit cellular uptake, and limit protein adsorption to the underlying active surface [27]. At the wound, the particle releases the PEG, revealing the active surface with which clotting is amplified. Our current studies for activation use a peptide with an IEGR sequence that connects the particle to the PEG (**Figure 12**). Activated Factor X (FXa) cleaves the peptide at the IEGR sequence, removing the PEG and leaving the activated TSP. As FXa only exists above threshold at bleeding sites, the targeting

mechanism will ensure that the “swarm” of TSP activates clotting only where necessary. Successful protection of the silica surface was shown at each functionalization stage (**Figures 13 and 14**). While this strategy would alleviate safety concerns, the linker was too small for FXa to cleave the peptide and release the PEG surface coating.

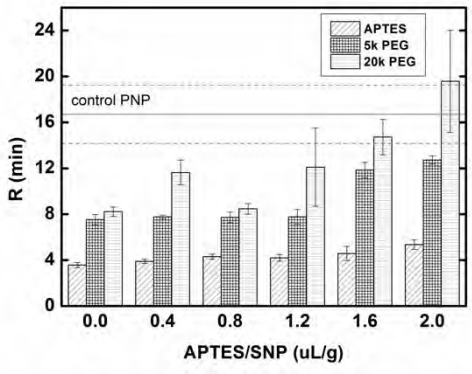

Figure 13. Optimization of APTES functionalization. At a ratio of 1.6 or 2.0 μL/g, SiO_2-APTES is pro-coagulant while SiO_2-PEG is not.

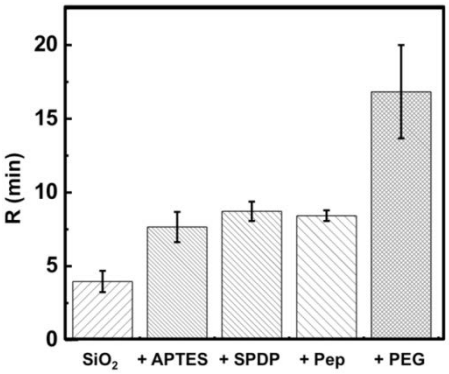

Figure 14. Clotting times of functionalized silica particles. (Pep: peptide, PEG used is 2k).

In addition to silica, calcium hydroxyapatite (HA), titania, and iron oxide were directly functionalized with polyP. HA particles functionalized with polyP (HA-P70) (**Figure 15**) showed promise as bare HA is anticoagulant in nature, while HA-P70 reduced clot times. Unfortunately, HA-P70 were never able to accelerate clotting function as well as polyP-SNP and were larger than 100 nm in size. We also saw that iron oxide was amenable to functionalization with polyP using both the traditional Lewis acid mechanism (**Figure 16**), as well as by esterification. Though functionalization was successful, polyP-functionalized iron oxide was not as effective as polyP-SNP.

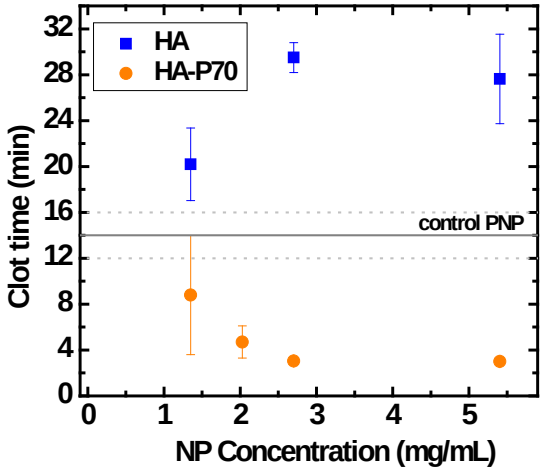

Figure 15. Attaching polyP to HA NPs creates a procoagulant from an anticoagulant scaffold. (Right) HA-P70 accelerates thrombin generation when compared to bare HA.

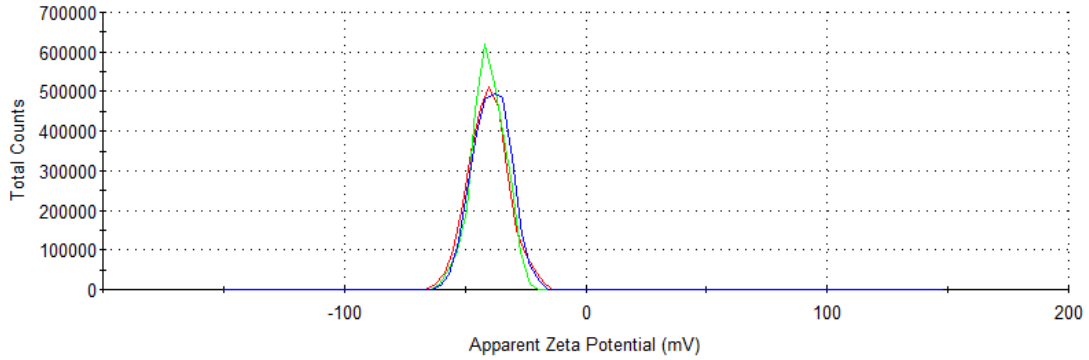

Figure 16. Zeta potential of iron oxide nanoparticles capped with P70 using the traditional Lewis acid mechanism (-40.3 ± 8.20 mV).

SUBTASK 3.c Attach clotting triggering/enhancing agents to particles identified in task 3.a; also attach molecules that allow targeting/clustering of these particles in order to create candidate TSPs.

Previously, we showed that bare silica nanoparticles can be functionalized with a targeting peptide and polyethylene glycol (PEG) to protect the molecule from clotting in healthy vessels (**Figures 117, 18**). We subsequently tested the same strategy with the SNP-P70 system. Aggregation remained the key issue. We used EDAC to bind P70 and APTES to limit aggregation via the cationic amine terminal on APTES and the anionic P70. Keeping the nanoparticle system in solution also resolved the aggregation issue.

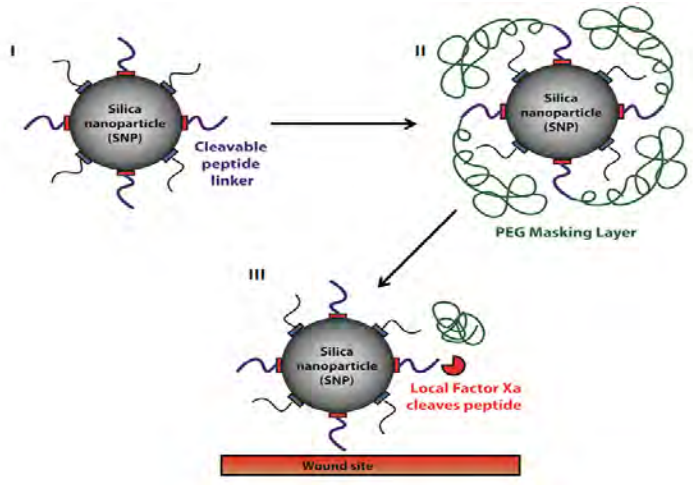

Figure 17. (I) TSP with peptide linker that cleaves at wound site. (II) PEG masking layer protects TSP from clotting in healthy vessels. (III) At injury site, the peptide is cleaved, PEG layer released and the TSP activates to accelerate clotting.

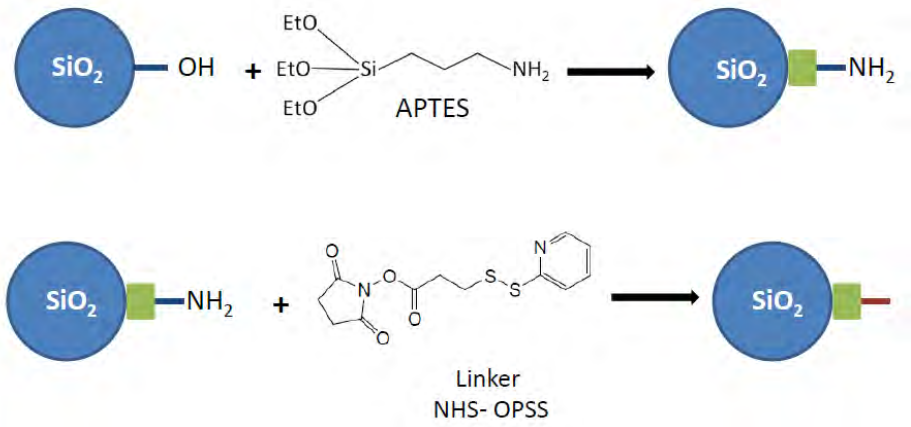

Figure 18. Functionalization of the TSP with APTES and an NHS- orthopyridyl disulfide (OPSS) cross-linker. The peptide is attached to the TSP via the cross-linker. PEG is attached to the peptide to fully protect the molecule.

Using a SNP particle functionalized with APTES (SNP-APTES) (**Figure 19**), we were able to further functionalize the TSP to attach a peptide and polyethylene glycol (PEG) (**Figure 20**). After attaching the cross-linker, peptide and PEG molecules, the average particle size remained below 100 nm. The polydispersity index (PdI) increased slightly above 0.1. Once we are able to fully synthesize a TSP with PdI below 0.1 at all steps, we will add P70 to the TSP system. This allowed us to test the particles' targeting and clotting ability in vitro.

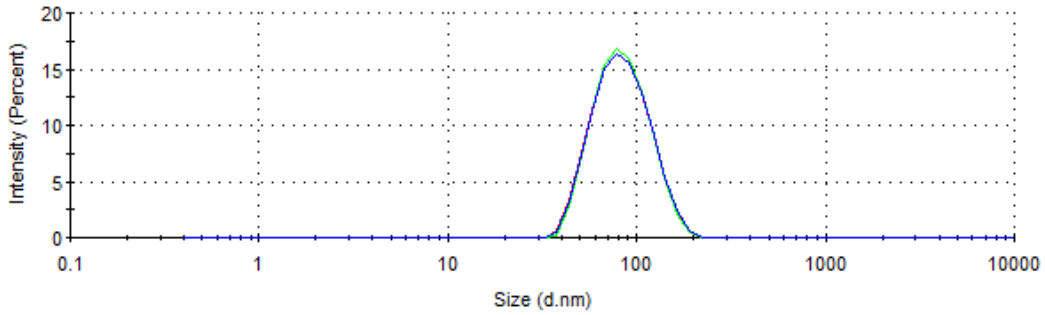

Figure 19. Attachment of cross-linker to SNP-APTES caused minimal aggregation (86.21 ± 28.83 nm, PdI 0.133).

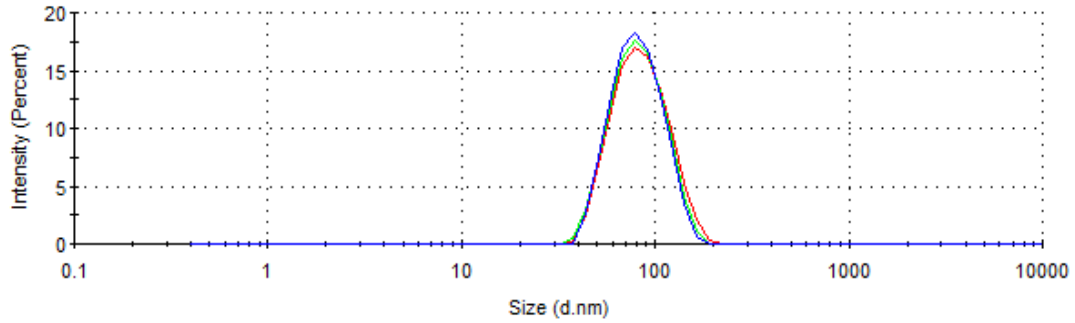

Figure 20. Upon PEGylation, the fully-functionalized TSP remained approximately the same size (86.99 ± 27.85 nm, PdI 0.093).

In addition, based on the work of Ruoslahti et al. [28] we identified a new targeting strategy (**Figure 21**). Rather than placing the linker inside the PEG coating, we used a peptide that targets the physical clot to deliver the particles to the injury site. Ruoslahti et al. used the peptide Cys-Arg-Glu-Lys-Ala (CREKA) to bind iron oxide nanoparticles to fibrin in tumors. Using the same strategy, we can attach TSPs to the forming clot at the wound site and safely deliver polyP to more quickly seal the wound with stronger clots. Having attached CREKA to iron oxide, produced a strong positive charge, which allows it to bind to fibrin (**Figure 22**).

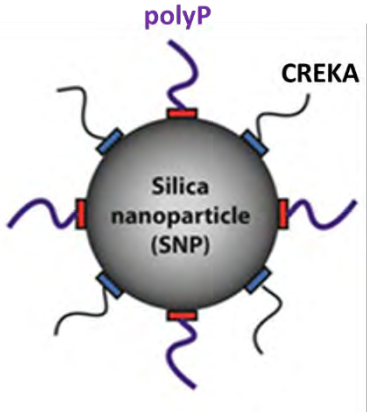

Figure 21. Scheme for targeting internal injuries. CREKA is attached to the surface of the nanoparticle and targets fibrin to attach the particle to the physical clot. Once attached, polyP accelerates clotting activity at the wound site.

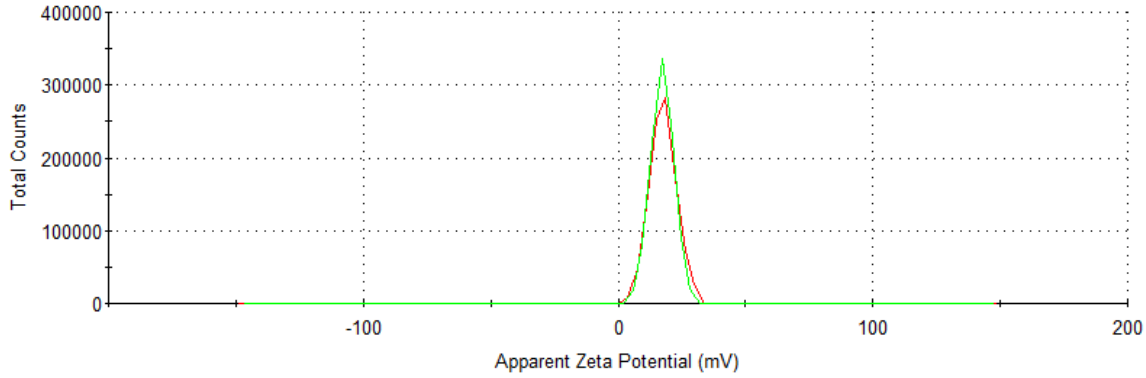

Figure 22. Zeta potential (17.6 ± 5.21 mV) of iron oxide particles functionalized with CREKA.

SUBTASK 3.d Quantify the procoagulant activities of the candidate TSPs created in task 3.c.

While most of the research has focused on the shorter chain polyP polymer because of its similarity to natural polyP, we also explored longer polyPs chains. The Morrissey lab developed large-scale preparations of size-fractionated polyPs, including ~700-mer polyP (P700). Although P700 was effective in reducing clot time, its mechanism of clot initiation through FXII was identical to silica and thus would have the same potential safety problems as injecting bare silica particles into the circulatory system.

In keeping with the goal of treating internal hemorrhage, we will focus on applying particles in concentrations well below the threshold level to prevent nonspecific clotting during general circulation. Spatially targeting the materials to the specific surfaces (i.e. wounded endothelial) or via other unique factors would then concentrate the material to above-threshold clotting behavior, though this is not

required for our near-future steps. Protecting the particles with PEG, which is cleaved off by factors present at the target site, would add an additional level of control.

In addition to testing the particles in the Stucky lab, 200-mg samples of SNP, polyP-SNP, and 700 polyP-SNP0 nanoparticles were sent to the Morrissey lab for polyP quantification and further coagulation tests. These tests revealed that polyP-SNP particles with a concentration of roughly 25 nmol PO_4 / mg SNP (quantified by hydrolysis) exhibited higher procoagulant activity than polyP-SNP particles with a higher nmol PO_4 / mg SNP concentration.

We also tested the coagulation threshold response using a thrombin-specific blue coumarin dye. Our experiments use the method established by the Ismagilov group in prior clotting threshold studies [29]. A small concentration of dye is added to the recalcified plasma. As clotting progresses and thrombin is produced, the thrombin cleaves the coumarin dye causing the solution to fluoresce. Signified by rapid fluorescence, the thrombin burst quickly leads to clot formation. A fluorescence microscope captures the qualitative change as shown in **Figure 23**.

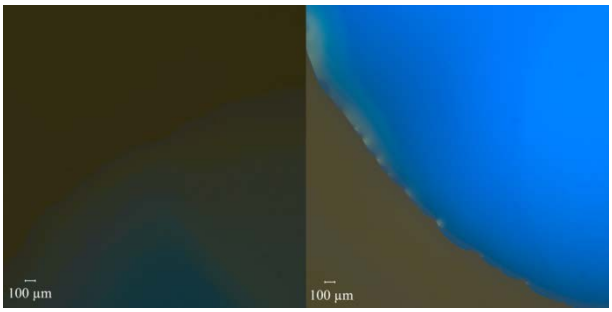

Figure 23. (Left) Blue coumarin dye experiment at time 0 min. (Right) Blue coumarin experiment at time 20 min.

Due to the microscope's limitations in quantifying thrombin expression, we instead monitored thrombin generation using a plate reader. By reading fluorescence every 10 seconds, we can clearly identify the thrombin burst. As clotting occurs near the rapid rise section of the thrombin burst, we can determine the clot time from the fluorescence data plot.

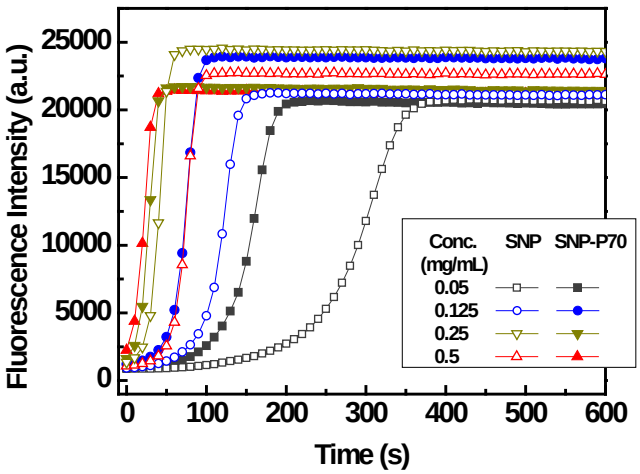

Figure 24. (Left) PolyP-SNP generates thrombin quicker than SNP.

After determining the procoagulant activity of polyP-SNP under normal conditions, we sought to apply the polyP-SNP TSPs under traumatic conditions. A traumatic injury can quickly develop into coagulopathy, the fundamental breakdown of the human coagulation cascade. Though coagulopathy

can exist either as a hypercoagulant or hypocoagulant form, we will define coagulopathy as the fundamental breakdown of the coagulation cascade that impairs clot formation. In the presence of trauma, the coagulopathic body becomes so weakened that anticoagulant pathways take over and a clot cannot form. Eventually, the patient succumbs to blood loss. Roughly 25% of trauma patients exhibit coagulopathy upon admission to hospitals [30].

Coagulopathy exists in three states known as the “lethal triad” -- dilution, hypothermia, and acidosis. Each damages the cascade in a specific way. In a coagulopathic state, all three states combine to inhibit clot formation. Left untreated, coagulopathic injuries often prove fatal. In our experiments we mimic dilution using a phosphate buffered solution (PBS). Incubating plasma below the usual 37^{o}C creates hypothermic conditions. Finally, we use a dilute phosphoric acid solution to acidify the plasma below a pH of 7.1. The experiments utilize a set concentration of lipidated tissue factor (LTF) – 0.5 ng/ml for TEG tests, 0.185 ng/ml for fluorescence dye tests – to ensure timely initiation of the coagulation cascade through the extrinsic pathway and the body’s main response to vessel injury. The polyP-SNP candidate TSP was tested at 0.25mg/ml without LTF to compare its ability to form clots.

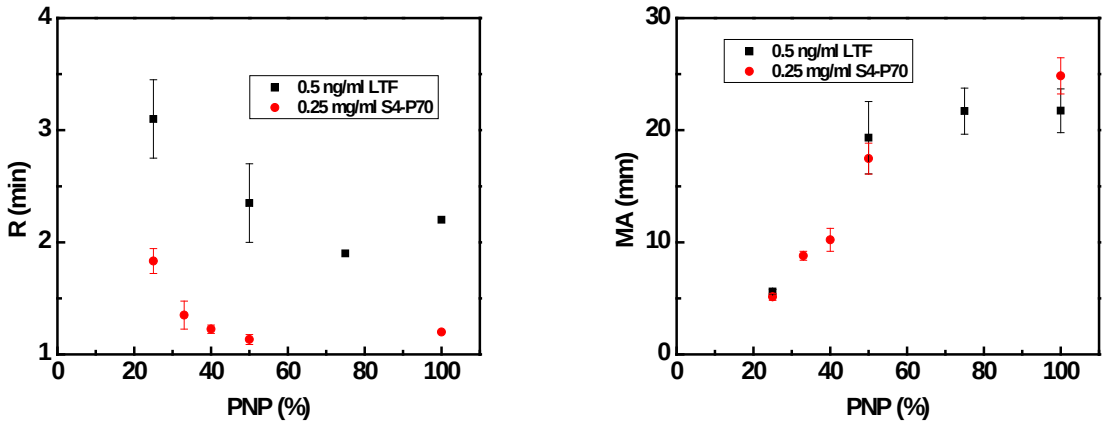

Figure 25. (Left) PolyP-SNP lowers clotting time in severely diluted samples. (Right) PolyP-SNP cannot increase clot size under severe dilution due to lack of fibrinogen.

As blood flows out of the body, the concentrations of proteins and factors in the blood flow out as well. Due to the loss of both procoagulant and anticoagulant factors, dilution only begins to significantly inhibit clotting at the ~50 % level. After reaching the 50 % threshold, the loss of procoagulant materials apparently is too much for the cascade to bear [31]. Using TEG and dye fluorescence, we established a dilution baseline. We then attempted to reverse the coagulopathic conditions using polyP-SNP at the threshold concentration of ~ 0.25mg/ml identified in our TEG experiments. PolyP-SNP successfully hastens thrombin burst and clot formation. However, polyP-SNP cannot improve the final clot size, which remains smaller than normal (**Figure 25**). The severe dilution of fibrinogen causes the small clot size. Without fibrinogen, the physical clot cannot form. In light of these data, we can consider delivering fibrinogen in addition to polyP-SNP to treat trauma patients suffering from massive bleeding and hemodilution.

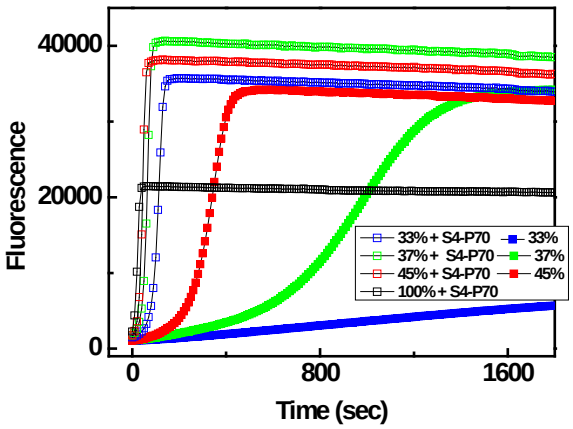

Figure 26. Adding polyP-SNP generates thrombin quickly even under severe plasma dilution (e.g., '33%' is 33% plasma and 67% dilutant).

Hypothermia, the second member of the lethal triad, occurs when the body temperature drops below 37° C. The drop in temperature leads to a decreased rate in the kinetics of many of the coagulation factors, especially formation of the tissue factor-FVIIa (TF-FVIIa) complex during the initiation phase of coagulation [32]. Unlike dilution where fibrinogen deficit triggers the drop in clotting, hypothermia slows coagulation but does not prevent it. The addition of polyP-SNP to hypothermic plasma results in improved coagulation across all TEG parameters. To highlight the excellence of polyP-SNP in clotting at sub-normal body temperature, we use the coagulation index formula to show robust procoagulant nature of the candidate TSP. Coagulation index (CI) combines all four TEG facets – R, K, alpha, and MA – into a single value; the more positive the CI, the stronger the procoagulant. While promising, our experiments on both the TEG and plate reader have showed some unexpected anomalies at 32°C and below (**Figure 27)**. We will continue to work on the hypothermic states in Y3 to ensure that the data are reliable.

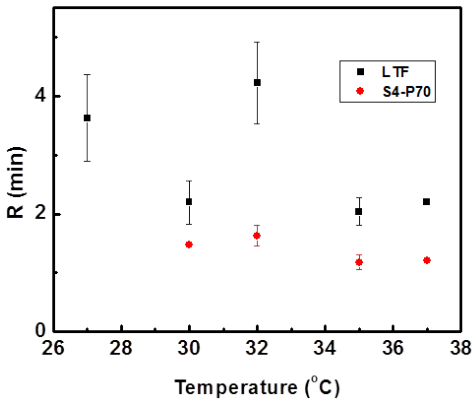

Figure 27. PolyP-SNP TSPs initiate clots quicker under hypothermia.

Of the triad, acidosis causes the greatest problem to trauma patients. Normal blood has a pH of 7.4, which drops as a result of trauma. While sodium bicarbonate can return the blood's pH to a normal level, effects from acidosis continue to plague coagulopathic patients for roughly 24 hours [33]. We will test the response of acidotic plasma to polyP-SNP in Y3. Our goal is to show polyP-SNP can correct deficiencies in clotting for all triad conditions, dilution, hypothermia, and acidosis.

In Y2, the research focus has shifted from designing and creating candidate TSPs to quantifying the procoagulant activities of TSPs. Our research has shown that polyP-SNP outperforms bare

SNP and LTF in lowering clot times while forming strong clots. As discovered by the Morrissey group, studies on FXII deficient plasma show that polyP-SNP initiates clotting through FXa coagulation pathway. Finally, polyP-SNP has been shown to decrease clot time and quicken thrombin generation under coagulopathic conditions often found in patients who have suffered a traumatic wound. In static conditions, polyP-SNP was excellent at promoting coagulation.

We showed that particles retain their clotting function even after months of storage at room temperature and pressure (**Figure 5** in **Publication 4**). The TSP is an improvement over polyP, which must be frozen to remain effective.

We tested the esterified SNP to determine their clotting activity in healthy and injured conditions. Particles suspended in water were considered healthy, while a phospholipid solution (PL) was used to mimic an in-progress clotting site. Ideally, the particles suspended purely in water would be within the recalcified range of 12-16 minutes, while the clot time would be lowered significantly in PL. In our initial tests, we found that the esterified particles in water clotted in approximately 9 min, while the clot time decreased to approximately 3 min in PL. This suggested that we have a potential TSP that minimally induces coagulation in healthy sites, while still accelerating coagulation at injury sites. We will continue to test the particles to increase the range between healthy (non-PL) and injured (PL) conditions to maximize safety.

The Stucky lab also conducted thrombin-generation assays using a pelleted version of polyP-SNP under static conditions (**Figures 28, 29**). These experiments showed a slightly lower clotting time compared to that of polyP-SNP in solution. The results favored nanoparticles in solution when run under static conditions. When attached to the well instead of in solution, the 100-μl sample of plasma had less surface area to activate on a pelleted polyP-SNP than polyP-SNP in solution. This was the reason for the slightly lengthened thrombin generation times. We are working to test the pelleted nanoparticles under flow to better estimate their clotting activity. Under flow, the clustering simulated by pelleting the polyP-SNP particles should reach the threshold faster than particles in solution, which may never aggregate in a sufficient concentration to achieve coagulation. Only under flow conditions can we closely mimic *in vivo* conditions.

After testing the pellet concentrations at above coagulation-threshold concentrations, we moved to sub-threshold concentrations. In the dye tests, we verified that sub-threshold concentrations of polyP-SNP in solution did not lead to increased thrombin production. Using pellets, thrombin generation times were elongated but not as long as the same conditions in solution. The plate reader measured the average thrombin generation over a 100-μl sample.

To better identify local clotting, we attempted to recreate previous Ismagilov experiments on a fluorescence microscope [34]. Using microscopy, we are able to identify local sources of thrombin generation within a plasma drop. At sub-threshold pellet concentrations, bright spots signify local sources of increased thrombin production and clot formation. Using the same analytical technique as the microfluidic experiments, we collected time-course images to generate thrombin curves. We found the threshold of polyP-SNP performance in solution to be close to 0.125mg/ml. We showed that clustered polyP-SNP at subthreshold (0.1mg/mL) concentrations outperformed 0.125mg/mL polyP-SNP solution.

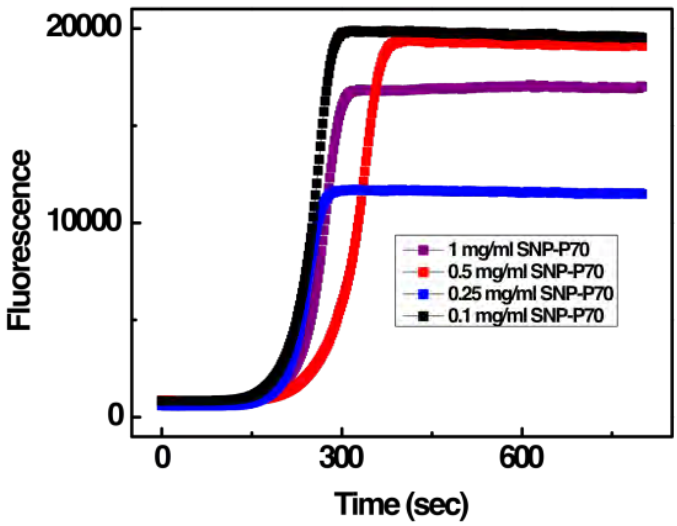

Figure 28. Clotting assay of pelleted polyP-SNP by microscopy. PolyP-SNP was patched onto a microscope slide via a 1 mm diameter by 250 µm height template prior to experiment.

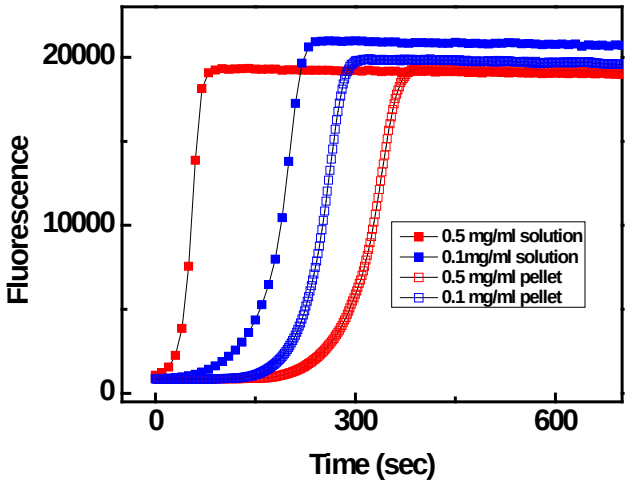

Figure 29. PolyP-SNP in solution generates thrombin faster than polyP-SNP pellets. The time difference decreases with decreasing concentration.

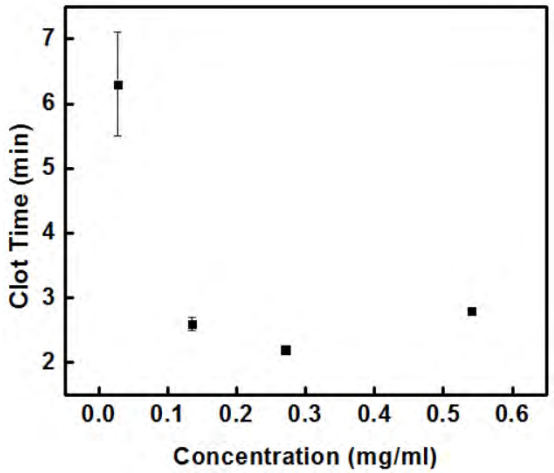

Figure 30. Clotting times of iron oxide particles functionalized with CREKA peptide. The ideal concentration is around 0.25 mg/ml

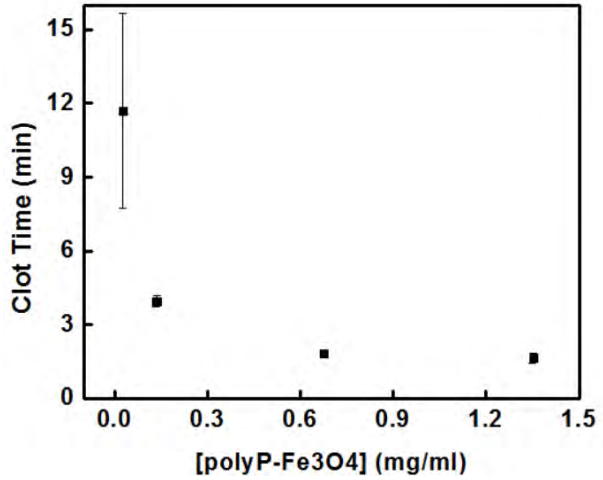

Figure 31. Clotting times of iron oxide particles functionalized with polyP peptide. The concentration required to minimize clotting is higher than iron oxide functionalized with CREKA.

Systematic data collection allowed for determining trends and conducting comparisons between the effectiveness of different functionalized types of inorganic nanoparticle carriers, such as silica and iron oxide; and to confirm that iron oxide core-silica nanoparticles exhibit the same clotting properties as silica nanoparticles (**Figures 30, 31**). We also considered size and charge of the nanoparticles as a function of blood-clotting ability in refining and determining the best nanoparticle system for TSPs. Clotting time decreased with an increase in concentration. The data are promising for use in determining the ideal concentration for this particular polyP-SNP nanoparticle system using ~50-nm SNPs. In determining the ideal TSP nanoparticle composition, we need to consider size and charge, as well as other properties unique to each formulation and type of inorganic nanoparticle.

Task 4 — Design and utilize microfluidic devices that reproduce shear flow and surface chemistries relevant to internal hemorrhage.

We used a microfluidic model of hemostasis to investigate whether the ability of localization to enhance clotting extends to short-chain polyP *in vitro* under flow. This microfluidic model enabled clotting of plasma, or lack thereof, to be monitored over many hours in the absence of tissue factor. The

experiments were designed to determine if localization of therapeutically-relevant concentrations of polyP could contribute to coagulation under flow.

To determine if surface immobilized polyP (SI-polyP) was able to accelerate clotting of flowing blood plasma, synthetic $polyP_{400}$ was immobilized onto the walls of microfluidic channels (**Figure 32**). Half of each chamber was patterned with biotinylated lipids followed by an excess of streptavidin. Biotinylated-$polyP_{400}$ was then flowed through the channel, becoming immobilized onto streptavidin. To test the ability of patterned polyP to induce clotting, platelet-poor human plasma was flowed through the chambers. The plasma clotted selectively on areas with immobilized $polyP_{400}$ (300 nmol/m^2) in 50-70 min at a shear rate of 1 s^{-1}. No clotting was observed over 5 hr in channels without $polyP_{400}$.

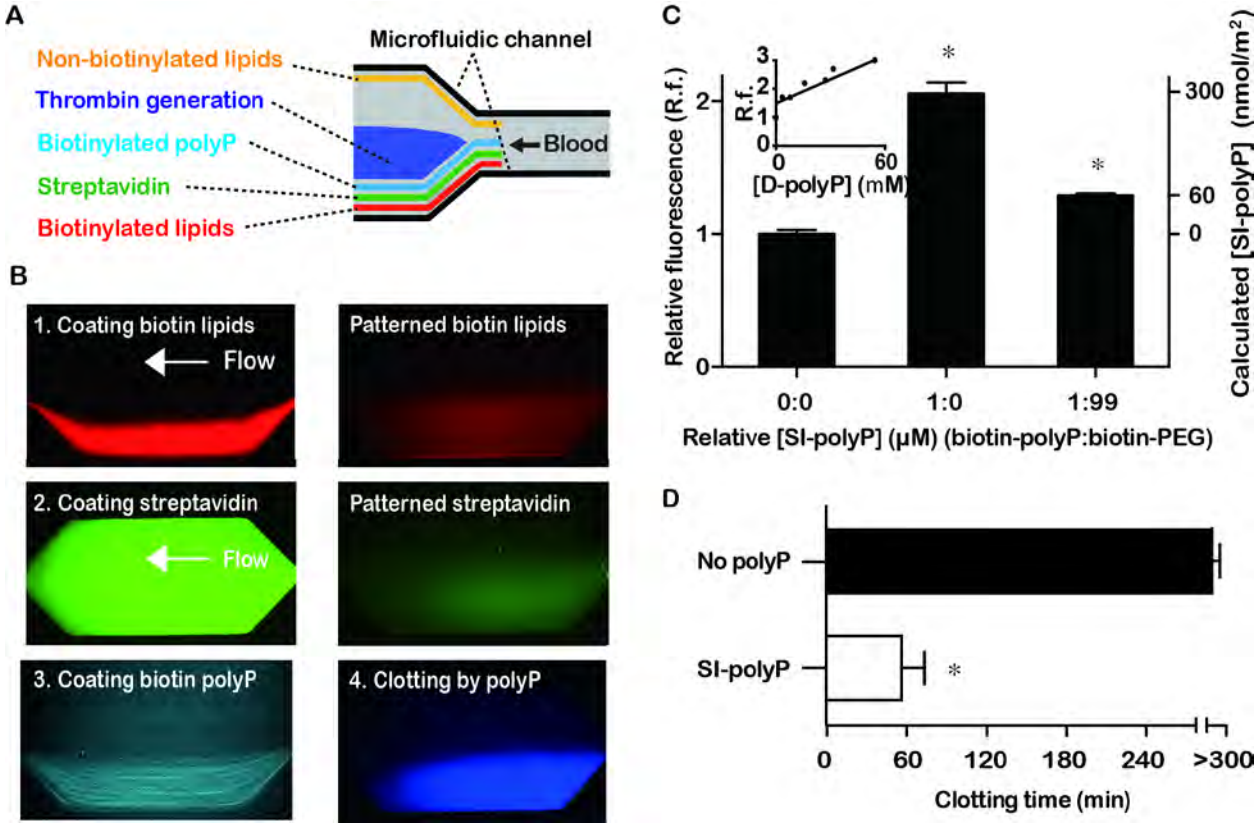

Figure 32. PolyP induces clotting of flowing blood plasma when localized on a surface. (A) Schematic of biotinylated synthetic polyP (cyan) patterned onto the surface of half of a microfluidic channel, which induces production of thrombin and clotting (blue) of flowing blood plasma (grey). (B) Images of fluorescent-labeled agents flowing and patterned along one side of a microfluidic channel. Biotinylated lipids (tagged red) self-assembled on the channel wall. Non-biotinylated lipids (not tagged in these images) were simultaneously flowed and patterned on the other side of the chamber using laminar flow patterning. Then, streptavidin (tagged green) was flowed through and bound to the biotinylated lipids, followed by flowing biotinylated polyP labeled with DAPI (cyan), which bound streptavidin. A substrate (blue) for thrombin was activated, indicating initiation of clotting, selectively on patterned $polyP_{400}$ (300 nmol/m^2). (C) Quantifying of the amount of SI-polyP by measuring the fluorescence of DAPI bound to it. Channels with SI-polyP were compared to channels without polyP and to channels treated with polyP diluted with biotinylated PEG. Inset is a standard curve of known concentrations of solubilized D-polyP, which was used to calculate the surface concentration of SI-polyP in coated channels. (D) The clotting times of normal human plasma flowing through channels coated with $polyP_{400}$ at a shear rate of 1 s^{-1}. *p = < 0.01 compared to controls without polyP. Data indicate mean ± SEM, n = 3.

A microfluidic system containing six regions with varying shear rates was used to measure clot times of flowing blood plasma (**Figure 33**). The range of shear rates was 1-110 s^{-1}, which occur in the inferior vena cava, venous valves, and large veins, and in wound pockets. To characterize and determine the range of clot times of flowing blood plasma in the microfluidic system, coagulation factor VIIa (FVIIa) was used, and added to plasma at a range of concentrations. In the device, plasma containing 16 µg/mL of FVIIa clotted in approximately 20-40 min, plasma containing 4 µg/mL of FVIIa clotted in approximately 60 min, and plasma containing 4 ng/mL did not clot within 6 hr.

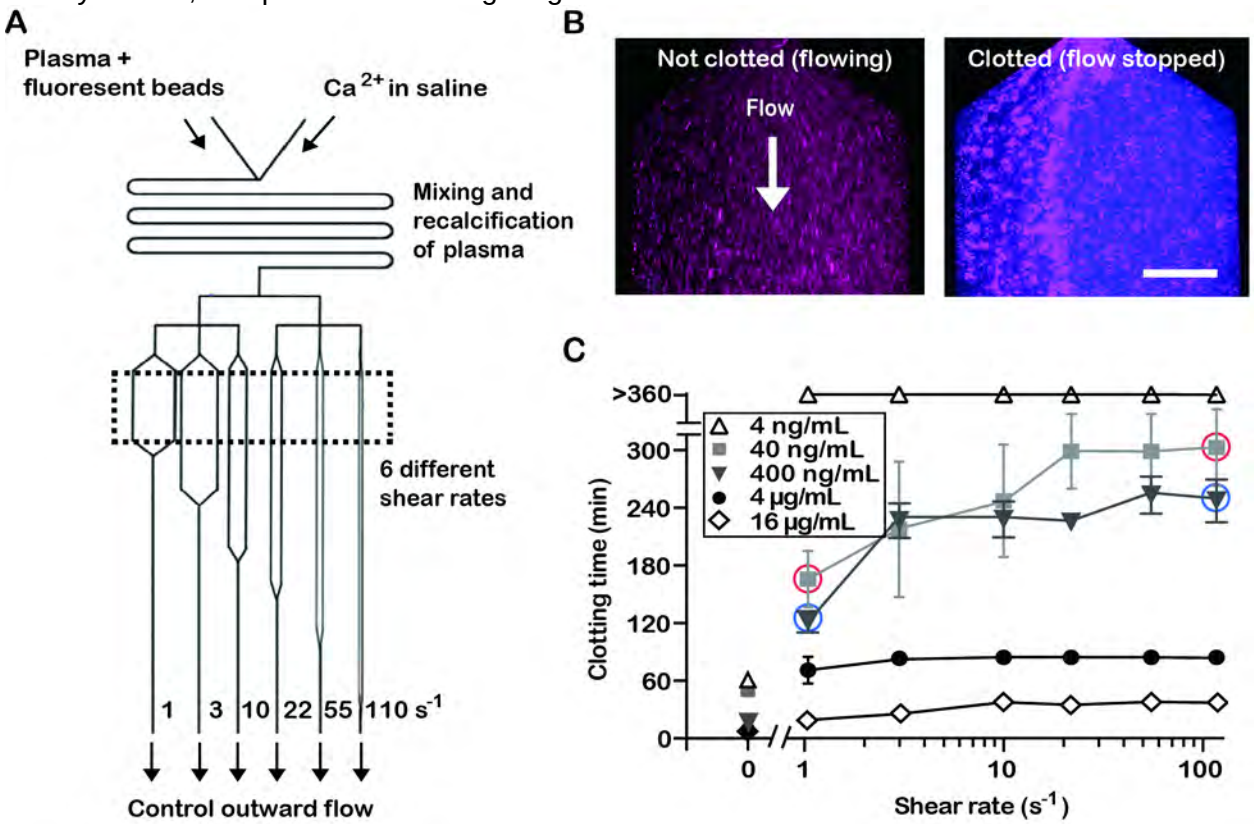

Figure 33. The microfluidic system used to measure clotting over a range of shear rates. (A) Schematic of the microfluidic system. Box (dashed lines) indicates the region where shear rates were varied and clot times were measured. (B) Fluorescence images showing that clotting was detected by the cessation of flow of tracer beads (pink) and by the cleavage of a substrate for thrombin (blue). Scale bar is 250 µm. (C) Assessing the range of clotting times in this flow system by adding various concentrations of FVIIa to the plasma. Data points indicate mean ± SEM, n = 3-4. Red circles indicate p = < 0.05 between the data points, and blue circles indicate p = < 0.01 between the data points.

We next examined if spatially localizing $polyP_{160}$ onto a surface (SI-$polyP_{160}$) would enhance its ability to contribute to clot formation compared to $polyP_{160}$ dispersed as nanoparticles (NP-$polyP_{160}$) or in solution (D-$polyP_{160}$) (**Figure 34**). With NP-$polyP_{160}$, clotting occurred in approximately 170 min and 200 min at a shear rate of 1 s^{-1} and 22 s^{-1} respectively. When a similar amount of $polyP_{160}$ was localized onto the channel surface, clotting occurred significantly faster than both NP-$polyP_{160}$ and D-$polyP_{160}$. Clotting with D-$polyP_{160}$ was 4- to 2.8-fold slower than SI-$polyP_{160}$ and 1.6- to 0-fold slower than NP-$polyP_{160}$ at all shear rates. Overall, clotting occurred fastest with SI-$polyP_{160}$ than dispersed $polyP_{160}$ in either soluble or NP forms, even with 6-43 fold less SI-$polyP_{160}$ in the channels.

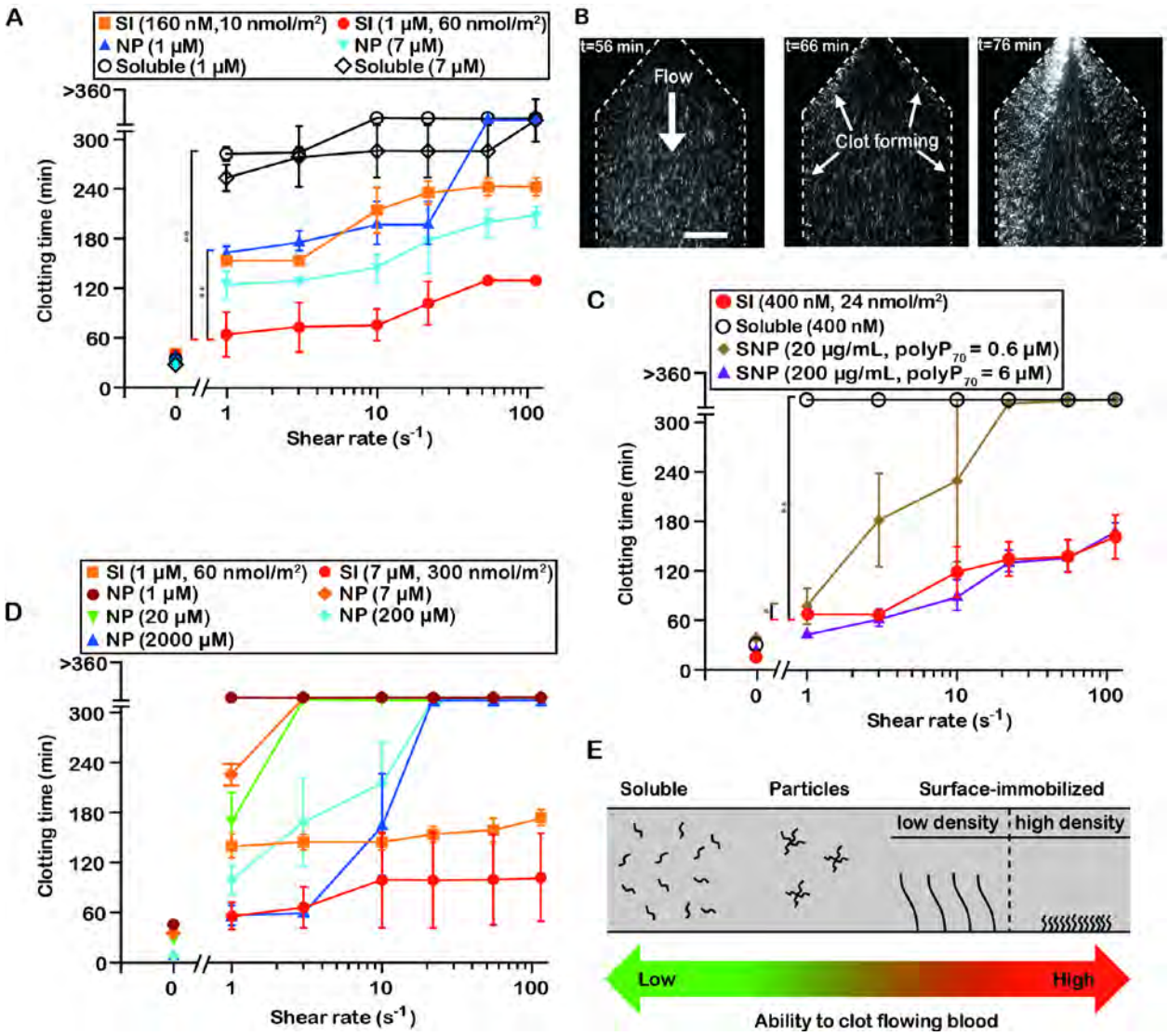

Figure 34. PolyP accelerates clotting best when spatially localized onto surfaces, compared to soluble polyP and nanoparticles of polyP. (A) Clotting times of plasma by $polyP_{160}$ at varying shear rates, comparing three states of $polyP_{160}$: solubilized, self-assembled nanoparticles, and surface-immobilized. (B) Time-lapse images showing SI-$polyP_{160}$ initiating clotting (detected by non-flowing beads) from the channel wall (dashed lines). Scale bar is 250 µm. (C) Comparing three states of polyP$_{70}$: solubilized, surface-immobilized onto the microfluidic channels, and immobilized onto silica nanoparticles. Clotting tendencies of plasma containing silica nanoparticles coated with $polyP_{70}$ (SNP-$polyP_{70}$) compared to soluble and surface-immobilized $polyP_{70}$ under shear in the microfluidic device. (D) Comparing two states of long-chain polyP: surface immobilized $polyP_{400}$ and nanoparticles of self-assembled $polyP_{>1000}$. (E) Schematic summarizing the relationship between spatial distribution of polyP and the acceleration of clotting in the above experiments. Data points indicate mean ± SEM, *p < 0.001, **p < 0.0001, *n* = 3-4. Statistical analysis represents comparisons between whole curves.

To test whether synthetic polyP similar in length to those found in human platelets can clot flowing blood at physiological concentrations, $polyP_{70}$ was tested. Soluble $polyP_{70}$ (D-$polyP_{70}$) at 400 nM did not accelerate clotting of flowing blood plasma at the shear rates tested. In contrast, an equivalent amount of SI-$polyP_{70}$ substantially accelerated clotting, to 70 min and 160 min at shear rates of 1 s^{-1} and 110 s^{-1} respectively.

To understand if the effect of surface localization extends to long-chain polyP, we tested a range of concentrations of long-chain polyP either surface localized (SI-polyP$_{400}$) or dispersed as nanoparticles (NP-polyP$_{>1000}$). PolyP$_{>1000}$ naturally self-assembles, localizing into nanoparticles of 150 ± 30 nm in diameter in solutions containing Ca^{2+} at low millimolar concentrations. It is a known activator of clotting under static conditions when dispersed throughout plasma. When plasma was flowed over SI-polyP$_{400}$, clotting occurred in approximately 60 min to 100 min. The clot times using NP-polyP$_{>1000}$ demonstrated robust shear- and concentration-dependence at 2000, 200, 20, 7 and 1 μM. NP-PolyP$_{>1000}$ was most potent at 2000 μM, initiating clotting at 60 min at 1 and 3 s^{-1}.

Together, these microfluidic results show that the spatial localization of synthetic polyP onto surfaces affects its ability to activate clotting under flow. It also shows that polyP is able to initiate coagulation under flow, particularly at low shear rates. Clotting occurs most rapidly at zero shear (no flow), and does not contribute to clotting at shear rate typical of arterial flow. This shear-dependence of polyP may enable polyP therapeutics to be safely delivered intravenously and only contribute to coagulation in wounds, where very low-flow shear regions exist along with natural triggers of coagulation, such as tissue factor.

Task 5 — In vivo tests of TSP activities in an animal model of incompressible hemorrhage.

During the final, no-cost extension, we had planned to test candidate TSPs in a mouse tail bleeding model. Loss of key, trained personnel in the final year of the project precluded our moving forward with the bleeding model. We therefore did not have a chance to initiate studies in experimental animals under this project and Task #5 remains unaddressed.

4. KEY RESEARCH ACCOMPLISHMENTS

Numerical simulations

- Numerical simulations were completed that reflect the activity of polyP on clotting.
- Simulations successfully predicted that the localization of polyP increases its coagulability, including when blood is flowing.

Raw materials for conjugation to nanoparticles:

- Synthesized and characterized silica and iron oxide nanoparticles as a carrier for polyP.
- Prepared and characterized a series of carefully size-fractionated polyP preparations of varying polymer lengths. Since polyP polymer length governs its procoagulant activity, these preparations are designed to help “tune” the procoagulant activity of candidate TSPs.

Coupling chemistries for conjugation of polyP to nanoparticles:

- We optimized the EDAC-mediate coupling chemistry for attaching not only primary amines (via phosphoramidate linkages) but also alcohol groups (via phosphoester linkages) covalently onto the terminal phosphates of polyP.
- We increased the scope of EDAC-mediated coupling chemistry by coupling a variety of peptides (each with different functional groups) onto the terminal phosphates. In addition, this allowed us to attach biotin, dyes and peptide epitopes covalently to the termini of polyP. We also coupled cystamine to the terminal phosphates of polyP to use sulfhydryl coupling chemistries for preparing nanoparticles.
- Applied both adsorbed and covalently bound polyP techniques to silica.
- For covalently bound polyP to silica, used APTMS or APTES to form the amide bond followed by EDAC cross-linker.

- An alternative to EDAC as a cross-linker for covalent binding of polyP to silica was through the use of NHS-OPSS.
- Esterification was used to couple polyP to silica and iron oxide particles.
- Iron oxide-polyP conjugates were prepared using Lewis acid chemistry.
- PolyP was conjugated to biotin, and this enabled polyP to be patterned on microfluidic devices.

Microfluidics:

- Devices were used to measure clot times simultaneously at various shear rates.
- Found that polyP with chain-lengths similar to platelet polyP can initiate clotting when surface-localized far more efficiently than when present in bulk solution.
- Found that particles of polyP initiate clotting faster than solubilized macromers of polyP under flow.

PolyP-based procoagulant nanoparticles:

- Reported that size-controlled nanoprecipitation of polyP in aqueous solutions containing biologically relevant concentrations of divalent metal cations (e.g. Ca^{2+}, Mg^{2+}, Zn^{2+} etc.)
- Reported Artificial Dense Granules as a drug delivery system (DDS) for treating incompressible hemorrhage
- Reported that particles of polyP initiate clotting faster than solubilized macromers of polyP.
- Found that polyP nanoparticles initiate clotting in a shear-dependent manner, where they clot plasma at the low shear rates typical of blood that is pooling in wound pockets.

5. CONCLUSION

We completed a series of studies that involved synthesizing, characterizing, and understanding the properties of iron oxide, silica, and iron oxide core-silica shell nanoparticles with respect to the blood clotting process, and to leverage their properties in developing an effective TSP upon conjugation with polyP. Using systematic methods of synthesis and characterization of SNP functionalized with linkers, such as APTES followed by EDAC, to covalently bind polyP, we enhance our understanding of the chemistry involved in developing procoagulant agents. Chemical and morphological characterization methods were expanded to include scanning and transmission electron microscopy; elemental analysis; dynamic and electrophoretic light scattering; and Raman, Fourier transform infrared, x-ray photoelectron, energy dispersive x-ray spectroscopy. In vitro studies of nanoparticle-polyP conjugate systems to determine blood clotting time as a function of simulated environmental conditions and nanoparticle-polyP composition continue to be conducted using properties such as thromboelastography, fibrin aggregometry, and thrombin production.

We successfully created “Artificial Dense Granules” via the size-controlled synthesis of monodisperse polyP NPs at physiological concentrations of calcium and magnesium, reported in **Publication 6**. We found that the solubility is related nonlinearly to the polymer length, with very long-chain polyP precipitating much more facilely than platelet-sized polyP.

Of all the formulations tested, attaching polyP directly to SNP scaffolds (see Publication 4) proved to be most effective in accelerating clotting. PolyP-SNPs were also effective in a variety of abnormal blood samples that attempted to mimic in vivo conditions. Our polyP-functionalized NPs can serve as a foundation for the future development of targeted procoagulant nanotechnologies to control internal hemorrhage.

6. PUBLICATIONS, ABSTRACTS, AND PRESENTATIONS (from project inception to date)

A. Publications resulting from this work (a copy of each is included in appendix):

1. Lay press – none

2. Peer-reviewed scientific journals

PUBLICATION 1: Li Y, Sawvel AM, Jun Y-S, Nownes S, Ni M, Kudela D, Stucky GD, and Zink D. Cytotoxicity and potency of mesocellular foam-26 in comparison to layered clays used as hemostatic agents. *Toxicol. Res.* 2013, 2:136-144. DOI: 10.1039/C2TX20065A

PUBLICATION 2: Hebbard CF, Wang Y, Baker CJ, and Morrissey JH. Synthesis and evaluation of chromogenic and fluorogenic substrates for high-throughput detection of enzymes that hydrolyze inorganic polyphosphate. *Biomacromolecules*. 2014, 15(8):3190-3196. DOI: 10.1021/bm500872g

PUBLICATION 3: Donovan AJ, Kalkowski J, Smith SA, Morrissey JH, and Liu Y. Size-controlled synthesis of granular polyphosphate nanoparticles at physiologic salt concentrations for blood clotting. *Biomacromolecules*. 2014, 15(11): 3976-3984. DOI: 10.1021/bm501046t

PUBLICATION 4: Kudela D, Smith SA, May-Masnou A, Braun GB, Pallaoro A, Nguyen CK, Chuong TT, Nownes S, Allen R, Parker NR, Rashidi HH, Morrissey JH, and Stucky GD. Clotting activity of polyphosphate functionalized silica nanoparticles. *Angew. Chem. Int. Ed. Engl.* 2015, 54(13):4018-4022. DOI: 10.1002/anie.201409639

PUBLICATION 5: Szymusiak M, Donovan AJ, Smith SA, Ransom R, Shen H, Kalkowski J, Morrissey JH, Liu Y. Colloidal confinement of polyphosphate on gold nanoparticles robustly activates the contact pathway of blood coagulation. *Bioconjug. Chem.* 2016, 27(1): 102-109. DOI: 10.1021/acs.bioconjchem.5b00524

PUBLICATION 6: Donovan AJ, Kalkowski J, Szymusiak M, Wang C, Smith SA, Klie RF, Morrissey JH, and Liu Y. Artificial Dense Granules: A procoagulant liposomal formulation modeled after platelet polyphosphate storage pools. *Biomacromolecules*. 2016, 17(8): 2572-2581. DOI: 10.1021/acs.biomac.6b00577

3. Invited articles – none

4. Abstracts – none

B. Presentations made during the funding period (international, national, local societies, military meetings, etc.)

Stucky GD, “Molecular assembly of material systems with integrated nanoscale to macroscale functionalities,” The 2nd International Symposium on Advanced Composite Materials, Tokyo, Japan, November 7-8, 2011.

Stucky GD, “Zeolites and R. M. Barrer Inspired Control of Bioprocesses: The Challenge of Hemostasis,” The Pennsylvania State University Barrer Lecture, University Park, PA, April 14, 2011.
Stucky GD, “Controlling Bioprocesses with Inorganic Nanostructured Systems: The Challenge of Hemostasis,” University of California, Berkeley Student-Hosted Inorganic Chemistry Series, Berkeley, CA, February 25, 2011.

Morrissey, JH. “Modulation of Hemostasis, Thrombosis, and Inflammation by PolyP “Special Symposium on the Basic Science of Hemostasis and Thrombosis, Annual Meeting of the American Society of Hematology, Atlanta, GA, December 11, 2012.

Stucky GD. "Hemostatic agents," Force Health Protection Future Naval Capability Science and Technology Program Review, Arlington VA, 2013.

Stucky GD. "Learning about the blood coagulation system from the outside and inside with simple, low-cost inorganic materials," Plenary Lecture, Symposium on Materials for Tomorrow, Göteborg, Sweden, 2013.

A.J. Donovan, J. Kalkowski, S.A. Smith, J.H. Morrissey, and Y. Liu. “Size-controlled synthesis of granular polyphosphate nanoparticles at physiologic salt concentrations for blood clotting.” 15th Annual Midwest Platelet Conference, 8-10th October 2014.

Damien Kudela, Stephanie A. Smith, Ju Hun Yeon, Anna May-Masnou, Gary B. Braun, Alessia Pallaoro, Tracy Chuong, James R. Baylis, Christian J. Kastrup, James H. Morrissey and Galen D. Stucky. "Treating non-compressible hemorrhage with functionalized nanoparticles," Military Health System Research Symposium (MHSRS), Orlando, Florida, 2014.

James Morrissey. “Polyphosphates and the Initiation of Coagulation via the Intrinsic Pathway,” Thrombosis and Hemostasis Summit of North America (THSNA); Chicago, IL; April 10, 2014.

James Morrissey. “New Roles for Polyphosphate in Blood Clotting, Thrombosis and Inflammation,” University of Georgia, Athens, GA; September 30, 2014.

Damien Kudela, Stephanie A. Smith, Ju Hun Yeon, Anna May-Masnou, Gary B. Braun, Alessia Pallaoro, Tracy Chuong, James R. Baylis, Christian J. Kastrup, James H. Morrissey and Galen D. Stucky. "Treating non-compressible hemorrhage with functionalized nanoparticles," Nanotech, Washington, D.C., 2014.

A.J. Donovan, J. Kalkowski, S.A. Smith, J.H. Morrissey, and Y. Liu. “Size-controlled synthesis of granular polyphosphate nanoparticles at physiologic salt concentrations for blood clotting.” 15th Annual Midwest Platelet Conference, 8-10th October 2014.

Damien Kudela, Stephanie A. Smith, Ju Hun Yeon, Anna May-Masnou, Gary B. Braun, Alessia Pallaoro, Tracy Chuong, James R. Baylis, Christian J. Kastrup, James H. Morrissey and Galen D. Stucky. "Treating non-compressible hemorrhage with functionalized nanoparticles," Military Health System Research Symposium (MHSRS), Orlando, Florida, 2014.

Damien Kudela, Stephanie A. Smith, Ju Hun Yeon, Anna May-Masnou, Gary B. Braun, Alessia Pallaoro, Tracy Chuong, James R. Baylis, Christian J. Kastrup, James H. Morrissey and Galen D. Stucky. "Treating non-compressible hemorrhage with functionalized nanoparticles," Nanotech, Washington, D.C., 2014.

James Morrissey. “Novel Concepts for Coagulation Activation,” 20th Congress of the European Hematology Association; Vienna, Austria; June 13 & 14, 2015.

Magdalena Szymusiak, Alexander Donovan, Stephanie A. Smith, Ross Ransom, Hao Shen, Joseph, Kalkowski, James H. Morrissey, and Ying Liu, “Comparison between colloidally-confined and molecularly-dissolved polyphosphates for activating the contact pathway of blood coagulation.” 10th World Biomaterials Congress, May 17-22, 2016, Montréal, Canada.

Alexander Donovan, Joseph, Kalkowski, Magdalena Szymusiak, Stephanie A. Smith, Robert F. Klie, James H. Morrissey, and Ying Liu. “Artificial dense granules, a potential, biomimetic procoagulant agent composed of inorganic polyphosphate, initiates autoactivation of factor XII.” 10th World Biomaterials Congress, May 17-22, 2016, Montréal, Canada.

Catherine J. Baker and James H. Morrissey. “Diversification of polyphosphate end-labeling via bridging molecules for development of novel hemostatic agents.” 10th World Biomaterials Congress, May 17-22, 2016, Montréal, Canada.

Stucky GD. "Learning about the blood coagulation system from the outside and inside with simple, low-cost inorganic materials," Symposium on Mesoporous and Nanostructured Hybrid Materials, American Chemical Society National Meeting, San Francisco, 2014.

Stucky GD. "Learning about the blood coagulation system from the outside and inside with simple, low-cost inorganic materials," UCSB Center for Bioengineering Faculty Seminar, 2016.

Chi K. Nguyen, Kyle Ploense, Damien Kudela, James H. Morrissey, Tod Kippin, Galen D. Stucky. "Hemorrhage control using biocompatible polyphosphate bound silica nanoparticles." 251st American Chemical Society National Meeting, San Diego, CA; March 13-17, 2016.

D. Kudela, K. Ploense, C. Nguyen, S.A. Smith, J. H. Morrissey, S. Hammond, G. D. Stucky. “Accelerating coagulation in traumatic injuries using inorganic polyphosphate-coated silica nanoparticles.” 10th World Biomaterials Congress, Montréal, Canada; May 21, 2016.

7. INVENTIONS, PATENTS AND LICENSES

Issued United States Patents:

Damien Kudela, Galen D. Stucky, Anna May-Masnou, Gary B. Braun, James H. Morrissey, and Stephanie A. Smith. "Polyphosphate-Functionalized Inorganic Nanoparticles as Hemostatic Compositions and Methods of Use." U. S. Patent number 9,186,417 (issued November 17, 2015).

Patent (including PCT) Applications:

Y. Liu and A.J. Donovan. “Artificial Platelets for Treatment of Catastrophic Bleeding.” PCT/US2015/051814 (WO2016049250), filed 24 September 2015.

Continuation application: “Polyphosphate-Functionalized Inorganic Nanoparticles as Hemostatic Compositions and Methods of Use.” Kudela, Damien; Stucky, Galen D.; May-Masnou, Anna; Braun, Gary B.; Morrissey, James H.; and Smith, Stephanie A. 20160213809 A1 14/883224. Filed October 14, 2015; published July 28, 2016.

8. REPORTABLE OUTCOMES

Cayuga Biotech is a startup company spun out of the Stucky laboratory at UCSB. Damien Kudela (PhD 2015, UCSB) founded Cayuga, which is based on his doctoral research supported primarily from this grant. Cayuga seeks to translate the polyP-functionalized nanoparticles -- developed and patented as a result of this research grant – into clinical use for both military and civilian trauma injuries by reaching patients whose needs are unmet by current treatment protocols. Cayuga collaborates with both the Stucky (UCSB) and Morrissey (UIUC) labs in addition to clinical collaborations with UCSF, UC Davis, and Travis AFB. Cayuga has been awarded a DARPA research contract to study

the effects of polyP-SNPs using a highly lethal swine liver injury model. In addition, Cayuga seeks to use this therapeutic in patients who are prone to bleeding due to underlying abnormal clotting functionalities.

9. OTHER ACHIEVEMENTS

Manuscript submitted to a peer-reviewed scientific journal:

- Yeon JH, Mazinani N, Schlappi T, Donovan A, Smith S, Baylis JR, Chan KYT, Kudela D, Stucky G, Ismagilov RF, Liu Y, Morrissey JH, Kastrup CJ. Localization of Short-Chain Polyphosphate Enhances its Ability to Clot Flowing Blood Plasma. *Scientific Reports*. Submitted 2016-09. (SA)

Degrees awarded:

- Sharon Choi (Ph.D. Summer 2014, University of Illinois at Urbana-Champaign
- Damien Kudela (Ph.D. Summer 2015, University of California Santa-Barbara)
- Chi K. Nguyen (Ph.D. Spring 2016, University of California Santa-Barbara)

Subsequent funding:

- Damien Kudela (PI, Cayuga Biotech). “Accelerating coagulation in traumatic injuries using inorganic polyphosphate-coated silica nanoparticles.” Defense Advanced Research Projects Agency. HR0011-16-C-0067. Contract awarded April 12, 2016

Employment opportunities:

- Damien Kudela, PhD, founded Cayuga Biotech, Inc. to translate this technology to clinical and commercial use and serves as the company’s CEO.

10. REFERENCES (literature cited)

[1] S.A. Smith, N.J. Mutch, D. Baskar, P. Rohloff, R. Docampo, J.H. Morrissey, Polyphosphate modulates blood coagulation and fibrinolysis, Proc. Natl. Acad. Sci. U. S. A. 103(4) (2006) 903-8.

[2] J.H. Morrissey, S.H. Choi, S.A. Smith, Polyphosphate: an ancient molecule that links platelets, coagulation, and inflammation, Blood 119(25) (2012) 5972-5979.

[3] F. Muller, N.J. Mutch, W.A. Schenk, S.A. Smith, L. Esterl, H.M. Spronk, S. Schmidbauer, W.A. Gahl, J.H. Morrissey, T. Renne, Platelet Polyphosphates Are Proinflammatory and Procoagulant Mediators In Vivo, Cell 139(6) (2009) 1143-1156.

[4] A.J. Shoffstall, K.T. Atkins, R.E. Groynom, M.E. Varley, L.M. Everhart, M.M. Lashof-Sullivan, B. Martyn-Dow, R.S. Butler, J.S. Ustin, E.B. Lavik, Intravenous hemostatic nanoparticles increase survival following blunt trauma injury, Biomacromolecules 13(11) (2012) 3850-7.

[5] F. Shen, R.R. Pompano, C.J. Kastrup, R.F. Ismagilov, Confinement regulates complex biochemical networks: initiation of blood clotting by "diffusion acting", Biophysical journal 97(8) (2009) 2137-45.

[6] S.H. Choi, S.A. Smith, J.H. Morrissey, Polyphosphate is a cofactor for the activation of factor XI by thrombin, Blood 118(26) (2011) 6963-6970.

[7] M.S. Chatterjee, W.S. Denney, H. Jing, S.L. Diamond, Systems biology of coagulation initiation: kinetics of thrombin generation in resting and activated human blood, PLoS computational biology 6(9) (2010).

[8] S.A. Smith, N.J. Mutch, D. Baskar, P. Rohloff, R. Docampo, J.H. Morrissey, Polyphosphate modulates blood coagulation and fibrinolysis, Proceedings of the National Academy of Sciences of the United States of America 103(4) (2006) 903-8.

[9] F. Müller, N.J. Mutch, W.A. Schenk, S.A. Smith, L. Esterl, H.M. Spronk, S. Schmidbauer, W.A. Gahl, J.H. Morrissey, T. Renné, Platelet polyphosphates are proinflammatory and procoagulant mediators in vivo, Cell 139(6) (2009) 1143-56.

[10] S.A. Smith, S.H. Choi, R. Davis-Harrison, J. Huyck, J. Boettcher, C.M. Rienstra, J.H. Morrissey, Polyphosphate exerts differential effects on blood clotting, depending on polymer size, Blood 116(20) (2010) 4353-9.

[11] S. Choi, S. SA, M. JH, Polyphosphate is a cofactor for the activation of factor XI by thrombin, Blood 118(26) (2011) 6963-6970.

[12] R. Engel, C.M. Brain, J. Paget, A.S. Lionikiene, N.J. Mutch, Single-chain factor XII exhibits activity when complexed to polyphosphate, Journal of thrombosis and haemostasis : JTH 12(9) (2014) 1513-22.

[13] T.J. Nevalainen, M.M. Haapamaki, J.M. Gronroos, Roles of secretory phospholipases A(2) in inflammatory diseases and trauma, Biochimica et biophysica acta 1488(1-2) (2000) 83-90.

[14] K. Jorgensen, J. Davidsen, O.G. Mouritsen, Biophysical mechanisms of phospholipase A2 activation and their use in liposome-based drug delivery, FEBS letters 531(1) (2002) 23-7.

[15] R. Flaumenhaft, Molecular basis of platelet granule secretion, Arterioscl Throm Vas 23(7) (2003) 1152-1160.

[16] L.F. Brass, C.C. Shaller, E.J. Belmonte, Inositol 1,4,5-Triphosphate-Induced Granule Secretion in Platelets - Evidence That the Activation of Phospholipase-C Mediated by Platelet Thromboxane Receptors Involves a Guanine-Nucleotide Binding Protein-Dependent Mechanism Distinct from That of Thrombin, J Clin Invest 79(4) (1987) 1269-1275.

[17] M.J. Gray, W.Y. Wholey, N.O. Wagner, C.M. Cremers, A. Mueller-Schickert, N.T. Hock, A.G. Krieger, E.M. Smith, R.A. Bender, J.C.A. Bardwell, U. Jakob, Polyphosphate Is a Primordial Chaperone, Mol Cell 53(5) (2014) 689-699.

[18] S.H. Choi, J.N. Collins, S.A. Smith, R.L. Davis-Harrison, C.M. Rienstra, J.H. Morrissey, Phosphoramidate end labeling of inorganic polyphosphates: facile manipulation of polyphosphate for investigating and modulating its biological activities, Biochemistry 49(45) (2010) 9935-41.

[19] R. Docampo, W. de Souza, K. Miranda, P. Rohloff, S.N. Moreno, Acidocalcisomes - conserved from bacteria to man, Nature reviews. Microbiology 3(3) (2005) 251-61.

[20] F.A. Ruiz, C.R. Lea, E. Oldfield, R. Docampo, Human platelet dense granules contain polyphosphate and are similar to acidocalcisomes of bacteria and unicellular eukaryotes, J. Biol. Chem. 279(43) (2004) 44250-44257.

[21] F.A. Ruiz, C.R. Lea, E. Oldfield, R. Docampo, Human platelet dense granules contain polyphosphate and are similar to acidocalcisomes of bacteria and unicellular eukaryotes, The Journal of biological chemistry 279(43) (2004) 44250-7.

[22] C.H. Wang, Q. Qiao, T. Shokuhfar, R.F. Klie, High-Resolution Electron Microscopy and Spectroscopy of Ferritin in Biocompatible Graphene Liquid Cells and Graphene Sandwiches, Adv Mater 26(21) (2014) 3410-3414.

[23] W. Stöber, A. Fink, E. Bohn, Controlled growth of monodisperse silica spheres in the micron size range, J. Colloid Interface Sci. 26(1) (1968) 62-69.

[24] J. Margolis, The effect of colloidal silica on blood coagulation, Aust. J. Exp. Biol. Med. Sci. 39 (1961) 249-58.

[25] F. Gao, P. Botella, A. Corma, J. Blesa, L. Dong, Monodispersed mesoporous silica nanoparticles with very large pores for enhanced adsorption and release of DNA, J. Phys. Chem. B 113(6) (2009) 1796-804.

[26] S.E. Baker, A.M. Sawvel, J. Fan, Q. Shi, N. Strandwitz, G.D. Stucky, Blood clot initiation by mesocellular foams: dependence on nanopore size and enzyme immobilization, Langmuir : the ACS journal of surfaces and colloids 24(24) (2008) 14254-60.

[27] V. Cauda, A. Schlossbauer, T. Bein, Bio-degradation study of colloidal mesoporous silica nanoparticles: Effect of surface functionalization with organo-silanes and poly(ethylene glycol), Microporous Mesoporous Mater. 132(1–2) (2010) 60-71.

[28] G. von Maltzahn, J.H. Park, K.Y. Lin, N. Singh, C. Schwoppe, R. Mesters, W.E. Berdel, E. Ruoslahti, M.J. Sailor, S.N. Bhatia, Nanoparticles that communicate in vivo to amplify tumour targeting, Nat. Mater. 10(7) (2011) 545-52.

[29] C.J. Kastrup, F. Shen, M.K. Runyon, R.F. Ismagilov, Characterization of the threshold response of initiation of blood clotting to stimulus patch size, Biophys. J. 93(8) (2007) 2969-77.

[30] P.I. Johansson, J. Stensballe, Hemostatic resuscitation for massive bleeding: the paradigm of plasma and platelets--a review of the current literature, Transfusion 50(3) (2010) 701-10.

[31] B.S. Bull, K.L. Hay, P.C. Herrmann, Postoperative bypass bleeding: a bypass-associated dilutional (BAD) coagulopathy?, Blood Cells. Mol. Dis. 43(3) (2009) 256-9.

[32] A.J. Ramaker, P. Meyer, J. van der Meer, M.M. Struys, T. Lisman, W. van Oeveren, H.G. Hendriks, Effects of acidosis, alkalosis, hyperthermia and hypothermia on haemostasis: results of point-of-care testing with the thromboelastography analyser, Blood Coagul. Fibrinolysis 20(6) (2009) 436-9.

[33] W.Z. Martini, Coagulopathy by hypothermia and acidosis: mechanisms of thrombin generation and fibrinogen availability, J. Trauma 67(1) (2009) 202-8; discussion 208-9.

[34] C.J. Kastrup, J.Q. Boedicker, A.P. Pomerantsev, M. Moayeri, Y. Bian, R.R. Pompano, T.R. Kline, P. Sylvestre, F. Shen, S.H. Leppla, W.J. Tang, R.F. Ismagilov, Spatial localization of bacteria controls coagulation of human blood by 'quorum acting', Nat. Chem. Biol. 4(12) (2008) 742-50.

11. APPENDIX

PDF "reprints" of the following 6 papers resulting from this project are attached as an appendix:

PUBLICATION 1: Li Y, Sawvel AM, Jun Y-S, Nownes S, Ni M, Kudela D, Stucky GD, and Zink D. Cytotoxicity and potency of mesocellular foam-26 in comparison to layered clays used as hemostatic agents. *Toxicol. Res.* 2013, 2:136-144. DOI: 10.1039/C2TX20065A

PUBLICATION 2: Hebbard CF, Wang Y, Baker CJ, and Morrissey JH. Synthesis and evaluation of chromogenic and fluorogenic substrates for high-throughput detection of enzymes that hydrolyze inorganic polyphosphate. *Biomacromolecules*. 2014, 15(8):3190-3196. DOI: 10.1021/bm500872g

PUBLICATION 3: Donovan AJ, Kalkowski J, Smith SA, Morrissey JH, and Liu Y. Size-controlled synthesis of granular polyphosphate nanoparticles at physiologic salt concentrations for blood clotting. *Biomacromolecules*. 2014, 15(11): 3976-3984. DOI: 10.1021/bm501046t

PUBLICATION 4: Kudela D, Smith SA, May-Masnou A, Braun GB, Pallaoro A, Nguyen CK, Chuong TT, Nownes S, Allen R, Parker NR, Rashidi HH, Morrissey JH, and Stucky GD. Clotting activity of polyphosphate functionalized silica nanoparticles. *Angew. Chem. Int. Ed. Engl.* 2015, 54(13):4018-4022. DOI: 10.1002/anie.201409639

PUBLICATION 5: Szymusiak M, Donovan AJ, Smith SA, Ransom R, Shen H, Kalkowski J, Morrissey JH, Liu Y. Colloidal confinement of polyphosphate on gold nanoparticles robustly activates the contact pathway of blood coagulation. *Bioconjug. Chem.* 2016, 27(1): 102-109. DOI: 10.1021/acs.bioconjchem.5b00524

PUBLICATION 6: Donovan AJ, Kalkowski J, Szymusiak M, Wang C, Smith SA, Klie RF, Morrissey JH, and Liu Y. Artificial Dense Granules: A procoagulant liposomal formulation modeled after platelet polyphosphate storage pools. *Biomacromolecules*. 2016, 17(8): 2572-2581. DOI: 10.1021/acs.biomac.6b00577

Publication 1

Toxicology Research

RSC Publishing

PAPER

View Article Online
View Journal | View Issue

Cite this: *Toxicol. Res.*, 2013, **2**, 136

Cytotoxicity and potency of mesocellular foam-26 in comparison to layered clays used as hemostatic agents†

Yao Li,[a] April M. Sawvel,‡[b] Young-Si Jun,[b] Sara Nownes,[b] Ming Ni,[a] Damien Kudela,[b] Galen D. Stucky*[b] and Daniele Zink*[a]

Received 27th August 2012,
Accepted 15th November 2012

DOI: 10.1039/c2tx20065a

www.rsc.org/toxicology

Uncontrolled hemorrhage is a leading cause of potentially preventable death. The most effective commercial hemostatic products employ layered clays. Due to safety concerns only a product containing kaolin is currently recommended by the U. S. Department of Defense. A problem related to layered clays, including kaolin, is their cytotoxicity. Also, material left in the wound can lead to thrombosis and other adverse effects. Recently, it has been shown that pure silica mesocellular foams (MCF) with cell window sizes >20 nm are effective in promoting blood clotting. Here, we tested the potency and cytotoxicity of layered clays in comparison to MCF with a cell window size of 26 nm (MCF-26) *in vitro*. The results showed that the potencies of MCF-26 and layered clays in promoting clotting were comparable. Effects on cell viability were assessed with relevant primary human cell types. The cytotoxic effects of all compounds were cell type-specific and most sensitive were endothelial cells. The IC50 values of MCF-26 were in the mg ml^{-1} range and its cytotoxicity was ~1–2 orders of magnitude lower than the cytotoxicity of layered clays. Further, MCF-26 did not adhere strongly to cell surfaces and was not taken up by cells as observed for the layered clays. This suggests that it would be easier to remove MCF-26 from wounds. Altogether, the results suggest that MCF-26 would be effective and safer than currently used hemostatic agents.

Introduction

Uncontrolled hemorrhage is the leading cause of potentially preventable death in combat casualties[1,2] and is the second leading cause of death in civilian trauma.[3,4] Several enhanced hemostatic dressings have been developed to prevent fatal exsanguinations. The active compounds of these dressings are mainly based on chitosan, zeolite, purified procoagulant factors or layered clays, such as smectite clays or kaolin.[5] They act as blood factor concentrators, mucoadhesive agents, procoagulent supplementors, or by initiating the intrinsic clotting cascade.

Since 2004, two products, namely HemCon and QuikClot, have been deployed by United States and United Kingdom Armed Forces and clinical data supported their efficacy.[5,6] HemCon consists of deacetylated chitosan acetate salt on a sterile foam backing pad and QuikClot is a granular preparation of zeolite. Due to the exothermic reaction between zeolite and water QuikClot can cause severe burns.[6,7] Based on these observations modified versions of the product have been developed that reduce wound temperature.[8]

It was found that HemCon and QuikClot were outperformed by WoundStat (WS, smectite granules), Celox (granular chitosan compounds) and QuikClot CombatGauze (CG, kaolin-coated surgical gauze) in animal models of lethal hemorrhage.[5,9,10] As a result, the US Army replaced HemCon dressing with CG and WS in 2008. However, in 2009 the US Army permanently suspended the use of WS due to safety concerns over embolization and tissue inflammation (http://www.stripes.com/news/army-halts-use-of-woundstat-1.90678). CG currently remains the number one recommended agent by the U. S. Department of Defense for treating uncontrolled hemorrhage in the battlefield.

Both, CG and WS obtained clearance by the U. S. Food and Drug Administration (FDA) in 2007. However, one study using a swine model published in 2010 revealed that WS use was associated with substantial local inflammatory response, endothelial and neuronal degeneration and myocyte necrosis.[11]

[a]*Institute of Bioengineering and Nanotechnology, 31 Biopolis Way, The Nanos, Singapore 138669, Singapore. E-mail: dzink@ibn.a-star.edu.sg*
[b]*Department of Chemistry and Biochemistry and Materials Department, University of California, Santa Barbara, California 93106, USA. E-mail: stucky@chem.ucsb.edu*
†Electronic supplementary information (ESI) available. See DOI: 10.1039/c2tx20065a
‡Currently at the Molecular Foundry, Lawrence Berkeley National Laboratory, Berkeley, California 94720.

Another study published in the same year demonstrated that WS led to formation of occlusive thrombi in the injured blood vessels.[12] Furthermore, it was observed that WS caused endothelial injury and damage of the vessels that could interfere with surgical repair. It was also found that the non-biodegradable particles could not be completely removed from the wounds and could enter systemic circulation, causing distal thrombosis in vital organs.[12] The study concluded that more relevant *in vitro* and *in vivo* tests should be performed for clearance of new hemostatic agents. In this regard it was outlined that according to the manufacturer, the cytotoxicity of WS was tested with fibroblast cell cultures and other standard tests, as recommended by the International Organization for Standardization (ISO) guidelines. It was pointed out that these standard tests might not be sufficient and did not include exposure to endothelial cells, which are a relevant cell type in this setting.

The view that it would be important to perform *in vitro* tests with endothelial cells and other relevant cell types is supported by studies that demonstrated profound cytotoxic effects of WS and/or layered clays on primary human umbilical vein endothelial cells (HUVEC), primary murine neurons and RAW267.4 murine macrophage-like cells.[13–15] However, different human and animal cell lines, such as HeLa cells or murine neuroblastoma cells, remained largely unaffected by these agents,[13–15] suggesting that cytotoxic effects were cell type-specific.

In addition to cytotoxicity other major safety-relevant problems associated with WS, such as local and distal thrombosis, were due to the fact that WS was difficult to remove from the wounds. In one case, residual kaolin powder was also detected in a vessel specimen treated with CG.[12]

These results suggest that safer and less cytotoxic hemostatic agents are needed. Improved materials should be at least as effective as layered clays, but have decreased cytotoxicity. Silica materials provide a negative surface that promotes coagulation *via* contact activation, or the intrinsic pathway. A promising strategy to develop more effective agents is to increase the surface area accessible to contact activation proteins. Mesocellular foams (MCF) are mesoporous silica materials, with a large surface area and open framework structure. The silica framework structure is made up of cages connected by windows, both of which are monodispersed in size. Both the cages and cage window sizes can be tuned over a relatively large size range. It has been suggested that the nanoporous cage windows play a critical role in providing contact activation proteins access to the inner cell surfaces, and it has been demonstrated that a MCF with a cell window size >20 nm is highly effective in accelerating blood clotting.[16] 2 mg of MCF-33 (cage window size of 33 nm) accelerated clot formation similarly to 20 mg of QuikClot.[16]

Here, we examined the potency of MCF-26 (cell window size of 26 nm) in promoting clot formation *in vitro*. Cytotoxicity, adhesion to the cell surface and cellular uptake were investigated with different relevant primary human cell types and two standard cell lines. The results obtained with MCF-26 are compared to data obtained with layered clays.

Materials and methods

Materials

Kaolin, bentonite, montmorillonite and dimethyl sulfoxide (DMSO) were purchased from Sigma-Aldrich (St. Louis, MO, USA). 10 nm silver nanoparticels (Ag NP) were purchased from Meliorum Technologies (Rochester, NY, USA).

Synthesis of MCF-26

MCF-26 was synthesized by dissolving 1.1 g of Pluronic P123 surfactant (poly(ethylene glycol)-*block*-poly(propylene glycol)-*block*-poly(ethylene glycol) (BASF, Ludwigshafen, Germany) into a solution of 2.5 ml concentrated HCl (Sigma-Aldrich) and 16.25 ml of 18.2 mΩ water. After stirring at room temperature for two hours or until the surfactant dissolved, 1.447 ml mesitylene (Sigma-Aldrich) was added and the solution was heated at 40 °C for 2 hours under vigorous stirring. Next, 2.3 ml tetraethyl orthosilicate (TEOS, Sigma-Aldrich) was added and the solution was stirred for an additional 5 minutes. The solution was then transferred to a Teflon-lined autoclave device and baked in an oven at 40 °C for 20 hours. After removal from the oven, the device cooled to room temperature overnight. 11.5 mg NH_4F (Sigma-Aldrich) was dissolved in 0.1 ml 18.2 mΩ water and added to the solution. The autoclave device was again sealed and placed in an oven at 140 °C for 24 hours. The resulting solution was filtered and the filtrate was washed with water and with ethanol. Calcination at 550 °C for six hours removed any impurities from the resulting white solid.

Characterization of MCF-26

The surface area, pore volume, and window size of MCF-26 were determined using a Micromeritics Tristar 3000 Porosimeter (Chemical Instruments AB, Sollentuna, Sverige). Prior to measurement, the samples were dried under 220 °C nitrogen gas overnight. Brunauer–Emmett–Teller (BET) analysis was used to calculate the surface area. Pore size and window size were derived from the adsorption and desorption isotherms using the Broekhoff–de Boer method.

Scanning electron microscopy (SEM)

SEM used to identify particle size and morphology was performed either with an XL30 Sirion FEG microscope (FEI, Hillsboro, OR, USA) or with an JSM-7400 field emission scanning electron microscope (Jeol, Tokyo, Japan) after coating with gold.

Dynamic light scattering (DLS)

DLS was performed with a ZetaPLAS particle size analyzer (Brookhaven Instruments, Holtsville, NY, USA).

Surface area and pore size determination

A Tristar 3000 (Micromeritics Instrument Corporation, Norcross, GA, USA) was used for nitrogen gas sorption analysis of clay and MCF-26 surface areas. Before the surface area measurement these compounds were dried at 220 °C for 12 hours under nitrogen. Data presented for surface areas were

calculated using the BET analysis, and pore sizes and external surface area were calculated using the BJH (Barrett–Joyner–Halenda) analysis.

Thrombelastography

All samples were pre-weighed into 1 dram glass vials prior to use and MCF-26 was used after calcination at 550 °C. A thrombelastograph (Haemoscope Corporation, Niles, Illinois, USA) was used to determine the clotting properties of all materials investigated. This instrument provides quantitative data regarding time until clot initiation (R), rate of clot formation (Alpha) and strength of the clot formed (MA) by measuring the torsion of a small sample of blood around a wire during coagulation. First, 20 μl of 0.2 M $CaCl_2$ were added to a plastic cup heated to 37.0 °C. Next, 340 μl of pooled human plasma (PHP) was added to the cup, followed immediately by addition of the clotting agent from a 1 dram glass vial. Finally, the sample cup was quickly loaded into position for commencement of the measurement.

PHP was purchased in 1 ml aliquots from George King Biomedical (Overland Park, KS, USA) and stored at −80 °C. Samples were warmed to 37 °C for 20 minutes immediately prior to use. All plasma samples were used or discarded within one hour of heating to 37 °C. Experiments involving PHP were approved by and carried out in accordance with the guidelines put forth by the Human Subjects Committee at the University of California, Santa Barbara, USA.

Cell culture

Different batches of primary human umbilical vein endothelial cells (HUVEC) and primary adult human epidermal keratinocytes (HEK) were purchased from ScienCell Research Laboratories (Carlsbad, CA, USA). Different batches of primary adult human dermal fibroblasts (HDF) were purchased from ScienCell Research Laboratories, the American Type Culture Collection (ATCC, Manassas, VA, USA), and Promocell (Heidelberg, Germany). Human primary renal proximal tubular cells (HPTC), HK-2 cells and NIH/3T3 cells were obtained from ATCC. The different cell types were cultivated in the media recommended by the vendors as described.[17–20]

Cell viability assays

The neutral red uptake (NRU) assay was performed as described[21] and as recommended by the International Standard for the Biological Evaluation of Medical Devices (Part 5: Tests for *In Vitro* Cytotoxicity, ISO 10993-5:2009 (E)), with the following modifications: different cell types were used and cells were seeded at a density of 50 000 cells cm^{-2} into 96-well microplates. Cells were cultivated for 24 h and were then treated overnight with the test materials. Before the NRU assay was performed the cells were washed with phosphate-buffered saline (PBS). Data acquisition and analysis was performed as described.[17] The NRU assay was used for the generation of all data on cell viability shown in the main manuscript. Some data that were generated by using assays employing 5-(3-carboxymethoxyphenyl)-2-(4-sulfophenyl)-2*H*-tetrazolium (MTS) or measuring lactate dehydrogenase (LDH) leakage are provided in the ESI† and details on these assays are described in the ESI.†

Adhesion of test materials to the cell surface

HUVEC were seeded on glass coverslips (Menzel-Gläser, Braunschweig, Germany) and were cultivated for 24 h. 1 mg ml^{-1} of test material was added for 10 minutes. Subsequently, all samples were rinsed in similar ways with 3 × 10 ml PBS and the samples were fixed with 3.7% formaldehyde/PBS. Imaging was performed with the CytoViva™ high resolution imaging system (CytoViva, Auburn, AL, USA), which is suitable for the imaging of nanoparticles and other types of particles.

Cellular uptake of test materials

HUVEC and HDF were seeded on cover slips and were cultivated for 24 h before treatment with the test materials was performed overnight. After treatment cells were washed with PBS, fixed and imaged with the CytoViva™ system.

Zeta potential measurements

Measurements of the zeta potentials of layered clays and MCF-26 were performed with 10 μg ml^{-1} of the materials suspended in PBS or complete endothelial cell culture medium (ScienCell Research Laboratories, Carlsbad, CA, USA; supplemented with 5% fetal bovine serum). Zeta potentials were measured with a Zen 3690 Zetasizer Nano ZS90 (Malvern Instruments, Malvern, Worcestershire, UK).

Measurement of reactive oxygen species (ROS)

Intracellular ROS generation was detected using 5-(and-6) chloromethyl-2′,7′-dichlorodihydrofluorescein diacetate, acetyl ester (CM-H_2DCFDA) (Invitrogen, Carlsbad, CA, USA). Assays were performed after cells had been treated for 24 h with kaolin or MCF-26 at concentrations of up to 250 μg ml^{-1}. Cells were incubated with 10 μM CM-H_2DCFDA for 60 min followed by incubation in PBS for 15 min. Fluorescence at an emission wavelength of 528 nm was measured using a Tecan Safire$^{2™}$ microplate reader (Männedorf, Switzerland).

Statistical analysis

Microsoft Office Excel 2003 was used for all calculations and statistics (unpaired *t*-test).

Results and discussion

Sizes and shapes of the particles in the samples of MCF-26, kaolin, bentonite and montmorillonite were determined by using SEM and DLS. MCF-26 consisted of smooth spheres with a narrow size distribution in the range of ~2000 nm (Fig. 1). The layered clays consisted of irregularly shaped particles, which showed broader size distributions. In case of bentonite and montmorillonite the sizes of most particles were in the range of ~1000 nm. Kaolin particles were smaller and the majority displayed sizes in the range of ~500 nm.

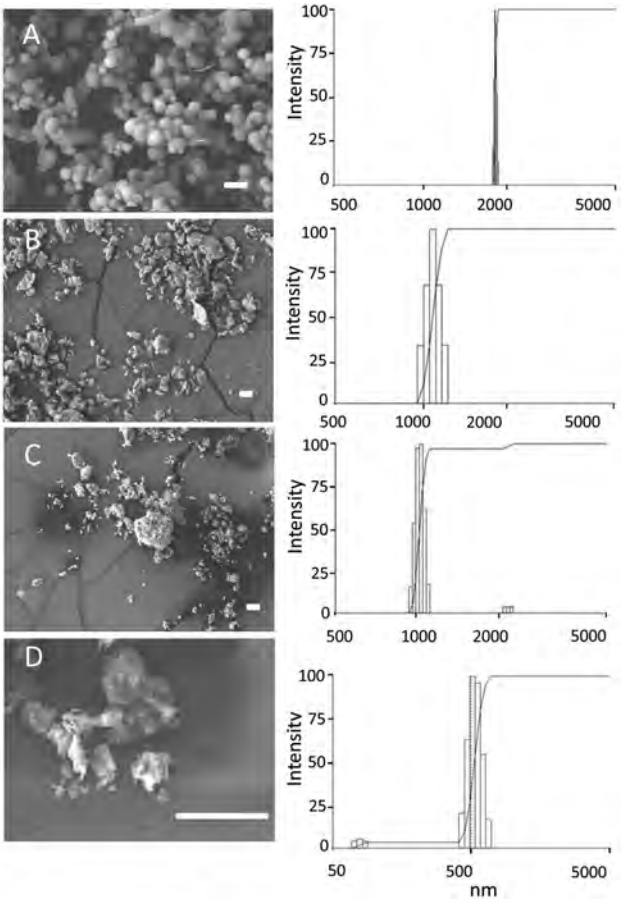

Fig. 1 Particle shapes and sizes. MCF-26 (A), bentonite (B), montmorillonite (C) and kaolin (D) were imaged by SEM (left-hand panels). Scale bars: 10 μm. Particle sizes were determined by DLS (right-hand panels).

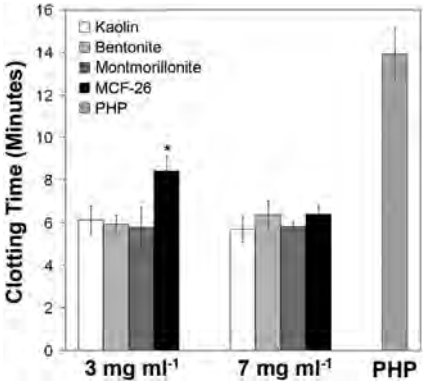

Fig. 2 Clotting times in the presence of different hemostatic agents. The clotting times of pure PHP without hemostatic agents (right-hand grey bar) or of PHP exposed to the indicated concentrations of hemostatic agents were determined. The bars show the mean ± standard deviation (s.d., $n = 4$). Significant differences ($p < 0.05$) between MCF-26 and layered clays are indicated by an asterisk.

In addition, surface areas and pore sizes were determined by BET and BJH analysis. MCF-26 had the largest total and external surface areas and the values were 364 $m^2\ g^{-1}$ (total surface area) and 278 $m^2\ g^{-1}$ (external surface area), respectively. The pore volume was 2.3 $cm^3\ g^{-1}$ and the average pore diameter was 26.4 nm. The external surface area of montmorillonite was 51 $m^2\ g^{-1}$, and the internal surface area of the layered structure contributed substantially to the total surface area, which was 174 $m^2\ g^{-1}$. The spacing of the layered structures was smaller in case of bentonite and kaolin, which resulted in smaller differences between the total surface area (20 $m^2\ g^{-1}$ for both compounds) and the external surface area (16 $m^2\ g^{-1}$ for both compounds). These results also showed that bentonite and kaolin had the smallest surface areas from the 4 compounds investigated.

The potency of MCF-26, kaolin, bentonite and montmorillonite in promoting clot formation was investigated by measuring the time to clot formation in pooled human plasma (PHP). Bentonite and montmorillonite are smectite clays with hemostatic effects. All of the materials investigated here led to decreased clotting times compared to PHP alone (Fig. 2). This is consistent with previous reports on accelerated clot formation by layered clays and MCFs.[16,22] There were no significant differences between the times to clot formation when the effects of layered clays were compared at a given concentration (Fig. 2). At the lowest concentration examined (3 mg ml^{-1}) the time to clot formation was slightly but significantly increased with MCF-26 in comparison to the layered clays. At 7 mg ml^{-1} no significant differences were observed with respect to all of the materials tested.

Next, we examined the effects of kaolin on the viability of different cell types *in vitro*. We examined HUVEC as well as primary human HEK and HDF to investigate the effects on primary human endothelial and skin cells. Three different batches of each cell type were included to address for inter-donor variability. For comparison we examined immortalized NIH/3T3 mouse fibroblasts, which represent a widely used standard cell line. We also assessed the effects on cells from a vital internal organ by including human primary (HPTC) and immortalized (HK-2) renal proximal tubular cells. These cell types are well-characterized and widely applied in *in vitro* nephrotoxicology.

In order to address effects on cell viability and cell damage we compared the results of the NRU, MTS and LDH assays. LDH leakage was not observed when different cell types were treated with increasing concentrations of up to 7 mg ml^{-1} of bentonite, montmorillonite and MCF-26 (Fig. S1†). This suggested that membrane damage did not play a major role in the cytotoxic effects of these compounds and that the LDH assay was not useful for this study.

Results obtained with the MTS assay (Fig. S2†) and the NRU assay were similar. However, the NRU assay is more reliable as it is not influenced by cell density,[17] which compromised the results of the MTS assay (Fig. S3†). Therefore, all experiments shown in the results section below were performed with the NRU assay. This assay is also recommended by the International Standard ISO 10993–5:2009(E).

When cells were treated with kaolin and other layered clays we observed that these compounds strongly adhered to the cell

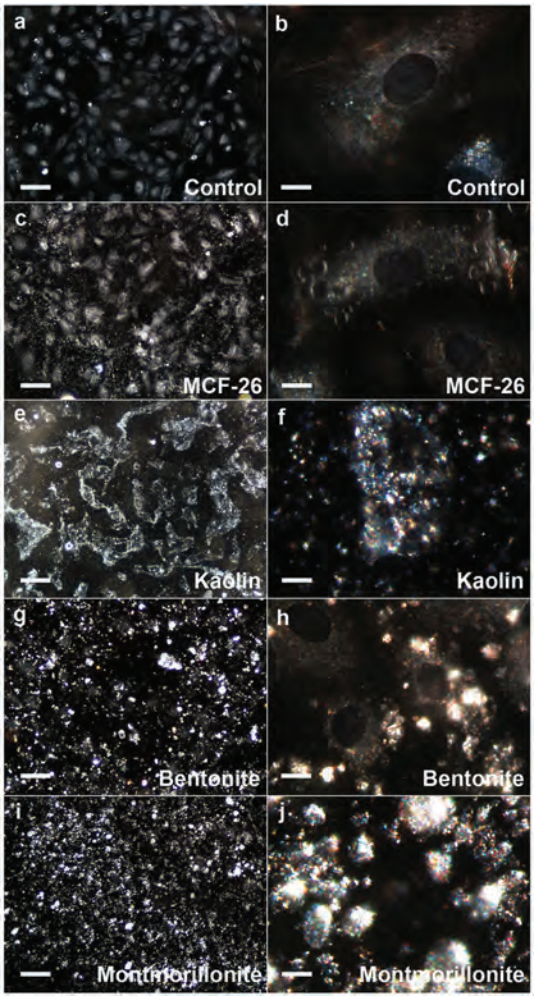

Fig. 3 Adhesion of layered clays and MCF-26 to the cell surface. HUVEC were exposed for 10 minutes to 1 mg ml^{-1} of kaolin, bentonite, montmorillonite or MCF-26 (control: untreated). Subsequently, cells were washed. Images were captured with the CytoViva system after fixation and particles appear white on the images. The left-hand images show fields of cells (scale bars: 100 μm), whereas the right-hand images show individual cells (scale bars: 10 μm).

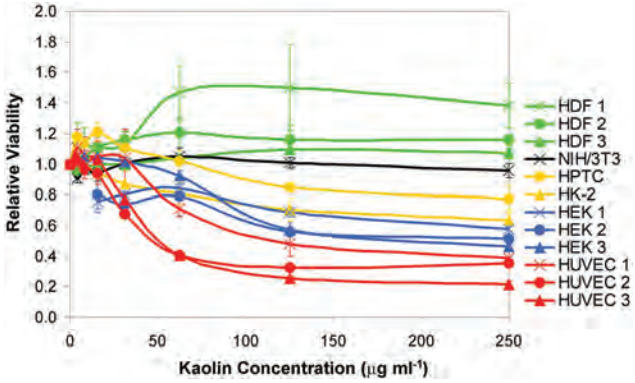

Fig. 4 Dose-dependent effects of kaolin on cell viability. Kaolin was applied at concentrations of up to 250 μg ml^{-1} to the cell types indicated on the right-hand side. Three different batches of HDF, HEK and HUVEC were tested. Cell viability was determined with the NRU assay and all values were normalized to the values obtained with untreated control cells. Error bars show the s.d. (n = 3).

and substrate surface and could not be washed away completely (Fig. 3). Tests with kaolin applied in cell culture medium to cell-free multi-well plates revealed that kaolin interfered with the absorbance measurements of multi-well plate-based assays (data not shown). Therefore, kaolin could not be tested at concentrations >250 μg ml^{-1}. Any potential artifacts due to residual kaolin in the NRU assays would lead to an overestimation of cell viability, as kaolin increased the values measured in the NRU assay.

Kaolin was applied at different concentrations to the cells in order to determine its effects on cell viability and Fig. 4 displays the dose-response curves. Table 1 (left-hand column) provides the IC50 values as well as the percentages of cell viability at the highest concentration tested (250 μg ml^{-1}). The results showed that the effects of kaolin were strongly cell type-specific. The numbers of NIH/3T3 fibroblasts were not significantly decreased by kaolin (P > 0.05) and the numbers of two batches of human skin fibroblasts (HDF1 and HDF2) were even increased (P < 0.05; Fig. 4 and Table 1). In contrast, a dose-dependent decrease of cell viability was observed in all other cases. HUVEC were most sensitive and the IC50 values of the three HUVEC batches ranged between ~50 μg ml^{-1} and ~125 μg ml^{-1}. Substantial cell death was also observed in case of HEK and here the IC50 values ranged between ~180 μg ml^{-1} and ~250 μg ml^{-1} (Table 1, the cell viability of two HEK batches was slightly above 50% at 250 μg ml^{-1}). Primary and immortalized human renal cells were only moderately affected and their IC50 values were clearly >250 μg ml^{-1}.

Overall, the results demonstrated cell type-specific cytotoxicity of kaolin and the sensitivity of the cell types used here could be ranked in the following order HUVEC > HEK > HK-2/HPTC > NIH/3T3 > HDF. Of note, the fibroblastic cell types (either immortalized murine or primary human) did not display any significantly reduced cell viability, even at the highest concentration of kaolin. It is also worth mentioning that, although some interdonor variability was observed, cell viability was mainly influenced by cell type-specific effects.

In the following we tested the cytotoxicity of bentonite and montmorillonite. These compounds interfered less strongly with the NRU assay than kaolin and were tested at higher concentrations of up to 1000 μg ml^{-1}. The same cell types were used as before and the results of the NRU assays are displayed in Fig. 5 (black and grey graphs) and Table 1.

The results revealed that all layered clays tested had substantial cytotoxic effects. As observed with kaolin, HUVEC were also most sensitive to the effects of bentonite and montmorillonite and the IC50 values ranged from ~11 μg ml to ~17 μg ml^{-1} (bentonite) and from ~33 μg ml^{-1} to ~95 μg ml^{-1} (montmorillonite). The effects of bentonite and montmorillonite on the different cell types were somewhat variable. However, all cell types and batches displayed IC50 values clearly below 1000 μg ml^{-1} with at least one of the two compounds, with exception of HK-2 cells and HEK batch 1.

Table 1 IC50 values and cell viability (%) at the maximal concentrations of kaolin, bentonite, montmorillonite and MCF-26. The maximal concentration of kaolin was 250 μg ml^{-1}, whereas the maximal concentration of the other compounds tested was 1000 μg ml^{-1}. The table provides the mean values ± s.d. (n = 3)

	Kaolin		Bentonite		Montmorillonite		MCF-26	
Cell type	IC50 (μg ml^{-1})	% at 250 μg ml^{-1}	IC50 (μg ml^{-1})	% at 1000 μg ml^{-1}	IC50 (μg ml^{-1})	% at 1000 μg ml^{-1}	IC50 (μg ml^{-1})	% at 1000 μg ml^{-1}
HUVEC 1	125 ± 47	39 ± 5	11 ± 1	18 ± 1	65 ± 3	18 ± 0	>1000	75 ± 2
HUVEC 2	48 ± 4	35 ± 2	17 ± 2	37 ± 3	33 ± 2	25 ± 3	>1000	73 ± 12
HUVEC 3	51 ± 2	21 ± 2	17 ± 4	34 ± 2	95 ± 13	33 ± 4	>1000	65 ± 3
HDF 1	>250	138 ± 14	300 ± 85	45 ± 3	272 ± 99	29 ± 1	>1000	66 ± 13
HDF 2	>250	119 ± 8	>1000	60 ± 3	335 ± 32	38 ± 5	>1000	130 ± 4
HDF 3	>250	107 ± 3	468 ± 18	52 ± 4	454 ± 120	57 ± 1	>1000	122 ± 3
HEK 1	>250	58 ± 2	>1000	60 ± 6	>1000	78 ± 6	>1000	100 ± 3
HEK 2	>250	51 ± 12	58 ± 14	41 ± 6	>1000	62 ± 2	>1000	66 ± 8
HEK 3	181 ± 44	46 ± 2	34 ± 10	41 ± 2	>1000	69 ± 2	>1000	102 ± 12
NIH/3T3	>250	96 ± 5	>1000	56 ± 1	461 ± 22	38 ± 2	>1000	93 ± 9
HK-2	>250	62 ± 6	>1000	82 ± 4	>1000	66 ± 2	>1000	71 ± 13
HPTC	>250	77 ± 9	>1000	55 ± 3	280 ± 27	34 ± 2	>1000	89 ± 11

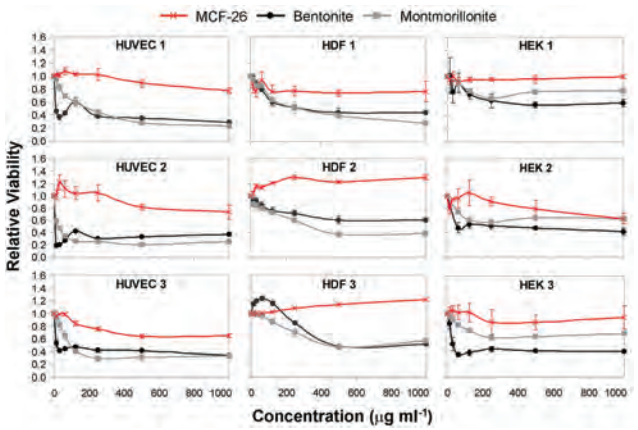

Fig. 5 Dose–response curves. HUVEC, HDF and HEK were treated with up to 1000 μg ml^{-1} of MCF-26 (red graphs), bentonite (black graphs) or montmorillonite (grey graphs). Cell viability was determined and all values were normalized to the values obtained with untreated control cells. Error bars show the s.d. (n = 3).

Table 2 MCF-26 was applied in the mg ml^{-1} range and the maximal concentration tested was 7 mg ml^{-1}. IC50 values and cell viability (%) at the maximal concentration of MCF-26 are shown (mean ± s.d.)

Cell type	IC50 (mg ml^{-1})	% at 7 mg ml^{-1}
HUVEC 1	6.3 ± 0.2	50 ± 3
HUVEC 2	2.1 ± 0.8	27 ± 7
HUVEC 3	0.7 ± 0.0	21 ± 2
HDF 1	2.0 ± 0.2	13 ± 3
HDF 2	5.6 ± 1.4	40 ± 8
HDF 3	5.0 ± 0.7	41 ± 3
HEK 1	>7.0	92 ± 9
HEK 2	>7.0	60 ± 4
HEK 3	>7.0	78 ± 3

Next, we addressed the cytotoxicity of MCF-26 by performing similar assays. When cells were treated with MCF-26 cell viability was generally higher as compared to bentonite and montmorillonite (Fig. 5), and in all cases the IC50 values were >1000 μg ml^{-1} (Table 1). This applied also to HUVEC, which were most sensitive to the cytotoxic effects of the layered clays. These results showed that MCF-26 had strongly reduced cytotoxicity in comparison to the layered clays.

As the IC50 values were in all cases >1000 μg ml^{-1} we assessed the cytotoxicity of MCF-26 also at higher concentrations in the mg ml^{-1} range with the most relevant cell types (primary human skin cell types and HUVEC). The IC50 values are displayed in Table 2 and the results revealed again cell type-specific effects. HEK were least sensitive with IC50 values of >7.0 mg ml^{-1} in all cases.

In addition, interdonor variability was observed and the IC50 values of the different batches of HDF and HUVEC ranged between ~2.0 mg ml^{-1} and ~6.3 mg ml^{-1} with the exception of HUVEC batch 3, where an IC50 value of ~0.7 mg ml^{-1} was determined. The difference to the previous result, where an IC50 value of >1000 μg ml^{-1} was obtained with this batch (Table 1), can probably be explained by the fact that this cell batch was used at a higher passage number (P6) when higher concentrations of MCF-26 were tested (P4 was used in the other experiments). Nevertheless, the lowest IC50 value obtained with this cell batch and MCF-26 (0.70 mg ml^{-1}, Table 2) was still ~7-fold higher than the highest value obtained with this cell batch and a layered clay (95.0 ± 12.5 μg ml^{-1}, Table 1, montmorillonite).

Overall, these results confirmed that MCF-26 was less cytotoxic than layered clays and the IC50 values were in the mg ml^{-1} range when relevant primary human cell types were tested.

In order to compare the cytotoxicity of MCF-26 and layered clays to the effects of other cytotoxic compounds we performed similar assays with DMSO and Ag NP. DMSO is a mildly cytotoxic agent that is used in concentrations of 10% for the

cryopreservation of cells and as solvent for pharmaceuticals in clinical applications. The IC50 values of this compound with low cytotoxicity ranged from ~25 mg ml^{-1} to >100 mg ml^{-1} (Table S1†) and were about 1–2 orders of magnitude higher than the IC50 values obtained with MCF-26 (Table 2 and Table S1†). Again, HUVEC displayed lower IC50 values than most other cell types. The lowest IC50 value was obtained here with HK-2 cells, which were relatively insensitive to layered clays.

Ag NP are applied in consumer products, cosmetics and wound dressings as antibacterial agents.[23,24] The cytotoxicity of Ag NP, which is probably due to the leaching of silver ions, is well documented and a point of concern.[23,25] Here, the IC50 values of Ag NP were in the same range as those of layered clays (Table 1 and Table S1†). Again, the lowest values were obtained with HUVEC and HK-2 cells. Overall, the IC50 values of Ag NP were at least an order of magnitude lower than those of MCF-26.

Together, the data showed that the cytotoxicity of MCF-26 is relatively mild and ~1–2 orders of magnitude lower than the cytotoxicity of other materials applied in wound dressings, such as kaolin and AgNP.

It would be important that non-biodegradable wound dressing materials can be effectively removed from the wound and are not taken up by the cells. Material remaining in the body can cause local and systemic effects including thrombosis, inflammation and foreign body reaction. We observed that layered clays strongly adhered to the cell surface and could not be completely washed away (Fig. 3), which would be a problem in this regard. Adhesion of MCF-26 to the cell surface was strongly reduced in comparison to layered clays (Fig. 3). To further address processes that might interfere with efficient removal we also studied cellular uptake of materials currently used in wound dressings in comparison to MCF-26. Fig. 6 shows that kaolin and Ag NP were efficiently taken up by HUVEC and HDF. Although kaolin also strongly adhered to the cell surface (Fig. 3) the fact that much lower concentrations of particles appeared in the nuclear area after overnight exposure (Fig. 6) showed that most particles were taken up into the cytoplasm and were not just distributed over the cell surface. In contrast, no uptake of MCF-26 by HUVEC and HDF could be detected after overnight exposure, even when MCF-26 was applied at 5- to 10-fold higher concentrations than Ag NP or kaolin (Fig. 6). The observed differences in cellular uptake and interactions with the cell surface could account for differences in the cytotoxicity of MCF-26 and layered clays.

As differences in cytotoxicity could also be potentially due to differences in the zeta potential of the particles, which could also account for the observed differences in the interactions with the cell surface, we measured the zeta potential of MCF-26, kaolin and the two smectite compounds. Positively charged compounds are usually cytotoxic. However, all of the compounds investigated here had negative zeta potentials. No significant differences between the zeta potentials of bentonite, kaolin and MCF-26 were observed when the different materials were suspended in cell culture medium (Fig. S4a†).

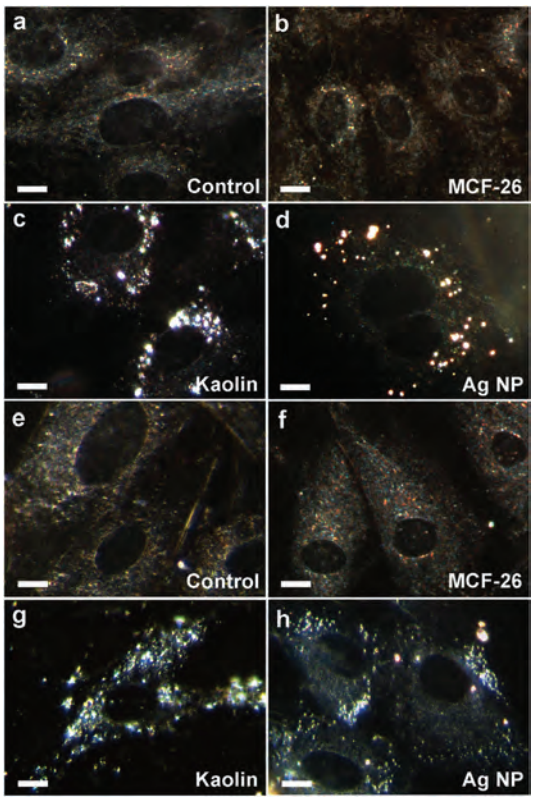

Fig. 6 Cellular uptake. HUVEC (a–d) and HDF (e–h) were left untreated (control) or were treated with MCF-26, kaolin or Ag NP as indicated. Ag NP and kaolin were applied at concentrations of 10 μg ml^{-1} (HUVEC) or 20 μg ml^{-1} (HDF). MCF-26 was applied to all samples at 100 μg ml^{-1}. Cells were washed after overnight exposure before images were captured with the CytoViva system. Cell nuclei appear as dark ovals within the cells. Scale bars: 10 μm.

The generation of ROS is another mechanism that could potentially account for the cytotoxic effects observed. Intracellular ROS generation in the presence of kaolin and MCF-26 was assessed with HUVEC batch 2 (Fig. S4b†). ROS generation in the presence of kaolin peaked when this compound was added at a concentration of 62.5 μg ml^{-1} and declined at higher concentrations. This could probably be explained by cell death. Only when kaolin and MCF-26 were added at a concentration of 62.5 μg ml^{-1} kaolin led to higher levels of ROS generation than MCF-26 (~24%). The concentration of ROS in the presence of MCF-26 increased linearly with the concentration of MCF-26 at higher concentrations of this compound. At 250 μg ml^{-1} of MCF-26 the concentration of ROS was ~1.8-fold higher than in untreated controls (Fig. S4b†). However, no negative effects on cell viability were observed at this concentration of MCF-26 (Fig. 5, HUVEC 2). Altogether, the data suggested that generation of ROS was not a primary cause for the negative effects on cell viability observed here.

Here, we addressed the cytotoxicity of MCF-26 and its potency in promoting clot formation in comparison to layered clays with hemostatic activity. Effects on cell viability were investigated *in vitro* by using different types of primary human cells and two well-characterized standard cell lines. The results

revealed that the cytotoxicity of MCF-26 is ~1–2 orders of magnitude lower than the cytotoxicity of layered clays. The effects of layered clays are strongly cell type-dependent and HUVEC are most sensitive. This result is in agreement with the findings of previous studies demonstrating cell type-specific cytotoxicity of layered clays and high sensitivity of HUVEC.[13–15]

The results showing a high sensitivity of HUVEC *in vitro* are in agreement with the finding that WS induced endothelial damage and other degenerative processes *in vivo*.[11,12] WS had been approved by the FDA in 2007 and the adverse effects observed in the more recent *in vivo* studies[11,12] suggested that standard *in vitro* safety tests with fibroblast cultures are not sufficient (discussed in ref. 12). In agreement with this notion we observed here that fibroblastic cell types are insensitive to the cytotoxic effects of layered clays. Although cell type-specific effects are also observed in case of MCF-26, this compound was only mildly cytotoxic to all cell types tested, and the IC50 values were in the mg ml^{-1} range.

It is not clear yet why the cytotoxicity of MCF-26 is reduced in comparison to layered clays. The mechanism of cell type-specific toxicity of layered clays does not appear to involve leaching of toxicants or binding of nutrients from the cell culture medium, and direct contact between the cell surface and the layered clay material is required.[13] We and others[14] observed that layered clays adhered strongly to the cell surface, and it has been discussed that the negative charge of the clay materials is important for associating with and lysing the cells.[14] However, we found that MCF-26, which has a similar zeta potential as kaolin and bentonite in cell culture medium, adheres less strongly to the cell surface and is less cytotoxic. Thus, reduced interactions with the cell surface might explain the reduced cytotoxicity of MCF-26, although this does not appear to be charge-dependent. It is also important to note that the results on LDH leakage did not indicate that membrane damage plays a major role in the cytotoxic effects observed.

Cellular uptake might be important for the cytotxic effects, which occurred in case of kaolin, but not in case of MCF-26. If cellular uptake was important for the cytotoxic effects of layered clays, it remains to be explained why the effects are cell type-specific. Substantial cellular uptake of kaolin, for instance, was observed in case of HDF and HUVEC (other cell types not tested), but only HUVEC displayed compromised viability. Our results suggested that the generation of ROS did not play a major role in the negative effects on cell viability observed.

Apart from potential effects on cell viability, adhesion to the cell surface and cellular uptake aggravates removal of non-biodegradable hemostatic agents from the wound. In fact, using porcine vascular injury models it was observed that it was difficult to remove WS from the wound.[9,12] Residual material led to local thrombus formation as well as to distal thrombosis in vital organs after entering systemic circulation.[12] In another study it was found that WS use was associated with substantial local inflammatory response and neurovascular degeneration up to 5 weeks post injury.[11] Severe problems with removal of the agent from the wound and thrombosis were not observed when CG was applied.[12] This was attributed to the fact that only a small amount of kaolin powder is incorporated into CG, whereas WS consists of smectite granules that are directly poured into the wound. However, in one case traces of kaolin were found in a specimen and it would be safer to use a compound that does not strongly adhere to the cells and does not show cellular uptake, as has been observed in case of MCF-26.

While we have demonstrated that MCF-26 has decreased cytotoxicity in comparison to layered clays and can be removed more easily, its potency to promote clot formation was in the same range. Previous data suggest that MCFs with larger pore window diameters than those investigated here could be more effective.[16] Furthermore, the ability of MCFs to uptake and immobilize proteins can be used to functionalize the surface with thrombin or other factors promoting blood clotting. It has been already demonstrated that the clotting times of plasma exposed to MCFs were dramatically reduced by immobilizing thrombin in the pores.[16] Also, the ability to sequester and release proteins[26] would allow to use MCFs as delivery vectors for procoagulant clotting factors. Using these strategies it would be possible to generate not only safer, but also more effective hemostatic agents.

Conclusions

Our results showed that MCF-26 displays a strongly reduced cytotoxicity to relevant human cell types in comparison to kaolin and other layered clays. Also, MCF-26 can be more easily removed from cellular material. This suggests that the use of MCF-26 would be safer, while its potency in promoting clot formation is comparable to that of the most effective commercial hemostatic agents. The potency of MCFs in promoting clot formation can be further increased by various strategies, which include increasing the pore window diameter and surface functionalization with thrombin.

Acknowledgements

This work was supported by the Institute of Bioengineering and Nanotechnology (Biomedical Research Council, Agency for Science, Technology and Research, Singapore). Part of this work was funded through the Casualty Care and Management Program at the Office of Naval Research, ONR grant numbers N00014-06-1-0145 and N00014-10-1-0191, and by the U. S. Army Medical Research & Materiel Command and the Telemedicine & Advanced Technology Research Center under Contract Number WQ81XWH-11-2-0021. The MRL Central Facilities are supported by the MRSEC Program of the NSF under Award No. DMR 1121053; a member of the NSF-funded Materials Research Facilities Network (www.mrfn.org).

Notes and references

1 R. F. Bellamy, *Mil. Med.*, 1984, **149**, 55–62.
2 H. R. Champion, R. F. Bellamy, C. P. Roberts and A. J. Leppaniemi, *Trauma*, 2003, **54**, S13–S19.
3 J. A. Acosta, J. C. Yang, R. J. Winchell, R. K. Simons, D. A. Fortlage, P. Hollingsworth-Fridlund and D. B. Hoyt, *J. Am. Coll. Surg.*, 1998, **186**, 528–533.
4 A. Sauaia, F. A. Moore, E. E. Moore, K. S. Moser, R. Brennan, R. A. Read and P. T. Pons, *J. Trauma*, 1995, **38**, 185–193.
5 J. Granville-Chapman, N. Jacobs and M. J. Midwinter, *Injury*, 2011, **42**, 447–459.
6 E. D. Cox, M. A. Schreiber, J. McManus, C. E. Wade and J. B. Holcomb, *Transfusion*, 2009, **49**(Suppl 5), 248S–255S.
7 P. Rhee, C. Brown, M. Martin, A. Salim, D. Plurad, D. Green, L. Chambers, D. Demetriades, G. Velmahos and H. Alam, *J. Trauma*, 2008, **64**, 1093–1099.
8 F. Arnaud, T. Tomori, W. Carr, A. McKeague, K. Teranishi, K. Prusaczyk and R. McCarron, *Ann. Biomed. Eng.*, 2008, **36**, 1708–1713.
9 B. S. Kheirabadi, J. W. Edens, I. B. Terrazas, J. S. Estep, H. G. Klemcke, M. A. Dubick and J. B. Holcomb, *J. Trauma*, 2009, **66**, 316–328.
10 B. S. Kheirabadi, M. R. Scherer, J. S. Estep, M. A. Dubick and J. B. Holcomb, *J. Trauma*, 2009, **67**, 450–460.
11 T. Gerlach, J. K. Grayson, K. O. Pichakron, M. J. Sena, S. D. DeMartini, B. Z. Clark, J. S. Estep and D. Zierold, *J. Trauma*, 2010, **69**, 1203–1209.
12 B. S. Kheirabadi, J. E. Mace, I. B. Terrazas, C. G. Fedyk, J. S. Estep, M. A. Dubick and L. H. Blackbourne, *J. Trauma*, 2010, **68**, 269–278.
13 P. D. Bowman, X. Wang, M. A. Meledeo, M. A. Dubick and B. S. Kheirabadi, *J. Trauma*, 2011, **71**, 727–732.
14 E. J. Murphy, E. Roberts, D. K. Anderson and L. A. Horrocks, *Neuroscience*, 1993, **57**, 483–490.
15 E. J. Murphy, E. Roberts and L. A. Horrocks, *Neuroscience*, 1993, **55**, 597–605.
16 S. E. Baker, A. M. Sawvel, J. Fan, Q. Shi, N. Strandwitz and G. D. Stucky, *Langmuir*, 2008, **24**, 14254–14260.
17 Y. Li, Y. Zheng, K. Zhang, J. Y. Ying and D. Zink, *Nanotoxicology*, 2012, **6**, 121–133.
18 M. Ni, J. C. M. Teo, M. S. Bin Ibrahim, K. Zhang, F. Tasnim, P. Y. Chow, D. Zink and J. Y. Ying, *Biomaterials*, 2011, **32**, 1465–1476.
19 M. Ni, P. K. Zimmermann, K. Kandasamy, W. Lai, Y. Li, M. F. Leong, A. C. A. Wan and D. Zink, *Biomaterials*, 2012, **33**, 353–364.
20 Z. Y. Oo, R. Deng, M. Hu, M. Ni, K. Kandasamy, M. S. Bin Ibrahim, J. Y. Ying and D. Zink, *Biomaterials*, 2011, **32**, 8806–8815.
21 G. Repetto, A. del Peso and J. L. Zurita, *Nat. Protoc.*, 2008, **3**, 1125–1131.
22 S. E. Baker, A. M. Sawvel, N. Zheng and G. D. Stucky, *Chem. Mater.*, 2007, **19**, 4390–4392.
23 H. J. Johnston, G. Hutchison, F. M. Christensen, S. Peters, S. Hankin and V. Stone, *Crit. Rev. Toxicol.*, 2010, **40**, 328–346.
24 L. J. Wilkinson, R. J. White and J. K. Chipman, *J. Wound Care*, 2011, **20**, 543–549.
25 M. Ahamed, M. S. Alsalhi and M. K. Siddiqui, *Clin. Chim. Acta*, 2010, **411**, 1841–1848.
26 Y.-J. Han, G. D. Stucky and A. Butler, *J. Am. Chem. Soc.*, 1999, **121**, 9897–9898.

Publication 2

BioMACROMOLECULES

Article

pubs.acs.org/Biomac

Open Access on 07/07/2015

Synthesis and Evaluation of Chromogenic and Fluorogenic Substrates for High-Throughput Detection of Enzymes That Hydrolyze Inorganic Polyphosphate

Carleigh F. F. Hebbard,[†,§] Yan Wang,[†] Catherine J. Baker,[†] and James H. Morrissey*[,†]

[†]Department of Biochemistry and [§]College of Medicine, University of Illinois at Urbana−Champaign, Urbana, Illinois 61801, United States

ABSTRACT: Inorganic polyphosphates, linear polymers of orthophosphate, occur naturally throughout biology and have many industrial applications. Their biodegradable nature makes them attractive for a multitude of uses, and it would be important to understand how polyphosphates are turned over enzymatically. Studies of inorganic polyphosphatases are, however, hampered by the lack of high-throughput methods for detecting and quantifying rates of polyphosphate degradation. We now report chromogenic and fluorogenic polyphosphate substrates that permit spectrophotometric monitoring of polyphosphate hydrolysis and allow for high-throughput analyses of both endopolyphosphatase and exopolyphosphatase activities, depending on assay configuration. These substrates contain 4-nitrophenol or 4-methylumbelliferone moieties that are covalently attached to the terminal phosphates of polyphosphate via phosphoester linkages formed during reactions mediated by EDAC (1-ethyl-3-(3-(dimethylamino)propyl)carbodiimide). This report identifies Nudt2 as an inorganic polyphosphatase and also adds to the known coupling chemistry for polyphosphates, permitting facile covalent linkage of alcohols with the terminal phosphates of inorganic polyphosphate.

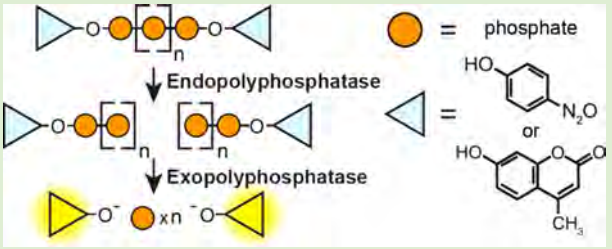

INTRODUCTION

Inorganic polyphosphates (polyP) are linear polymers of orthophosphate joined by high-energy phosphoanhydride bonds and can range in length from tens to thousands of phosphates. PolyP is widespread throughout biology and implicated in a multitude of physiologic processes in organisms from bacteria to man,[1−4] although many of its biological functions likely remain to be discovered and characterized. PolyP is also an industrial chemical with applications in areas such as water treatment, food processing, fertilizers, and flame retardants.[3] The biodegradable and versatile nature of polyP makes it an attractive material with many uses, and it would be desirable to understand how polyP is turned over. Known polyP-digesting enzymes include exopolyphosphatases which sequentially remove terminal phosphates from polyP, and endopolyphosphatases which hydrolyze internal phosphoanhydride bonds.[1] Although some of the enzymes responsible for degrading polyP have been identified in unicellular organisms, they remain relatively poorly studied in higher eukaryotes, with a few notable exceptions.[1,5] Two examples are mammalian alkaline phosphatase,[6] a highly potent exopolyphosphatase, and the human protein, h-prune, a short-chain exopolyphosphatase implicated as a regulator of metastasis.[7] Recent work has shown that polyP is secreted from activated human platelets[8] and mast cells[9] and that it is an important regulator of blood clotting[4] and complement.[10] PolyP is degraded in human plasma with a half-life of about 90 min,[11] which is no doubt important in controlling polyP's biological action, yet the mechanism of its degradation in vivo is currently unknown.

An impediment to identifying and studying the properties of polyP-degrading enzymes is the dearth of high-throughput means for detecting inorganic polyphosphatases and quantifying their activities. Many of the existing methods for quantifying enzymatic polyP degradation are cumbersome, of low sensitivity, or require the use of specialized equipment. The methods also typically rely on multiple steps including chromatography, gel electrophoresis, laborious physical extraction protocols coupled with chemical detection of liberated inorganic orthophosphate, or the use of radiolabeled polyP.[1] On the other hand, recently reported, more facile methods for detecting exopolyphosphatase activity include the continuous recording of released inorganic monophosphate, which was successfully employed to determine the kinetic parameters of the exopolyphosphatase, h-prune.[7] Detecting and quantifying the action of endopolyphosphatases remains substantially more time-consuming, however, as it typically involves resolving the digested polyP products using gel electrophoresis.[12] We therefore sought to develop chromogenic and fluorogenic polyP substrates that would allow polyP degradation to be followed spectrophotometrically and, in particular, a method that would allow high-throughput detection of endopolyphos-

Received: June 13, 2014
Revised: July 2, 2014
Published: July 7, 2014

phatase activity. Ideally, we would covalently attach chromogenic or fluorogenic dyes to the terminal phosphates of polyP. Chromogenic and fluorogenic substrates are available for a number of hydrolases and are readily adaptable to high-throughput assays in multiwell formats. We previously showed that primary amines can be covalently coupled via phosphoramidate linkages to the terminal phosphates of polyP in a reaction promoted by the zero-length cross-linking reagent, 1-ethyl-3-(3-(dimethylamino)propyl)carbodiimide (EDAC).[13] In the present study, we now show that EDAC can also be used to promote the efficient formation of phosphoester linkages with the terminal phosphates of polyP, and we apply this chemistry to create chromogenic or fluorogenic polyphosphatase substrates in which polyP is end-labeled with either 4-nitrophenol (NOL) or 4-methylumbelliferone (MU). We also show that these polyP derivatives can be used to detect the action of endo- and exopolyphosphatases, depending on assay configuration.

EXPERIMENTAL SECTION

Materials. Specified reagents were purchased from Sigma-Aldrich (St. Louis, MO) unless otherwise noted. NOL was recrystallized using hot water and ethanol. All experiments in this report used a polyP preparation (Natriumpolyphosphat P70) that was a kind gift from BK Giulini GmbH (Ludwigshafen, Germany). The polymer lengths of this preparation ranged from about 20 to 100 phosphates, with a mean length of approximately 45 to 50. PolyP concentrations were quantified using malachite green after acid hydrolysis[14] and are reported here in terms of phosphate monomer (monomer formula: $NaPO_3$). PolyP was end-labeled with spermidine via phosphoramidate linkages as described.[13]

Methods. *EDAC-Mediated End-Labeling of PolyP by Esterification with Methanol.* A mixture of 5.9 mM polyP, 150 mM freshly dissolved EDAC, and 6.4 M methanol in 100 mM MES buffer pH 6.5 was incubated for either 5 h at 37 °C or 1 h at 65 °C, after which the reaction mixtures were cooled on ice. Reaction volumes varied from 0.35 to 6.5 mL. PolyP-methanol was purified by acetone precipitation; briefly, NaCl was added to the reaction mixture (to 535 mM) followed by two reaction volumes of acetone, with mixing after each addition. The mixture was then centrifuged at 11,000 × *g* for 7 min at room temperature, after which the supernatant was discarded. The polyP pellet was washed twice by adding acetone to the tube followed by centrifugation. Pellets were then dried and redissolved in water.

Prior to NMR analyses, polyP-methanol was further purified by adsorption to a suspension of silica particles ("glass milk"). Glass milk was produced by a modification of the method of Vogelstein and Gillespie,[15] in which 250 mL silica (325 mesh) was stirred in 400 mL water for 1 h, then allowed to settle for 1 h to remove large particles. The supernatant was then centrifuged for 4000 × *g* for 15 min after which the pellet was collected and resuspended in 200 mL 50% nitric acid. This was then stirred and heated to close to boiling, after which it was cooled to room temperature. The silica fines were then collected by centrifugation and washed five times with water by resuspension and centrifugation. The final pellet of washed silica fines was resuspended as a 50% slurry by volume (glass milk). PolyP was purified by binding to, and elution from, glass milk as described,[14] except that the solutions were kept chilled throughout, and the polyP was eluted with 95 °C water instead of buffer.

EDAC-Mediated End-Labeling of PolyP by Esterification with NOL. A mixture of 5.9 mM polyP, 150 mM freshly dissolved EDAC, and 200 to 525 mM NOL was incubated for 1 h at 65 °C. Reaction volumes varied from 0.35 to 40 mL, and mixtures were agitated throughout, since the NOL concentrations exceeded solubility limits even in hot water. Completed reactions were cooled on ice and polyP was isolated by acetone precipitation. Because some free NOL coprecipitated with polyP in the first acetone precipitation, three full cycles of acetone precipitation were employed in which the collected polyP pellets were completely resuspended in water and reprecipitated by addition of NaCl and acetone followed by centrifugation. PolyP-NOL was then further purified using Bio-Gel P-6 desalting columns (Bio-Rad; Hercules, CA). The polyP-containing column fractions were identified by toluidine blue staining,[16] pooled, and lyophilized.

EDAC-Mediated End-Labeling of PolyP by Esterification with MU. A mixture of 5.5 mM polyP, 150 mM freshly dissolved EDAC, and 280 mM MU in a reaction volume of 1 mL was incubated for 1 h at 65 °C with agitation because the concentrations of MU used exceeded solubility limits. The reactions were then cooled on ice and polyP-MU was isolated using acetone precipitation as described above for the preparation of polyP-NOL.

NMR Analyses. Purified polyP and polyP derivatives were dissolved in water containing 10% (v/v) D_2O. All solution NMR spectra were collected on a Varian Unity INOVA 600 MHz proton frequency spectrometer with a 5 mm Varian AutoTuneX 1H/X PFG Z probe at 23 °C. 1D ^{31}P and ^{13}C spectra were acquired with a 2 s recycle delay. 1D ^{1}H spectra were acquired with a 1 s recycle delay, and solvent suppression was done by presaturation. 2D $^{1}H-^{13}C$ Heteronuclear Single Quantum Coherence (HSQC) spectra were acquired with 2048 and 160 points in the ^{1}H and ^{13}C dimensions, respectively. ^{1}H and ^{13}C spectra were referenced with external tetramethylsilane at 0 ppm, and ^{31}P spectra were referenced with external phosphoric acid at 0 ppm. 1D spectra were processed with MNOVA (MestreLab Research), and 2D spectra with NMRPipe.[17] polyP: ^{31}P NMR (90% H_2O 10% D_2O, 243 MHz) δ: −7.01 (s), −21.14, −21.65. polyP-methanol: ^{31}P NMR (90% H_2O 10% D_2O, 243 MHz) δ: −9.36 (d, $J_{P,P}$ = 17.8 Hz), −21.67. ^{1}H NMR (90% H_2O 10% D_2O, 600 MHz) δ: 3.51 (d, $J_{H,P}$ = 11.42 Hz). ^{13}C NMR (90% H_2O 10% D_2O, 151 MHz) δ: 53.7. polyP-NOL: ^{31}P NMR (90% H_2O 10% D_2O, 243 MHz) δ: −10.43, −16.81(d, $J_{P,P}$ = 17.7 Hz), −21.43, −21.61.

Gel Electrophoresis of PolyP. PolyP preparations were resolved on urea-containing 15% polyacrylamide gels and visualized using DAPI negative staining as described.[18]

Alkaline Phosphatase Digestion of PolyP. Protection against exopolyphosphatase-mediated degradation was employed to determine the extent to which polyP molecules were doubly end-labeled, as previously described.[13] Such digestions used calf intestinal alkaline phosphatase (CIAP, Promega; Madison, WI), a highly active exopolyphosphatase.[6] Typical reactions included 250 μM polyP and 20 units/mL CIAP; the liberated monophosphate was quantified using malachite green analysis.[14]

PolyP-NOL preparations often varied in the extent to which both ends of polyP were derivatized. To rid these preparations of singly labeled polyP, some were digested to completion with recombinant shrimp alkaline phosphatase (SAP, New England BioLabs; Ipswich, MA) by incubating 50 mM derivatized polyP with 50 U/mL SAP for 2 h at 37 °C in the manufacturer's buffer. SAP then was inactivated by heating at 65 °C (7 min), after which the remaining polyP was repurified by acetone precipitation. These preparations were termed SAP-treated polyP-NOL.

Endopolyphosphatase Digestion of PolyP. Certain nudix hydrolases were examined for endopolyphosphatase activity, typically in a two-stage assay. In the first stage, polyP-MU or SAP-treated polyP-NOL was incubated with endoacting enzyme (Nudt2 or Nudt3, Fitzgerald Industries International; Acton, MA) in the appropriate buffer at 37 °C, after which the reactions were chilled on ice. Buffer conditions were the following: for Nudt2, 8 mM SAP-treated polyP-NOL or 2 mM polyP-MU, 50 mM HEPES pH 7.4, and 5 mM $MgCl_2$; for Nudt3: 5.5 mM SAP-treated polyP-NOL or 2 mM polyP-MU, 25 mM HEPES pH 7.4, 20 mM NaCl, 10 mM $MgCl_2$, and 1 mM dithiothreitol.

For the second stage, a solution of CIAP in 100 mM Tris-HCl pH 8.8, 0.2 mM $ZnCl_2$ was prepared and warmed to 37 °C in 96-well polystyrene plates (Corning; Tewksbury, MA). The second stage was initiated by pipetting 100 μL of the chilled nudix-polyP reaction into prewarmed wells containing 100 μL CIAP solution, after which the rate of dye release was monitored spectrophotometrically at 37 °C. For polyP-NOL substrate, absorbance at 400 nm was measured using a SpectraMax M2 microplate reader (Molecular Devices; Sunnyvale, CA); for polyP-MU substrate, fluorescence was quantified in

Scheme 1. EDAC-Mediated Esterification of the Terminal Phosphates of PolyP[a]

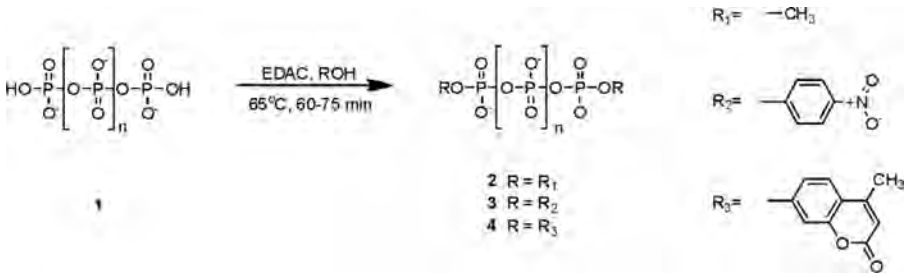

[a]Compounds: **1**, polyP; **2**, polyP-methanol; **3**, polyP-NOL; **4**, polyP-MU.

fluorescence mode using excitation at 360 nm, emission at 450 nm, and a 435 nm cutoff filter.

RESULTS

EDAC-Mediated Esterification of the Terminal Phosphates of PolyP with Methanol. EDAC has been used to promote the formation of ester linkages between alcohols and carboxylates,[19] as well as phosphoester linkages between alcohols and certain organic phosphates.[20] We therefore examined whether EDAC could promote the formation of ester linkages between alcohols and the terminal phosphate groups of inorganic polyP (Scheme 1).

As proof of principle, and to identify reaction conditions more readily, we examined EDAC-mediated esterification of polyP with methanol. The reaction resulted in a product that was protected from exopolyphosphatase (CIAP) digestion to an extent comparable to polyP that had been end-labeled with spermidine via phosphoramidate linkages (Table 1).

Table 1. Resistance of PolyP Derivatives to Hydrolysis by Alkaline Phosphatase (CIAP)

reactant	end label	% hydrolysis		
(none)	–	96.0	±	16.7
spermidine	$NH_2(CH_2)_3NH(CH_2)_4NH$–	20.8	±	2.1
methanol	H_3CO–	19.8	±	2.0
NOL	$O_2NC_6H_4O$–	27.0	±	2.0
MU	$C_{10}H_7O_3$–	3.9	±	1.6

We used solution-state NMR to further verify the product's identity. In the ^{31}P spectra, unmodified polyP displayed a relatively broad alpha (terminal) phosphorus peak at about 7 ppm (Figure 1A); the broadness likely reflects exchange of protonation states of the phosphate group.

Methylated polyP displayed an alpha peak shifted to 9.4 ppm (Figure 1B), which was also much sharper than the alpha peak of underivatized polyP. The methylated polyP alpha peak sharpness likely is caused by attenuation of the exchange broadening. This shifted alpha peak displayed as a doublet (Figure 1C) owing to the $^{31}P–^{31}P$ *J*-coupling between the alpha- and beta-phosphorus atoms. We next utilized the $^3J_{H–P}$ coupling between the methyl protons and alpha-phosphorus atom to confirm end modification and map connectivity. When proton decoupling was turned off, each peak of the alpha phosphorus doublet signal was split into a quartet pattern (Figure 1D), indicating the presence of three neighboring protons. To assign the chemical shift of the methyl protons, we acquired a 1D ^1H spectrum with heteronuclear decoupling irradiation at the alpha phosphorus frequency. The resulting spectrum, when compared to the spectrum without decoupling (compare Figure 1E and F), shows that the peak at around 3.5 ppm is converted from a doublet to a singlet. This transformation is consistent with a proton signal being coupled to a single neighboring phosphorus atom. To identify the carbon signal of the methyl group, we used ^{13}C-enriched (20%) methanol to synthesize methylated polyP. The resulting 1D ^{13}C spectrum (Figure 1H) shows significant enhancement of the carbon peak at ~53.6 ppm, which was almost unobservable in natural abundance methyl-polyP preparation (Figure 1G). To confirm that coupling existed between the carbon peak and the previously identified methyl proton signal, we performed 2D $^1H–^{13}C$ HSQC on the ^{13}C-enriched sample, with clearly observable correlation between the two signals (Figure 1I).

PolyP End-Labeled with NOL or MU. NOL is used often in making chromogenic substrates, as its absorption spectrum shifts dramatically when ester-linked to carboxylates or a single phosphate. MU is also extensively employed in synthesizing fluorogenic substrates because its fluorescence is quenched when ester-linked to carboxylates. Reacting polyP with NOL and EDAC resulted in a polyP preparation that was nearly as resistant to CIAP digestion as was polyP end-labeled with spermidine or methanol (Table 1). Reacting polyP with MU and EDAC resulted in a product with even greater CIAP resistance (Table 1) than that of polyP derivatized with spermidine or methanol. Absorption spectra of polyP-NOL before and after hydrolysis reveal an absorption maximum of 285 nm before hydrolysis (indicating covalent coupling of the NOL dye to phosphate) and 398 nm after hydrolysis (characteristic of free NOL; Figure 2C).

Analyzing polyP-NOL by 1D ^{31}P NMR produced an alpha peak shifted from ~7 ppm in underivatized polyP (Figure 1A) to a doublet at ~17 ppm in polyP-NOL (Figure 3A), consistent with covalent modification of the terminal phosphates. Resolving polyP and polyP-NOL by gel electrophoresis indicated little change in the distribution of polymer lengths after reacting the polyP with NOL and EDAC (Figure 3B).

Exopolyphosphatase (CIAP) Digestion of PolyP-NOL. End-labeling efficiency was calculated after complete acid hydrolysis of polyP-NOL and quantification and comparison of liberated NOL and monophosphate ratios (and assuming a mean polymer length of 50 phosphates). Using a polyP-NOL preparation in which approximately 40% of the polyP molecules were singly end-labeled, we added CIAP and monitored A_{400} versus time at 37 °C (Figure 3C). These results show that singly labeled polyP-NOL can be used to follow the progress of exopolyphosphatase digestion. The curvilinear progress curves probably reflect the fact that the substrate is ~50 phosphates long but the chromophore is

dx.doi.org/10.1021/bm500872g | *Biomacromolecules* 2014, 15, 3190–3196

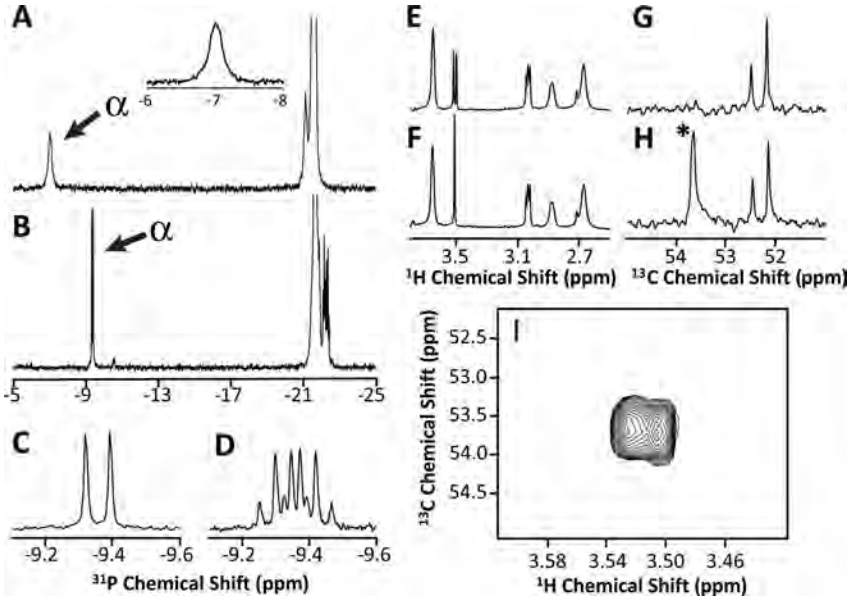

Figure 1. NMR analyses of end-methylated polyP. 1D ^{31}P spectra of (A) unmodified polyP and (B) polyP following reaction with methanol and EDAC. The terminal phosphate (alpha) peaks are indicated by arrows, and the inset in panel A is an expanded view of the alpha peak region of this spectrum. (C) The expanded view shows that the sharp alpha peak in panel B is resolved as a doublet. (D) Without ^{1}H decoupling, the alpha peak from methylated polyP expands into quartets as a result of *J* couplings from methyl protons. (E,F) 1D ^{1}H spectra of methylated polyP with (E) and without (F) applied decoupling irradiation at the alpha-phosphate frequency. The doublet peak at ~3.5 ppm (E) converts into a singlet (F) after irradiation because the proton peak is coupled to a phosphorus atom. (Other peaks in the ^{1}H spectra are from the MES buffer used in product purification and thus not affected by the decoupling.) 1D ^{13}C spectra of methylated polyP prepared with (G) natural abundance methanol or (H) 20% ^{13}C-enriched methanol. Use of ^{13}C-enriched methanol in the reaction greatly enhanced the signal at ~53.7 ppm (asterisk). (Other ^{13}C peaks are from the MES buffer.) (I) 2D HSQC analysis of the 53.7 ppm ^{13}C peak confirmed that the ^{13}C atoms are connected to the methyl protons.

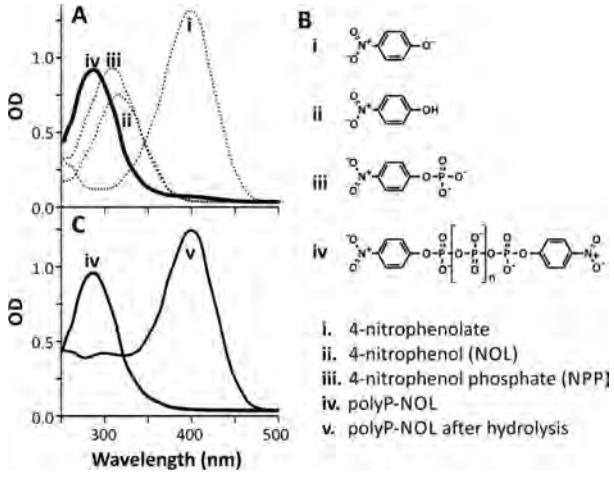

Figure 2. Product analysis and NOL substitution series using UV−vis spectroscopy. (A) Absorbance spectra of NOL substitution series with (B) the accompanying compounds' chemical structures. Each compound (except (ii)) was brought to a final concentration of 150 μM in alkaline conditions (1.5 M Tris-HCl buffer pH = 8.8, final) and scanned spectrally; NOL (ii) was scanned under acidic conditions. Absorbance maxima were the following: 398 nm (i), 317 nm (ii), 310 nm (iii), and 285 nm (iv). (C) Absorption spectra of polyP end-labeled with NOL, before (iv) and after (v) acid hydrolysis (1 M HCl for 1 h at 100 °C) followed by alkalization to pH 8.8.

released only when the last phosphate is removed from the substrate.

Endopolyphosphatase Digestion of PolyP-NOL and PolyP-MU. Covalent modification of polyP on both ends protects polyP against exopolyphosphatase (CIAP) digestion (Table 1). We therefore reasoned that two-stage assays for endopolyphosphatase activity could be devised using polyP that is completely labeled on both ends with chromophore or fluorophore. Digestion by exopolyphosphatase should be possible only after the action of endopolyphosphatase has exposed free polyP ends. In such an assay one could employ either sequential or simultaneous digestion with endo- and exopolyphosphatases. Accordingly, polyP-NOL was predigested to completion with SAP to eliminate singly labeled molecules, after which the polyP-NOL was repurified. We then used this SAP-treated polyP-NOL in a two-stage endopolyphosphatase assay in which we first digested the substrate with either Nudt3 (a hydrolase with known endopolyphosphatase activity[12]) or Nudt2 (another nudix hydrolase that cleaves dinucleotide polyphosphates, "Np$_n$Ns", but whose endopolyphosphatase activity was not known) and then monitored product release during digestion with CIAP. Figure 4 shows that few dye molecules from SAP-treated polyP-NOL were released upon incubating the substrate with either endopolyphosphatase (Nudt2 or Nudt3) or exopolyphosphatase (CIAP) alone. However, polyP-NOL was readily hydrolyzed by CIAP following pretreatment with either Nud2 or Nudt3. Additionally, this experiment demonstrated that Nudt2 has endopolyphosphatase activity (Figure 4B).

The efficiency of polyP labeling with MU was usually greater than that with NOL (Table 1), so predigestion of polyP-MU (Figure 5A) with SAP was typically not required before using this substrate to detect endopolyphosphatase activity. Figure 5B shows the reaction curves for two-stage assays of polyP-MU digestion with Nudt2 followed by CIAP. Neither Nudt2 nor CIAP alone released significant MU, while polyP-MU was efficiently digested by CIAP after incubation with Nudt2.

This experiment also demonstrates the amount of CIAP required for maximal rates of product release. Figure 5C shows

dx.doi.org/10.1021/bm500872g | *Biomacromolecules* 2014, 15, 3190−3196

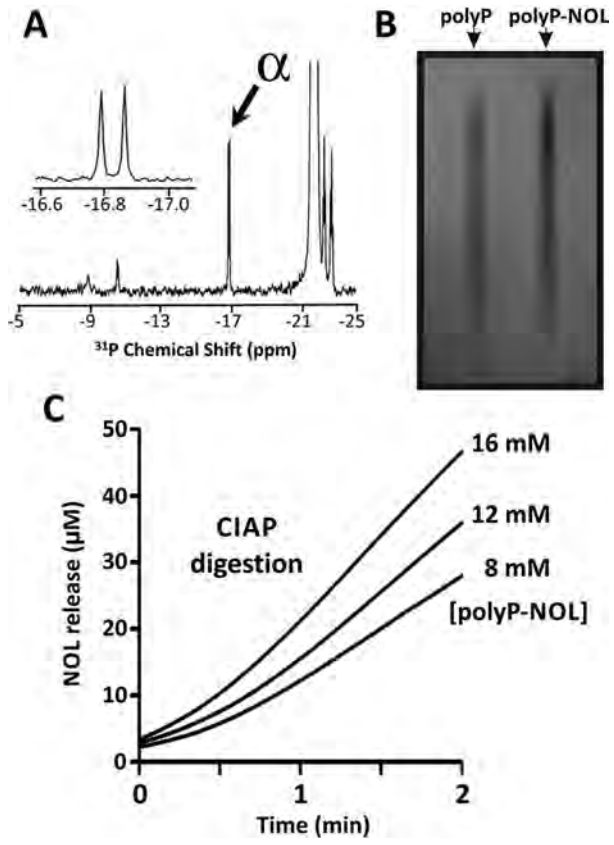

Figure 3. Analysis of polyP end-labeling with NOL. (A) 1D ^{31}P spectrum of polyP-NOL highly labeled at both ends. The alpha phosphate peak, indicated by an arrow, is resolved as a doublet (inset) upon axis expansion. (B) Comparison of polyP and polyP-NOL resolved by gel electrophoresis and detected by DAPI negative staining. (C) Enzymatic degradation of varying concentrations of incompletely end-labeled polyP-NOL (8 to 16 mM phosphate) by CIAP, with NOL release detected spectrophotometrically at 400 nm.

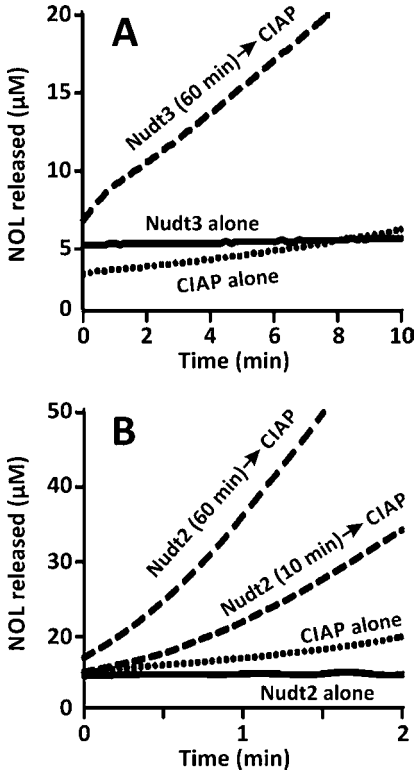

Figure 4. Sequential digestion of doubly end-labeled polyP-NOL with endopolyphosphatases and exopolyphosphatases. In both panels, doubly end-labeled polyP-NOL was first incubated with or without endopolyphosphatase (Nudt2 or Nudt3) for 10 or 60 min at 37 °C. Exopolyphosphatase (120 U/mL CIAP) was then added to the indicated samples and NOL release was quantified over time. (A) Treatment with 850 nM Nudt3. (B) Treatment with 250 nM Nudt2.

a much shorter time course of the second stage of this two-stage assay, using saturating levels of CIAP. We tested Nudt1 (a nudix hydrolase known to cleave Ap_3A but not long-chain Np_nN molecules) in a similar two-stage assay, but under the various conditions we used, the enzyme did not support MU release by CIAP (data not shown). We also examined a one-stage assay employing polyP-MU incubated simultaneously with CIAP plus varying concentrations of Nudt2. We found limited product release with CIAP alone but robust product release by the combination of CIAP and Nudt2 (Figure 5D).

■ DISCUSSION

This study had two goals: expand the covalent coupling chemistry for polyP, allowing for facile linkage of alcohols to the terminal phosphates of polyP via phosphoester bonds; and use this chemistry to develop high-throughput methods for detecting and quantifying the enzymatic digestion of polyP. We now report that the water-soluble cross-linker, EDAC, can be used to efficiently generate phosphoester linkages between alcohols and the terminal phosphates of polyP. We utilized this coupling chemistry to generate new chromogenic and fluorogenic substrates for detecting the enzymatic hydrolysis of polyP, based on phosphoester end-labeling of polyP with NOL or MU, respectively. Additionally, with our polyP substrates, we were able to monitor and distinguish endo- and exopolyphosphatase activities in real time.

Previously, we reported that EDAC could be used efficiently to couple compounds with primary amines to the terminal phosphates of polyP via phosphoramidate linkages, and this chemistry has allowed us to link a variety of probes to polyP;[13] for example, we used this method to biotinylate polyP, which we then employed to detect and quantify interactions between polyP and blood clotting proteins.[21,22] Although phosphoramidate linkages are relatively stable under neutral and alkaline conditions, the linkages are highly acid-labile.[23] It would be advantageous, therefore, to be able to efficiently link the terminal phosphates of polyP to organic compounds via phosphoester linkages, which, unlike phosphoramidate linkages, resist acid hydrolysis at physiological temperatures.[23] A previous study used combinations of carbodiimides (other than EDAC) in conjunction with polyP and alcohols in anhydrous organic solvents to generate phosphoester linkages to polyP; however, the reactions also caused substantial polyP hydrolysis to much shorter polyP chains and the apparent formation of cyclic and branched polyP adducts (which are unstable in aqueous solution).[24] In this report we identified aqueous coupling conditions for EDAC-mediated formation of phosphoester linkages to polyP that resulted in labeling just the terminal phosphates and that did not appreciably shorten the polyP chains.

Full-length polyP capped on either end with chromogenic or fluorogenic dyes was used to detect phosphatase activity. PolyP-

dx.doi.org/10.1021/bm500872g | Biomacromolecules 2014, 15, 3190−3196

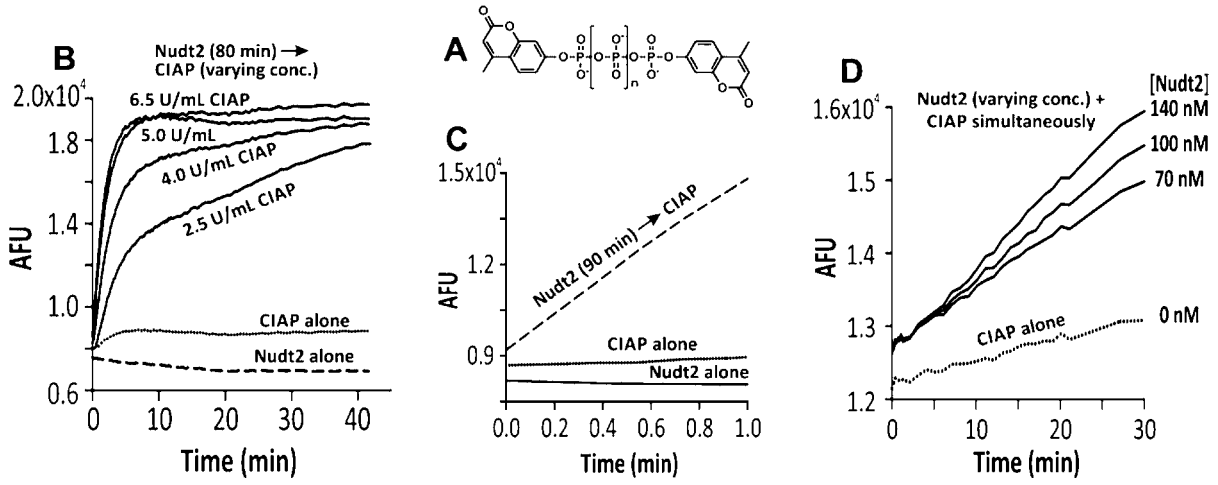

Figure 5. Digestion of polyP-MU by mixtures of endo- and exopolyphosphatases. (A) Structure of doubly end-labeled polyP-MU. (B) Sequential digestion of doubly end-labeled polyP-MU with endopolyphosphatase and exopolyphosphatase. PolyP-MU was first incubated with or without endopolyphosphatase (250 nM Nudt2) for 80 min at 37 °C, after which varying concentrations of exopolyphosphatase (CIAP) were added to the indicated samples and the increase in fluorescence (AFU) was quantified over time. (C) Sequential digestion of doubly end-labeled polyP-MU, first, with or without 250 nM Nudt2 for 90 min at 37 °C, after which 5 U/mL CIAP was added to the indicated samples and fluorescence was quantified over time. (D) Simultaneous digestion of polyP-MU with the indicated concentrations of Nudt2 and 55 U/mL CIAP, during which fluorescence was quantified over time.

NOL preparations that were incompletely labeled on both polyP ends were useful substrates for detecting exopolyphosphatase activity, which released free NOL upon the complete hydrolysis of the singly end-labeled polyP. On the other hand, polyP-NOL and polyP-MU preparations that were fully labeled on both polyP ends were highly resistant to exopolyphosphatase digestion, and this property was used as the basis of a two-stage assay in detecting endopolyphosphatase activity. In such assays, endopolyphosphatase digestion creates free polyP ends which are then substrates for exopolyphosphatase (CIAP) digestion, which in turn releases free dye from polyP-NOL or polyP-MU.

Not surprisingly, assays using the fluorogenic substrate, polyP-MU, could be conducted using lower substrate concentrations than those using the chromogenic substrate, polyP-NOL, owing to the greater sensitivity of fluorescence-based detection methods; however, assays using fluorogenic substrates require more specialized equipment and sample handling than do simple chromogenic assays, prompting us to develop both types of substrates in this study.

We constructed a two-stage assay to demonstrate the activity of a known endopolyphosphatase (Nudt3), and to demonstrate that another nudix hydrolase (Nudt2) also exhibits endopolyphosphatase activity. Nudt3, sometimes called DIPP1, or simply DIPP, is a nudix-type enzyme with multiple known in vitro substrates: capped mRNA, oxo-8-dGTPase, inositol pyrophosphates, dinucleotide polyphosphates, and inorganic polyphosphate (reviewed by McLennan[25]). Many nudix-type phosphatases are clinically important enzymes and their overexpression can be markers of disease. Nudt2 (Apah1), for example, is an Ap_4A hydrolase that, when overexpressed in breast cancer, correlates with poor prognosis.[26] In addition to processing Ap_4A, Nudt2 can hydrolyze long-chain Np_nNs such as Ap_6A. We hypothesized that this nudix enzyme, though previously not described as having endopolyphosphatase activity on inorganic polyP, might be able to cleave polyP and that we might detect this cleavage using our substrates in conjunction with CIAP. This was confirmed with our novel substrates. Like Nudt2, the human short-chain exopolyphosphatase, h-prune, is also implicated in tumor survival,[7] again providing a connection between alterations in polyP degradation and human health.

It should also be noted that the substrates only release a signal (free dye) when the last phosphate of the polyP chain is removed by an exopolyphosphatase. While this reaction was efficiently catalyzed by CIAP, other exopolyphosphatases might digest polyP to very short chains but not completely to monophosphate and therefore would not be expected to release the dye from these substrates. Such enzymes could be studied using these substrates in sequential assays employing CIAP.

We anticipate that the utilization of chromogenic and fluorogenic polyP substrates will aid further inquiry into how polyphosphates are turned over enzymatically. For example, an additional class of enzymes that could conceivably be studied using these substrates are kinases that utilize polyP as a substrate/phosphate donor. Also important is the development of a method for making stable ester linkages to the ends of polyP. Applications for such phosphoester linkages could include attaching polyP to surfaces, fabricating polyP-containing nanoparticles, and attaching fluorescent probes to polyP, in addition to creating the chromogenic and fluorogenic substrates for polyP-degrading enzymes reported here.

■ CONCLUSIONS

Using carbodiimide-mediated chemistry, we selectively esterified the terminal phosphates of inorganic polyP polymers with various alcohols. In a proof-of-principle experiment, we used methanol in esterification reactions and confirmed the product through 1D and 2D ^{31}P, ^{1}H, and ^{13}C NMR analyses. We also showed that polyP could be similarly end-labeled with chromogenic or fluorogenic alcohols to form adducts. These adducts were shown to be useful substrates for polyP-degrading enzymes, allowing us to monitor enzyme activity spectrophotometrically in real time; furthermore, we used these substrates to identify a new function for the clinically significant enzyme,

dx.doi.org/10.1021/bm500872g | Biomacromolecules 2014, 15, 3190−3196

Nudt2. The chemistry and substrates developed in this work are likely to be useful for synthetic and clinical applications.

AUTHOR INFORMATION

Corresponding Author

*E-mail: jhmorris@illinois.edu. Telephone: (217) 265-5424. Fax: (217) 265-5290.

Notes

The authors declare no competing financial interest.

ACKNOWLEDGMENTS

We thank Dr. M. Burke for helpful discussions about chemical synthesis and Dr. A. Jahromi for help with recrystallization. This work was supported in part by grant R01 HL047014 from the National Heart, Lung and Blood Institute of the NIH, and by Award WQ81XWH-11-2-0021 from the U.S. Army Medical Research and Materiel Command. The U.S. Army Medical Research Acquisition Activity, 820 Chandler Street, Fort Detrick, MD 21702−5014 is the awarding and administering acquisition office. The contents of this article do not necessarily reflect the position or the policy of the Government, and no official endorsement should be inferred.

REFERENCES

(1) Rao, N. N.; Gomez-Garcia, M. R.; Kornberg, A. *Annu. Rev. Biochem.* **2009**, *78*, 605−647.

(2) Moreno, S. N.; Docampo, R. *PLoS Pathol.* **2013**, *9* (5), e1003230.

(3) Kulakovskaya, T. V.; Vagabov, V. M.; Kulaev, I. S. *Process Biochem.* **2012**, *47* (1), 1−10.

(4) Morrissey, J. H.; Choi, S. H.; Smith, S. A. *Blood* **2012**, *119* (25), 5972−5979.

(5) Azevedo, C.; Saiardi, A. *Biochem. Soc. Trans.* **2014**, *42* (1), 98−102.

(6) Lorenz, B.; Schröder, H. C. *Biochim. Biophys. Acta* **2001**, *1547* (2), 254−261.

(7) Tammenkoski, M.; Koivula, K.; Cusanelli, E.; Zollo, M.; Steegborn, C.; Baykov, A. A.; Lahti, R. *Biochemistry* **2008**, *47* (36), 9707−9713.

(8) Ruiz, F. A.; Lea, C. R.; Oldfield, E.; Docampo, R. *J. Biol. Chem.* **2004**, *279* (43), 44250−44257.

(9) Moreno-Sanchez, D.; Hernandez-Ruiz, L.; Ruiz, F. A.; Docampo, R. *J. Biol. Chem.* **2012**, *287* (34), 28435−28444.

(10) Wat, J. M.; Foley, J. H.; Krisinger, M. J.; Ocariza, L. M.; Lei, V.; Wasney, G. A.; Lameignere, E.; Strynadka, N. C.; Smith, S. A.; Morrissey, J. H.; Conway, E. M. *Blood* **2014**, *123* (5), 768−776.

(11) Smith, S. A.; Mutch, N. J.; Baskar, D.; Rohloff, P.; Docampo, R.; Morrissey, J. H. *Proc. Natl. Acad. Sci. U. S. A.* **2006**, *103* (4), 903−908.

(12) Lonetti, A.; Szijgyarto, Z.; Bosch, D.; Loss, O.; Azevedo, C.; Saiardi, A. *J. Biol. Chem.* **2011**, *286* (37), 31966−31974.

(13) Choi, S. H.; Collins, J. N.; Smith, S. A.; Davis-Harrison, R. L.; Rienstra, C. M.; Morrissey, J. H. *Biochemistry* **2010**, *49* (45), 9935−9941.

(14) Smith, S. A.; Choi, S. H.; Davis-Harrison, R.; Huyck, J.; Boettcher, J.; Reinstra, C. M.; Morrissey, J. H. *Blood* **2010**, *116* (20), 4353−4359.

(15) Gailani, D.; Broze, G. J., Jr. FXI and the contact system. In *Metabolic and Molecular Basis of Inherited Disease*; Scriver, C., Beaudet, A., Sly, W., Valle, D., Childs, B., Kinzler, K., Vogelstein, B., Eds.; McGraw-Hill: New York, 2001; Vol. *8*, pp 4433−4453.

(16) Damle, S. P.; Krishnan, P. S. *Arch. Biochem. Biophys.* **1954**, *49* (1), 58−70.

(17) Delaglio, F.; Grzesiek, S.; Vuister, G. W.; Zhu, G.; Pfeifer, J.; Bax, A. *J. Biomol. NMR* **1995**, *6* (3), 277−293.

(18) Smith, S. A.; Morrissey, J. H. *Electrophoresis* **2007**, *28* (19), 3461−3465.

(19) Otera, J.; Nishikido, J. Reaction of alcohols with carboxylic acids and their derivatives. In *Esterification: Methods, Reactions and Applications*, 2nd ed.; Wiley-VCH Verlag GmbH & Co. KGaA, 2010; pp 3−157.

(20) Jordan, S. W.; Cronan, J. E., Jr. *J. Bacteriol.* **2003**, *185* (5), 1582−1589.

(21) Choi, S. H.; Smith, S. A.; Morrissey, J. H. *Blood* **2011**, *118* (26), 6963−6970.

(22) Smith, S. A.; Choi, S. H.; Collins, J. N.; Travers, R. J.; Cooley, B. C.; Morrissey, J. H. *Blood* **2012**, *120* (26), 5103−5110.

(23) Duclos, B.; Marcandier, S.; Cozzone, A. J. *Methods Enzymol.* **1991**, *201*, 10−21.

(24) Glonek, T.; Kleps, R. A.; Van Wazer, J. R.; Myers, T. C. *Bioinorg. Chem.* **1976**, *5* (4), 283−310.

(25) McLennan, A. G. *Cell. Mol. Life Sci.* **2013**, *70* (3), 373−385.

(26) Oka, K.; Suzuki, T.; Onodera, Y.; Miki, Y.; Takagi, K.; Nagasaki, S.; Akahira, J.; Ishida, T.; Watanabe, M.; Hirakawa, H.; Ohuchi, N.; Sasano, H. *Int. J. Cancer* **2011**, *128* (8), 1770−1782.

Publication 3

BioMACROMOLECULES

Article

pubs.acs.org/Biomac

Size-Controlled Synthesis of Granular Polyphosphate Nanoparticles at Physiologic Salt Concentrations for Blood Clotting

Alexander J. Donovan,[†] Joseph Kalkowski,[†] Stephanie A. Smith,[‡] James H. Morrissey,[‡] and Ying Liu*[,†,§]

[†]Department of Chemical Engineering, University of Illinois at Chicago, Chicago, Illinois 60607, United States

[‡]Department of Biochemistry, University of Illinois at Urbana−Champaign, Urbana, Illinois 61801, United States

[§]Department of Biopharmaceutical Sciences, University of Illinois at Chicago, Chicago, Illinois 60607, United States

Supporting Information

ABSTRACT: Size-controlled granular polyphosphate (PolyP) nanoparticles were synthesized by precipitation in aqueous solutions containing physiological concentrations of calcium and magnesium. We demonstrate using dynamic light scattering (DLS) that the solubility is correlated inversely with PolyP chain length, with very long chain PolyP (PolyP1000+, more than 1000 repeating units) normally found in prokaryotes precipitating much more robustly than shorter chains like those found in human platelet dense granules (PolyP80, range 76−84 repeating units). It is believed that the precipitation of PolyP is a reversible process involving calcium coordination to phosphate monomers in the polymer chain. The particles are stable in aqueous buffer and albumin suspensions on time scales roughly equivalent to catastrophic bleeding events. Transmission electron microscopy images demonstrate that the PolyP nanoparticles are spherical and uniformly electron dense, with a particle diameter of 200−250 nm, closely resembling the content of acidocalcisomes. X-ray elemental analysis further reveals that the P/Ca ratio is 67:32. The granular nanoparticles also manifest promising procoagulant effects, as measured by *in vitro* clotting tests assaying contact pathway activity.

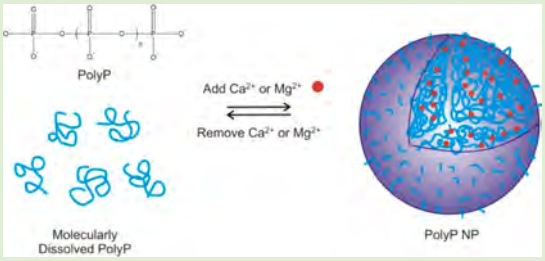

INTRODUCTION

Inorganic polyphosphate (PolyP) is an anionic linear polymer composed of orthophosphate subunits found in a broad array of organisms, ranging from the simplest prokaryotes to the most complex mammals including humans.[1] Dating from evolution's primordial stages, PolyP exhibits a diversity of functions depending upon its environment and polymer length, including highly regulated cellular tasks such as biofilm formation,[2] pathogen virulence,[3] cell motility,[4] quorum sensing,[5] transmembrane ion conductance,[6,7] metal chelation,[8] blood coagulation,[9−14] and energy storage.[15] PolyP's chemical simplicity despite its ubiquity, age, and biological versatility suggests that its precipitation into condensed granules may play a part in its myriad of biochemical tasks. Present across nearly all phylogenetic taxa are acidic subcellular storage compartments containing large quantities of PolyP.[16] Acidocalcisomes are acidic intracellular compartments found in prokaryotes that contain extremely high levels of ionized alkali earth and transition metal cations. Electron microscopy has revealed that these structures are electron dense, and elemental analysis confirms the presence of phosphate-containing compounds.[17] Ruiz et al. recently showed that this structure is conserved through the evolutionary tree to humans in the form of dense granules in human platelets.[18]

PolyP precipitates could wield different procoagulant effects than the molecularly dissolved polymer, possibly serving as an anionic contact "surface" for activation of FXII like kaolin and collagen.[19] Alternatively, these bodies could have evolved in evolution's early stages merely as condensed stores of large concentrations of PolyP for later downstream cellular functions requiring rapid nonlinear responses. PolyP has been known for approximately a century to reversibly bind to calcium, magnesium, iron, copper, zinc, barium, and other metals.[20] The calcium concentration within the platelet dense granules is as high as 2.2 M,[21] and the dissociation constants for Ca^{2+} and Mg^{2+} have even been quantified.[22]

Although successful synthesis of aluminum PolyP nanoparticles has been reported, the established synthetic routes require harsh organic solvents and intensive separation processes and lead to inadequate size control.[23] Momeni et al. investigated polyphosphate gels, or "coacervates," for potential utilization as hemostatic agents and examined the chelation of Ca^{2+}, Ba^{2+}, and Sr^{2+} to PolyP glasses of varied polymer lengths and its effects on solution pH and chain degradation of the PolyP solution.[24,25] However, systematic measurements of PolyP precipitation into particles with controlled sizes have never been reported. Moreover, the potential downstream therapeutic potential of PolyP precipitation has not been adequately addressed in the literature.

Herein, we show that the precipitation of inorganic PolyP into granular nanostructures is based on polymer length, with very long polymer lengths condensing much more robustly

Received: July 17, 2014
Revised: September 26, 2014
Published: September 30, 2014

than shorter chains like those found in human platelet dense granules. Furthermore, these condensed PolyP granules are stable in aqueous buffer and albumin suspensions on the same time scale as catastrophic bleeding events and possess potent procoagulant function, when assaying for activation of the contact pathway. Precipitation of inorganic PolyP in aqueous calcium and/or magnesium could potentially serve as a facile therapy to mitigate the deleterious effects of serious trauma via the delivery of high concentrations of PolyP stores locally to bleeding sites to rapidly induce coagulation.

EXPERIMENTAL SECTION

Materials and Reagents. Tris(hydroxymethyl)aminomethane, $CaCl_2 \cdot 6H_2O$, $MgCl_2 \cdot 6H_2O$, NaCl, KCl, and bovine serum albumin (BSA) were purchased from Sigma-Aldrich (St. Louis, MO). Water was deionized to 18.2 MΩ-cm (Nanopure II, Barnstead, Dubuque, IA). Citrated, pooled normal plasma was purchased from George King Biomedical (Overland Park, KS). L-α-Phosphatidylcholine (PC), L-α-phosphatidylserine (PS), and Avanti Mini-Extruder with 200 nm pore diameter polycarbonate membrane were purchased from Avanti Polar Lipids (Alabaster, AL). All materials were purchased at standard grades and used as received. PolyP80 (76−84 repeating units), PolyP250, (100−390 repeating units), PolyP305 (242−383 repeating units), and PolyP1000+ (more than 1000 repeating units) was size fractionated via preparative electrophoresis as previously described[14] or by differential isopropanol precipitation of heterogeneous long chain PolyP. Natriumpolyphosphat P70 (BKGP70, 20−125 repeating units, mode ∼45) was purchased from BK Guilini GmbH (Ludwigshafen am Rhein, Germany). PolyP concentrations are given throughout in terms of the concentration of phosphate monomer (monoP).

PolyP Nanoprecipitation. Aqueous size-fractionated PolyP was micropipetted into 8 mM Tris·HCl, pH 7.4 solutions containing combinations of the following: 1.2 mM, 5.0 mM, or 7.5 mM $CaCl_2$; 0.4 mM $MgCl_2$; 4.35 mM KCl; and 150 mM NaCl. The nanoparticles were then vortexed for 5 s. Precipitation was characterized by dynamic light scattering (DLS) (Brookhaven NanoDLS, Brookhaven, NY).

Determination of PolyP Solubility. The measurements of PolyP solubility are similar to the procedure used to determine the critical micelle concentration (CMC) of surfactants, copolymers, and phospholipids using DLS. PolyP samples were prepared as described above and injected into the DLS, beginning at exceedingly low concentrations (typically 100 nM to 1 μM monoP), where the scattering count rate resembled that of molecularly dissolved PolyP. The PolyP concentration was slowly titrated up until the scattering count rate increased and the correlation function was a well-behaved exponential decay on the baseline, suggesting that the PolyP sample was supersaturated. The scattering count rate was then plotted against the logarithm of the monoP concentration, producing a plot with two clear regimes representing: (1) molecularly dissolved PolyP and (2) precipitated PolyP. A linear regression was then performed on each regime and the point of intersection was found, which was defined as the solubility concentration. For consistency, all measurements were done on low laser intensity.

PolyP Nanoparticle (NP) Stability. *Stability in Aqueous Buffer.* NPs were synthesized using PolyP250 (125 μM) in either 1.2 mM or 5 mM $CaCl_2$ buffered with 8 mM Tris·HCl, pH 7.4 as discussed previously. Immediately after vortexing, particle size was characterized by DLS using at least a 1 min scattering time every 5 min for 1 h at room temperature.

Stability in BSA Suspensions. A solution of BSA (70 mg/mL) containing 8 mM Tris·HCl, pH 7.4 was prepared both with and without 2.5 mM $CaCl_2$ the day before experiments were conducted. PolyP250 (125 μM) was nanoprecipitated in 5 mM $CaCl_2$, 8 mM Tris·HCl, pH 7.4, and the particle diameter was determined immediately by DLS. The PolyP NPs were then mixed 1:1 (v:v) with the BSA suspensions. The resulting BSA and $CaCl_2$ concentrations were thus 35 mg/mL and 1.25 mM, respectively. Particle size was measured using DLS every 5 min for 1 h and subsequently every 30 min until 3 h had elapsed. The dispersion viscosity was calculated to be 1.2 cP,[26] and the refractive index was kept the same as water (1.331).

Transmission Electron Microscopy. *Sample Preparation.* PolyP250 (125 μM) was nanoprecipitated in 5 mM $CaCl_2$, 8 mM Tris·HCl, pH 7.4 as described above. The sample (10 μL) was micropipetted onto a 300-mesh carbon-coated Formvar grid (Structure Probe Inc., West Chester, PA) and allowed to dry in air for 10 min. The remaining liquid was wicked away with a Kim wipe and the process was repeated two more times to increase particle density and minimize aggregation. The sample was viewed in a JEOL JEM-1220 transmission electron microscope (JEOL, Japan).

X-ray Microanalysis. PolyP250 NPs (10 μL) were micropipetted onto a 300-mesh Holey Formvar carbon grid. The sample was dried for 15 min and examined in a JEOL JEM-3010 transmission electron microscope (JEOL, Japan).

Preparation of Large Unilamellar Vesicles (LUV). LUVs (200 nm) of PC to PS (80:20 molar ratio) were made by extrusion.[27] Briefly, 158 μL of 10 mg/mL L-α-PC and 42 μL of 10 mg/mL L-α-PS dissolved in chloroform were pipetted into a glass scintillation vial and dried under argon gas. The resulting lipid film was then placed under vacuum for an additional 1 h to remove any residual chloroform. The lipid cake was subsequently rehydrated with 1 mL Tris buffer, pH 7.4 and passed through an extruder with a polycarbonate membrane with 200 nm pore size 11 times to generate monodisperse LUV. Liposome diameter and polydispersity were verified by DLS.

Clotting Assays. Clotting was evaluated using a microplate-based assay as previously described[9] with minor modifications. The citrated plasma was prewarmed to 37 °C for 20 min, and PolyP was nanoprecipitated at room temperature and evaluated by DLS before proceeding with the assay. Wells contained 50 μL of citrated pooled normal plasma, 50 μL of PolyP NPs in 5 mM $CaCl_2$, 8 mM Tris·HCl, pH 7.4, and coagulation was initiated with 50 μL of 25 mM $CaCl_2$, 75 μM LUV, 8 mM Tris·HCl, pH 7.4. Final excess free calcium was estimated to be 4.72 mM. LUVs containing a small amount of phosphatidylserine (∼20 mol %) were added in contact activation assays, because the prothrombinase complex, consisting of Factor Va and Factor Xa, assembles on negatively charged phospholipid membranes in the presence of calcium. In the absence of negatively charged phospholipids, thrombin formation would be significantly hindered. Absorbance was read at 405 nm at room temperature on a Finstriments Microplate Reader (MTX Lab Systems Inc., Vienna, Virginia) every minute for 30 min. The sigmoidal absorbance traces were fitted to a standard Boltzmann growth function in Origin Pro 8.6 (OriginLab Corp., Northampton, MA). The *x*-coordinate of the inflection point (parameter x0) was defined as the time at which clotting occurred.

RESULTS AND DISCUSSION

In this study, the solubilities of PolyP of differing polymer lengths were first investigated by employing DLS. Analogous to determining the critical micelle concentration of a surfactant, the light scattering count rate begins to markedly increase when PolyP begins to precipitate into NPs. The scattering intensity of very long chain PolyP (PolyP1000+, similar to the long chains in prokaryotes) in aqueous solutions containing various concentrations of mono- and divalent cations is shown in Figure 1A. PolyP precipitated in the presence of divalent metal cations at biologically relevant concentrations (5 and 1.2 mM $CaCl_2$ and 1.2 mM $CaCl_2$ + 0.4 mM $MgCl_2$); however, monovalent cations exerted far less precipitative effects than their divalent counterparts. At 5 mM $CaCl_2$, concentrations typical of conventional clotting assays, PolyP nanoprecipitated much more easily than at physiological concentrations (1.2 mM $CaCl_2$). K^+ at normal physiological concentration does not statistically change the scattering intensity profile, while Na^+ at a relatively high ionic strength of 150 mM combined with 5 mM $CaCl_2$ causes the scattering intensity to increase at a

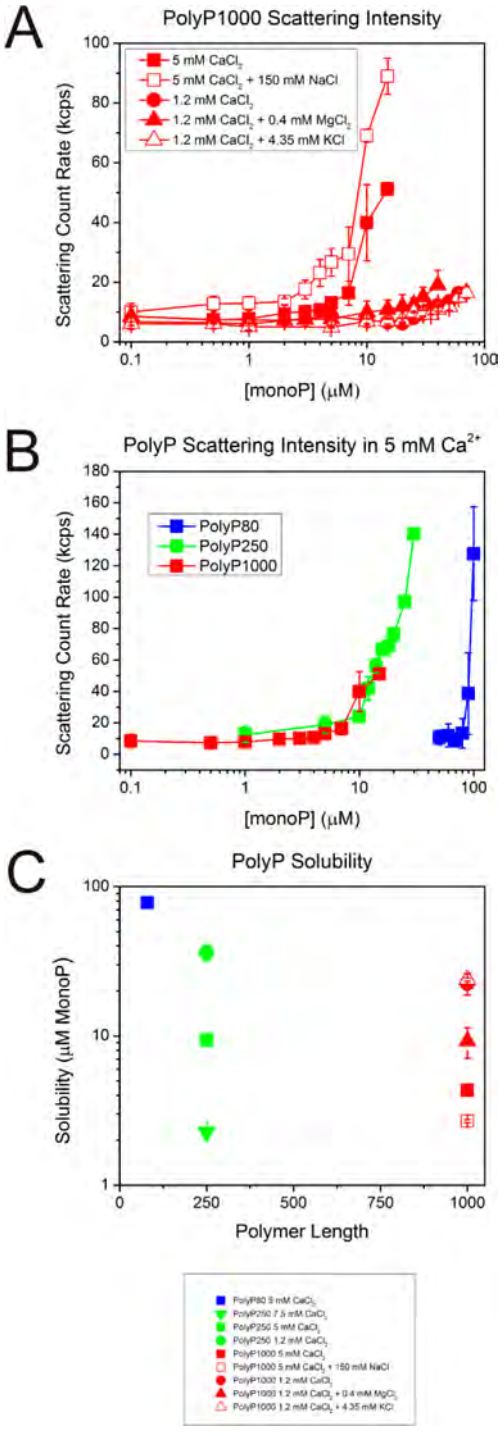

Figure 1. Solubility of PolyP as determined by DLS. (A) The precipitative effects of different metal cations on very long chain PolyP. Divalent metal cations such as Ca^{2+} and Mg^{2+} cause PolyP1000+ to robustly nanoprecipitate at physiological concentrations, as evidenced by the steep rise in the scattering intensity count rate, whereas monovalent cations such as Na^{+} and K^{+} at biologically relevant concentrations exert negligible effects on the polymer's solubility. (B) 5 mM $CaCl_2$ wields divergent precipitative effects on PolyP depending on the polymer length. PolyP1000+ precipitates most robustly with a steep rise in scattering intensity at 4.3 μM monoP concentration. PolyP250 is more soluble than PolyP1000+, with the count rate increasing near 9.4 μM. Platelet-size PolyP (PolyP80) is more soluble than both very long- and intermediate-chain length PolyP, with the scattering intensity markedly increasing at a monoP concentration almost a magnitude higher than PolyP250. (C) Solubility of PolyP of different polymer lengths. PolyP's solubility in various aqueous salt solutions buffered with 8 mM Tris·HCl, pH 7.4 plotted against polymer length in monoP units. There is a strongly nonlinear relationship, with very long chains (i.e., PolyP1000+) being much more readily precipitated than shorter polymers, e.g., polyP80. Divalent metal cations like Ca^{2+} and Mg^{2+}, which are known to chelate strongly to phosphate-containing compounds, exert precipitative effects at biologically relevant concentrations, while monovalent ions such as Na^{+} and K^{+} induce little or no significant effects on PolyP's solubility.

modestly lower monoP concentration. Ca^{2+} and Mg^{2+} function synergistically to promote nanoprecipitation. The solubility in 1.2 mM $CaCl_2$ + 0.4 mM $MgCl_2$ is more than 60% lower than in 1.2 mM $CaCl_2$ alone.

Nanoprecipitation was also a function of polymer length, with very long chains precipitating much more robustly than intermediate-length PolyP (PolyP250) or platelet-size polyP (PolyP80) at 5 mM $CaCl_2$ (Figure 1B). The solubility for each precipitative condition was determined by finding the intersection of the two linear regressions representing molecularly dissolved PolyP and PolyP NP regimes as plotted in Figure 1C. The solubilities for PolyP1000+ and PolyP250 at 5 mM $CaCl_2$ were 4.3 and 9.4 μM, respectively, while platelet-sized PolyP's solubility at the same condition was about 78 μM. Although not measured, it is safe to assume that PolyP80s solubility concentration is at or above 78 μM in 1.2 mM $CaCl_2$. Upon platelet activation, the concentration of PolyP in whole blood can reach up to 2−7 μM,[14] which suggests that platelet PolyP likely exerts its procoagulant effects while remaining largely molecularly dissolved. However, the next experiments demonstrate that PolyP nanoparticles exhibit dilution hysteresis, keeping open the possibility that condensed PolyP precipitates remain in NP format after secretion from activated platelets, despite being below the thermodynamic solubility limit. In addition, the local concentration of secreted PolyP could be orders of magnitude higher than 2−7 μM inside platelet-rich thrombi.

The solubility of platelet-sized PolyP in 5 mM $CaCl_2$ as a function of pH was also investigated. PolyP is stored intracellularly under mildly acidic conditions (~pH 5.4) together with extremely concentrated levels of calcium cations, serotonin, and pyrophosphate under the tight regulation of a H^{+}-ATPase pump in human platelet dense granules.[18] Given that this is the case in prokaryotic organisms as well, one could speculate that PolyP may be more easily precipitated under acidic conditions. However, at least for platelet-sized PolyP, the solubility is nearly identical at both mildly acidic and basic conditions (see Supporting Figure S5 and Supporting Table S3 in the Supporting Information).

PolyP250 was chosen as a paradigmatic polymer to study nanoparticle stability. First, nanoparticle growth kinetics were examined in an aqueous buffer containing biologically relevant concentrations of ionic calcium for 1 h, a time scale approximating a traumatic bleeding event and the half-life of PolyP in plasma or serum.[9] PolyP250 was nanoprecipitated in 8 mM Tris·HCl, pH 7.4 with 1.2 mM and 5 mM $CaCl_2$ (Figure 2A). Particle aggregation behavior follows power law kinetics, typical of metastable colloidal dispersions. Initial particle diameters were 169 and 58 nm for 5 mM and 1.2 mM $CaCl_2$, respectively. This suggests that the phosphate/calcium

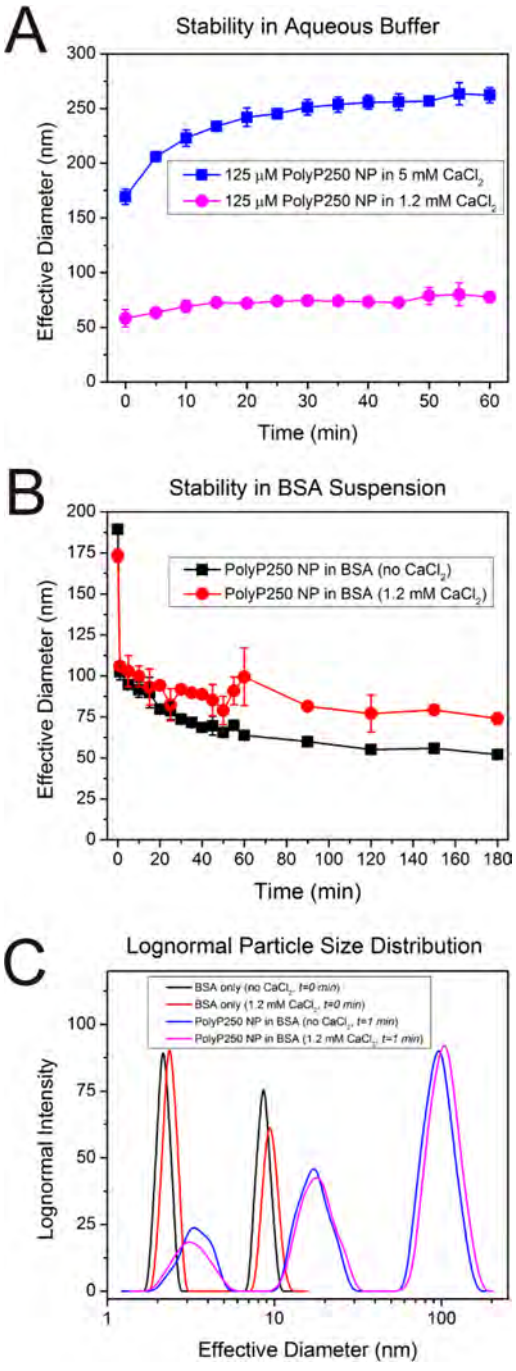

Figure 2. PolyP nanoparticle stability. (A) PolyP250 nanoparticle stability in aqueous buffer. 125 μM PolyP250 was nanoprecipitated in 8 mM Tris·HCl, pH 7.4 containing 1.2 mM or 5 mM $CaCl_2$. Average effective diameter was assessed every 5 min for 1 h, a typical time scale for a bleeding event. At 5 mM $CaCl_2$, the initial particle diameter was 169 nm and slowly grew to be approximately 260 nm after 1 h. At 1.2 mM $CaCl_2$ the particles were initially 58 nm and steadily increased to ~80 nm. The growth behavior of both suspensions appears to follow power-law kinetics typical of many metastable colloidal dispersions. (B) PolyP250 nanoparticle stability in suspensions containing BSA. 125 μM PolyP250 was precipitated in aqueous buffer containing 5 mM $CaCl_2$ as described previously and then mixed 1:1 (v:v) with 70 mg/mL BSA suspension buffered to pH 7.4 with or without 1.2 mM $CaCl_2$. Final BSA and $CaCl_2$ concentrations were 35 mg/mL and 1.2 mM, respectively. In both cases, the PolyP250 NPs shrank from approximately 170−180 nm before mixing with the BSA solution to 100 nm immediately after mixing with the BSA solution. This was not due to changes in dispersion viscosity or multiple scattering effects (confirmed by more measurements presented in the Supporting Information, Table S1). After 3 h, the PolyP NPs in BSA without $CaCl_2$ equilibration shrank to approximately 50 nm in diameter, while the NPs in the BSA equilibrated with 1.2 mM $CaCl_2$ were roughly the same size (~80 nm). It is hypothesized that BSA may be initially forming a complex with PolyP (the rapid shrinkage upon addition to the suspension) and then competitively binding Ca^{2+}, unless it has been pre-equilibrated. (C) Lognormal size distributions for (1) BSA suspension without Ca^{2+} pretreatment; (2) BSA suspension with 1.2 mM $CaCl_2$; (3) immediate addition of PolyP 250 NPs in 35 mg/mL BSA without $CaCl_2$ pre-equilibration; and (4) immediate addition of PolyP 250 NPs in 35 mg/mL BSA with 1.2 mM $CaCl_2$.

ratio may be the major driving force in the thermodynamic equilibrium of PolyP nanoprecipitation. Stoichiometry and PolyP supersaturation ratio as it relates to nanoparticle formation will be discussed systematically below. The stability of PolyP1000+ NPs precipitated at mildly acid conditions was also examined (see Supporting Figure S3 in the Supporting Information), resembling the environment in acidocalcisomes. The growth behavior manifests power law kinetics identical to physiologic pH. However, the scattering count rate remains more stable.

Aqueous buffer is only a poor approximation of the environment in circulation as it lacks many of the proteins and peptides that contribute to hemostasis and that regulate pH and plasma ionic strength. In addition to examining the nanoparticle growth behavior in aqueous buffer, stability was also investigated in Tris-buffered suspensions containing 35 mg/mL BSA to better approximate the conditions found in human serum. Serum albumin is the most abundant protein in circulation. It binds to a myriad of pharmaceuticals and foreign substances,[28] tightly regulates serum pH,[29] and robustly and competitively binds to metal cations,[30−35] most notably Ca^{2+}, Zn^{2+}, and Cu^{2+}. Because of BSA's functionality, two conditions were considered for PolyP250 NP stability: (1) BSA not pre-equilibrated with $CaCl_2$ and (2) BSA pre-equilibrated with 1.2 mM $CaCl_2$. Briefly, 125 μM PolyP250 NPs were nanoprecipitated in 5 mM $CaCl_2$ as described previously and mixed 1:1 (v:v) with the BSA suspensions. The particle size evolution was then monitored for 3 h (Figure 2B). At both salt conditions, the particles immediately shrank from 170 to 180 nm to approximately 100 nm when they were added to the BSA suspensions. The shrinkage is too rapid to suggest that this is due to enzymatic degradation. Moreover it is not an artifact of multiple scattering or changes in dispersion viscosity (see the Supporting Information, Table S1). PolyP250 NPs in BSA not pretreated with $CaCl_2$ continued to shrink to ~50 nm after 3 h, whereas the PolyP250 NPs in BSA pre-equilibrated with 1.2 mM $CaCl_2$ maintained approximately the same particle diameter, with the final size after 3 h being ~80 nm. It is conjectured that serum albumin may extract Ca^{2+} from the PolyP-Ca^{2+} complex. However, much further study is needed to prove this claim conclusively.

Figure 2C shows the log-normal particle population for the following conditions: (1) BSA without Ca^{2+} pre-equilibration; (2) BSA with 1.2 mM $CaCl_2$ pre-equilibration; (3) immediate addition of 125 μM PolyP250 NPs to BSA not pre-equilibrated with Ca^{2+}; and (4) immediate addition of PolyP250 NPs to BSA pre-equilibrated with 1.2 mM $CaCl_2$. BSA without PolyP in the presence or absence of calcium displayed two peaks. The

dx.doi.org/10.1021/bm501046t | Biomacromolecules 2014, 15, 3976−3984

first peak centered around 3 nm represents the hydrodynamic diameter of the BSA monomer. The second peak at approximately 15 nm constitutes multimeric BSA. The hydrodynamic radius has been previously reported in the literature to be 3.42 nm.[36] Quasielastic light scattering data demonstrates that the BSA monomer is a prolate ellipsoid. BSA dimerizes side-to-side, with significant overlap, leading to the dimer being less than twice the size of the monomer.[37]

Addition of $CaCl_2$ has minimal effects on the size distribution of the BSA protein. The particle populations representing conditions 3 and 4 show that there is an additional peak with a mean diameter of approximately 100 nm. This peak must be the effective diameter of the PolyP250 NPs. Moreover, the middle peak representing the BSA dimer has shifted to the right, further evidence that PolyP may be interacting directly with BSA and forming an adduct mediated by calcium. The striking discrepancy in the hydrodynamic diameter of the PolyP NPs in aqueous buffer and in BSA suspension deserves special scrutiny. Further study is needed to measure PolyP-Ca^{2+} binding constants at these conditions to corroborate the hypothesis that the evolution in PolyP particle diameter, characterized first by a steep drop and then a gradual shrinkage over a time scale of hours, is due to a competitive equilibrium process governed by the differential Ca^{2+} binding affinities of BSA and PolyP.

The initial effective diameter of the PolyP granular NPs was systemically investigated against the polymer's supersaturation ratio at three different calcium concentrations: 1.2 mM (free calcium concentration in human plasma), 5 mM (calcium concentration in *in vitro* coagulation assays), and 7.5 mM. Figure 3A shows the particle size plotted against monoP concentrations up to 1 mM for intermediate-length PolyP (PolyP250). PolyP precipitated in 5 mM $CaCl_2$ at monoP concentrations of 250 μM or greater had to be diluted with more Tris-buffered 5 mM $CaCl_2$ solution before being characterized by DLS (PolyP NP diameter is hysteretic after dilution; see the Supporting Information, Table S2). No trends between particle diameter and monoP concentration are manifest at first glance until the monoP concentration is divided by the solubility of PolyP250 at the given calcium concentration and plotted nondimensionally as the supersaturation ratio, as in Figure 3B. At low to moderate superaturation ratios (~1−50) the particle size is only a function of the calcium concentration.

After it was established that the solubility of PolyP250 was 9.4 μM in 5 mM $CaCl_2$, 8 mM Tris·HCl, pH 7.4, a sample well above the solubility concentration (in this case 30 μM) was diluted progressively with more 5 mM $CaCl_2$ to decrease the PolyP concentration and keep the calcium concentration constant, and the scattering intensity was measured after each dilution. As can be seen in Figure 3C, the system exhibits hysteresis: the count rate remains much higher even below the solubility concentration despite a thermodynamic driving force for some of the particles to resolubilize. Evidence that PolyP NP formation manifests dilution-dependent hysteresis has potentially profound ramifications: for example, a bolus of condensed PolyP could be delivered to a trauma site at locally high concentrations and be dispersed further downstream in the circulation without losing its NP format due to its hysteretic behavior, maintaining its associated biological functionality as a procoagulant and proinflammatory agent. However, in human plasma other mechanisms may come into play, such as binding of PolyP to membrane-associated proteins on vessel walls

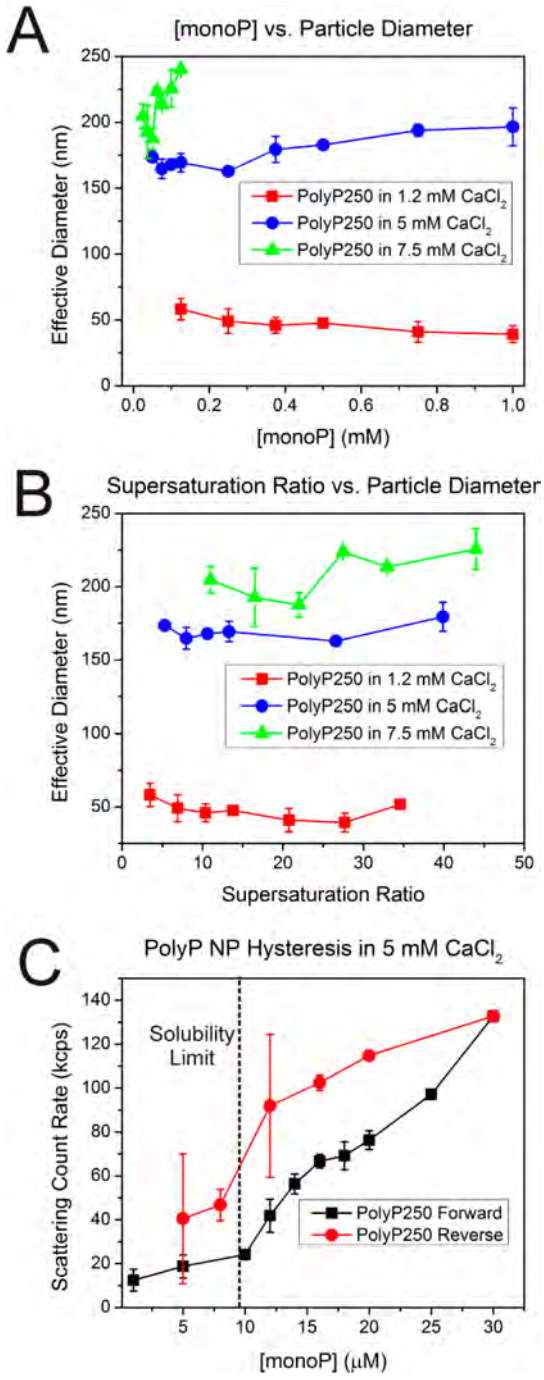

Figure 3. PolyP NP effective diameter as a function of supersaturation ratio. (A) PolyP250 NP initial effective diameter versus monoP and Ca^{2+} concentrations. Initial PolyP250 NP sizes were measured with up to 1 mM monoP concentration at three different calcium concentrations: 1.2, 5, and 7.5 mM Ca^{2+}. No trends are manifest except for a dependence on calcium concentration. (B) PolyP250 NP initial effective diameter as a function of supersaturation ratios and Ca^{2+} concentrations. When the monoP concentrations are divided by the solubility of PolyP250 at the respective calcium concentrations, it appears that at moderate supersauration ratios (~1−50), the PolyP particle diameter is only a function of the calcium concentration. (C) PolyP NP solubility hysteresis. The 30 μM PolyP250 was nanoprecipitated in 5 mM $CaCl_2$, generating a supersaturated colloidal dispersion of PolyP250 NPs. The suspension was then serially diluted with 5 mM $CaCl_2$, 8 mM Tris·HCl, pH 7.4 in order to decrease monoP concentration, while maintaining constant [Ca^{2+}]. As is evident from the reverse solubility curve (shown in red above), the

dx.doi.org/10.1021/bm501046t | *Biomacromolecules* 2014, 15, 3976−3984

Figure 3. continued

scattering intensity remains elevated, even approaching PolyP250s solubility (9.4 μM) in 5 mM $CaCl_2$ despite a thermodynamic driving force for resolubilization. This suggests that PolyP colloidal dispersions manifest hysteresis, a characteristic that may have profound ramifications for potential downstream therapeutic usage of PolyP NPs as clotting agents.

adjacent to thrombi, which may prevent PolyP NPs from being convected away from the wound site, thereby curtailing a potentially disastrous or even fatal scenario.

We have found that PolyP exerts its most robust procoagulant effects at roughly the 10−500 μM when assayed at 5 mM $CaCl_2$.[14] Indeed, this concentration range almost exactly corresponds to a supersaturation ratio of 1−50 for PolyP250 at 5 mM Ca^{2+}. However, at physiological calcium concentration, the particle diameter for this polymer length is roughly constant between 36 μM and 1.8 mM. One could speculate that organisms have specifically developed techniques to store and condense PolyP in subcellular compartments such as acidocalcisomes and platelet dense granules in a controlled manner by exploiting PolyP's roughly constant particle diameter at low to moderate supersaturation ratios. Upon secretion, these PolyP precipitates could potentially serve as concentrated stores of the polymer for biochemical processes requiring rapid, nonlinear, or threshold-switchable behavior such as coagulation or quorum sensing.

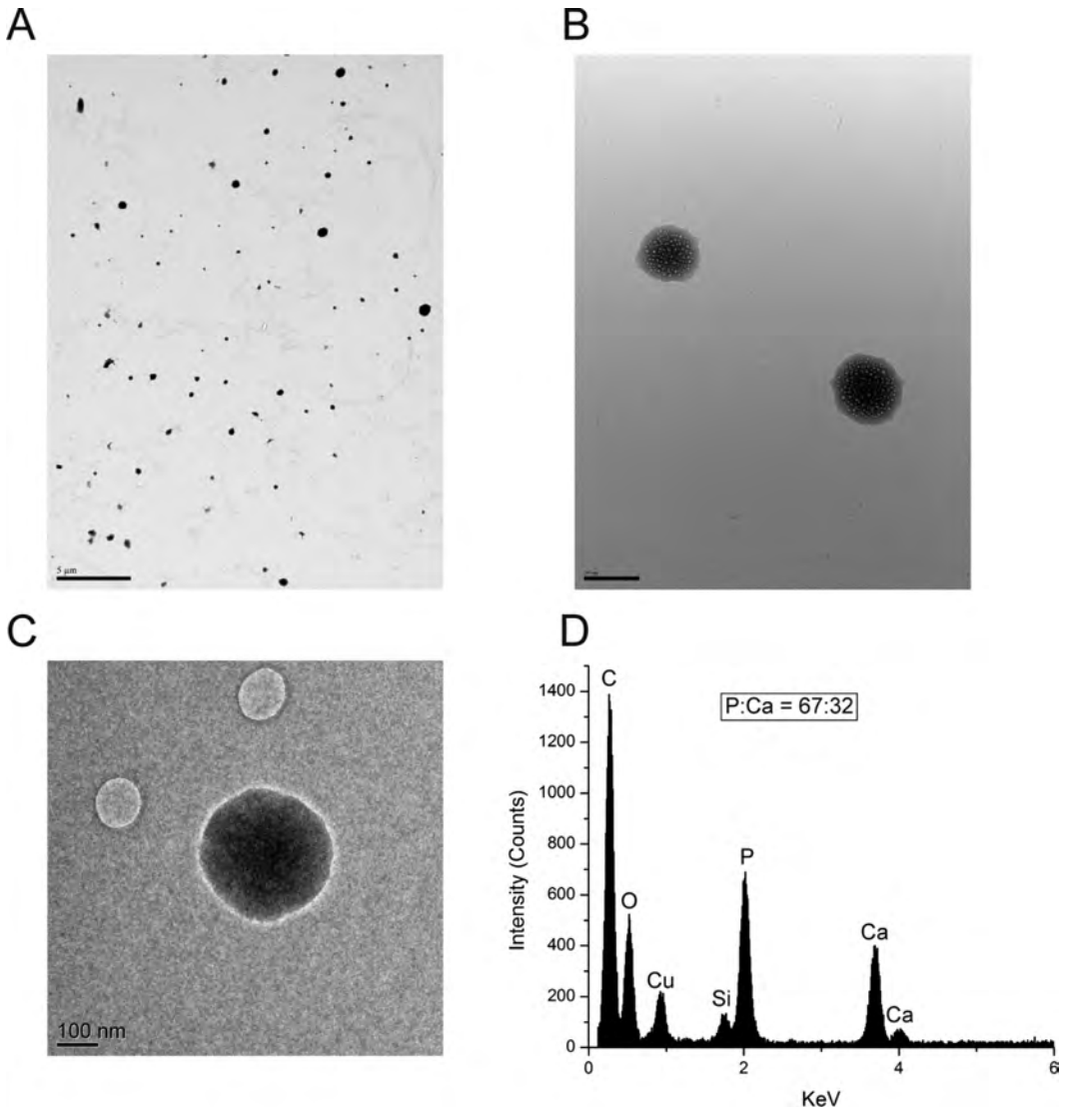

Figure 4. PolyP NP morphology, structure and elemental composition. (A) PolyP forms monodisperse particles in solution. The 125 μM PolyP250 was precipitated in 5 mM $CaCl_2$, 8 mM Tris·HCl, pH 7.4. PolyP250 forms monodisperse particle populations in the presence of 5 mM $CaCl_2$. Scale bar: 5 μm. (B) PolyP NPs appear spongy after prolonged electron beam exposure just like acidocalcisomes and platelet dense granules. Even though PolyP250 NPs are uniformly electron dense, after sustained exposure to the electron beam, white spots begin to appear so that the particles appear like round sponges or porous balls. This same phenomenon was also observed in Ruiz et al.'s investigation[18] of PolyP-containing dense granules in platelets. (C) A granular PolyP250 nanoparticle. A single PolyP 250 NP is shown at higher magnification revealing that the granule is roughly spherical and approximately 200−250 nm in diameter, in good agreement with DLS data. Scale bar: 100 nm. (D) Elemental composition of the synthetic PolyP250 NPs. Copper, carbon, and silicon are from the grid. The ratio of the phosphorus to the calcium peak is 67:32. Ruiz et al. performed the equivalent analysis with human platelet dense granules, and their resulting X-ray microspectrum is quasi-identical, except for the presence of a small K peak.[18] However, potassium was not used here for PolyP nanoprecipitation.

dx.doi.org/10.1021/bm501046t | *Biomacromolecules* 2014, 15, 3976−3984

Transmission electron microscopy was used to examine the PolyP particle structure, elemental composition, and morphology. Figure 4A is an electron micrograph taken at low magnification with a large population of PolyP250 NPs, showing that the granules are spherical in shape and relatively monodisperse, despite the presence of some larger aggregates. The particle diameter is a function of the calcium concentration; inevitably, some aggregation is bound to occur during the drying process and grid preparation. When the particles undergo substantial exposure from the electron beam, the PolyP250 NPs develop white spherical spots, resulting in the granules resembling round sponges or soccer balls, despite their uniform electron density as seen in Figure 4B. Indeed, Ruiz et al. has shown using TEM that PolyP bodies in acidocalcisomes and human platelet dense granules also appear spongy after bleaching with the electron beam, resembling the PolyP NPs synthesized here.[18]

Figure 4C shows a single PolyP250 nanoparticle at high magnification. The PolyP granule is spherical and approximately 200−250 nm in diameter, corroborating DLS data. Figure 4D is an X-ray microspectrum of the particle in part C showing its elemental composition. Copper, carbon, and silicon are from the grid. It is very typical for X-ray microspectra to have small peaks (∼1−2%) of Si and alkali earth metals arising from the detector itself or, more rarely, from silicon-containing oils deposited on the Formvar grids during the manufacturing process. In fact, a small Si peak was also observed in the X-ray microanalysis of human platelet dense granules in the past.[18] The P/Ca ratio is 67:32. Ruiz et al., in their investigation of human platelet dense granules, also determined the elemental composition of the PolyP bodies, yielding very similar results.[18] The P/Ca was 1.76 with trace amounts of K^+. However, dense granules are mildly acidic subcellular compartments, which may lead to a different P/Ca stoichiometry, and platelets contain substantial cellular stores of potassium.[38] Potassium was not used here to precipitate PolyP into synthetic PolyP granules.

Smith et al. demonstrated that PolyP is a potent activator of the contact pathway of coagulation, and its activity is related nonlinearly with its polymer length,[14] with long polymers being more robust activators than shorter chains, which exert their effects at different points in the cascade such as via acceleration of FV activation and alteration of fibrin clot architecture and morphology. Figure 5B shows a schematic representation of the intrinsic pathway of coagulation and the points in which PolyP exerts its effects. It is well accepted in the literature that anionic "surfaces" such as collagen, glass, or kaolin are required to form the primary complex consisting of FXII (Hageman Factor) and its activation partners, plasma prekallikrein and high molecular weight kininogen (HMWK).[19] However, countless other soluble substances serve as scaffolds for the (auto)activation of FXII. Examples include ellagic acid, lipopolysaccharides, dextran sulfate, and phospholipids.[39] It has been reported previously that there exists a threshold molecular weight for activation of the intrinsic pathway for polystyrene polymers and dextran derivatives, with contact activity for both polymer types rising sharply ∼25 000 Da.[40] Others have communicated that the threshold molecular weight for dextran sulfate is as low as 10 000 Da.[41] Nonetheless, the mechanism by which PolyP acts on FXII has yet to be clearly elucidated.

Previous studies assaying the procoagulant effects of PolyP were performed under conditions where the polymer would presumably exist in its molecularly dissolved state. Typically, PolyP was incubated together with pooled normal plasma

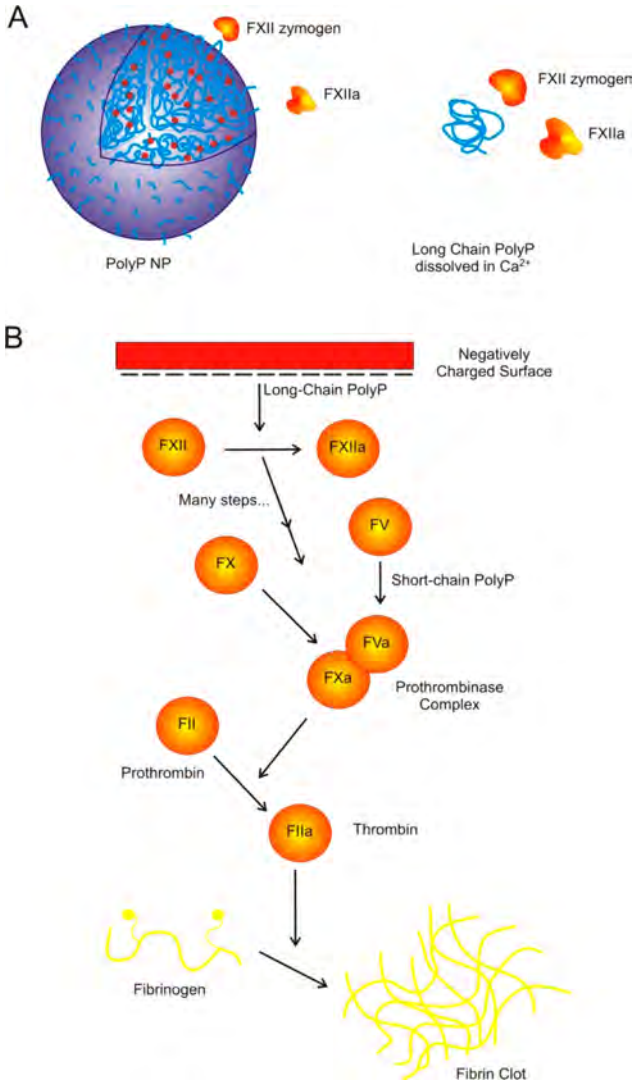

Figure 5. PolyP NPs as contact activators. (A) Possible mechanisms by which PolyP exerts its contact pathway activity. PolyP could serve as a surface for FXII activation as a colloidal particle like kaolin (left) or as a soluble anionic polymer like dextran sulfate (right) with a threshold molecular weight needed to elicit a conformational change in the FXII zymogen. (B) Schematic of the intrinsic pathway of blood coagulation. A negatively charged surface serves as the site for assembly of the primary complex consisting of FXII, kallikrein, and high molecular weight kininogen. Long-chain PolyP is able to support activation of the contact pathway, while shorter polymer lengths (like those in human platelets) are weak contact activators. PolyP also exhibits procoagulant effects further downstream in the final common pathway of blood clotting.

(PNP) for 3−5 min prior to recalcification. Since the plasma is citrated, there would be very little ionic calcium available to chelate PolyP, and thus no calcium-dependent precipitation would take place. The activation of contact enzymes and the generation of FXIIa are calcium-independent; therefore, prior studies investigating PolyP's contact activity are confined to an examination of the polymer in the absence of calcium-dependent precipitation. Moreover, plasma contains countless proteins and peptides such as serum albumin which may prevent or hinder its precipitation after recalcification. Because of PolyP's role in the early stages of natural selection, predating the arrival of polypeptides and quite possibly serving as the

precursor to deoxyribonucleic and ribonucleic acid, it is only natural that PolyP would serve as the paradigmatic anionic scaffold for plasma and cytosolic proteins, emerging as a favored binding partner for peptides with cationic amino acid residues.

Figure 6 shows the clotting time of PolyP molecules or nanoparticles when assaying for contact activity using citrated

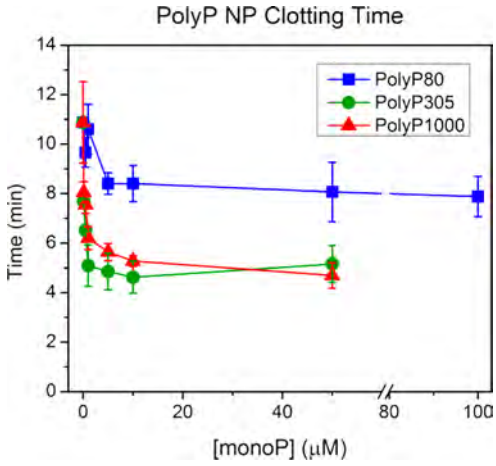

Figure 6. Initiation of the contact pathway by PolyP based on polymer length and concentration. Clotting time of PolyP is plotted as a function of monoP concentration from 0 to 100 μM. PolyP was added to 5 mM $CaCl_2$, 8 mM Tris·HCl, pH 7.4 at concentrations above and below its solubility. The presence of precipitated PolyP was monitored by DLS before addition to plasma. Intermediate- and very long-chain length PolyP (PolyP305 and PolyP1000+) are clearly more robust contact activators than platelet-sized PolyP (PolyP80). The concentration dependence on clotting time for PolyP305 and PolyP1000+ are identical, suggesting that a "saturating condition" has been established.

PNP. The polyphosphates (PolyP80, PolyP305, and PolyP1000+) were first added to 5 mM $CaCl_2$, 8 mM Tris·HCl, pH 7.4 at three times the final assay concentration and characterized by DLS (data not shown). Once the PolyP was incubated with the calcium solution, it was added to the PNP and immediately recalcified to initiate coagulation. Platelet-size PolyP (PolyP80) weakly shortened time to clot formation, saturating near 10−50 μM monoP. PolyP305 and PolyP1000+, on the other hand, were robust contact activators, drastically reducing clotting times even at submicromolar concentrations. Interestingly, the clotting activities of the two longer polymer sizes are quasi-identical (the error bars overlap for every concentration except one).

These data suggest that platelet PolyP only weakly promotes the activation of FXII, with the reduction in clotting time deriving mostly from effects on the final common pathway of clotting. On the other hand, the longer polymer sizes are large enough to serve as scaffolds for primary complex formation after treatment with calcium. One possibility is that there is a threshold polymer length (molecular weight) (as was previously reported for polystyrene and dextran sulfate) needed to exert the conformation change on the FXII zymogen (or to recruit a sufficiently high local surface density of FXII and its activators) as shown in Figure 5A. Interestingly, PolyP305's molecular weight is approximately 24 kDa, corroborating past results on threshold contact activation measured using polystyrene and dextran sulfate polymers. The fact that the concentration dependence is identical for PolyP305 and PolyP1000+ also suggests that the nanoparticle solubility is not the threshold condition for contact pathway activation for polymers over the threshold size, as PolyP1000+'s solubility is approximately 2-fold lower in 5 mM $CaCl_2$. If the solubility were the limiting condition, then PolyP1000+'s clotting time would drop at ∼4 μM, whereas PolyP305's would drop at ∼9 μM. However, there are several important caveats that limit the completeness of this analysis: (1) PolyP NPs have been shown to exhibit dilution-dependent hysteresis; (2) the solubility of PolyP in plasma or serum with its diversity of proteins and peptides and additional polyvalent cations such as Mg^{2+}, Cu^{2+}, Zn^{2+}, Mn^{2+}, and Fe^{2+}/Fe^{3+} (see Supporting Figures S2 and S4 in the Supporting Information) could be vastly different than in aqueous buffer containing only calcium; and (3) the effect of citrate and other calcium chelators such as EDTA on PolyP nanoparticle stability has yet to be investigated.

The zeta potential of the PolyP NPs was determined to be between −15 and −20 mV independent of particle diameter and polymer length (see Supporting Tables S4 and S5 in the Supporting Information). The negative surface charge of PolyP precipitates could therefore conceivably support autoactivation of Factor XII or recruitment of its activators, plasma prekallikrein, and high molecular weight kininogen independent of polymer molecular weight, discounting other factors that would influence PolyP NP stability in human plasma mentioned above.

Regardless of the physical interpretation, the fact remains that PolyP precipitation under aqueous conditions at physiologic salt concentrations is a facile means to synthesize large amounts of condensed PolyP granules similar in structure to human platelet dense granules for potential downstream uses such as a biocompatible procoagulant agent.

CONCLUSION

Herein, we demonstrate the size-controlled synthesis of monodisperse PolyP NPs at physiological concentrations of calcium and magnesium. The solubility is related nonlinearly to the polymer length, with very long-chain PolyP precipitating much more facilely than platelet PolyP. Further, the NP size is only a function of the calcium concentration across a wide supersaturation range. The granules are stable for at least an hour in aqueous buffer solutions, displaying typical power-law growth kinetics and are stable in BSA suspensions for 3 h.

The PolyP NPs possess promising procoagulant activity. Given that the PolyP particles are stable on the same time scale as a catastrophic bleeding event raises the question that PolyP's powerful procoagulant effects on the intrinsic pathway may be related to its precipitation into micron or submicron granular particles serving as negatively charged surfaces for FXII activation. The facile, size-controlled synthesis of these particles in the laboratory serves as a foundation for the future development of targeted procoagulant nanotechnologies exploiting PolyP precipitation to mitigate the effects of a diversity of bleeding phenomena such as internal hemorrhage and hemophilia in a minimally invasive manner.

ASSOCIATED CONTENT

Supporting Information

Scattering intensity of PolyP250 in 7.5 mM $CaCl_2$, 8 mM Tris·HCl, pH 7.4. Determination of any multiple scattering effects in BSA suspensions containing PolyP250 NPs. PolyP250 NP diameter hysteresis after dilution with more 5 mM $CaCl_2$. PolyP1000+ precipitation and log-normal particle size dis-

dx.doi.org/10.1021/bm501046t | Biomacromolecules 2014, 15, 3976−3984

tribution in 5 mM $MgCl_2$, 8 mM Tris·HCl, pH 7.4. Stability of PolyP1000+ NPs in acidic and basic conditions. Particle size distribution of PolyP1000+ NPs in Fe^{2+}/Fe^{3+}. Scattering intensity of platelet-sized PolyP as a function of monoP concentration at acidic and basic conditions. Solubility of PolyP as a function of molecular weight and pH. Zeta potential and particle effective diameter as a function of polymer length in 5 mM $CaCl_2$, pH 7.4. Zeta potential and particle effective diameter of PolyP at various precipitating conditions. This material is available free of charge via the Internet at http://pubs.acs.org.

AUTHOR INFORMATION

Corresponding Author

*Phone: +1(312) 996-8249. Fax: +1(312) 996-0808. E-mail: liuying@uic.edu.

Author Contributions

Experiments were conducted by A.J.D and J.K. and were designed and interpreted by Y.L., A.J.D, J.K., S.A.S., and J.H.M. Polyphosphates were prepared by S.A.S. The manuscript was composed by A.J.D. and Y.L. with editorial contributions from S.A.S. and J.H.M. All authors have given approval to the final version of the manuscript.

Notes

The authors declare no competing financial interest.

ACKNOWLEDGMENTS

The authors would like to extend their gratitude to Dr. Alan Nicholls and Linda Juarez of the UIC Research Resource Center for their excellent technical assistance with transmission electron microscopy characterization. The study was sponsored by the U.S. Army Medical Research and Material Command (Grant WQ81XWH-11-2-0021). The U.S. Army Medical Research Acquisition Activity, 820 Chandler Street, Fort Detrick MD 21702-5014 is the awarding and administering acquisition office. The contents of this article do not necessarily reflect the position or the policy of the government, and no official endorsement should be inferred.

REFERENCES

(1) Morrissey, J. H.; Choi, S. H.; Smith, S. A. *Blood* **2012**, *119* (25), 5972−5979.
(2) Shi, X. B.; Rao, N. N.; Kornberg, A. *Proc. Natl. Acad. Sci. U.S.A.* **2004**, *101* (49), 17061−17065.
(3) Kim, K. S.; Rao, N. N.; Fraley, C. D.; Kornberg, A. *Proc. Natl. Acad. Sci. U.S.A.* **2002**, *99* (11), 7675−7680.
(4) Rashid, M. H.; Rao, N. N.; Kornberg, A. *J. Bacteriol.* **2000**, *182* (1), 225−227.
(5) Brown, M. R. W.; Kornberg, A. *Proc. Natl. Acad. Sci. U.S.A.* **2004**, *101* (46), 16085−16087.
(6) Reusch, R. N.; Huang, R. P.; Bramble, L. L. *Biophys. J.* **1995**, *69* (3), 754−766.
(7) Fleischer, B.; Xie, J. P.; Mayrleitner, M.; Shears, S. B.; Palmer, D. J.; Fleischer, S. *J. Biol. Chem.* **1994**, *269* (27), 17826−17832.
(8) Kornberg, A.; Rao, N. N.; Ault-Riche, D. *Annu. Rev. Biochem.* **1999**, *68*, 89−125.
(9) Smith, S. A.; Mutch, N. J.; Baskar, D.; Rohloff, P.; Docampo, R.; Morrissey, J. H. *Proc. Natl. Acad. Sci. U.S.A.* **2006**, *103* (4), 903−908.
(10) Smith, S. A.; Morrissey, J. H. *Blood* **2008**, *112* (7), 2810−2816.
(11) Muller, F.; Mutch, N. J.; Schenk, W. A.; Smith, S. A.; Esterl, L.; Spronk, H. M.; Schmidbauer, S.; Gahl, W. A.; Morrissey, J. H.; Renne, T. *Cell* **2009**, *139* (6), 1143−1156.
(12) Choi, S. H.; Smith, S. A.; Morrissey, J. H. *Blood* **2011**, *118* (26), 6963−6970.
(13) Smith, S. A.; Morrissey, J. H. *J. Thromb. Haemost.* **2008**, *6* (10), 1750−1756.
(14) Smith, S. A.; Choi, S. H.; Davis-Harrison, R.; Huyck, J.; Boettcher, J.; Rienstra, C. M.; Morrissey, J. H. *Blood* **2010**, *116* (20), 4353−4359.
(15) Kornberg, A. *J. Bacteriol.* **1995**, *177* (3), 491−496.
(16) Docampo, R.; de Souza, W.; Miranda, K.; Rohloff, P.; Moreno, S. N. J. *Nat. Rev. Microbiol.* **2005**, *3* (3), 251−261.
(17) Docampo, R.; Moreno, S. N. J. *Parasitol. Today* **1999**, *15* (11), 443−448.
(18) Ruiz, F. A.; Lea, C. R.; Oldfield, E.; Docampo, R. *J. Biol. Chem.* **2004**, *279* (43), 44250−44257.
(19) Renne, T.; Schmaier, A. H.; Nickel, K. F.; Blomback, M.; Maas, C. *Blood* **2012**, *120* (22), 4296−4303.
(20) Jensen, T. E.; Baxter, M.; Rachlin, J. W.; Jani, V. *Environ. Pollut. A* **1982**, *27* (2), 119−127.
(21) Holmsen, H.; Weiss, H. J. *Annu. Rev. Med.* **1979**, *30*, 119−134.
(22) Bonting, C. F. C.; Kortstee, G. J. J.; Boekestein, A.; Zehnder, A. J. B. *Arch. Microbiol.* **1993**, *159* (5), 428−434.
(23) Monteiro, V. A. D.; de Souza, E. F.; de Azevedo, M. M. M.; Galembeck, F. *J. Colloid Interface Sci.* **1999**, *217* (2), 237−248.
(24) Momeni, A.; Filiaggi, M. J. *J. Non-Cryst. Solids* **2013**, *382*, 11−17.
(25) Momeni, A.; Filiaggi, M. J. *Langmuir* **2014**, *30* (18), 5256−5266.
(26) Einstein, A. *Ann. Phys.* **1906**, *19* (2), 289−306.
(27) Mui, B.; Chow, L.; Hope, M. J. *Methods Enzymol.* **2002**, *367*, 3−14.
(28) Sjoholm, I.; Ekman, B.; Kober, A.; Ljungstedtpahlman, I.; Seiving, B.; Sjodin, T. *Mol. Pharmacol.* **1979**, *16* (3), 767−777.
(29) Van Slyke, D. D.; Hastings, A. B.; Hiller, A.; Sendroy, J. *J. Biol. Chem.* **1928**, *79* (2), 769−780.
(30) Pedersen, K. O. *Scand. J. Clin. Lab. Inv.* **1972**, *30* (1), 89−94.
(31) Pedersen, K. O. *Scand. J. Clin. Lab. Inv.* **1972**, *29* (4), 427−432.
(32) Pedersen, K. O. *Scand. J. Clin. Lab. Inv.* **1971**, *28* (4), 459−469.
(33) Foghandersen, N. *Clin. Chem.* **1977**, *23* (11), 2122−2126.
(34) Pedersen, K. O. *Scand. J. Clin. Lab. Inv.* **1972**, *29* (1), 75−83.
(35) Masuoka, J.; Saltman, P. *J. Biol. Chem.* **1994**, *269* (41), 25557−25561.
(36) Axelsson, I. *J. Chromatogr.* **1978**, *152* (1), 21−32.
(37) Squire, P. G.; Moser, P.; O'Konski, C. T. *Biochemistry* **1968**, *7* (12), 4261−4272.
(38) Zieve, P. D.; Gamble, J. L., Jr.; Jackson, D. P. *J. Clin. Invest.* **1964**, *43*, 2063−2069.
(39) Samuel, M.; Pixley, R. A.; Villanueva, M. A.; Colman, R. W.; Villanueva, G. B. *J. Biol. Chem.* **1992**, *267* (27), 19691−19697.
(40) Corretge, E.; Nigretto, J. M. *Thromb. Res.* **1990**, *59* (3), 463−473.
(41) Silverberg, M.; Diehl, S. V. *Biochem. J.* **1987**, *248* (3), 715−720.

Publication 4

Medicinal Chemistry

International Edition: DOI: 10.1002/anie.201409639
German Edition: DOI: 10.1002/ange.201409639

Clotting Activity of Polyphosphate-Functionalized Silica Nanoparticles**

Damien Kudela, Stephanie A. Smith, Anna May-Masnou, Gary B. Braun, Alessia Pallaoro, Chi K. Nguyen, Tracy T. Chuong, Sara Nownes, Riley Allen, Nicholas R. Parker, Hooman H. Rashidi, James H. Morrissey,* and Galen D. Stucky**

Abstract: *We present a silica nanoparticle (SNP) functionalized with polyphosphate (polyP) that accelerates the natural clotting process of the body. SNPs initiate the contact pathway of the blood-clotting system; short-chain polyP accelerates the common pathway by the rapid formation of thrombin, which enhances the overall blood-clotting system, both by accelerating fibrin generation and by facilitating the regulatory anticoagulation mechanisms essential for hemostasis. Analysis of the clotting properties of bare SNPs, bare polyP, and polyP-functionalized SNPs in plasma demonstrated that the attachment of polyP to SNPs to form polyP-SNPs creates a substantially enhanced synergistic effect that lowers clotting time and increases thrombin production at low concentrations. PolyP-SNP even retains its clotting function at ambient temperature. The polyP-SNP system has the potential to significantly improve trauma-treatment protocols and outcomes in hospital and prehospital settings.*

Controlling hemorrhage is a major focus in the treatment and stabilization of many trauma patients. Uncontrolled blood loss is the leading cause of battlefield deaths, even though less than 5% of soldiers who subsequently reach a hospital die of their wounds.[1] In civilian hospitals, hemorrhage results in 15–25% of trauma deaths.[2] These data suggest that treatment should focus on stopping bleeding prior to hospital arrival. Bleeding management is currently aimed at volume resuscitation and surgical intervention to limit blood loss.[3] However, these measures often do not address the source or mechanism of the bleeding and ultimately can limit the possible options to control it, especially in the prehospital setting.

Currently, there are three major approaches for controlling prehospital hemorrhage. The oldest method employs mechanical devices that compress the wound to minimize the area through which blood can escape the damaged vessel.[4] Agents such as kaolin or chitosan (Figure 1) are useful as field therapeutics for the management of external hemorrhage and are widely utilized by military forces as a first-response treatment.[5,6] However, these compounds cannot be administered systemically and therefore lack utility for internal injuries with an intrinsic noncompressible hemorrhage.

Recombinant human factor VIIa (rFVIIa) is currently licensed for the management of bleeding episodes in patients with hemophilia and certain cases of warfarin overanticoagulation. Off-label use of rFVIIa is also commonly seen in certain other hemorrhagic conditions.[7] Although anecdotal reports of clinical response abound, a significant number of concerns regarding safety remain owing to reported thrombotic complications.[7] Drug-storage requirements and the

[*] D. Kudela, A. May-Masnou, A. Pallaoro, C. K. Nguyen, T. T. Chuong, S. Nownes, R. Allen, Prof. G. D. Stucky
Department of Chemistry and Biochemistry
University of California, Santa Barbara
Santa Barbara, CA 93106 (USA)
E-mail: dkudela@chem.ucsb.edu
stucky@chem.ucsb.edu

S. A. Smith, Prof. J. H. Morrissey
Department of Biochemistry, College of Medicine
University of Illinois at Urbana-Champaign
Urbana, IL 61801 (USA)
E-mail: jhmorris@illinois.edu

A. May-Masnou
Departament d'Enginyeria Química, Universitat de Barcelona
c/Martí i Franquès, 1–11, 08028 Barcelona, Catalunya (Spain)

G. B. Braun
Sandford-Burnham Medical Research Institute
10901 North Torrey Pines Road, La Jolla, CA 92037 (USA)

N. R. Parker
Department of Mechanical Engineering
University of California, Santa Barbara

Prof. H. H. Rashidi
Department of Pathology and Laboratory Medicine
University of California, Davis, Sacramento, CA 95817 (USA)

Prof. G. D. Stucky
Materials Department, University of California, Santa Barbara

[**] This research was funded by the US Army Medical Research and Material Command under Contract Number WQ81XWH-11-2-0021, by the US Army Medical Research and Materiel Command and the Telemedicine and Advanced Technology Research Center under Contract Number W911NF-10-2-0114, and by NIH grant R01 HL047014. Partial support was provided by the Institute for Collaborative Biotechnologies grant W911NF-09-0001 from the U.S. Army Research Office. The content of the information does not necessarily reflect the position or the policy of the Government, and no official endorsement should be inferred. The MRL Shared Experimental Facilities are supported by the MRSEC Program of the NSF under Award No. DMR 1121053; a member of the NSF-funded Materials Research Facilities Network. A.M.-M. thanks the Spanish MINECO for financial support within the framework of project number CTQ2011-29336-C03-02.

Supporting information for this article, including experimental details of the synthesis and characterization of all new compounds as well as clotting assays, is available on the WWW under http://dx.doi.org/10.1002/anie.201409639.

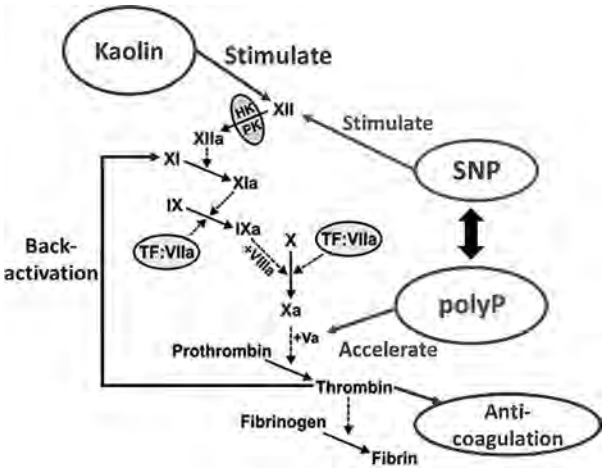

Figure 1. Simplified coagulation cascade. The SNP surface induces the activation of FXII, whereas short-chain polyP enhances the rates of activation of FV and FXI, thus leading to an earlier thrombin burst. Rapid thrombin generation leads to back-activation of FXIa to accelerate the coagulation cascade and facilitate increased activity in the anticoagulation pathway, which is designed to limit the spread of coagulation to uninjured vessels. Kaolin acts only to activate FXII through the intrinsic pathway.

extreme cost of recombinant-protein medication further limit field use.[8]

The ideal agent to control noncompressible hemorrhage in the prehospital setting would have the following properties: 1) long shelf life and stability in weather extremes, 2) reasonable cost, 3) promotion of key functions of the blood-clotting system at the injury site through the common pathway, including coagulation, regulatory anticoagulation, and fibrin formation, and 4) lack of off-target adverse effects. Such an agent could initiate treatment during the transport phase when the patient is at the greatest risk for exsanguination. We propose that targeted short-chain-polyphosphate-laden silica nanoparticles (polyP-SNPs) have the potential to fulfill these requirements.

Because it accelerates through the common pathway the key functions of the blood-clotting system rather than initiating endogenous-coagulation-enzyme production, short-chain polyP is a reasonable candidate for the management of hemorrhage.[9] The delivery of a polyP payload on a nanoparticle carrier could potentially be optimized to target the site of injury while minimizing the impact on the systemic circulation. Effective targeting and control would in theory minimize the risk of thrombotic complications that limit procoagulant therapy. Besides the potential for better biosystem safety, the production cost for polyP is low as compared to that of recombinant proteins. Upon attachment to inorganic oxides, polyP also has the potential for long-term stability under a variety of storage conditions.

In response to an injury, human platelets secrete short-chain polyP of approximately 60–100 monomers. Platelet-secreted polyP has a variety of wound-healing therapeutic effects, including enhanced activation of factors XI and V, which ultimately leads to enhanced factor X activity, and limitation of the activity of tissue factor pathway inhibitor, thus resulting in accelerated thrombin generation.[10] The incorporation of polyP also impacts clot structure and leads to resistance to fibrinolysis.[11] As a result of the approximately 90 min half-life of polyP in plasma, the procoagulant effects are temporally limited.[10–12] This endogenous metabolism of polyP offers much better biocompatibility than currently available agents, such as kaolin, which are not metabolized.

Whereas long-chain polyP is a potent activator of the contact pathway, short-chain polyP released from platelets has a relatively poor capacity to activate factor XII.[9] We employed polyP with a relatively short chain length for these studies to maximize the enhancement of downstream coagulation enzymatic steps (common pathway), while minimizing contact-pathway activation.

As noted above, platelets serve as a polyP-delivery agent, secrete procoagulants and clotting factors that promote blood coagulation, and initiate the formation of a clot-dissolving enzyme that degrades blood clots during the healing process. In our studies following up on the extensive research originally carried out by the Morrissey group,[9–12] we used free polyP as a benchmark. In the research we report herein, delivery-agent bifunctionality is introduced by using SNPs as a procoagulant carrier for the polyP.

Silica is generally considered to be a nontoxic material, and it is often used in drug-delivery studies.[13] However, owing to its negative surface charge, silica is also a contact activator.[5a,14] Consequently, the ideal construction of a polyP-bearing silica nanoparticle would shield the silica from exposure to the systemic circulation, with targeting and exposure of the silica carrier surface and polyP at the site of internal hemorrhage. Current materials used for treating external hemorrhage generally contain particles in the micrometer range, which are too large to readily traverse capillaries and unsuitable for use as intravenous therapeutics.[15] We consequently developed an approach for the synthesis of particles with a diameter of 50–100 nm (Figure 2a, Table 1).[5a,15]

Table 1: ζ potential and surface charge of the particles when dispersed in water or phosphate-buffered saline solution (pH 7.4).

Compound, medium[a]	ζ potential [μV]	Size [nm]
SNPs, H_2O	-24.4 ± 0.3	55.97 ± 2.19
SNPs, PBS	-52.5 ± 2.1	74.00 ± 6.24
PolyP-SNPs, H_2O	-44.3 ± 0.3	53.79 ± 1.75
PolyP-SNPs, PBS	-52.0 ± 3.2	78.18 ± 2.86

To attach the highly anionic polyP to an oxide, we followed the model of Lorenz et al., who used zirconia, which like silica has a negative surface potential, as the scaffold for applications in protein separation and purification.[16] This attachment strategy exploits the Lewis acid properties of an oxide surface to bind polyP, thus overcoming the electrostatic repulsion.[17]

^{31}P NMR spectroscopy and the change in surface charge qualitatively demonstrated polyP attachment. PolyP-SNPs were digested in acid to break down polyP into phosphate monomers. ^{31}P NMR spectroscopic tests on the digested

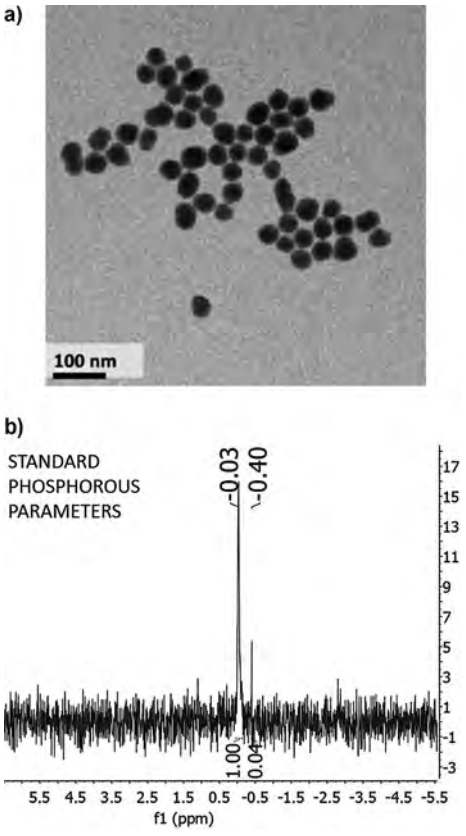

Figure 2. a) TEM images of polyP-SNPs. b) ^{31}P NMR spectrum of digested polyP-SNPs showing evidence of phosphorous.

sample detected the presence of phosphorous. The change in surface charge also suggested the presence of polyP in undigested polyP-SNPs (Table 1; see Figure 2 in the Supporting Information). Under physiological pH conditions in phosphate-buffered saline solution (PBS), both SNPs and polyP displayed a negative surface charge. In deionized water, the SNP surface charge ranged from −15 to −25 mV (Table 1; see Figure 2 in the Supporting Information). In simulated body fluid (SBF) under physiological pH conditions, SNPs had a surface charge between −50 and −60 mV. PolyP is negatively charged at this pH value as a result of a pK_{a1} value between pH 1 and 2 (for all internal phosphates) and a pK_{a2} value between pH 7.2 and 8.2 (for the two terminal phosphates).[18] Upon functionalization of the SNP surface with polyP, the ζ potential of the nanoparticles decreased from −20 to −30 mV to roughly −40 to −50 mV in water, thus confirming the attachment of the polyP. In SBF, both types of particles exhibited a strongly negative charge below −45 mV.

To quantify the polyP loaded on the SNP surface, we examined the digested phosphate solutions with a malachite green assay and by inductively coupled plasma atomic emission spectroscopy (ICP-AES). Malachite green identified PO_3 concentrations of 56, 26, and 23 nmol per milligram of SNPs. ICP-AES indicated that the 26 nmol PO_3 sample had a PO_3 concentration of 29.6 nmol per milligram of SNPs. Assuming each polyP chain has 70 PO_3 monomers, these data suggest 100–200 polyP molecules are attached to each SNP.

By not using tissue factor to initiate clotting, we focused our clotting assays on the intrinsic (common) and the contact activation pathways. Negatively charged particles, such as the aluminosilicate kaolin (QuikClot Combat Gauze) used for external injuries, activate the contact pathway.[4,5a] Because polyP is a poor clot initiator, polyP attachment shields SNPs in the systemic circulation, which is beneficial for intravenous control of haemorrhage. We measured the impact of both bare SNPs and polyP-SNPs on clot time by thromboelastography (TEG) on pooled normal plasma (PNP; Figure 3a; see

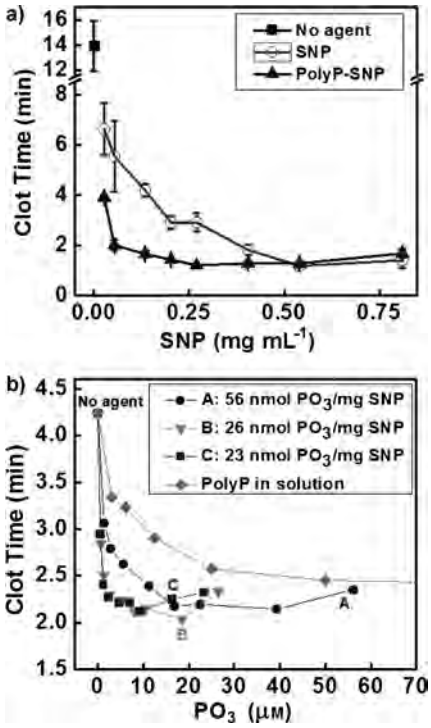

Figure 3. a) Graph showing that polyP-SNPs cut clot time (*R* value by TEG) roughly by half relative to that observed with bare SNPs below 0.3 mg mL^{-1}. b) Graph showing that polyP loaded onto silica lowers clot time relative to that observed with bare polyP, as measured by fibrometry.

Figures 4 and 5 in the Supporting Information). Both particles decreased the time to initial clot formation (*R*) in a concentration-dependent manner; however, polyP-SNP was more potent at concentrations below 0.5 mg mL^{-1}. The clot time reported in Figures 3 and 5 refers to the time to initial clot formation, which is key in illustrating how polyP-SNP successfully accelerates clotting. The agent used did not affect the overall size of the clot formed, only the time required to reach peak clot size. However, polyP has previously been shown to improve overall clot formation, in part by limiting the effect of fibrinolysis in plasma containing tissue plasminogen activator.[11,12]

Next we evaluated the procoagulant activity of polyP-SNPs formed with differing loads of polyP. The ability to promote coagulation was measured by adding polyP-SNP or polyP in solution to PNP. Coagulation was evaluated by measuring the time to clot formation on a fibrometer (Fig-

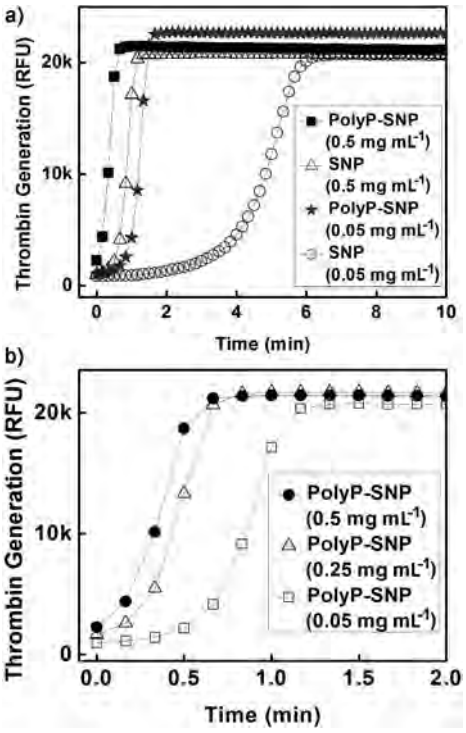

Figure 4. a) Graph showing that thrombin generation is more rapid with polyP-SNPs than with bare SNPs. b) Graph showing that polyP-SNPs are able to generate a rapid thrombin burst even at low concentrations. Thrombin generation was measured by the use of a thrombin-sensitive fluorescent dye.

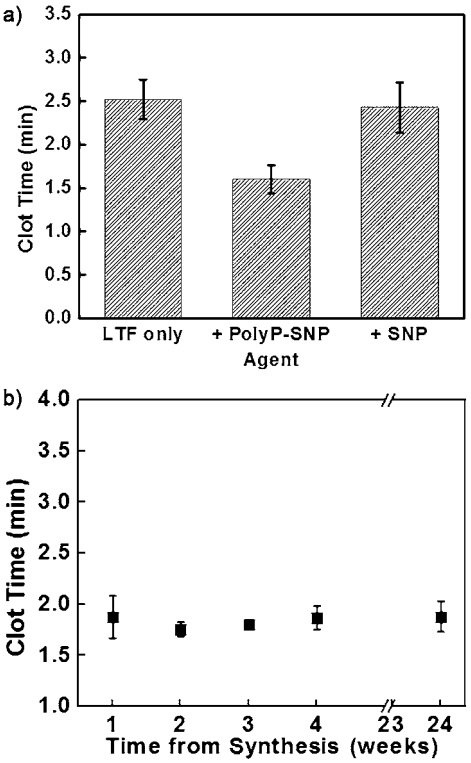

Figure 5. a) Graph showing that the addition of polyP-SNPs to LTF shortens clot time in FXII-deficient plasma relative to that observed with LTF only or LTF + SNP. LTF is required to initiate clotting. b) Graph showing that polyP-SNPs suspended in aqueous solution retained their procoagulant function after weeks of storage under ambient conditions.

ure 3b). In comparing the polyP payload, polyP-SNPs were more potent at activating the contact pathway than polyP in solution.

To further explore the relative activities of our materials, we evaluated the ability of the materials to generate thrombin, the terminal enzyme of the coagulation cascade and the primary determinant of the rate of fibrin formation.[19] PolyP-SNP again substantially outperformed its bare counterpart (Figure 4a).

We next evaluated whether polyP-SNPs were able to enhance the generation of downstream coagulation enzymes (common pathway). We eliminated any potential impact on contact activation by utilizing factor XII deficient plasma and initiating coagulation with a small amount of relipidated tissue factor (LTF, 63 pM). As expected, bare SNPs did not affect TEG clot time in this system (Figure 5a). In contrast, polyP-SNP did shorten the time to physical clot formation. This result indicates that the polyP is accessible for binding to the relevant downstream coagulation proteins. Additionally, this response could also be evaluated in the clinical setting by comparing tests such as prothrombin time (PT) and partial thromboplastin time (PTT).

One of the problems facing emergency medical personnel is that current intravenous treatments have a significantly short half-life at ambient temperature. Even pure polyP nanoparticles remain stable for hours.[9b] In comparison, the attachment of polyP to silica greatly enhanced the stability and procoagulant function of polyP from hours to weeks. After bench-top storage at room temperature as both a powder and an aqueous suspension, polyP-SNP clotting times remained constant for weeks (Figure 5b). The strong negative surface charge of polyP-SNPs also minimized aggregation in aqueous suspensions over the same time period. Injectable drugs with a long shelf life can be used by emergency medical personnel prior to hospital arrival without concern that the particles will degrade without refrigeration. Thus, the polyP-SNP system could become the first prehospital intravenous injection designed to treat internal injuries by accelerating the clotting system at bleeding sites.

In this study, we successfully attached polyP to the surface of small-diameter SNPs and demonstrated that these polyP-SNPs are more potent than bare SNPs at promoting coagulation, probably owing to the ability of polyP to accelerate the common pathway for active clotting processes. PolyP-SNPs, like polyP in solution, are able to enhance downstream coagulation reactions, thus resulting in a shorter time to clot formation. Even after long-term storage at regular room temperature, the polyP-SNP system retained its procoagulant ability. The polyP-SNP construct is consequently promising as a prohemostatic agent. Further exploration of methods to limit contact activation in vivo will be necessary for its use as a systemic agent.

Keywords: hemorrhage · nanoparticles · polyphosphates · silicates · trauma

How to cite: *Angew. Chem. Int. Ed.* **2015**, *54*, 4018–4022
Angew. Chem. **2015**, *127*, 4090–4094

[1] a) J. B. Holcomb, N. R. McMullin, L. Pearse, J. Caruso, C. E. Wade, L. Oetjen-Gerdes, H. R. Champion, M. Lawnick, W. Farr, S. Rodriguez, F. K. Butler, *Ann. Surg.* **2007**, *245*, 986–991; b) R. F. Bellamy, *Mil. Med.* **1984**, *149*, 55–62; c) H. R. Champion, R. F. Bellamy, C. P. Roberts, A. J. Leppaniemi, *Trauma* **2003**, *54*, S13–S19.
[2] R. Pfeifer, I. S. Tarkin, B. Rocos, H.-C. Pape, *Injury* **2009**, *40*, 907–911.
[3] P. I. Johansson, J. Stensballe, *Transfusion* **2010**, *50*, 701–710.
[4] B. S. Kheirabadi, I. B. Terrazas, M. A. Hanson, J. F. Kragh, Jr., M. A. Dubick, L. H. Blackbourne, *J. Trauma. Acute. Care. Surg.* **2013**, *74*, 1260–1265.
[5] a) S. E. Baker, A. M. Sawvel, N. Zheng, G. D. Stucky, *Chem. Mater.* **2007**, *19*, 4390–4392; b) D. Johnson, B. Gegel, J. Burgert, J. Gasko, C. Cromwell, M. Jaskowska, R. Steward, A. Taylor, *ISRN Emerg. Med.* **2012**, *2012*, 927678.
[6] a) B. G. Kozen, S. J. Kircher, J. Henao, F. S. Godinez, A. S. Johnson, *Acad. Emerg. Med.* **2008**, *15*, 74–81; b) Y. Li, A. M. Sawvel, Y.-S. Jun, S. Nownes, M. Ni, D. Kudela, G. D. Stucky, D. Zink, *Toxicol. Res.* **2013**, *2*, 136–144; c) P. D. Bowman, X. Wang, M. A. Meledeo, M. A. Dubick, B. S. Kheirabadi, *J. Trauma* **2011**, *71*, 727–732.
[7] J. F. Barletta, C. L. Ahrens, J. G. Tyburski, R. F. Wilson, *J. Trauma* **2005**, *58*, 646–651.
[8] P. M. Mannucci, M. E. Mancuso, E. Santagostino, *Blood* **2012**, *119*, 4108–4114.
[9] a) S. A. Smith, S. H. Choi, R. Davis-Harrison, J. Huyck, J. Boettcher, C. M. Rienstra, J. H. Morrissey, *Blood* **2010**, *116*, 4353–4359; b) A. J. Donovan, J. Kalkowski, S. A. Smith, J. H. Morrissey, Y. Liu, *Biomacromolecules* **2014**, *15*, 3976–3984.
[10] S. A. Smith, J. H. Morrissey, *J. Thromb. Haemostasis* **2008**, *6*, 1750–1756.
[11] S. A. Smith, J. H. Morrissey, *Blood* **2008**, *112*, 2810–2816.
[12] S. A. Smith, N. J. Mutch, D. Baskar, P. Rohloff, R. Docampo, J. H. Morrissey, *Proc. Natl. Acad. Sci. USA* **2006**, *103*, 903–908.
[13] a) V. Cauda, H. Engelke, A. Sauer, D. Arcizet, C. Brauchle, J. Radler, T. Bein, *Nano Lett.* **2010**, *10*, 2484–2492; b) D. Tarn, C. E. Ashley, M. Xue, E. C. Carnes, J. I. Zink, C. J. Brinker, *Acc. Chem. Res.* **2013**, *46*, 792–801.
[14] J. Margolis, *J. Exp. Biol.* **1961**, *39*, 249–258.
[15] N. Singh, A. Karambelkar, L. Gu, K. Lin, J. S. Miller, C. S. Chen, M. J. Sailor, S. N. Bhatia, *J. Am. Chem. Soc.* **2011**, *133*, 19582–19585.
[16] B. Lorenz, S. Marmé, W. E. G. Müller, K. Unger, H. C. Schröder, *Anal. Biochem.* **1994**, *216*, 118–126.
[17] W.-C. J. Wei, S.-C. Wang, F.-Y. Ho, *J. Am. Ceram. Soc.* **1999**, *82*, 3385–3392.
[18] A. Lee, G. M. Whitesides, *Anal. Chem.* **2010**, *82*, 6838–6846.
[19] a) T. Myles, T. H. Yun, S. W. Hall, L. L. K. Leung, *J. Biol. Chem.* **2001**, *276*, 25143–25149; b) Y. Xiao, A. A. Lubin, A. J. Heeger, K. W. Plaxco, *Angew. Chem. Int. Ed.* **2005**, *44*, 5456–5459; *Angew. Chem.* **2005**, *117*, 5592–5595.

Received: September 30, 2014
Revised: December 19, 2014
Published online: January 29, 2015

Publication 5

Bioconjugate Chemistry

Article

pubs.acs.org/bc

Colloidal Confinement of Polyphosphate on Gold Nanoparticles Robustly Activates the Contact Pathway of Blood Coagulation

Magdalena Szymusiak,[#,†] Alexander J. Donovan,[#,†] Stephanie A. Smith,[‡] Ross Ransom,[†] Hao Shen,[†] Joseph Kalkowski,[†] James H. Morrissey,[‡] and Ying Liu*[,†,§]

[†]Department of Chemical Engineering and [§]Department of Biopharmaceutical Sciences, University of Illinois at Chicago, Chicago, Illinois 60607, United States

[‡]Department of Biochemistry, University of Illinois at Urbana−Champaign, Urbana, Illinois 61801, United States

Supporting Information

ABSTRACT: Platelet-sized polyphosphate (polyP) was functionalized on the surface of gold nanoparticles (GNPs) via a facile conjugation scheme entailing EDAC (*N*-(3-(dimethylamino)propyl)-*N*′-ethylcarbodiimide hydrochloride)-catalyzed phosphoramidation of the terminal phosphate of polyP to cystamine. Subsequent reduction of the disulfide moiety allowed for anchoring to the colloidal surface. The ability of the synthesized polyP-GNPs to initiate the contact pathway of clotting in human pooled normal plasma (PNP) was then assayed by quantifying changes in viscous, mechanical, and optical properties upon coagulation. It is revealed that the polyP-GNPs are markedly superior contact activators compared to molecularly dissolved, platelet-sized polyP (of equivalent polymer chain length). Moreover, the particles' capacity to mobilize Factor XII (FXII) and its coactivating proteins appear to be identical to very-long-chain polyP typically found in bacteria. These data imply that nanolocalization of anionic procoagulants on colloidal surfaces, achieved through covalent anchoring, may yield a robust contact surface with the ability to sufficiently cluster active clotting factors together above their threshold concentrations to cease bleeding. The polyP-GNPs therefore serve as a promising foundation in the development of a nanoparticle hemostat to treat a range of hemorrhagic scenarios.

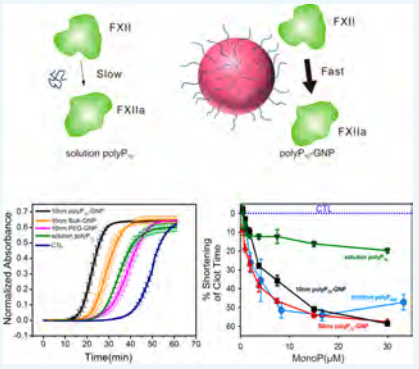

INTRODUCTION

Polyphosphate (polyP) is an inorganic linear macromolecule consisting of orthophosphates connected by phosphoanhydride bonds.[1] The prevailing thought in the biochemistry community for decades contended that polyP was an early evolutionary casualty in Nature's endeavor to design information-dense, multifunctional biomacromolecules.[2] Arthur Kornberg and others[3] in the last two decades have reasserted polyP's significant role in a multitude of organismal processes blurring across taxonomic boundaries: the polymer possesses potent hemostatic, inflammatory, and thrombotic properties,[4−7] hinders tumor growth and angiogenesis,[8] modulates bacterial pathogenicity,[9] chelates toxic metals,[10] aids in DNA transport,[11] and directs histological differentiation,[12,13] among innumerable other functions. PolyP arguably performs its variegated cellular duties, even with its simple polyphosphoanhydride chemistry, by adopting different macrostructures depending on polymer length, local environment, and incoming stimuli similar (but perhaps on a much more rudimentary level) to the plethora of possible tertiary structures encountered with polypeptides. Some prokaryotes surface-pattern long-chain polyPs at varying surface densities on their exterior, with the polymer projecting outward from the cell membrane into their surroundings. For example, the human infectious agents *N. meningitditis* and *N. gonorrheae*, responsible for bacterial meningitis and gonorrhea, respectively, derive their resilience and virulence in large part from storing a significant fraction of their inorganic phosphate as high-molecular-weight polyP on their capsules.[14] The intensely anionic charge density on the exterior is hypothesized to confer protection from a myriad of environmental insults. DoCampo and co-workers discovered condensed polyP on the nanometer-scale in several protozoan species known to infect insects, notably *T. cruzi* and *T. brucei*, in spherical, mildly acidic organelles called acidocalcisomes,[15] colocalized with concentrations of metal ions at levels orders of magnitude higher than in the cytosol. More recently, short-chain polyP has been found in nearly identical subcellular compartments called dense granules in human platelets.[16] We recently established that polyP spontaneously self-assembles into granular nanoparticles in aqueous media containing concentrations of divalent metal cations such as Ca^{2+} and Mg^{2+}, at levels normally found in human blood plasma.[17] The nanoprecipitation is a thermodynamic process governed by the polyP polymer size and the metal ion concentration, with the salt concentration controlling the nanoparticle diameter regardless of polymer supersaturation ratio.[17]

Considerable effort in recent years has centered on implementing novel conjugation chemistries for modifying

Received: September 26, 2015
Revised: November 20, 2015

DOI: 10.1021/acs.bioconjchem.5b00524
Bioconjugate Chem. XXXX, XXX, XXX−XXX

polyP with various moieties, e.g., fluorescent dyes, biotin, chromogenic substrates, or primary amines, and attaching the polymer to solid substrates for facilitating in vitro and in vivo detection, quantitating interactions with various binding partners like thrombin, Factor XIIa (FXIIa), Factor XIa (FXIa), and kallikrein, and preventing or slowing enzymatic degradation.[18,19] Phosphoramidation of the terminal phosphates does not abrogate polyP's physiological functionality, and polyP attached to solid supports retains robust procoagulant ability.[18]

The fact that polyP can exist in a variety of physical manifestations, be it molecularly dissolved, surface-immobilized, granular, or even supported on a colloidal particle scaffold, suggests that these forms might manifest differential procoagulant properties. The varied ability of inorganic polyP to initiate the contact pathway of blood coagulation could be interpreted to substantiate this hypothesis. It has been previously demonstrated that polyP exerts differential clotting effects as a function of polymer length,[6] with high-molecular-weight polymers serving as powerful activators of the contact pathway, while intermediate and platelet-sized polyP are less potent contact activators. These shorter polymers are procoagulant through mechanisms impacting enzymes and inhibitors of other portions of the coagulation cascade.[4,7] It has been shown that negatively charged surfaces are necessary to initiate the contact pathway of blood coagulation.[20] Foreign colloidal particles like ellagic acid[21] and silicate minerals[22] and highly anionic polymers of sufficient molecular weight like sulfated polysaccharides[23] present the FXII zymogen and its enzymatic binding partners (i.e., high-molecular-weight kininogen (HMWK) and prekallikrein) a sufficiently large nanosurface to trigger clotting. Sulfated polysaccharides such as heparin are generally considered powerful anticoagulants because of binding to antithrombin; however, in the absence of this enzyme inhibitor, we have previously demonstrated that heparin in actuality is a robust procoagulant molecule in many respects similar to polyP.[24] FXII has a molecular weight of 80 000 Da,[25] so its radius of gyration would be ~2−5 nm. As such, long-chain polyP should possess significant ability to activate the contact pathway due its high molecular weight and large surface area, with both the molecularly dissolved and nanoprecipitated forms arguably being large enough to activate FXII. On the other hand, the ability of molecularly dissolved, short-chain polyP to initiate the contact pathway is a matter of some dispute.[26−28] Recent work by Mutch and colleagues provides evidence that platelet-sized polyP autoactivates FXII in vitro, with activity catalyzed by the presence of zinc cations.[29]

In the present investigation we demonstrate that polyP of approximately the size released from platelets conjugated to colloidal gold nanoparticles (GNPs) via phosphoramidate linkages is able to robustly activate the contact pathway of coagulation, with potency equivalent to that of molecularly dissolved, long-chain polyP like that predominately found in bacteria. With further functionalization, polyP−GNP conjugates may be potentially used for targeted delivery as procoagulant agents to the bleeding site, especially benefiting the first-aid treatment of internal hemorrhage. As polyP is already secreted upon platelet activation and naturally exists in the human body, it is anticipated that the introduction of a colloidally anchored polyP drug delivery vehicle would have minimal side effects compared to other foreign procoagulants. In order to achieve hemostasis, polyP concentrations typically approach the micromolar range in near-vascular injury sites and could potentially be much higher within a platelet-dense thrombus.[6] PolyP-GNPs could potentially be of use in the management of bleeding episodes and provide further corroboration that polyP is able to wield its divergent effects by manifesting in a myriad of macrostructural forms.

RESULTS AND DISCUSSION

Binding of $polyP_{70}$ to GNPs was achieved by two-stage reaction: (1) $PolyP_{70}$ was first allowed to react with cystamine. (2) The $polyP_{70}$-cystamine conjugate was then reacted with GNPs by replacing the citrate groups (Figure 1).

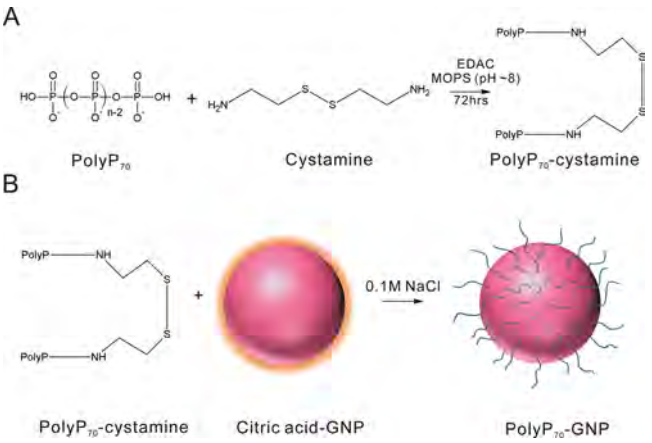

Figure 1. Process of synthesizing GNPs conjugated with $polyP_{70}$. (A) $PolyP_{70}$ is conjugated to cystamine. (B) $PolyP_{70}$-cystamine is attached to the surface of GNPs.

The primary amine-containing compounds like polyethylenimine, amine-PEG_2-biotin, and spermidine were used previously to study the covalent attachment of primary amine groups with the terminal phosphates of polyP via EDAC-mediated reaction.[18] We modified this method for the coupling of $polyP_{70}$ with cystamine—a disulfide molecule, containing two primary amine groups. Reduction of the disulfide moiety in cystamine then allowed for the attachment to the GNP surface. Reaction conditions (including temperature, reaction time, pH, and buffering environment) were optimized to control the coupling of $polyP_{70}$ with cystamine. For the optimal conditions, $polyP_{70}$ was allowed to react with cystamine at room temperature and pH around 8 for 48 to 72 h. Higher temperature (37 °C) did not improve the yield. A fluorescamine assay was used to test the amount of the unreacted primary amines on cystamine, which indicated the conjugation efficiency. The highest yield of the reaction was approximately 90% as seen in Table 1.

An investigation of P−N bond hydrolysis was carried out to test the stability of the $polyP_{70}$-cystamine ligand. After 72 h of reaction, a fluorescamine assay was performed to detect the concentration of the unreacted cystamine. The samples were monitored for 2 weeks and hydrolysis of the P−N bonds was quantified. The P−N bond hydrolyzed in acidic conditions at pH 6.02. It was stable at pH above 7 as presented in Table 2 below. These results were in good agreement with other literature data on P−N bond hydrolysis.[30−34]

The $polyP_{70}$-cystamine conjugate was allowed to react with GNPs of two different sizes (10 and 50 nm) by displacing the citrate group. After 24 h of reaction, salt addition was initiated to increase free GNP surface area available for $polyP_{70}$

DOI: 10.1021/acs.bioconjchem.5b00524
Bioconjugate Chem. XXXX, XXX, XXX−XXX

Table 1. Conjugation Efficiency of polyP$_{70}$ and Cystamine at Various pH Conditions

buffer	pH of reaction	efficiency (24 h)	efficiency (48 h)	efficiency (72 h)
MOPS (100 mM)	7.1	61.5%	65.0%	71.1%
MOPS (100 mM)	7.6	72.7%	74.3%	78.7%
MOPS (100 mM)	8.1	79.6%	87.3%	88.1%
MOPS (100 mM)	8.5	83.5%	87.3%	88.6%
MES (100 mM)	7.8	81.4%	89.5%	-

attachment.[35] The slow increase in salt concentration in the reaction over a period of 4 days (0.1 M NaCl final concentration) allowed the already attached polyP$_{70}$ to extend, creating more space for the unreacted ligands to access the gold surface, thus resulting in an increase in the number of polyP$_{70}$ chains per particle. The reaction conditions were modified from the conditions used to conjugate DNA on the surface of gold nanoparticles[35] and their detailed description is presented in the Experimental Procedures. The full coverage is estimated from the theoretical calculations based on the ideal maximum ligand density of 0.22 per square nanometer[36,37] and found to be 69 and 1727 for 10 and 50 nm GNPs, respectively. The maximized conjugation efficiencies were found to be 24.7% and 46.0% for 10 and 50 nm GNPs, respectively, comparing the number of conjugated ligands with the theoretical maxima.

Removal of excess, unreacted polyP$_{70}$ left in the solution was achieved via centrifugation. The detailed description of the centrifugation conditions and the centrifugation optimization experiments is provided in the Experimental Procedures and Supporting Information. After each centrifugation, the supernatant was removed and the pellets were resuspended with a buffer at pH 7.2 to ensure the stability of the polyP$_{70}$-cystamine ligand and prevent polyP$_{70}$ hydrolysis.

Morphology and stability of the polyP$_{70}$-GNPs were confirmed by TEM (Figure 2), revealing that the polyP$_{70}$-GNP dispersion is largely free of aggregation, and the morphology of the GNPs is indistinguishable from commercially available citrated gold suspensions, that being spherical and uniformly electron dense. High magnification micrographs of 10 nm polyP$_{70}$-GNPs reveal the recognizable atomic lattices of the particles, clearly suggesting that the GNPs are nanocrystals.

After purification using centrifugation, concentrations of polyP$_{70}$ were measured using the malachite green assay and concentrations of GNPs were obtained by UV−vis spectroscopy. The number of polyP$_{70}$ on the surface of GNPs was calculated on the basis of the above measurements. The following polyP$_{70}$-GNPs were synthesized and characterized (Table 3) to investigate their ability to initiate the contact pathway of blood coagulation in a concentration-dependent manner.

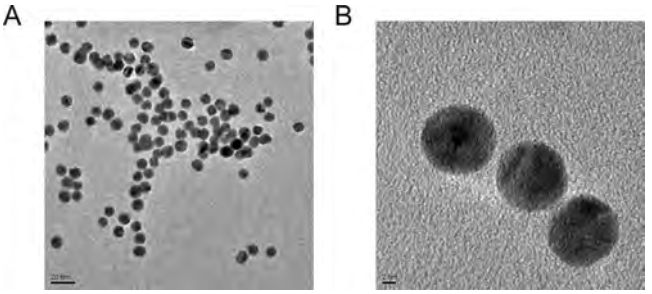

Figure 2. Typical transmission electron micrographs of 10 nm polyP$_{70}$-GNPs. (A) polyP$_{70}$-GNPs are spherical and largely free of aggregation several days after synthesis. Scale bar: 20 nm. (B) Trio of polyP$_{70}$-GNPs with the crystal lattices very apparent. Scale bar: 2 nm.

Table 3. Synthesized polyP$_{70}$-GNPs

sample	MonoP conc. (μM)	GNP conc. (nM)	number of polyP$_{70}$ chains per particle	UV−vis peak for bulk GNP	UV−vis peak after centrifuging
10 nm polyP$_{70}$-GNP	90	75.399	17.052	519	521
50 nm polyP$_{70}$-GNP	90	1.619	794.195	531	532

PolyP$_{70}$-GNPs markedly reduce the time of coagulation in human plasma when assayed for contact activity using a mechanical coagulometer, a standard technique to measure clotting of both whole blood and plasma (Figure 3). Molecularly dissolved polyP$_{70}$ and polyP$_{800}$ were added as a positive control to citrated pooled normal plasma (PNP) at monoP concentrations ranging from 0 to 30 μM. Clotting was initiated by adding excess $CaCl_2$. Concentration for polyP$_{70}$-GNPs is given in terms of moles of GNPs (not elemental gold). Reduction in clotting time for polyP$_{70}$-GNPs follows typical kinetics of a surface-modulated reaction mechanism,[38] suggesting that the polyP$_{70}$-GNPs provide a templating surface for FXII activation. PolyP$_{70}$-cystamine ligands conjugated to GNPs of 10- and 50-nm diameter robustly activate the contact pathway of coagulation much more efficiently as compared to polyP$_{70}$ in solution.

The clotting activity of both 10 and 50 nm polyP$_{70}$-GNPs is comparable to that of much longer polyP (polyP$_{800}$) and even greater at monoP concentrations exceeding 20 μM. These results raise the question that colloidal confinement of polyP may yield divergent outcomes in complex, nonlinear biological processes such as blood coagulation, where threshold concentrations of activators must be attained before a response is generated. In this instance, chemical conjugation of platelet-

Table 2. Free Cystamine Concentration (μM) before and after pH Adjustment

	primary amine concentration (μM)				
pH	before pH adjustment	after 1 day	after 5 days	after 8 days	after 13 days
6.02	16.4 ± 0.49	30.0 ± 0.68	26.4 ± 0.82	27.6 ± 0.17	37.18 ± 1.41
7.07	16.4 ± 0.49	18.6 ± 1.29	14.5 ± 0.31	12.9 ± 0.12	13.72 ± 0.78
9.05	16.4 ± 0.49	17.1 ± 0.85	14.8 ± 0.44	14.2 ± 0.26	15.31 ± 1.36
10.01	16.4 ± 0.49	17.2 ± 0.90	14.8 ± 0.28	12.7 ± 1.2	14.73 ± 0.10

DOI: 10.1021/acs.bioconjchem.5b00524
Bioconjugate Chem. XXXX, XXX, XXX−XXX

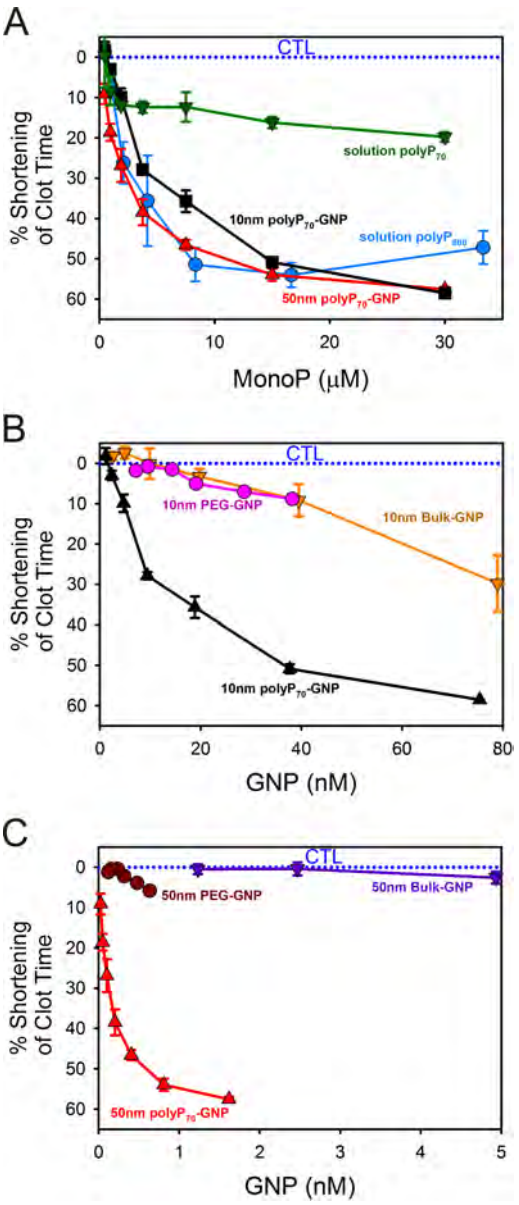

Figure 3. Shortening of clotting time of $polyP_{70}$-GNPs in human plasma when assayed for contact activation as a function of monoP and GNP concentration. (A) Reduction in clotting time of 10 nm $polyP_{70}$-GNPs and 50 nm $polyP_{70}$-GNPs compared to equivalent concentration of molecularly dissolved $polyP_{70}$ and heterogeneous long-chain $polyP_{800}$. (B) Reduction of clotting time of 10 nm $polyP_{70}$-GNPs compared to the equivalent concentration of 10 nm bulk-GNPs and 10 nm PEG-GNPs. (C) Shortening of clotting time of 50 nm $polyP_{70}$-GNPs compared against the same concentration of 50 nm bulk-GNPs and 50 nm PEG-GNPs.

sized polyP, itself a mediocre activator of the contact pathway, to an essentially inert colloidal surface, transforms the small polymer into an excellent contact activator comparable to polyP approximately ten times larger. Initiation of the contact pathway almost always necessitates a nanosurface of sufficient negative charge density and cross-sectional area to recruit the FXII zymogen. Subsequently, its fellow contact pathway components high-molecular-weight kininogen (HWMK) and prekallikrein must come in close proximity to FXII to accelerate and propagate the procoagulant stimulus. Anchoring highly anionic $polyP_{70}$ onto 10 and 50 nm GNPs likely generates such an activating surface for the triad of proteins, whereas short-chain polymers that are molecularly dissolved like platelet-sized $polyP_{70}$ do not have adequate radii of gyration to localize FXII, HMWK, and prekallikrein together into the primary complex and propagate the signal. As prekallikrein and HMWK have been found to have a complexed molecular weight of 285 kDa in plasma, a surface larger than 5 nm would most likely be required to properly anchor these proteins together with FXII.[39] Bacterial polyPs, typically several hundred to thousands of orthophosphate residues, have molecular weights and radii of gyration comparable to large globular proteins, suggesting that these polymers are already above this threshold size for anchoring the primary complex, given that they robustly initiate the contact pathway of clotting in a fashion similar to foreign colloidal procoagulant agents.[6] Long-chain polyP with robust contact-pathway activity can accordingly be used as a ruler for the measurement of hemostatic activity of $polyP_{70}$-GNPs and molecularly dissolved $polyP_{70}$ (Figure 3A).

The reduction in clotting time elicited by the $polyP_{70}$-GNPs was further analyzed as a function of the GNP concentration (Figure 3B,C). 50 nm $polyP_{70}$-GNPs are more procoagulant, as contrasted with the 10 nm $polyP_{70}$-GNPs, at equivalent GNP concentration: the 50 nm GNPs reduce the time to clot by 60% at less than 2 nM GNP concentration, whereas it takes approximately 80 nM for the equivalent drop with the 10 nm GNPs. This effect can be attributed to the 25-fold increase in the surface area of the 50 nm GNPs when compared with 10 nm GNPs, indicating larger localization of $polyP_{70}$ that could lead to a better recruitment of active clotting factors above their threshold concentration. The curvature of the particles may also affect the structural change of FXII. It is reported by Kushida et al. that nanoparticles of larger size with low curvature effect facilitated higher degree of FXII denaturation, whereas smaller size nanoparticles (high curvature) led to little or no denaturation/unfolding of FXII resulting in much weaker effects on the intrinsic coagulation.[40] Citrated (bulk) and PEGylated GNPs are used as controls to demonstrate that the GNPs themselves are not responsible for the marked reduction in clotting time. PEGylation of 10 nm citrated GNPs after 3−4 days of reaction reveals that the zeta potential drops from −20 to −5 mV, implying that the negatively charged citrate is being replaced by the neutral PEG-thiol (see Table 4). The zeta potential of the synthesized polyP-GNPs is found to be −25 mV to −30 mV, which is comparable to silica particles with the zeta potential range from −25 mV to −40 mV and kaolin suspensions with the zeta potentials ranging from −20 mV to −30 mV.[41,42] The silica particles and kaolin have been previously reported to be potent surfaces for contact pathway activation.[43,44]

Table 4. ζ Potential Measurements of the Synthesized Samples

sample	ζ potential (mV)
10 nm bulk	−19.5
10 nm $polyP_{70}$-GNPs	−27.5
10 nm PEG-GNP	−3.49
50 nm bulk	−22.3
50 nm $polyP_{70}$-GNP	−26.53
50 nm PEG-GNP	−2.30

The contact activity of the $polyP_{70}$-GNPs was further corroborated by A_{405} turbidity assays in pooled normal plasma

DOI: 10.1021/acs.bioconjchem.5b00524
Bioconjugate Chem. XXXX, XXX, XXX−XXX

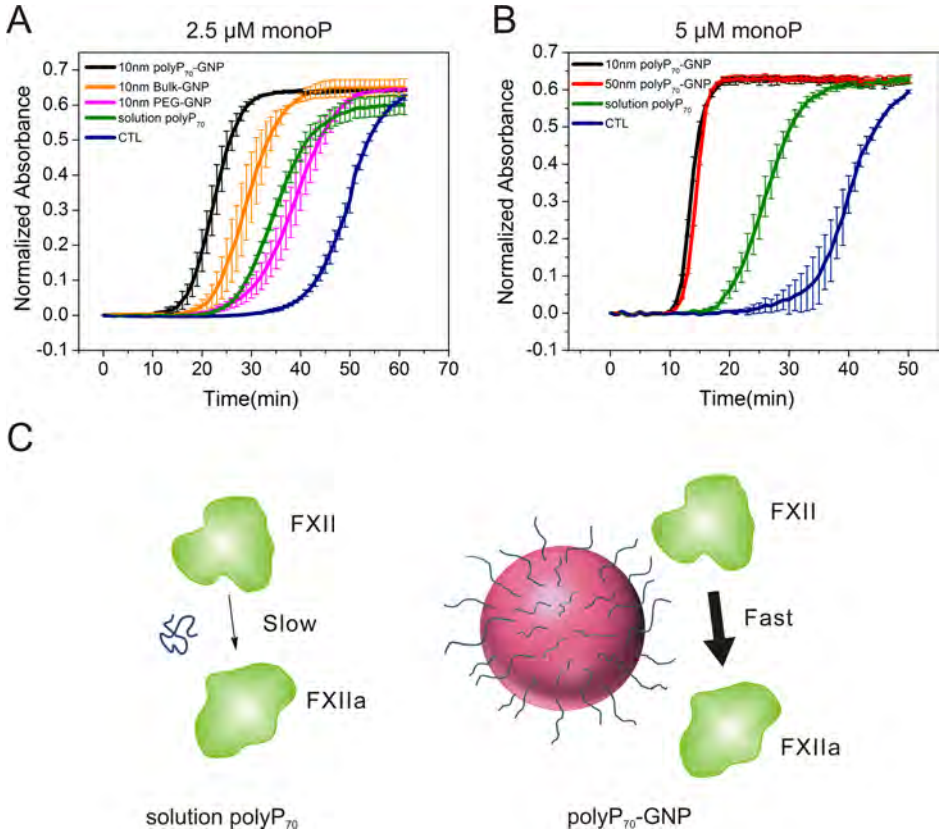

Figure 4. Procoagulant activity of polyP$_{70}$-GNPs assayed by A_{405} turbidity in PNP. (A) Normalized absorbance traces of 10 nm polyP$_{70}$-GNPs at 2.5 μM monoP (n = 3, ±S.E.) compared to PEGylated GNP and citrate GNP with the same GNP concentration, and molecularly dissolved polyP$_{70}$. (B) Normalized absorbance traces of 10 and 50 nm polyP$_{70}$-GNPs at 5 μM monoP (n = 3, ±S.E.) compared to molecularly dissolved polyP$_{70}$. (C) Differential clotting activation of colloidally anchored and solution-phase polyP$_{70}$. Colloidal clustering of polyP promotes rapid initiation of the contact pathway of clotting by serving as a surface for the assembly of the primary complex, whereas polyP$_{70}$ in solution is only marginally capable of FXII zymogen activation.

(PNP). 10 and 50 nm GNPs have intrinsic absorbance at 405 nm; hence, changes in absorbance values must be interpreted cautiously. As the coagulometric assay measures the mechanical and viscous properties of the clotting plasma, the turbidity tests provide complementary information on the optical density of the polymerizing fibrin mesh. Although fibrin clot density is being directly observed, and is a consequence of thrombin kinetics, it is linked to activation of FXII from interaction with a contact surface. Therefore, these two techniques can be used synergistically to evaluate the efficacy of the polyP$_{70}$-GNPs at initiating the contact pathway of clotting.

Before proceeding with the turbidity tests a series of control experiments were performed to ensure that the absorbance of citrated and polyP$_{70}$ conjugated GNPs does not change after incubation in PNP, and that the absorbance detector does not reach a saturating value during or after coagulation. SI Figure S2B,C,D demonstrates that the GNPs are colloidally stable in human plasma for at least 1 h, and that A_{405} remains constant. These observations also provide evidence that the GNPs did not aggregate during the clotting assays and that the quantified procoagulant outcomes emerge from the physical parameters we measured in the laboratory. SI Figure S2A,E,F shows that GNPs at considerably higher concentrations than used in the clotting tests still display a linear relationship with A_{405} turbidity, implying that absorbance values after coagulation will be well below the saturation limit of the detector. Therefore, the absorbance traces can be normalized by subtracting their initial values and directly compared between samples to quantify their procoagulant efficacy. SI Figure S2A gives a representative raw absorbance trace of the polyP$_{70}$-GNPs at 5 μM monoP before normalization. The time to initial fibrin formation is typically determined by fitting a line to the point at which the absorbance begins to increase and subsequently finding the intersection with the baseline absorbance value. Figure 4A shows the clotting outcomes (measured by increase in turbidity) of the 10 nm polyP$_{70}$-GNPs. PolyP$_{70}$-GNPs manifest a marked increase in turbidity long before polyP$_{70}$ in solution or control with no activator present. Completely PEGylated GNPs likewise do not robustly initiate the contact pathway, with a clotting time between molecularly dissolved polyP$_{70}$ in solution and the control (with no activator present). The citrated 10 nm GNPs (bulk), at the same GNP concentration as the 10 nm polyP$_{70}$-GNP sample, possess some ability to initiate the contact pathway of clotting, but they are significantly less efficacious than the 10 nm polyP$_{70}$-GNPs. Figure 4B depicts the clotting behavior of 10 and 50 nm polyP$_{70}$ -GNPs at 5 μM monoP. All GNPs conjugated with polyP$_{70}$ clot in approximately 10 min, while polyP$_{70}$ in solution coagulates at approximately 25 min, while the control (with no activator present) trails at 35−40 min. The turbidity measurements were all performed at room temperature, and the time to coagulation will in practice be much longer than those obtained by coagulometry at 37 °C. Regardless, the equivalent trends in procoagulant efficacy

DOI: 10.1021/acs.bioconjchem.5b00524
Bioconjugate Chem. XXXX, XXX, XXX−XXX

between samples are apparent after short inspection. These data further corroborate coagulometric measurements presented above that nanoscale confinement of polyP$_{70}$ onto a colloidal surface transforms the weak contact activator polyP$_{70}$ into a robust agent, mimicking polyP chains more than ten times larger.

In the present investigation we lay the groundwork for the implementation of a novel, potentially injectable hemostat for treating a constellation of internal and external hemorrhagic phenomena through the conjugation of platelet-sized polyP to colloidal GNPs, facilitated by phosphoramidation to the disulfide cystamine. Although many negatively charged moieties have been shown to initiate the contact pathway of blood clotting,[45] using polyP has unique advantages, in that it is naturally secreted by human platelets and, in addition to FXII, polyP also interacts with FXI, FV, and thrombin to accelerate clotting. Moreover, our data indicated that the procoagulant effect of polyP conjugated on gold nanoparticles is orders of magnitude greater than any other (as yet) identified anionic polymer.[4,6,7] Procoagulant outcomes, measured by conventional contact activity assays in human blood plasma, indicate that they exert significant reductions in the time to clot. Covalent conjugation to the colloidal surface transforms platelet-sized polyP$_{70}$ into a very robust contact surface, similar to that of the potent activator long-chain polyP. These data offer strong support to the claim that clustering of shorter polymers at high local concentrations is equivalent to having much longer polymers dispersed in solution phase for modulation of blood coagulation and other threshold-switchable networks.

The procoagulant activity characteristic of the polyP$_{70}$-GNPs is a meaningful step forward in the development of an on-demand, minimally invasive, targeted hemostat, and surprisingly reminiscent of the threshold-switchable properties of the coagulation cascade itself. Localization of procoagulant activators above crucial threshold concentrations accomplished in physiological contexts allows for swift propagation of the hemostatic signal to achieve wound healing. Organisms have adapted these nonlinear processes capable of exponential amplification, counterbalanced by negative feedback mechanisms, to harbor a rapid response to potentially catastrophic injury, always maintaining this delicate equilibrium of hemostasis essential for survival. The synthesis of polyP$_{70}$-GNPs therefore may fulfill a need for the treatment of a variety of bleeding phenomena, its methodology inspired by nature's nonlinear, threshold-switchable processes.

EXPERIMENTAL PROCEDURES

Materials and Reagents. Cystamine, EDAC (*N*-(3-(dimethylamino)propyl)-*N*′-ethylcarbodiimide hydrochloride), MES (2-(*N*-morpholino)ethanesulfonic acid), 4-morpholineethanesulfonic acid), NaCl, MOPS (3-(*N*-morpholino)-propanesulfonic acid, 4-morpholinepropanesulfonic acid), imidazole, phosphorus standard solution, ammonium molybdate IV tetrahydrate, malachite green carbinol base, and poly(ethylene) glycol methyl ether thiol (Mn: 1000) were purchased from Sigma-Aldrich (St. Louis, Mo, U.S.A.). Colloidal gold citrate nanoparticles (10 and 50 nm diameter) were purchased from Ted Pella (Redding, CA). PolyP$_{70}$ ("Natrium polyphosphat", range 20−125 orthophosphates) was a kind gift from BK Giulini GmbH (Ludwigshafen am Rhein, Germany). PolyP$_{800}$ (range 200−1600) was prepared as previously described.[6]

Synthesis of PolyP$_{70}$-Cystamine Ligand. PolyP$_{70}$-cystamine ligand was conjugated via EDAC mediated reaction.[18] PolyP$_{70}$ (70 mM monophosphate) was added to cystamine (0.1 mM) in the presence of EDAC (300 mM) and MES or MOPS (300 mM) buffers at various pH values (ranging from 6 to 10) and allowed to mix for 72 h at room temperature (20 °C). Control reactions containing all reagents except EDAC were also performed. The efficiency and stability of the reaction at different pH values (ranging from 6 to 10) were tested by the fluorescamine assay. Briefly, 10 μL of the reaction sample was added to 95 μL of 250 mM borate pH 10, and 45 μL of fluorescamine reagent in acetone (1 mg/mL) in a 96-well black plate. The fluorescamine reagent is known to rapidly bind to the unreacted primary amine group in cystamine, which was measured by using a fluorescence plate reader with excitation wavelength of 365 nm and emission wavelength of 470 nm. A calibration curve was prepared with known concentrations of free cystamine to quantify the amounts of unreacted cystamine in the reaction.

Conjugation of PolyP$_{70}$-Cystamine to GNPs. PolyP$_{70}$-cystamine ligand was allowed to react with GNPs in eight 4 mL reaction vials for 10 nm GNPs and eight 2 mL reaction vials for 50 nm GNPs. Depending on the nanoparticle size (supplied in different starting particle concentrations or preconcentrated), the following reagent volumes and concentrations were chosen as indicated in Table 5 below.

Table 5. Experimental Conditions for Conjugation of polyP$_{70}$-Cystamine to GNPs

GNP size (nm)	GNP starting concentration (nM)	GNP suspension volume (μL)	ligand solution (0.1 mM) volume (μL)	MOPS buffer (pH 8) (μL)
10	9.43	3850	30	120
50	0.374	1970	15	15

Control reactions of PEG-thiol (0.2 mM) with GNPs were also set up. The same reaction volumes were chosen for consistency. The ligands (polyP$_{70}$-cystamine or PEG-thiol) were used in a 2:1 excess ratio to GNP available binding sites. The reaction vials were first kept for 24 h at room temperature with constant slow mixing on a rotator. To increase binding efficiency, the salt addition was initiated to increase the ionic strength of the solution. 10 μL of 5 M NaCl was added to the reaction vials while mixing. The procedure of salt addition was repeated eight times (two times a day with at least a 6 h break in between). The final concentration of salt was 0.1 M NaCl.

Removal of Unreacted PolyP$_{70}$. Unreacted polyP$_{70}$ and ligands were removed by using centrifugation in a Labnet Spectrafuge 16 M Microcentrifuge (Labnet International, Woodbridge, NJ). The samples from the polyP$_{70}$-cystamine ligand reactions with GNPs were distributed into 1.6 mL microcentrifuge tubes and centrifuged using optimized conditions (Table 6). After each centrifugation, the supernatant was collected and the GNP pellet was resuspended with the buffer (imidazole, pH 7.2) by vortexing for 30 s. After final

Table 6. Size-Dependent Centrifugation Conditions

GNP size (nm)	RPM	G-force	pelleting time (min)	centrifuge repeat
10	10000	8176	60	3×
50	8000	5223	10	3×

DOI: 10.1021/acs.bioconjchem.5b00524
Bioconjugate Chem. XXXX, XXX, XXX−XXX

centrifugation for all GNP types, the pellets were resuspended with a smaller amount of buffer in order to achieve desired concentrations of $polyP_{70}$ and GNP.

Determination of Number of $PolyP_{70}$ Chains per Particle. The number of $polyP_{70}$ chains per particle was calculated by quantifying the concentrations of $polyP_{70}$ and GNPs in the concentrated samples after completion of the purification step. To quantify the amount of $polyP_{70}$ present in the sample, 101 μL of sample was mixed with 9.1 μL of 12.1 M HCl and heated at 100 °C for 30 min to first hydrolyze the $polyP_{70}$ chains into monophosphate (monoP). Then, 50 μL of hydrolyzed sample was mixed with 100 μL of malachite green reagent (mixing 0.1% malachite green and 42 mg/mL ammonium molybdate acid solution (5 M HCl) at 3:1 volume ratio) in a 96-well clear plate and allowed to react for 5 min. The amount of monoP present was quantified by measuring the absorbance at 620 nm using a plate reader and comparing the readings with the standardized curve. The amount of GNPs was determined by measuring the absorbance at 405 nm (for 10 nm GNPs) and 492 nm wavelengths (for 50 nm GNPs) and comparing it with the standard calibration. The final number of $polyP_{70}$ chains per particle was determined by the following formula:

$$\text{number of polyP}_{70}\text{chains per particle} = \frac{\text{monoP concentration/repeating unit}}{\text{gold nanoparticle concetration}}$$

Transmission Electron Microscopy (TEM). $PolyP_{70}$-GNPs or unmodified Au citrate suspension (10 μL) was micropipetted onto a 300-mesh Formvar grid (Structure Probe Inc., West Chester, PA). After 10 min the liquid which had not evaporated was wicked away with the tip of a Kim Wipe. The samples were examined in a JEM-3010 transmission electron microscope (JEOL Inc., Tokyo, Japan).

Zeta (ζ) Potential Measurements. Zeta potentials of the synthesized $polyP_{70}$-GNPs and PEG-GNPs were measured by using a Zetasizer Nano ZS instrument (Malvern Instruments, Worcestershire, U.K.) in DI water at 20 °C.

Clotting Assays. Contact pathway activity of $polyP_{70}$-GNPs was determined by coagulometric assay.[6] Clotting times of citrated human pooled normal plasma (PNP) (George King Biomedical, Overland Park, KS) were quantified at 37 °C using a Start 4 coagulometer (Diagnostica Stago, France). Prewarmed polyP or $polyP_{70}$-GNPs in imidazole buffer was incubated in coagulometer cuvettes with prewarmed plasma for 3 min, after which clotting was initiated by addition of phospholipid and $CaCl_2$. Tests of the contact pathway of blood clotting were conducted using final concentrations of GNPs as indicated, 33% plasma, 25 μM phospholipid, 1.67 mM imidazole pH 7.0, and 8.33 mM $CaCl_2$.

A_{405} Turbidity Measurements. Turbidity measurements of the same GNPs used above in the coagulometric assays were performed in clear, medium-binding 96-well microplates. A_{405} was typically measured every min for 40−60 min at room temperature (20 °C). Each well contained 50 μL of citrated human pooled normal plasma (George King Biomedical, Overland Park, KS) prewarmed to 37 °C containing 75 μM phospholipid; 50 μL of GNPs or $polyP_{70}$ (BKGP70) in solution in 5 mM imidazole, pH 7.2; and 50 μL of 25 mM $CaCl_2$. GNPs and $polyP_{70}$ were preincubated in the citrated plasma on the microplate at 37 °C for 3 min before recalcification to ensure FXII activation.

■ ASSOCIATED CONTENT

Ⓢ Supporting Information

The Supporting Information is available free of charge on the ACS Publications website at DOI: 10.1021/acs.bioconjchem.5b00524.

Centrifugation Optimization. Supporting Figures: Control centrifugation experiments for 10 nm GNPs, Control absorbance experiments, Clotting of 50 nm $polyP_{70}$-GNPs as a function of surface coverage. (PDF)

■ AUTHOR INFORMATION

Corresponding Author

*E-mail: liuying@uic.edu. Tel: (312) 996-8249. Fax: (312) 996-0808.

Author Contributions

M.S., A.J.D., S.A.S., R.R., H.S., and J.K. conceived and conducted experiments. M.S., A.J.D., S.A.S., R.R., H.S., J.K., J.H.M., and Y.L. interpreted the results. M.S., A.J.D., Y.L., and S.A.S. composed the manuscript, with editorial contributions from J.H.M. All authors have given consent to the final version of the manuscript.

Notes

The authors declare the following competing financial interest(s): J.H.M. and S.A.S. are co-inventors on patents and pending patent applications related to therapeutic usage of polyP. Y.L. and A.J.D. are co-inventors on a pending patent application associated with the pharmacologic application of polyP nanoparticles. The remaining authors declare no competing financial interests..

[#]Equivalent first authors.

■ ACKNOWLEDGMENTS

The study was sponsored by the U.S. Army Medical Research and Material Command (WQ81XWH-11−2−0021). The U.S. Army Medical Research Acquisition Activity, 820 Chandler Street, Fort Detrick MD 21702−5014 is the awarding and administering acquisition office. The contents of this article do not necessarily reflect the position or the policy of the government, and no official endorsement should be inferred. We would like to thank Dr. Seungpyo Hong at UIC for allowing us to access Malvem Zetasizer in his laboratory and Dr. Tad Daniel at UIC for assisting with TEM imaging.

■ REFERENCES

(1) Brown, M. R. W., and Kornberg, A. (2004) Inorganic polyphosphate in the origin and survival of species. *Proc. Natl. Acad. Sci. U. S. A. 101*, 16085−16087.

(2) Morrissey, J. H., Choi, S. H., and Smith, S. A. (2012) Polyphosphate: an ancient molecule that links platelets, coagulation, and inflammation. *Blood 119*, 5972−5979.

(3) Kornberg, A. (1995) Inorganic Polyphosphate - toward Making a Forgotten Polymer Unforgettable. *J. Bacteriol. 177*, 491−496.

(4) Smith, S. A., Mutch, N. J., Baskar, D., Rohloff, P., Docampo, R., and Morrissey, J. H. (2006) Polyphosphate modulates blood coagulation and fibrinolysis. *Proc. Natl. Acad. Sci. U. S. A. 103*, 903−908.

(5) Smith, S. A., and Morrissey, J. H. (2008) Polyphosphate enhances fibrin clot structure. *Blood 112*, 2810−2816.

(6) Smith, S. A., Choi, S. H., Davis-Harrison, R., Huyck, J., Boettcher, J., Reinstra, C. M., and Morrissey, J. H. (2010) Polyphosphate exerts differential effects on blood clotting, depending on polymer size. *Blood 116*, 4353−4359.

DOI: 10.1021/acs.bioconjchem.5b00524
Bioconjugate Chem. XXXX, XXX, XXX−XXX

(7) Choi, S. H., Smith, S. A., and Morrissey, J. H. (2011) Polyphosphate is a cofactor for the activation of factor XI by thrombin. *Blood 118*, 6963−6970.
(8) Han, K. Y., Hong, B. S., Yoon, Y. J., Yoon, C. M., Kim, Y. K., Kwon, Y. G., and Gho, Y. S. (2007) Polyphosphate blocks tumour metastasis via anti-angiogenic activity. *Biochem. J. 406*, 49−55.
(9) Rashid, M. H., Rumbaugh, K., Passador, L., Davies, D. G., Hamood, A. N., Iglewski, B. H., and Kornberg, A. (2000) Polyphosphate kinase is essential for biofilm development, quorum sensing, and virulence of Pseudomonas aeruginosa. *Proc. Natl. Acad. Sci. U. S. A. 97*, 9636−9641.
(10) Keasling, J. D. (1997) Regulation of intracellular toxic metals and other cations by hydrolysis of polyphosphate. *Ann. N. Y. Acad. Sci. 829*, 242−249.
(11) Reusch, R. N., and Sadoff, H. L. (1988) Putative Structure and Functions of a Poly-Beta-Hydroxybutyrate Calcium Polyphosphate Channel in Bacterial Plasma-Membranes. *Proc. Natl. Acad. Sci. U. S. A. 85*, 4176−4180.
(12) Gezelius, K. (1974) Inorganic polyphosphates and enzymes of polyphosphate metabolism in the cellular slime mold Dictyostelium discoideum. *Arch. Microbiol. 98*, 311−329.
(13) Zhang, H., Gomez-Garcia, M. R., Brown, M. R., and Kornberg, A. (2005) Inorganic polyphosphate in Dictyostelium discoideum: influence on development, sporulation, and predation. *Proc. Natl. Acad. Sci. U. S. A. 102*, 2731−2735.
(14) Noegel, A., and Gotschlich, E. C. (1983) Isolation of a High Molecular-Weight Polyphosphate from Neisseria-Gonorrhoeae. *J. Exp. Med. 157*, 2049−2060.
(15) Docampo, R., and Moreno, S. N. J. (1999) Acidocalcisome: A novel Ca2+ storage compartment in trypanosomatids and apicomplexan parasites. *Parasitol. Today 15*, 443−448.
(16) Ruiz, F. A., Lea, C. R., Oldfield, E., and Docampo, R. (2004) Human platelet dense granules contain polyphosphate and are similar to acidocalcisomes of bacteria and unicellular eukaryotes. *J. Biol. Chem. 279*, 44250−44257.
(17) Donovan, A. J., Kalkowski, J., Smith, S. A., Morrissey, J. H., and Liu, Y. (2014) Size-Controlled Synthesis of Granular Polyphosphate Nanoparticles at Physiologic Salt Concentrations for Blood Clotting. *Biomacromolecules 15*, 3976−3984.
(18) Choi, S. H., Collins, J. N. R., Smith, S. A., Davis-Harrison, R. L., Rienstra, C. M., and Morrissey, J. H. (2010) Phosphoramidate End Labeling of Inorganic Polyphosphates: Facile Manipulation of Polyphosphate for Investigating and Modulating Its Biological Activities. *Biochemistry 49*, 9935−9941.
(19) Hebbard, C. F. F., Wang, Y., Baker, C. J., and Morrissey, J. H. (2014) Synthesis and Evaluation of Chromogenic and Fluorogenic Substrates for High-Throughput Detection of Enzymes That Hydrolyze Inorganic Polyphosphate. *Biomacromolecules 15*, 3190−3196.
(20) Renne, T., et al. (2012) In Vivo Roles for Factor XII. *Blood 120*, 4296−4303.
(21) Bock, P. E., Srinivasan, K. R., and Shore, J. D. (1981) Activation of Intrinsic Blood-Coagulation by Ellagic Acid - Insoluble Ellagic Acid-Metal Ion Complexes Are the Activating Species. *Biochemistry 20*, 7258−7266.
(22) Heimark, R. L., Kurachi, K., Fujikawa, K., and Davie, E. W. (1980) Surface Activation of Blood-Coagulation, Fibrinolysis and Kinin Formation. *Nature 286*, 456−460.
(23) Tans, G., Rosing, J., and Griffin, J. H. (1983) Sulfatide-dependent autoactivation of human-blood coagulation factor-XII (Hageman-Factor). *J. Biol. Chem. 258*, 8215−8222.
(24) Smith, S. A., and Morrissey, J. H. (2008) Heparin is procoagulant in the absence of antithrombin. *Thromb. Haemostasis 100*, 160−162.
(25) Griffin, J. H. (1978) Role of Surface in Surface-Dependent Activation of Hageman-Factor (Blood-Coagulation Factor-Xii). *Proc. Natl. Acad. Sci. U. S. A. 75*, 1998−2002.
(26) Faxalv, L., Boknas, N., Strom, J. O., Tengvall, P., Theodorsson, E., Ramstrom, S., and Lindahl, T. L. (2013) Putting polyphosphates to the test: evidence against platelet-induced activation of factor XII. *Blood 122*, 3818−3824.
(27) Nickel, K. F., Spronk, H. M., Mutch, N. J., and Renne, T. (2013) Time-dependent degradation and tissue factor addition mask the ability of platelet polyphosphates in activating factor XII-mediated coagulation. *Blood 122*, 3847−3849.
(28) Muller, F., Mutch, N. J., Schenk, W. A., Smith, S. A., Esterl, L., Spronk, H. M., Schmidbauer, S., Gahl, W. A., Morrissey, J. H., and Renne, T. (2009) Platelet polyphosphates are proinflammatory and procoagulant mediators in vivo. *Cell 139*, 1143−1156.
(29) Engel, R., Brain, C. M., Paget, J., Lionikiene, A. S., and Mutch, N. J. (2014) Single-chain factor XII exhibits activity when complexed to polyphosphate. *J. Thromb. Haemostasis 12*, 1513−1522.
(30) Haake, P., and Koizumi, T. (1970) Hydrolysis of phosphinamides and the nature of the P-N bond. *Tetrahedron Lett. 11*, 4845−4848.
(31) Garrison, A. W., and Boozer, C. E. (1968) The acid-catalized hydrolysis of a series of phosphoroamidates. *J. Am. Chem. Soc. 90*, 3486−3494.
(32) Mucha, A., Grembecka, J., Cierpicki, T., and Kafarski, P. (2003) Hydrolysis of the phosphonamidate bond in phosphono dipeptide analogues - The influence of the nature of the N-terminal functional group. *Eur. J. Org. Chem. 2003*, 4797−4803.
(33) Mucha, A., Kunert, A., Grembecka, J., Pawelczak, M., and Kafarski, P. (2006) A phosphonamidate containing aromatic N-terminal amino group as inhibitor of leucine aminopeptidase - design, synthesis and stability. *Eur. J. Med. Chem. 41*, 768−772.
(34) Jacobsen, N. E., and Bartlett, P. A. (1981) A Phosphonamidate Dipeptide Analog as an Inhibitor of Carboxypeptidase-A. *J. Am. Chem. Soc. 103*, 654−657.
(35) Demers, L. M., Mirkin, C. A., Mucic, R. C., Reynolds, R. A., 3rd, Letsinger, R. L., Elghanian, R., and Viswanadham, G. (2000) A fluorescence-based method for determining the surface coverage and hybridization efficiency of thiol-capped oligonucleotides bound to gold thin films and nanoparticles. *Anal. Chem. 72*, 5535−5541.
(36) Corbierre, M. K., Cameron, N. S., and Lennox, R. B. (2004) Polymer-stabilized gold nanoparticles with high grafting densities. *Langmuir 20*, 2867−2873.
(37) Liu, Y. L., Shipton, M. K., Ryan, J., Kaufman, E. D., Franzen, S., and Feldheim, D. L. (2007) Synthesis, stability, and cellular internalization of gold nanoparticles containing mixed peptide-poly(ethylene glycol) monolayers. *Anal. Chem. 79*, 2221−2229.
(38) Jackson, C. M., and Nemerson, Y. (1980) Blood-Coagulation. *Annu. Rev. Biochem. 49*, 765−811.
(39) Mandle, R. J., Colman, R. W., and Kaplan, A. P. (1976) Identification of Prekallikrein and High-Molecular-Weight Kininogen as a Complex in Human-Plasma. *Proc. Natl. Acad. Sci. U. S. A. 73*, 4179−4183.
(40) Kushida, T., Saha, K., Subramani, C., Nandwana, V., and Rotello, V. M. (2014) Effect of nano-scale curvature on the intrinsic blood coagulation system. *Nanoscale 6*, 14484−14487.
(41) Kim, K. M., Kim, H. M., Lee, W. J., Lee, C. W., Kim, T. I., Lee, J. K., Jeong, J., Paek, S. M., and Oh, J. M. (2014) Surface treatment of silica nanoparticles for stable and charge-controlled colloidal silica. *Int. J. Nanomed. 9*, 29−40.
(42) Greenwood, R., Lapcikova, B., Surynek, M., Waters, K., and Lapcik, L. (2007) The zeta potential of kaolin suspensions measured by electrophoresis and electroacoustics. *Chem. Pap. - Chem. Zvesti 61*, 83−92.
(43) Margolis, J. (1961) The effect of colloidal silica on blood coagulation. *Immunol. Cell Biol. 39*, 249−258.
(44) Zhu, S., and Diamond, S. L. (2014) Contact activation of blood coagulation on a defined kaolin/collagen surface in a microfluidic assay. *Thromb. Res. 134*, 1335−1343.
(45) Oslakovic, C., Cedervall, T., Linse, S., and Dahlback, B. (2012) Polystyrene nanoparticles affecting blood coagulation. *Nanomedicine 8*, 981−986.

DOI: 10.1021/acs.bioconjchem.5b00524
Bioconjugate Chem. XXXX, XXX, XXX−XXX

BioMACROMOLECULES

Article

pubs.acs.org/Biomac

Artificial Dense Granules: A Procoagulant Liposomal Formulation Modeled after Platelet Polyphosphate Storage Pools

Alexander J. Donovan,[†] Joseph Kalkowski,[†] Magdalena Szymusiak,[†] Canhui Wang,[‡] Stephanie A. Smith,[§] Robert F. Klie,[‡] James H. Morrissey,[§] and Ying Liu*[,†,∥]

[†]Department of Chemical Engineering, University of Illinois at Chicago, Chicago, Illinois 60607, United States

[‡]Department of Physics, University of Illinois at Chicago, Chicago, Illinois 60607, United States

[§]Department of Biochemistry, University of Illinois at Urbana−Champaign, Urbana, Illinois 61801, United States

[∥]Department of Biopharmaceutical Sciences, University of Illinois at Chicago, Chicago, Illinois 60607, United States

Supporting Information

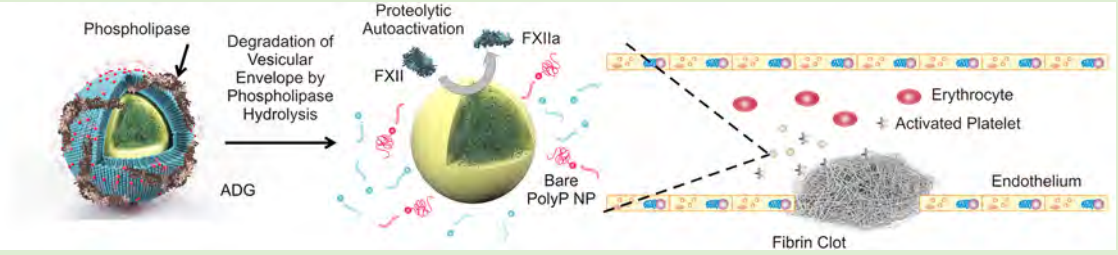

ABSTRACT: Granular platelet-sized polyphosphate nanoparticles (polyP NPs) were encapsulated in sterically stabilized liposomes, forming a potential, targeted procoagulant nanotherapy resembling human platelet dense granules in both structure and functionality. Dynamic light scattering (DLS) measurements reveal that artificial dense granules (ADGs) are colloidally stable and that the granular polyP NPs are encapsulated at high efficiencies. High-resolution scanning transmission electron microscopy (HR-STEM) indicates that the ADGs are monodisperse particles with a 150 nm diameter dense core consisting of P, Ca, and O surrounded by a corrugated 25 nm thick shell containing P, C, and O. Further, the ADGs manifest promising procoagulant activity: Detergent solubilization by Tween 20 or digestion of the lipid envelope by phospholipase C (PLC) allows for ADGs to trigger autoactivation of Factor XII (FXII), the first proteolytic step in the activation of the contact pathway of clotting. Moreover, ADGs' ability to reduce the clotting time of human plasma in the presence of PLC further demonstrate the feasibility to develop ADGs into a potential procoagulant nanomedicine.

INTRODUCTION

Hemorrhagic events arising from trauma in either a civilian or military setting contribute to a significant proportion of avoidable fatality.[1−3] In countless combat scenarios, proper management of hemorrhage is not immediately feasible without invasive surgical intervention. Topical hemostatic wound dressings and other pharmacological agents, which can be delivered on-demand on the battlefield, are therapeutically inferior in mitigating internal, incompressible bleeding sources.[4]

Clinical guidelines created to diminish poor outcomes in patients experiencing an uncontrolled post-traumatic bleeding event have focused on restoring normal circulatory perfusion to the wounds after swiftly determining and suppressing the source of bleeding by a trained clinician rather than via administration of a hemostat as a first-line therapy.[5,6] However, these guidelines have largely failed to eradicate trauma-related complications even in developed countries with relatively more medical resources.[7] Both private and public entities have invested heavily into developing a targeted, on-demand, broad-spectrum procoagulant agent.[4] The Food and Drug Administration (FDA) has approved a myriad of pharmacological therapies in recent years to address external compressible trauma, enhancing survival, and reestablishing hemostasis without surgery.[8] Hemcon, for example, is a commercially available bandage composed of a biodegradable polysaccharide, chitosan, which rapidly marginates negatively charged erythrocytes at the trauma site due to the macromolecule's high positive charge density.[9] Nonetheless, Hemcon is not suitable for the treatment of incompressible wounds. Factor VIIa has also been used to treat internal bleeding.[10] However, the efficacy of factor VIIa therapy for treating traumatic injuries is controversial.[11] The recombinant clotting factor is expensive and requires special storage and handling conditions.

Nanoscale drug delivery has emerged as a novel therapeutic platform in recent decades with the potential to drastically transform medical treatment,[12] promising reduced side effects, enhanced efficacy, and targeted delivery to only effected organs and tissues.[13] The conventional strategy to design this next

Received: April 22, 2016
Revised: July 7, 2016
Published: July 13, 2016

DOI: 10.1021/acs.biomac.6b00577
Biomacromolecules 2016, 17, 2572−2581

generation of smart drugs entails the encapsulation of therapeutic and/or imaging agents into supramolecularly assembled depots[14] such as phospholipid vesicles,[15] polymersomes,[16,17] viral capsids,[18] polymeric micelles,[19] and other self-assembled nanostructures.[20] Among these candidate drug architectures, vesicles have garnered the most tangible success, with several liposomal nanoformulations being approved by the FDA to treat a myriad of disorders, especially cancer.[21,22] The liposomal envelope of these smart drugs usually contains a small molar percentage of poly(ethylene glycol)−phosphatidylethanolamine (PEG−PE), which is used for steric stabilization and long blood circulation time.[23,24]

Given both the limitations of the available treatments to improve hemostasis and the promise of nanotherapeutics, numerous candidate nanoparticle hemostats have been developed in recent years. These nanotherapeutics attempt to imitate at least some aspects of platelet morphology and the procoagulant response adjacent to the bleeding site. Anselmo and Mitragotri approach mimicry with their platelet-like nanoparticles (PLNs), synthesized by alternative deposition of the polyelectrolytes bovine serum albumin (BSA) and poly(allylamine) hydrochloride on a polystyrene (PS) core.[25,26] Further functionalization of the PLN with targeting peptide ligands allow PLNs to accumulate at the bleeding site, bind and interact synergistically with the body's own activated platelets, and rapidly induce coagulation at the site of trauma.[26] However, the synthesis of the PLNs involves multiple steps and toxic organic solvents to dissolve the nonbiodegradable polymer.

Inorganic polyphosphate (polyP), on the contrary, is virtually omnipresent in biology and degradable in human blood plasma on therapeutic time scales.[27] The polymer is a highly negatively charged macromolecule of orthophosphates, and is often stored intracellularly in a precipitated form as ∼250 nm granules[28−30] in conjunction with calcium and other divalent and multivalent cations. These organelles, generally termed "acidocalcisomes," are present in all species including humans.[31] These subcellular phosphate-containing bodies are called dense granules in human platelets[28] due to their uniformly high electron density. Their contents are secreted upon platelet activation, where they exert potent procoagulant and proinflammatory effects,[32] especially on Factor V[33] and thrombin-promoted Factor XI activation.[34] We have previously shown that polyP self-assembly into granular NPs in the presence of physiological amounts of metal cations is thermodynamically controlled, and that these particles retain their robust procoagulant effects.[29]

Herein we envision a biomimetic procoagulant nanoparticle composed of a granular polyP NP core encapsulated in a sterically stabilized liposome, which we call an artificial dense granule (ADG). The ADG assembly process is scalable and highly reproducible, and there are no toxic organic solvents or nonbiodegradable materials involved. The size distribution of the ADGs was characterized by dynamic light scattering (DLS) measurements. Electron microscopy techniques demonstrate that the ADGs are virtually indistinguishable from dense granules isolated from human platelets in terms of morphology and structure,[28] consisting of a 150 nm uniformly dense core surrounded by a 200 nm lipid shell. Electron energy loss spectroscopy (EELS) confirms the colocalization of P, Ca, and O in the core and P, C, and O in the phospholipid lamella. The ADGs are procoagulant as demonstrated by *in vitro* clotting factor assays: The ADGs can be triggered to initiate FXII autoactivation, the initial step in the contact pathway of blood clotting, via enzymatic hydrolysis by PLC, which modulates platelet degranulation. Furthermore, ADGs manifest contact activity in human plasma, and are roughly equivalent to molecularly dissolved, long-chain polyP at physiologically relevant concentrations.

EXPERIMENTAL SECTION

Materials and Reagents. $CaCl_2{\cdot}6H_2O$, phospholipase C (PLC) from *Clostridium perfringens (C. welchii)*, and secretory phospholipase A_2 from honey bee venom (bvsPLA$_2$) were purchased from Sigma-Aldrich (St. Louis, MO). Water was deionized using a Nanopure II filtration system (Barnstead, Dubuque, IA) to 18.2 MΩ-cm. 1,2-dipalmitoly *sn*-glycero-3-phosphoethanolamine-*N*-[methoxy-(polyethylene glycol)-2000] (ammonium salt) (PEG$_{2k}$DPPE), L-*α*-phosphatidylcholine (L-*α*-PC), and Avanti Mini Extruder Kit, together with a 200 nm pore-diameter polycarbonate membrane, were purchased from Avanti Polar Lipids (Alabaster, AL). Citrated human pooled normal plasma (PNP) from 30 healthy donors was purchased from George King Biomedical (Overland Park, KS). The polyP preparation used throughout for synthesis of ADGs was Natriumpolyphosphat P70 (BKGP70, approximate range 20−125 phosphate units, mode ∼45) from BK Guilini GmbH (Ludwigshafen am Rhein, Germany). polyP$_{>600}$ ("long chain polyP") used in clotting assays, and polyP$_{>1000}$, used to synthesize "Artificial Acidocalcisomes," were size-fractioned as previously described by differential isopropanol precipitation.[33] All materials were purchased at standard grades and used as received.

PolyP Nanoprecipitation. Molecularly dissolved polyP was precipitated in aqueous 5 mM $CaCl_2$, pH 5.4 as previously described.[29] Briefly, the polyP was micropipetted into the calcium solution and vortexed for 5 s. PolyP precipitated at supersaturation ratios exceeding 100 was diluted with more 5 mM $CaCl_2$, pH 5.4 prior to DLS characterization (Brookhaven NanoDLS, Brookhaven, NY). Dilution should not alter NP effective diameter as it is hysteretic as demonstrated previously.[29]

Synthesis of Sterically Stabilized Liposomes. Two hundred nanometer sterically stabilized liposomes composed of 95 mol % L-*α*-PC/5 mol % PEG$_{2k}$DPPE were synthesized by standard protocol via extrusion[35] through a 200 nm pore-diameter polycarbonate membrane. Briefly, 14.3 *μ*L of 25 mg/mL PEG$_{2k}$DPPE and 76.1 *μ*L of 25 mg/mL L-*α*-PC (both dissolved in chloroform) were micropipetted into a 7 mL glass scintillation vial and dried under a gentle stream of Argon gas. The dried lipid film was then placed under vacuum for an additional 60 min to remove any residual traces of organic solvent. The desiccated lipid cake was subsequently rehydrated with 1 mL of filtered, deionized H_2O (DI H_2O), and stored for up to 2 weeks at 4 °C. Liposome effective diameter and polydispersity index (PDI) were characterized by DLS after rehydration.

Synthesis of ADGs. Five millimolar polyP NPs were synthesized as described above. Following precipitation, the bare NP effective diameter, polydispersity, and scattering intensity were characterized by DLS before addition of 106.6 *μ*L of 2.6 mM 200 nm L-*α*-PC/PEG$_{2k}$DPPE liposomes in DI H_2O. The dispersion was bath sonicated for 10 min to encapsulate the granular polyP NPs at high efficiency.

FXII Autoactivation Assay with Detergent. FXII autoactivation was measured in 96-well microplates as described previously[36] with some small modifications. In short, ADGs were synthesized at 5 mM [monoP] in 5 mM $CaCl_2$, pH 5.4 as delineated in the Synthesis of ADGs section above. The ADGs were diluted with more 5 mM $CaCl_2$, pH 5.4 after solubilization with 0.5% (v:v) Tween 20 or an equivalent volumetric amount of pure DI H_2O (as a control) to a final monoP concentration of 500 *μ*M. Final concentrations of FXII zymogen and S-2302 substrate were 50 nM and 0.5 mM, respectively. FXII autoactivation was measured at room temperature.

FXII Autoactivation Assay with PLC from *C. welchii*. In lieu of solubilization with Tween 20, the 5 mM ADGs were prepared, as above, and diluted into 5 mM $CaCl_2$, 10 *μ*M $ZnCl_2$, 0.1% bovine serum albumin (BSA), 5 mM Tris·HCl, pH 5.5, and preincubated with 30 *μ*g/mL PLC for 20 min at 37 °C before addition of FXII zymogen

DOI: 10.1021/acs.biomac.6b00577
Biomacromolecules 2016, 17, 2572−2581

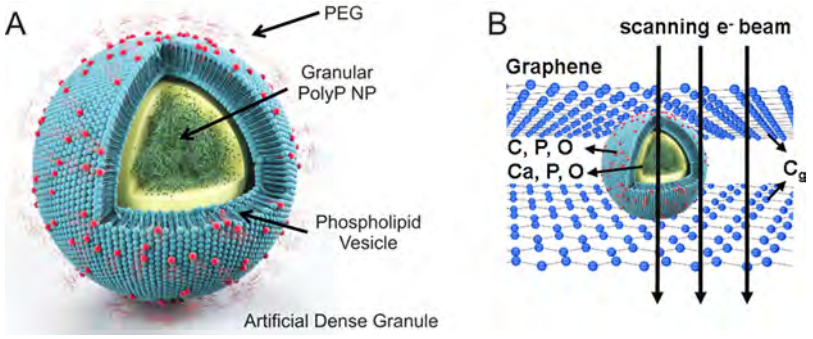

Figure 1. (A) Schematic of ADG design and structure. ADGs are 150 nm granular polyP NPs encapsulated in 200 nm sterically stabilized, PEGylated liposomes. (B) Illustration of a biocompatible graphene sandwich trapping an ADG for high resolution imaging. To prevent beam-induced morphology change and mass loss in the electron microscopy analysis, the ADG is directely sandwiched between two layers of free-standing graphene.

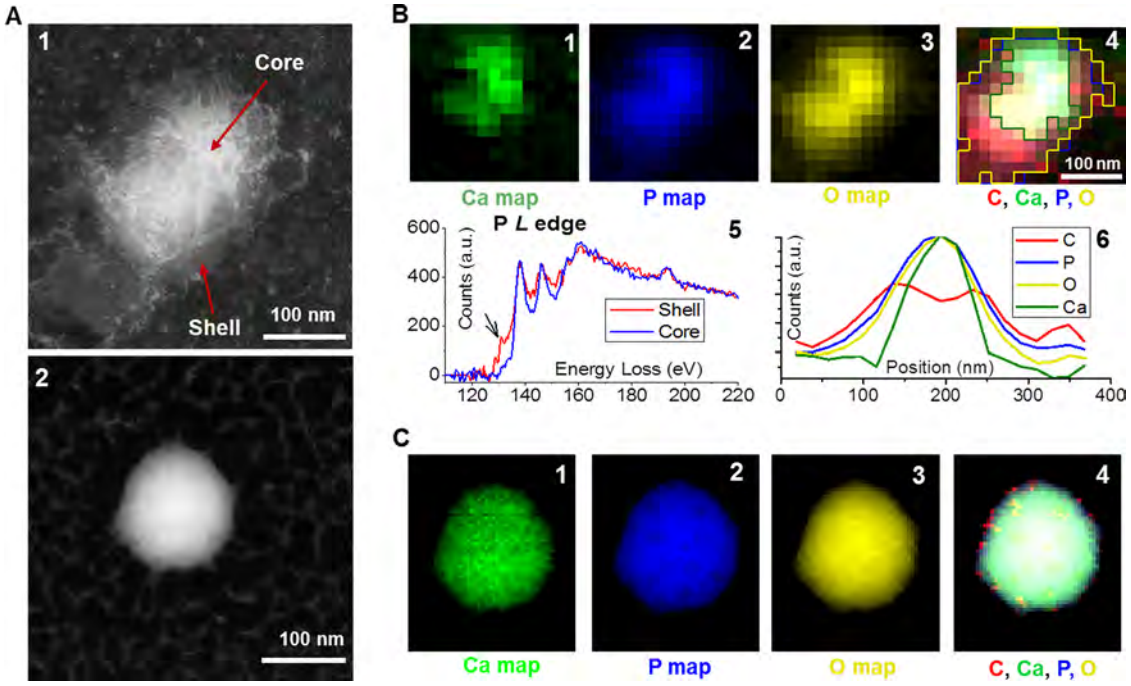

Figure 2. (A) HAADF images of the ADG (1) and the bare polyP NP (2). (B) Elemental and structural maps of the ADG. (B1−B4) Individual Ca, P, O and composite (C, Ca, P, O) map extracted from EEL spectrum images with the graphene background subtracted. The color-coded outlines of the Ca, P, and O distribution shown in B1−B3 are superimposed in composite map B4. (B5) Phosphorus *L*-edges extracted from the shell and core of the ADG shown in A. (B6) Elemental line scan of the C, O, P and Ca map extracted from the graphene background-subtracted spectrum image of the ADG (B1−4) from top left to lower right. (C) Elemental maps of the bare particle. (C1−C4) Individual Ca, P, and O maps as well as composite (C, Ca, P, O) map extracted from the background subtracted spectrum image.

and S-2032 chromogenic substrate. BSA was added as a carrier protein for maximal PLC activity. Final concentrations of ADG, FXII zymogen and S-2302 substrate were 500 μM, 50 nM, and 0.5 mM, respectively. FXII autoactivation was measured at room temperature.

Determination of PolyP NP Encapsulation Efficiency. A facile assay was devised employing DLS to measure the stability of ADGs after modulation of $[Ca^{2+}]$ with and without the presence of surface-active agents that would disrupt phospholipid vesicular integrity. Bare granular polyP NPs and ADGs at equivalent monoP concentration were monitored for stability by DLS at 5 mM $CaCl_2$ for 30 min. Immediately prior to the 30 min measurement, the calcium concentration was adjusted to 7.5 mM with gentle mixing (to prevent local concentration inhomogeneities) with or without the addition of 0.5% (v:v) Tween 20.

Monitoring Digestion of ADGs by bvsPLA$_2$ and PLC via DLS. The scattering intensity of 5 mM ADGs in 5 mM $CaCl_2$, pH 5.4 at room temperature (RT) was observed in 10 min increments for 30 min to ensure colloidal stability. The ADGs were then diluted 10X in enzyme buffer prewarmed to 37 °C containing either 25 mM Tris·HCl, pH 7.4, 100 mM NaCl, 7.5 mM $CaCl_2$ and 10 μg/mL bvsPLA$_2$ or 50 mM Tris·HCl, pH 5.5, 10 μM $ZnCl_2$, 7.5 mM $CaCl_2$, 0.1% (w:v) BSA, and 1 μg/mL PLC. The scattering intensity continued to be monitored in 10 min intervals at 37 °C as phospholipid hydrolysis occurred.

ADG Contact Activity in Human Plasma. Before addition to citrated PNP, 30 μM ADGs were digested with 100 ng/mL PLC from *C. perfringens* for 20 min in a buffer containing 5 mM $CaCl_2$, 10 μM $ZnCl_2$, 0.1% (w:v) BSA, and 50 mM Tris·HCl, pH 7.4 for 20 min at 37 °C. After phospholipase digestion, 50 μL citrated PNP was recalcified with 50 μL of 25 mM $CaCl_2$, 5 mM imidazole, pH 7.4 and 50 μL sample was immediately added (after recalcification). Final concentrations of molecularly dissolved, long-chain polyP ($polyP_{>600}$) and ADGs were 10 μM. Turbidity was measured at 405 nm every minute for 60 min at room temperature using a Finstriments Microplate

DOI: 10.1021/acs.biomac.6b00577
Biomacromolecules 2016, 17, 2572−2581

Reader (MTX Lab Systems, Vienna, Virginia). The resulting sigmoidal absorbance traces were fitted to a Boltzmann sigmoidal function in OriginPro 8.6 (OriginLab Corporation, Northhampton, MA). The time to clot was defined as the inflection point $x_0 \pm$ SE. The percent reduction in the time to clot was normalized against the control (with no activator present).

Conventional Transmission Electron Microscopy. *Sample Preparation.* Briefly, 10 μL of the undiluted sample was pipetted onto a 300-mesh Holey, copper-on-carbon Formvar grid (Structure Probe Inc., West Chester, PA). After 2 min the liquid that did not evaporate was wicked away by placing the tip of a Kim wipe in close proximity to the liquid droplet. The grid was subsequently allowed to dry at ambient conditions for at least 5 min before examination in a JEM-1220 transmission electron microscope (JEOL Ltd., Tokyo, Japan).

High-Resolution Scanning Transmission Electron Microscopy (HR-STEM). *Methods.* The biocompatible graphene sandwich containing the ADG was prepared by (1) etching the copper layer away from a copper/graphene film to expose the graphene monolayer before transfer to the surface of DI H_2O; (2) forming a thin liquid film containing the ADG sample on a standard TEM grid coated with monolayer graphene; and (3) exploiting the evanescent wave generated by total internal reflection to place the grid on top of the graphene monolayer to form the graphene sandwich.[37] The EELS spectrum images of the ADGs and the bare particles are background subtracted. In Figure 2B, the P *L*-edge in the shell EELS spectrum (red) is taken from the shell of the EELS map of the ADG. The P *L*-edge in the core EELS spectrum (blue) is generated by first extracting the spectrum from the core region of the EELS map, which contains both the core and the shell signal, and then by subtracting the shell spectrum. In Figure 2B, the O, P, and Ca line profiles are normalized to the maximum intensity, while the C line profile is normalized with P at the maximum intensity position.

Sample Preparation. Ten millimolar bare granular polyP NPs and 5 mM ADGs were prepared in biocompatible graphene sandwiches using previously established methodology[37] and transferred to JEOL JEM200CF STEM/TEM (JEOL Ltd., Tokyo, Japan) operated at 80 keV for imaging and EELS acquisition. HAADF and ABF images were taken simultaneously.

RESULTS AND DISCUSSION

A facile nanoprecipitation process was devised to encapsulate granular platelet-sized polyP into sterically stabilized liposomes rapidly on the benchtop, creating a nanoscale drug delivery platform modeled after the human body's intrinsic arsenal for controlling hemorrhage. The ADGs consist of a 150 nm granular polyP core surrounded by a 200 nm PEGylated liposome (Figure 1A), mimicking the size and structure of human platelet dense granules.[28]

The nanostructure of the ADGs was subsequently examined by imaging and spectroscopic methods. Conventional transmission electron microscopy (TEM) and high-resolution scanning transmission electron microscopy (HR-STEM) were employed to show that the ADGs possess narrow size distribution and a defined core−shell architecture, with a homogeneously dense polyP granule serving as the core and a ring of lighter electron-density consisting of the phospholipid lamella (Figure 2A, cf. Supporting Information **Figure S1**). Further, EELS was exploited to map the ADG's elemental components to prove unambiguously that the synthetic scheme yielded encapsulated polyP particles as intended.

An inherent disadvantage of conventional TEM for structural characterization of biological or biomimetic nanomaterials is radiation damage from the electron beam,[38] limiting imaging resolution to length scales of nanometers and spectroscopy to tens of nanometers.[39,40] Standard electron dose and dose rates directed at polyP bodies transform the granular structures into round sponges most likely due to electron beam-induced hydrogen gas bubbling and mass loss, and this therefore necessitates an alternative imaging and structural characterization tool for finer sample elucidation. To overcome these limitations, ADGs suspended in aqueous 5 mM $CaCl_2$ were directly sandwiched between two graphene layers, before transferal to the transmission electron microscope (JEOL JEM-ARM200CF) for high-resolution STEM and EELS analysis[37] (Figure 1B). The presence of the graphene monolayers has been shown to substantially abrogate the deleterious electronic effects on the sample, minimizing covalent bond cleavage during electron microscopy visualization of biological materials and biochemical reactions of experimental interest.[41−45] As a comparison, bare granular polyP NPs prepared in graphene sandwiches are spherical particles of uniform electron density, with the characteristic white spots, observed by Docampo and Ruiz[28] using conventional TEM, being absent (Figure 2A). The polyP granules are approximately 150−200 nm in diameter, in very good agreement with DLS measurements (cf. Supporting Information Figure S3). In contrast to the bare particles, the ADGs exhibit a clear core−shell nanoarchitecture characteristic of a polyP NP encapsulated in a liposome. A high angle annular dark-field (HAADF) image of an ADG reveals a dense, 150 nm core surrounded by an irregularly shaped 25 nm thick shell of decreased electron density (Figure 2A). These length scales are in good agreement with light scattering data, as the granular polyP NP was measured to have an initial hydrodynamic diameter of ∼160 nm, and the liposomes were formed via extrusion through a polycarbonate membrane with 200 nm pores.

To the best of our knowledge, this is the first time that EELS has been used to probe the elemental consituents of polyP NPs and their liposomally encapsulated counterparts, ADGs. Figure 2B shows the elemental distribution of Ca, P and O within the ADG particle. The compositional map reveals that the shell consists of C, O, and P, but not Ca, suggesting the presence of a phospholipid envelope. The carbon signal in the shell stems most likely from the PEG brushes and the hydrocarbon tails, glycerol backbone, and headgroup carbons of the phospholipid lamella (cf. Supporting Information Figure S2). The dense core exhibits a homogeneous distribution of Ca, P and O, demonstrating that the granular polyP NPs were successfully encapsulated by the phospholipid envelope. As a control group, Figure 2C shows the elemental distribution of Ca, P, and O of the bare particle. These elemental maps match well with the acquired HAADF image, and show a uniform distribution of Ca, P and O in the bare particle, consistent with the elemental composition of granular polyP NPs. The pixel-size in Figure 2B is larger than in Figure 2C to minimize the effects of electron-dose induced changes to the shell. In order to rule out the possibility that in the ADG, the O and P signals in the core region shown in Figure 2B are only coming from the phospholipid envelope, which also contains O and P, we perform elemental line scans of the C, O, P and Ca to show the distribution of these elements, shown in Figure 2B. Elemental line scans of C and Ca indicates the presence of a Ca core encapsulated by a ∼ 25 nm thick C shell. The shape of the C and Ca signal is consistent with the typical core−shell structure. Unlike the "saddle" shape of C, which indicates the absence of C in the core, the Gaussian shape of the O and P signals indicates that these two elements are present in both the core and the shell. Furthermore, analysis of the P *L*-edges is used to compare the local P bonding between the core and the shell.

DOI: 10.1021/acs.biomac.6b00577
Biomacromolecules 2016, 17, 2572−2581

Both spectra show a near-edge fine-structure typical for P_xO_y,[46] while the P spectrum from the shell shows an additional prepeak, indicating a loss in P−O bonding. These EELS data are consistent with our expectation of the P bonding structure in the granular polyP core as well as the liposome shell.

The stability of the ADGs was subsequently investigated for 1 h at room temperature in the same solution in which they were prepared (5 mM $CaCl_2$, pH 5.4) utilizing DLS, measured in 10 min intervals (Figure 3B). The initial effective diameter of the bare polyP granules is approximately 160 nm with a PDI ∼ 0.1 (t = −10 min in Figure 3B), in agreement with our previous report.[29] After addition of a stoichiometric excess of sterically stabilized liposomes and 10 min of bath sonication, encapsulated polyP granules are monodisperse with a PDI ∼ 0.2, (Supporting Figure S3), with an effective diameter only marginally bigger than their unencapsulated counterparts (t = 0 min in Figure 3B). Further DLS measurements reveal that the diameter remains unchanged ca. 165 nm after 60 min has elapsed, whereas bare polyP NPs (black symbols and line in Figure 3B) in the same solution environment manifest power-law type growth kinetics. At the time of nanoprecipitation the bare polyP granules are approximately 160 nm, ripening to ∼220 nm in 1 h. The equivalent power-law growth phenomenon is clearly absent with the ADGs (red symbols and line in Figure 3B). The particle diameter of the ADGs as determined by electron microscopy is comparable qualitatively to the hydrodynamic diameter measured by dynamic light scattering, which strongly suggests that the encapsulated particles observed in HR-STEM are stable in suspension for at least an hour, a time scale sufficient to potentially mitigate bleeding after a severe hemorrhagic event.

ADG encapsulation efficiency was investigated by modulating the calcium concentration, since the presence of calcium controls the thermodynamic equilibrium of granular polyP NP self-assembly.[29] Changes in the calcium concentration would have nearly immediate effects on the polyP NP effective diameter, as the polyP NP size is solely determined by the calcium concentration over an extensive range of polyP supersaturation values.[29] 5 mM ADGs were synthesized in 5 mM $CaCl_2$, pH 5.4, and monitored by DLS every 10 min. Once 30 min had elapsed the calcium concentration was increased to 7.5 mM, and an excess of a nonionic detergent, Tween 20, (which would not affect polyP nanoprecipitation in a measurable way, cf. Supporting Figure S4) was added to solubilize the vesicular envelope and expose the polyP cargo to the higher calcium environment (Figure 3C). Upon addition of 0.5% (v:v) Tween 20 and increasing the calcium concentration to 7.5 mM, the average particle size rapidly increases above 200 nm (red line with open circles in Figure 3C). Ten minutes after detergent solubilization, the particle population is no longer unimodal (data not shown), with a Gaussian-averaged effective diameter greater than 300 nm. Visible sedimentation of agglomerated granular polyP occurs 20 min after adding detergent, with the effective diameter bigger than the micron length scale and the scattering count rate tending to 0. In the absence of detergent, an increase in calcium concentration, by contrast, causes only a negligible change in size, with the average effective diameter centered around 165−180 nm (red line with solid circles in Figure 3C), comparable to the instance with no modulation in the calcium concentration (red line with solid circles in Figure 3B). Bare polyP NPs subjected to the same experimental scheme show typical power-law growth before calcium concentration increase and subsequently rapidly

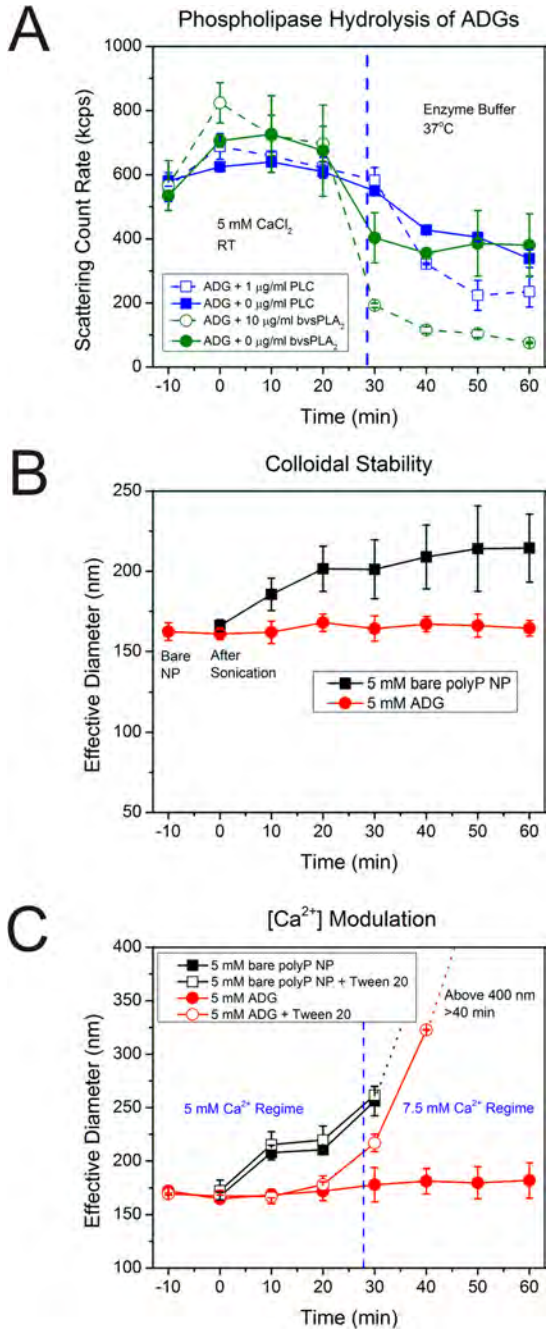

Figure 3. (A) Scattering intensity of ADGs after phospholipase digestion. ADGs were prepared in 5 mM $CaCl_2$ at room temperature (RT) and monitored for stability for 30 min before transferal to an enzyme buffer at 37 °C containing either 10 μg/mL $sPLA_2$ from bee venom ($bvsPLA_2$) or 1 μg/mL PLC from *C. perfringens*. The scattering count rate drops significantly for both 10 μg/mL $bvsPLA_2$ and 1 μg/mL PLC ADG digestions, implying that the phospholipases are inducing hydrolysis of the lipid envelope, leading to degradation and agglomeration of ADGs and precipitation of the polyP NP cargo. (B) Stability of ADGs in suspension. The average effective diameter was determined for the bare polyP NP (immediately before adding liposome, t = −10 min), immediately after sonication (t = 0 min), and every 10 min thereafter until 1 h had elapsed. The ADGs do not appreciably change in size over the duration of the experiment. The bare polyP NPs, on the other hand, prepared at the same supersaturation ratio, grow in a power-law manner to a mean effective diameter of approximately 220 nm in 1 h. (C) Verification of the ADG encapsulation efficiency by measuring ADG diameter shifts after

DOI: 10.1021/acs.biomac.6b00577
Biomacromolecules 2016, 17, 2572−2581

Figure 3. continued

exposure to detergent and changes in calcium concentration. Liposome solubilization by the nonionic detergent Tween 20, in conjunction with an increase in the calcium concentration, was exploited to judge the ADG encapsulation efficiency semiquantitatively. In the absence of Tween 20 and an increase in calcium concentration to 7.5 mM at t = 30 min, there is no statistically significant perturbation in the ADG effective diameter (solid red dots). However, increasing the calcium concentration after dissolution of the lipid envelope by detergent exposure allows for the polyP NPs to be exposed to the higher amount of calcium, resulting in an increased effective diameter (hollow red dots).

precipitate into micron-sized particles after 10 min independent of the presence of detergent. These results suggest that the particle encapsulation efficiency is close to the theoretically maximum value.

Not only do the ADGs structurally resemble human platelet dense granules, they also manifest potentially promising procoagulant effects *in vitro* like their biological counterparts when triggering agents are used to disassemble the phospholipid envelope and expose the procoagulant polyP cargo. Inspired by the platelet degranulation process that occurs *in vivo*, we present a paradigm through which hydrolytic enzymes present in human platelets or secreted into the circulation after hemorrhage can be exploited to induce clotting factor activity on a time scale sufficient to cease bleeding.

The targeted delivery of polyP relies on the presence of phospholipases (e.g., PLC and $sPLA_2$), which occur at much higher concentrations at local bleeding sites (at the scale of μg/mL) compared to global baseline physiological levels (at the scale of ng/mL) to quickly degrade phospholipid vesicles. Immediately after traumatic hemmorhage, a concatenation of carefully orchestrated biochemical events must occur near the wound site, with platelets serving as the principal actors in establishing primary hemostasis.[47] Platelets adjacent to the trauma site stick to the damaged endothelium creating a temporary "plug," recruit other platelets via secreted small molecule messengers, and initiate the coagulation cascade by supporting activation of circulating clotting factors.[48−50] PLC plays a major role in platelet activation, and is central to the platelet degranulation process[51,52]—the exocytosis of dense and α granules into the vasculature—ensuring that high local concentrations of polyP are established in platelet-rich thrombi. PLC is an intracellular lipase that hydrolyzes phospholipids at the 3 position,[51] leading to mobilization of intracellular calcium

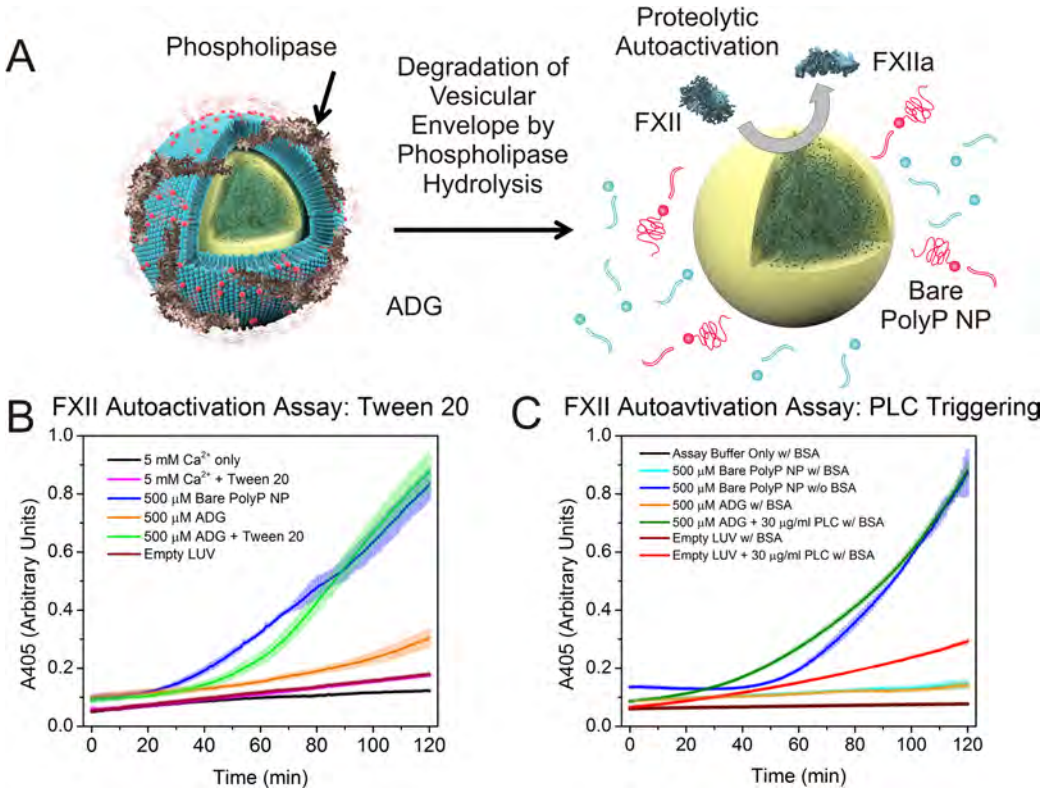

Figure 4. (A) Illustration of phospholipase-induced degradation of the lipid envelope. Secretory phospholipases such as human $sPLA_2$ encountered at locally high concentrations near sites of trauma and inflammation, as well as intracellular isoforms like PLC, involved in platelet degranulation, are envisioned to degrade the liposome vesicle, exposing the granular polyP NP to induce FXII autoactivation. (B) Autoactivation of FXII zymogen via detergent-triggered solubilization of ADG vesicular envelope. ADGs initiate autoactivation of FXII after addition of 0.5% (v:v) Tween 20, similar to the bare polyP NPs (as a positive control). In contrast, ADGs without detergent treatment yield no significant conversion of FXII to FXIIa. As a negative control empty liposomes at the same concentration elicit no FXII autoactivation. (C) FXII autoactivation after ADG preincubation with PLC. ADGs were incubated with 30 μg/mL PLC (from *C. perfringens*) at 37 °C for 20 min before initiation of FXII autoactivation in a buffer containing BSA to ensure optimal phospholipase digestion. Bare polyP NPs without BSA were included as a positive control. ADGs preincubated with PLC manifest a similar rate of absorbance increase to both bare polyP NPs and ADGs digested with Tween 20. ADGs without PLC do not measureably promote FXII autoactivation at the concentration tested. Empty liposomes digested with PLC show some absorbance increase, which is likely a result of vesicle aggregation after phospholipid hydrolysis.

DOI: 10.1021/acs.biomac.6b00577
Biomacromolecules 2016, 17, 2572−2581

stores and activation of G protein-coupled secondary messenger systems with diverse physiological consequences extending beyond hemostasis and inflammation.[53] Although PLC in human platelets exclusively hydrolyzes phosphoinositides,[54] numerous other PLC isoforms exist in nature that do not discriminate between phospholipids. Many bacterial toxins referred to as "lecithinases" possess robust PLC activity for phosphatidylcholines and phosphatidylethanolamines.[55,56]

An additional strategy employs secreted phospholipases at sites of inflammation, e.g. around tumors and sites of vascular injury, to promote hydrolysis of the vesicular envelope. It has been clinically documented that in human patients with a constellation of inflammatory diseases, such as rheumatism and atherosclerosis, that the serum concentration of secretory phospholipase A_2 ($sPLA_2$) can reach 10−30 ng/mL.[57] Local plasma concentrations of $sPLA_2$ in the boundary layer directly adjacent to sites of trauma can be 100- to 1000-fold higher, approaching 10 μg/mL. Moreover, several studies have shown that degradation of phospholipid vesicles by phospholipase hydrolysis could be an order faster when conjugated to PEG chains.[58] The likely mechanism is that PEG chains cause extrusion of the phospholipid to the exterior of the bilayer, promoting more rapid and facile phospholipase adsorption at the interface.[59] Therefore, PEGylated phospholid vesicles, as with our design of encapsulating polyP NPs, offer not only steric stabilization and immunoprotection, but also a means for controlling and targeting drug release upon phospholipid degredation at the sites where phospholipases are overexpressed.

The phenomenon of ADG liposomal envelope digestion by model phospholipases was explored by DLS to estimate time scales of hydrolysis and protein concentrations necessary for polyP cargo release to suitably modulate clotting factor activity. The colloidal stability of ADGs was surveyed in 5 mM $CaCl_2$, pH 5.4 at RT for 30 min before dilution into an enzymatic assay buffer at 37 °C. Upon transfer to the enzymatic buffers tailored for optimal PLC and $sPLA_2$ activity, respectively, the scattering intensity marginally drops, likely due to changes in liposome phase behavior and fluidity due to the low melting temperature of L-α-phosphatidylcholine, the major constituent in the sterically stabilized liposomes (Figure 3A). Moreover, the calcium concentration for both buffers is 7.5 mM in order to gauge polyP release after hydrolysis. In the absence of enzyme, the size of the ADGs does not change significantly, suggesting that the majority of the granular polyP NPs are completely encalpsulated. After addition of 1 μg/mL PLC or 10 μg/mL $sPLA_2$ at 30 min, however, the scattering intensities drop siginificantly. This suggests that the phospholipases have begun to hydrolyze the liposomal barrier surrounding the polyP NP, leading to polyP NP precipitation in the more calcium-enriched environment, decreasing the total number of colloidal particles due to sedimentation. Further investigation reveals that 30 μg/mL PLC is an ideal concentration for *in vitro* autoactivation of FXII (please see Supporting Figure S6).

The ability of ADGs to autoactivate isolated FXII zymogen after detergent-induced solubilzation was first assessed as a proof-of-principle demonstrating that the polyP NP cargo retains its procoagulant functionality. Corroborating Engel et al.'s results that platelet-sized polyP robustly supports zymogen conversion,[36] we show under similar experimental conditions that 500 μM ADGs are able to promote autoactivation of FXII after detergent solubilization by 0.5% (v:v) Tween 20, whereas ADGs not treated with detergent are largely inert, exhibiting minimal FXII autoactivity (Figure 4B). Empty sterically stabilized liposomes are also unable to initiate conversion of FXII to FXIIa, suggesting that promotion of autoactivation stems from release of the granular polyP NPs. FXII autoactivity of the bare granular polyP NPs is concentration-dependent, and manifests saturating kinetic behavior with maximal autoactivation occurring at 500 μM monoP for BKGP70, the same polyP used in this study (see Supporting Figure S5 for concentration dependence). Figure 4C shows that ADGs preincubated in a 0.1% (w:v) BSA suspension with PLC for optimal phospholipase activity for 20 min before addition of zymogen initiate conversion of FXII in a manner consistent with ADGs subjected to detergent treatment with Tween 20. ADGs preincubated in the same buffer without PLC are largely "contact inactive". Likewise, empty sterically stabilized liposomes are unable to support autoactivation of FXII zymogen. The absorbance intensity of empty sterically stabilized liposomes preincubated with the equivalent concentration of PLC does increase slightly during the duration of the experiment; however, this rise is likely due to vesicle aggregation or zymogen activation stemming from interaction with negatively charged degradation products.

Interestingly, 500 μM bare polyP NPs in the presence of 0.1% (w:v) BSA evince no contact activity over the 120 min assay, whereas bare polyP NPs without BSA elicit robust FXII autoactivation within 1 h (Figure 4C). BSA is an established divalent metal chelator, with low dissociation constants for Ca^{2+}, Zn^{2+}, and Cu^{2+}.[60,61] Moreover, zinc cations greatly accelerate FXII autoactivation, and hence signficantly reduce the autoactivation doubling time.[62,63] The presence of millimolar amounts of divalent metals like Ca^{2+} and Zn^{2+} ensures that the predominant polyP species is either an NP or polyP−metal complex (see Supporting Information Figure S7−8 for zinc's *nanoprecipitative* effects). It is well established that foreign contact activators manifest as either negatively charged colloids or granules like kaolin[64] or as polymer−metal complexes, e.g., ellagic acid coordinated with copper.[65] The fact that BSA effectively lowers the free ionic concentration of these precipitative divalent metal cations and completely abrogates polyP NP contact activity in this simplified *in vitro* model of the contact pathway of blood clotting suggests that divalent metal ion complexation to the polymer may be required for polyP to elicit FXII zyomgen autoactivation. Additionally, recent work by Ursula Jakob and colleagues at the University of Michigan provides compelling evidence that polyP is a nonspecific protein binder, facilitating protein folding in a fashion comparable to conventional protein chaperones.[66] Surface plasmon resonance measurements have identified numerous blood proteins that bind to polyP, including thrombin.[67] We have also observed by DLS that bare polyP NPs may complex with BSA via a calcium-mediated process.[29] However, enzymatically triggered hydrolysis of ADGs by PLC even in the presence of BSA still yields siginificant proteolytic autoactivation (Figure 4C). Although there is a high concentration of serum albumin in human plasma, polyP still manages to function as a very potent procoagulant agent, implying that the inhibitory effect of serum albumin cannot be too strong. Nonetheless, the precise mechanism by which BSA and polyP interact demands further investigation. Taken together, these data suggest that PLC hydrolysis of the lipid envelope is occurring, quickly exposing a negatively charged surface to autoactivate the FXII zymogen, and, further, that the sterically stabilized liposome shields the granular polyP NP

DOI: 10.1021/acs.biomac.6b00577
Biomacromolecules 2016, 17, 2572−2581

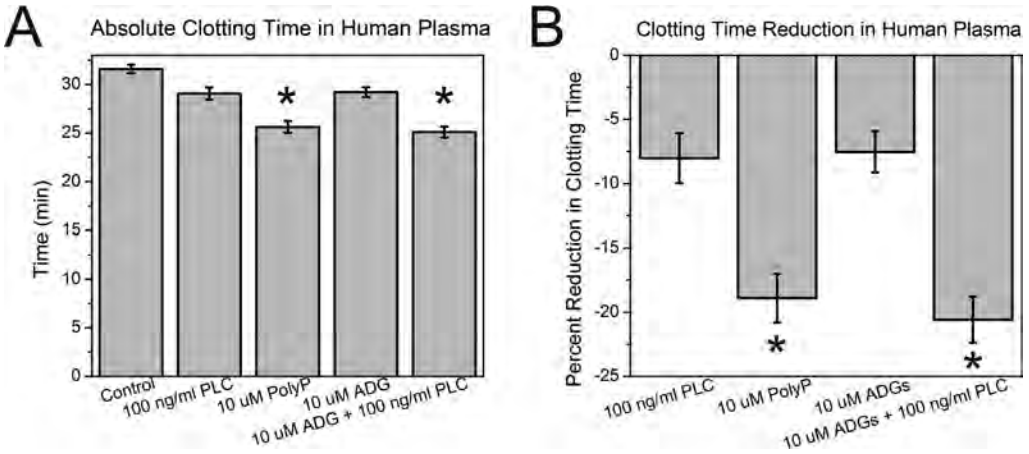

Figure 5. Contact activity of ADGs in human plasma. (A) Absolute clotting time in human plasma. 10 μM ADGs + 100 ng/mL PLC are comparably procoagulant to 10 μM molecularly dissolved, long-chain polyP. Ten micromolar ADGs without trigger and 100 ng/mL PLC alone marginally reduce the time to clot compared to the control (with no activator present). Absolute clotting time is given by the fitted inflection point of a Boltzmann sigmoidal growth function ± SE of the averaged absorbance traces of each sample group (n = 11). * represents $p < 0.05$ for a two-sided t test compared to control (without activator). (B) Clotting times given as percent reduction from the control.

from interacting with FXII and other proteins like BSA over a duration of at least 2 h.

In addition to assessing the ability of ADGs to catalyze the conversion of FXII zyomgen to FXIIa in isolation, the particles' contact activity was determined in pooled normal plasma (PNP) by measuring changes in turbidity upon coagulation. ADGs were preincubated for 20 min with 100 ng/mL PLC from *C. perfringens* before initiation of clotting. Figure 5 shows that 10 μM ADGs + 100 ng/mL PLC reduce the time to clot equivalently compared to 10 μM molecularly dissolved, long-chain polyP, with 21% and 19% diminutions compared to control, respectively. Ten micromolar ADGs and 100 ng/mL PLC alone both clot slightly more rapidly than control (with no activator present). The fact that ADGs minimally reduce the clotting time suggests that either a small fraction of the polyP remains unencapsulated, or that some polyP can be transported across the relatively fluid ADG bilayer, of which 95 mol % is the low T_m L-α-PC, when it is diluted into PNP. Given that PLC also reduces the time to coagulation compared to control implies that the phospholipase possesses marginal intrinsic contact activity at the concentration tested. It is also noteworthy that molecularly dissolved, long-chain polyP is not as robust a contact activator as previous reports in the literature demonstrate;[29,33] however, the assay protocol was suitably modified to gauge the ADG procoagulant activity, accounting for the divergent behavior. Altogether, PLC is able to digest the ADG lipid envelope, allowing the polyP granule inside to initiate the contact pathway of blood coagulation.

CONCLUSION

We present the facile, rapid, and inexpensive synthesis of a polyP NP encapsulated in a liposome as a potential procoagulant nanotherapy imitating human platelet dense granules. All the materials are biocompatible and biodegradable, and the process could conceivably be scaled in an economical manner. High-resolution TEM and EEL spectrum imaging of ADGs confirm the nanostructure of a 200 nm sterically stabilized lipid shell encapsulating a 150 nm diameter granular polyP NP core. A label-free direct graphene sandwich approach was used in electron microscopy experiments to prevent beam-induced mass loss and morphology change. Light scattering measurements of ADGs in suspension indicate that the procoagulant nanoparticle is colloidally stable. Triggered initiation of FXII autoactivation by ADGs via detergent solubilization or phospholipase hydrolysis of the liposomal envelope in an *in vitro* model lends direction in the future for an *in vivo* investigation into ADGs' efficacy in activating the contact system of clotting with the objective to limit blood loss following a severe hemorrhagic event.

ASSOCIATED CONTENT

Supporting Information

Calculation of PolyP Aggregation Number in a Representative Granular PolyP NP; Calculation of Stoichiometric Amount of Lipids for Theoretically Complete Encapsulation of the Granular PolyP NPs; Conventional TEM of ADGs; HR-STEM of ADGs and Bare PolyP NPs; Colloidal Stability & Particle Size Distribution of ADGs Prepared for HR-STEM Imaging; Nanoprecipitation of PolyP in Aqueous Media Containing Tween 20; FXII Autoactivity of Bare PolyP NPs; ADG-Induced FXII Autoactivity: Dependence on PLC Concentration; PolyP Nanoprecipitation in Aqueous Media Containing Ca^{2+}/Zn^{2+}; Colloidal stability of ADGs and Empty PEGylated Vesicles in BSA/Ca^{2+} Suspensions. The Supporting Information is available free of charge on the ACS Publications website at DOI: 10.1021/acs.biomac.6b00577.

(PDF)

AUTHOR INFORMATION

Corresponding Author

*Tel: +1(312) 996-8249. Fax: +1(312) 996-0808. E-mail: liuying@uic.edu.

Author Contributions

Experiments were conducted by A.J.D., J.K., M.S., and C.W. and designed and interpreted by A.J.D., J.K., M.S., C.W., S.A.S., R.F.K., J.H.M., and Y.L. The manuscript was composed by A.J.D. and Y.L., and edited by C.W., S.A.S., R.F.K., and J.H.M. All authors have given approval to the final version of the manuscript.

DOI: 10.1021/acs.biomac.6b00577
Biomacromolecules 2016, 17, 2572−2581

Funding

Synthesis of the nanoparticles was funded by Nanomanufacturing program of National Science Foundation CAREER award (NSF 1350731). The characterization of the ADG clotting activity was sponsored by the US Army Medical Research and Materiel Command (WQ81XWH-11-2-0021). The U.S. Army Medical Research Acquisition Activity, 820 Chandler Street, Fort Detrick MD 21702-5014 is the awarding and administering acquisition office. This work made use of the JEOL JEM-ARM200CF in the Electron Microscopy Service (Research Resources Center, UIC). The acquisition of the UIC JEOL JEM-ARM200CF was supported by a MRI-R2 grant from the National Science Foundation [DMR-0959470]. The contents of this article do not necessarily reflect the position or the policy of the government, and no official endorsement should be inferred.

Notes

The authors declare the following competing financial interest(s): Y.L. and A.J.D. are co-inventors on a pending patent application related to this work. S.A.S. and J.H.M. hold several patents and are co-inventors on pending patent applications on the therapeutic usage of polyP.

■ ACKNOWLEDGMENTS

The authors are indebted to L.J. at the UIC RRC EMS for her assistance with imaging ADGs, as well as her experience and judgment with evaluating biological materials. The authors would like to acknowledge Dr. Q.Q. from BNL for her help in writing the EELS background subtraction DigitalMicrograph script.

■ REFERENCES

(1) Sauaia, A.; Moore, F. A.; Moore, E. E.; Moser, K. S.; Brennan, R.; Read, R. A.; Pons, P. T. *J. Trauma Acute Care Surg.* **1995**, *38*, 185−193.
(2) Holcomb, J. B. *Crit. Care* **2004**, *8*, S57−S60.
(3) Kauvar, D. S.; Wade, C. E. *Crit. Care* **2005**, *9*, S1−S9.
(4) Alam, H. B.; Burris, D.; DaCorta, J. A.; Rhee, P. *Mil. Med.* **2005**, *170*, 63−69.
(5) Spahn, D. R.; Cerny, V.; Coats, T. J.; Duranteau, J.; Fernández-Mondéjar, E.; Gordini, G.; Stahel, P. F.; Hunt, B. J.; Komadina, R.; Neugebauer, E.; et al. *Crit. Care* **2007**, *11*, R17.
(6) Rossaint, R.; Bouillon, B.; Cerny, V.; Coats, T. J.; Duranteau, J.; Fernández-Mondéjar, E.; Hunt, B. J.; Komadina, R.; Nardi, G.; Neugebauer, E.; et al. *Crit. Care* **2010**, *14*, R52.
(7) Kauvar, D. S.; Lefering, R.; Wade, C. E. *J. Trauma* **2006**, *60*, S3−S11.
(8) Cox, E. D.; Schreiber, M. A.; McManus, J.; Wade, C. E.; Holcomb, J. B. *Transfusion* **2009**, *49*, 248S−255S.
(9) Brown, M. A.; Daya, M. R.; Worley, J. A. *J. Emerg. Med.* **2009**, *37*, 1−7.
(10) Beekley, A. C. *Crit. Care Med.* **2008**, *36*, S267−S274.
(11) Nishijima, D. K.; Zehtabchi, S. *Ann. Emerg. Med.* **2009**, *54*, 737−744.
(12) Farokhzad, O. C.; Langer, R. *ACS Nano* **2009**, *3*, 16−20.
(13) Murday, J. S.; Siegel, R. W.; Stein, J.; Wright, J. F. *Nanomedicine* **2009**, *5*, 251−273.
(14) Peer, D.; Karp, J. M.; Hong, S.; Farokhzad, O. C.; Margalit, R.; Langer, R. *Nat. Nanotechnol.* **2007**, *2*, 751−760.
(15) Torchilin, V. P. *Nat. Rev. Drug Discovery* **2005**, *4*, 145−160.
(16) Discher, D. E.; Ahmed, F. *Annu. Rev. Biomed. Eng.* **2006**, *8*, 323−341.
(17) Meng, F.; Zhong, Z.; Feijen, J. *Biomacromolecules* **2009**, *10*, 197−209.
(18) Kovacs, E. W.; Hooker, J. M.; Romanini, D. W.; Holder, P. G.; Berry, K. E.; Francis, M. B. *Bioconjugate Chem.* **2007**, *18*, 1140−1147.
(19) Huh, K. M.; Lee, S. C.; Cho, Y. W.; Lee, J. W.; Jeong, J. H.; Park, K. *J. Controlled Release* **2005**, *101*, 59−68.
(20) Gref, R.; Domb, A.; Quellec, P.; Blunk, T.; Muller, R. H.; Verbavatz, J. M.; Langer, R. *Adv. Drug Delivery Rev.* **2012**, *64*, 316−326.
(21) Jain, R. K.; Stylianopoulos, T. *Nat. Rev. Clin. Oncol.* **2010**, *7*, 653−664.
(22) Barenholz, Y. *J. Controlled Release* **2012**, *160*, 117−134.
(23) Papahadjopoulos, D.; Allen, T. M.; Gabizon, A.; Mayhew, E.; Matthay, K.; Huang, S. K.; Lee, K. D.; Woodle, M. C.; Lasic, D. D.; Redemann, C. *Proc. Natl. Acad. Sci. U. S. A.* **1991**, *88*, 11460−11464.
(24) Allen, T. M. *Adv. Drug Delivery Rev.* **1994**, *13*, 285−309.
(25) Zhou, Z.; Anselmo, A. C.; Mitragotri, S. *Adv. Mater.* **2013**, *25*, 2723−7.
(26) Anselmo, A. C.; Modery-Pawlowski, C. L.; Menegatti, S.; Kumar, S.; Vogus, D. R.; Tian, L. L.; Chen, M.; Squires, T. M.; Sen Gupta, A.; Mitragotri, S. *ACS Nano* **2014**, *8*, 11243−11253.
(27) Smith, S. A.; Mutch, N. J.; Baskar, D.; Rohloff, P.; Docampo, R.; Morrissey, J. H. *Proc. Natl. Acad. Sci. U. S. A.* **2006**, *103*, 903−908.
(28) Ruiz, F. A.; Lea, C. R.; Oldfield, E.; Docampo, R. *J. Biol. Chem.* **2004**, *279*, 44250−44257.
(29) Donovan, A. J.; Kalkowski, J.; Smith, S. A.; Morrissey, J. H.; Liu, Y. *Biomacromolecules* **2014**, *15*, 3976−3984.
(30) Docampo, R.; Moreno, S. N. *Parasitol. Today* **1999**, *15*, 443−448.
(31) Docampo, R.; de Souza, W.; Miranda, K.; Rohloff, P.; Moreno, S. N. *Nat. Rev. Microbiol.* **2005**, *3*, 251−261.
(32) Muller, F.; Mutch, N. J.; Schenk, W. A.; Smith, S. A.; Esterl, L.; Spronk, H. M.; Schmidbauer, S.; Gahl, W. A.; Morrissey, J. H.; Renne, T. *Cell* **2009**, *139*, 1143−1156.
(33) Smith, S. A.; Choi, S. H.; Davis-Harrison, R.; Huyck, J.; Boettcher, J.; Rienstra, C. M.; Morrissey, J. H. *Blood* **2010**, *116*, 4353−4359.
(34) Choi, S. H.; Smith, S. A.; Morrissey, J. H. *Blood* **2011**, *118*, 6963−6970.
(35) Mui, B.; Chow, L.; Hope, M. J. *Methods Enzymol.* **2003**, *367*, 3−14.
(36) Engel, R.; Brain, C. M.; Paget, J.; Lionikiene, A. S.; Mutch, N. J. *J. Thromb. Haemostasis* **2014**, *12*, 1513−1522.
(37) Wang, C. H.; Qiao, Q.; Shokuhfar, T.; Klie, R. F. *Adv. Mater.* **2014**, *26*, 3410−3414.
(38) Egerton, R. F.; Li, P.; Malac, M. *Micron* **2004**, *35*, 399−409.
(39) Egerton, R. F. *Electron Energy-Loss Spectroscopy in the Electron Microscope*. Springer: New York, 2011.
(40) Wu, J. S.; Kim, A. M.; Bleher, R.; Myers, B. D.; Marvin, R. G.; Inada, H.; Nakamura, K.; Zhang, X. F.; Roth, E.; Li, S. Y.; Woodruff, T. K.; O'Halloran, T. V.; Dravid, V. P. *Ultramicroscopy* **2013**, *128*, 24−31.
(41) Park, J.; Park, H.; Ercius, P.; Pegoraro, A. F.; Xu, C.; Kim, J. W.; Han, S. H.; Weitz, D. A. *Nano Lett.* **2015**, *15*, 4737−4744.
(42) Wojcik, M.; Hauser, M.; Li, W.; Moon, S.; Xu, K. *Nat. Commun.* **2015**, *6*, 7384.
(43) Chen, Q.; Smith, J. M.; Park, J.; Kim, K.; Ho, D.; Rasool, H. I.; Zettl, A.; Alivisatos, A. P. *Nano Lett.* **2013**, *13*, 4556−4561.
(44) Chen, Q.; Smith, J. M.; Rasool, H. I.; Zettl, A.; Alivisatos, A. P. *Faraday Discuss.* **2015**, *175*, 203−214.
(45) Kashyap, S.; Woehl, T. J.; Liu, X.; Mallapragada, S. K.; Prozorov, T. *ACS Nano* **2014**, *8*, 9097−9106.
(46) Favron, A.; Gaufrès, E.; Fossard, F.; Lévesque, P.; Phaneuf-L'Heureux, A.; Tang, N.; Loiseau, A.; Leonelli, R.; Francoeur, S.; Martel, R. *arXiv preprint arXiv:1408.0345*, 2014.
(47) Broos, K.; Feys, H. B.; De Meyer, S. F.; Vanhoorelbeke, K.; Deckmyn, H. *Blood Rev.* **2011**, *25*, 155−167.
(48) Coughlin, S. R. *Arterioscler., Thromb., Vasc. Biol.* **1998**, *18*, 514−518.
(49) Coughlin, S. R. *Nature* **2000**, *407*, 258−264.
(50) Furie, B.; Furie, B. C. *N. Engl. J. Med.* **2008**, *359*, 938−949.
(51) Brass, L. F.; Shaller, C. C.; Belmonte, E. J. *J. Clin. Invest.* **1987**, *79*, 1269−1275.

DOI: 10.1021/acs.biomac.6b00577
Biomacromolecules 2016, 17, 2572−2581

(52) Flaumenhaft, R. *Arterioscler., Thromb., Vasc. Biol.* **2003**, *23*, 1152−1160.
(53) Taylor, S. J.; Chae, H. Z.; Rhee, S. G.; Exton, J. H. *Nature* **1991**, *350*, 516−518.
(54) Rittenhouse-Simmons, S. *J. Clin. Invest.* **1979**, *63*, 580−587.
(55) Titball, R. W. *J. Appl. Microbiol.* **1998**, *84*, 127s−137s.
(56) Roberts, M. F.; Otnaess, A. B.; Kensil, C. A.; Dennis, E. A. *J. Biol. Chem.* **1978**, *253*, 1252−1257.
(57) Nevalainen, T. J.; Haapamaki, M. M.; Gronroos, J. M. *Biochim. Biophys. Acta, Mol. Cell Biol. Lipids* **2000**, *1488*, 83−90.
(58) Jorgensen, K.; Davidsen, J.; Mouritsen, O. G. *FEBS Lett.* **2002**, *531*, 23−27.
(59) Majewski, J.; Kuhl, T.; Gerstenberg, M.; Israelachvili, J.; Smith, G. *J. Phys. Chem. B* **1997**, *101*, 3122−3129.
(60) Foghandersen, N. *Clin. Chem.* **1977**, *23*, 2122−2126.
(61) Masuoka, J.; Saltman, P. *J. Biol. Chem.* **1994**, *269*, 25557−25561.
(62) Bernardo, M. M.; Day, D. E.; Olson, S. T.; Shore, J. D. *J. Biol. Chem.* **1993**, *268*, 12468−12476.
(63) Bernardo, M. M.; Day, D. E.; Halvorson, H. R.; Olson, S. T.; Shore, J. D. *J. Biol. Chem.* **1993**, *268*, 12477−12483.
(64) Renne, T.; Schmaier, A. H.; Nickel, K. F.; Blomback, M.; Maas, C. *Blood* **2012**, *120*, 4296−4303.
(65) Bock, P. E.; Srinivasan, K. R.; Shore, J. D. *Biochemistry* **1981**, *20*, 7258−7266.
(66) Gray, M. J.; Wholey, W. Y.; Wagner, N. O.; Cremers, C. M.; Mueller-Schickert, A.; Hock, N. T.; Krieger, A. G.; Smith, E. M.; Bender, R. A.; Bardwell, J. C. A.; Jakob, U. *Mol. Cell* **2014**, *53*, 689−699.
(67) Choi, S. H.; Collins, J. N.; Smith, S. A.; Davis-Harrison, R. L.; Rienstra, C. M.; Morrissey, J. H. *Biochemistry* **2010**, *49*, 9935−9941.

DOI: 10.1021/acs.biomac.6b00577
Biomacromolecules 2016, 17, 2572−2581